High-Throughput Automated Detection And Analyses Of Locomotor and Hunting Sequences In Larval Zebrafish Unveil The Role Of A Conserved Dopaminergic Diencephalospinal Tract In Locomotor Development and Goal-Directed Behavior

A THESIS
SUBMITTED TO THE FACULTY OF
UNIVERSITY OF MINNESOTA
BY

Aaron M. Lambert

IN PARTIAL FULFILLMENT OF THE REQUIREMENTS
FOR THE DEGREE OF
DOCTOR OF PHILOSOPHY

Adviser: Dr. Mark A. Masino

March 2015

Acknowledgements

I would like to thank all members of my immediate family for their continual support while I have been a doctorate student, through both good times and bad. Specifically, I would like to thank my mother, Rose Harris, and father, Thomas Lambert, for being excellent parents during my formative years and equally excellent friends during my adult years. I would like to thank my brother, Bill Lambert, and sister, Jenn Lambert, for always being compassionate siblings and even better friends. I would also like to thank my two cats, Zenan and Angel, for providing unwavering love. Specifically, Zenan is 16-years-old at the time of the submission of this dissertation, and she has been with me through: high school at Minooka, undergraduate college at Urbana-Champaign, two jobs I had as a research technician while living in Chicago, and throughout my doctoral work here in the Twin Cities. Conversely, Angel is still a kitten at the time of this dissertation submission, but she has provided much needed companionship in the final days of the writing of this dissertation. Finally, I would like to thank all members of the Masino lab, as well as all of my collaborators from six different labs at five different institutions, for their support and synergistic collaborations. Most of all, however, I would like to thank my advisor, Dr. Mark A. Masino, for providing me with the opportunity to work in his laboratory and continue the strong tradition of sound science that his predecessors instilled in him, with an even greater emphasis on fostering caring and constructive inter-dependent relationships with scientific colleagues, both inside and outside of the lab.

Dedication

This thesis is dedicated to myself, my immediate family, the Masino Lab, and the Department of Neuroscience and Graduate Program in Neuroscience at the University of Minnesota- Twin Cities. This thesis is also dedicated to: 1) the long-term pursuit of fully elucidating the multiple roles of the conserved dopaminergic diencephalospinal network in normal and disease states 2) providing novel analytical tools for high-throughput assaying of visual, oculomotor, visuomotor, motor, locomotor, appetitive, attentional, and engramic function in larval zebrafish 3) providing an analytical platform for high-throughput assaying in other model organisms.

Thesis Abstract

The dopaminergic diencephalospinal tract (DDT), and its source *orthopedia*-specified dopaminergic (DAergic) population, is the most conserved part of the vertebrate DAergic system. The source somata of the DDT have widespread ascending and descending projections that span and have potential to integrate the entire rostro-caudal axis of the central nervous system, from telencephalon to spinal cord. Mammalian studies confirm that the extensive DDT network is multifunctional, even via its direct influence within the spinal cord. While specific mechanosensory and nociceptive functions of the DDT acting in the spinal cord *in vivo* have been elucidated in adult mammals, whether or not the DDT also exerts locomotor influences in the spinal cord *in vivo*, as well as whether the DDT plays an early role during development, has remained unknown despite suggestive *in vitro* studies. My thesis explored the role of the vertebrate DDT in locomotor development and goal-directed behavior in zebrafish larvae, a premiere model to elucidate the neural bases of such behaviors at organismal, systems, circuit, cellular, and subcellular levels *in vivo*. To this aim, I developed new methodologies for high-throughput, unbiased, automated detection and analyses of locomotion and goal-directed hunting. This approach was combined with peripheral nerve recordings of the neural locomotor output of the spinal cord and employed during: DAergic pharmacological perturbations, demarcated transections at varying locations of the nervous system, selective chemogenetic

ablation of *orthopedia* neurons, and laser ablations of the DDT. Collectively, this thesis reveals that the DDT acts specifically through endogenous dopamine receptor 4 (D4R) signaling to mediate locomotor development and provide a multifunctional modulation of multiple locomotor parameters in a separable manner, by putatively influencing disparate neuronal targets concurrently. Moreover, this thesis elucidates that endogenous D4R signaling is crucial to goal-directed prey capture via a specific motor-centric role in shifting prey-directed motor strategies and providing precision of speed control during execution of advancing hunting maneuvers. From the collective elucidations of my thesis, I posit the existence of a modular organization subserving a versatile locomotor network, wherein separate neural modules are recruited spontaneously and during hunting and that the hunting module is further subdivided into separable orienting and advancing regimes. Integrated into this granular network, endogenous D4R signaling, perhaps through a widespread integrative impetus at disparate regions via the extensive DDT network, differentially influences multiple modules concurrently. These findings, integrated with the mammalian literature, suggest that the conserved vertebrate DDT is crucial for locomotor development, as well as motor planning and execution of goal-directed behavior.

Table of Contents (TOC)

-Use PDF bookmarks to navigate to each section.

-PDF bookmarks expand into nested bookmarks to navigate subsections.

Doctoral Projects (11 Total)

9 Original-Research (5 First-Author), **2 Reviews** (2 First-Author)

1) Friedrich T, **Lambert AM**, Masino MA, Downes GB (2012). Mutation of zebrafish dihydrolipoamide branched chain transacylase E2 results in motor dysfunction and models maple syrup urine disease. Dis Model Mech 5(2):248-58. Mar 1, 2012.

2) **Lambert AM**, Bonkowsky JL, Masino MA (2012). The conserved dopaminergic diencephalospinal tract mediates vertebrate locomotor development in zebrafish larvae. J Neurosci 32(39):13488-500. Sep 26, 2012. **Cover article**.

3) Decker AR*, McNeill MS*, **Lambert AM**, Overton JD, Chen YC, Lorca RA, Johnson NA, Brockerhoff S, Mohapatra DP, MacArthur H, Panula P, Masino MA, Runnels LW, Cornell RA (2014). Abnormal differentiation of dopaminergic neurons in zebrafish *trpm7* mutant larvae impairs development of the motor pattern. Dev Biol 386(2):428-39. Feb 15, 2014.

4) **Lambert AM** and Masino MA (In Preparation). A widespread conserved dopaminergic system exerts multi-site D4R-mediated meta-locomotor modulation.

5) **Lambert AM** and Masino MA (In Preparation). High-throughput automated detection and analyses of hunting sequences reveals a highly modular locomotor network with separable dopaminergic contributions to spontaneous and goal-directed behavior.

6) **Lambert AM** and Masino MA (In Preparation). Hunting experience unveils goal-directed visuomotor learning and long-term memory in zebrafish larvae.

7) **Lambert AM** and Masino MA (In Preparation). An ancient dopaminergic system: evolutionary conservation of the dopaminergic diencephalospinal tract and its multifunctional integration of the CNS . **Review article**.

8) **Lambert AM** and Masino MA (In Preparation). Zebrafish prey capture as a premiere model to elucidate visuomotor transformations, learning, and long-term memory of goal-directed behavior. **Review article**.

9) Koleilat A, **Lambert AM**, Masino MA, Ekker SC, Schimmenti, LA (Work In Progress). Amelioration of vestibular and auditory deficits in Myo7a mutants via high-throughput genomic and pharmacological interventions.

10) Chan JD, Grab T, **Lambert AM**, Masino MA, Marchant JS (Work In Progress). High-throughput genomic and pharmacological targeting of bioaminergic targets for regeneraton in the planarian Dugesia japonica.

11) **Lambert AM**, Montgomery JE, Peck JH, Masino MA (Work In Progress). Optogenetic and pharmacological advancement of vertebrate locomotor development via the dopaminergic diencephalospinal tract.

List of Figures (42 Total)

List of Tables (5 Total)

General Introduction

The primary goal of this thesis is to test the hypothesis, by developing new methodologies, that the vertebrate dopaminergic diencephalospinal tract is a necessary neural component of locomotor development and goal-directed behavior in zebrafish larvae. Successful completion of this goal could elucidate ancient and preserved fundamental functions of the vertebrate DDT, which could provide a heuristic for subsequent studies in mammalian models. Moreover, development of the proposed methodologies could be employed for further investigations of the disparate but integrative neural bases of locomotion and goal-directed behavior in zebrafish and other animal models.

Dopaminergic Diencephalospinal Tract (DDT): Conservation and Function

Conservation.

The diversity of dopaminergic (DAergic) systems across vertebrates is a paragon for comparative evolutionary biology. A rich exemplary palette of conservation, divergence, and evolution of DAergic systems provides both tractable and convoluted investigative pathways from which to traverse. A strikingly tractable target for investigating perpetual conservation of an ancient vertebrate DAergic system is the diencephalic population comprising the DAergic diencephalospinal tract (DDT). The DDT is present in the most ancient of vertebrates, lamprey

(Barreiro-Iglesias et al., 2008), as well zebrafish (Kastenhuber et al., 2010; Tay et al., 2011), salamander (Sánchez Camacho et al., 2001), frog (Sánchez Camacho et al., 2001), lizard (Smeets et al., 2001), mouse (Qu et al., 2005), rat (Skagerberg et al., 1982; Takada et al., 1988), cat (Doyle, 1994; Holstege et al., 1996), sheep (Kania, 1985; Tillet and Kitahama, 1998), monkey (Holstege et al., 1996), and even human (Kinkhabwala et al., 2011; Koyama et al., 2011). Conversely, the same continuity of conservation does not hold for the more prominently studied midbrain DAergic populations in mammals, namely the substantia nigra and ventral tegmental area (VTA) (Reiner et al., 1998; Smeets and González, 2000). These midbrain populations appear to be a more recent evolutionary development, as they do not exist in zebrafish or lamprey (McLean and Fetcho, 2004a; Barreiro-Iglesias et al., 2008). Moreover, the DDT is genetically conserved between zebrafish and mouse since it is conferred by the same homeodomain transcription factor, Orthopedia (Otp), across species (Ryu et al., 2007). In both animal models, genetic or morpholino knockdown of the gene/transcript for *orthopedia* (*otp*) eliminates the DDT but leaves all other DAergic neurons intact, including several other diencephalic populations, as well as the midbrain populations in mammals (Ryu et al., 2007; Kastenhuber et al., 2010). Hence, the DDT represents the most conserved part of the vertebrate DAergic system. These and the following data are voluminous evidence of the DDT's conserved transcriptional identity, somatic location, morphology, projection patterns, and potentially multifunctional nature.

In addition to conservation of transcriptional identity and somatic topology, the DDT across several model organisms exhibits conservation of somatic and neuritic morphology; much of this evidence comes from zebrafish and murine models. The bilateral ventro-caudal diencephalic cells of the DDT are large pear-shaped neurons with a dorsally-protruding t-shaped neuritic bifurcation (Doroshenko and Maĭskiĭ, 1987; Tay et al., 2011). The descending neuritic branch traverses and arborizes through the midbrain, hindbrain, and ultimately innervates and tiles virtually the entire rostro-caudal length of the spinal cord (Skagerberg et al., 1982; McLean and Fetcho, 2004a; Qu et al., 2005; Tay et al., 2011). This descending branch is largely ipsilaterally projecting, but a minority of contralateral projections exist (Takada et al., 1988; Qu et al., 2005; Tay et al., 2011). The ascending neuritic branch projects and arborizes, exclusively ipsilaterally, into the endohypothalamic tract and, in some cases, all the way dorso-rostrally to the highest-order telencephalic territories within a given organism: to the subpallium of zebrafish (Tay et al., 2011) and to many subcortical regions (nucleus accumbens, striatum, olfactory tubercle, amygdala) and even the prefrontal cortex of rodents (Takada et al., 1988; Takada, 1993). However, the long-range ascending branch of the source of the DDT has a notable diversity in fiber density across organisms, being particularly dense in lamprey (Barreiro-Iglesias et al., 2008) but sparse in zebrafish (Tay et al., 2011). Nevertheless, the source of the vertebrate DDT is poised to be a broadly

influencing neuromodulatory system with the potential to integrate the entire rostral-caudal extent of the central nervous system, from telencephalon to spinal cord.

The DDT's longitudinal projection pattern into the spinal cord is well characterized in most species, but finer analyses of the DDT's spinal arborization patterns have been done in most mammals but not non-mammals. The bilateral DDT projects caudally along a diffuse dorsal-ventral extent of the lateral spinal cord, making it strategically positioned to putatively influence both sensory and motor spinal regions (Skagerberg et al., 1982; McLean and Fetcho, 2004b; 2004a; Kastenhuber et al., 2010); however, in mammals there is a dorsal bias to these longitudinal projections (Skagerberg et al., 1982). The only further characterization in zebrafish is that the longitudinal DDT fibers traverse in direct apposition to spinal motor neurons and appear to form discrete synaptic boutons around these cells (McLean and Fetcho, 2004b). In mammals, these DDT fibers are known to innervate the dorsal horn, intermediolateral cell column, intermediate and central gray, other peri-ependymal regions and, to a lesser extent, the ventral horn (Skagerberg et al., 1982; Doroshenko and Maĭskiĭ, 1987; Ridet et al., 1992). Ultrastructural analyses of DDT spinal arborizations reveal primarily axodendritic contacts, but also a minority of axosomatic contacts (Ridet et al., 1992). Innervation of the DDT to the ventral horn and the IML, across the rostro-caudal extent of the spinal cord, appears to consist of mostly classical

synapses, whereas in the dorsal horn it's largely non-synaptic cervically but with more classical synapses at thoraco-lumbar levels (Ridet et al., 1992).

Function.

Given the widespread ascending and descending anatomical connectivity, the source of the DDT likely subserves several disparate but integrative functions. Even restricting its potential influence to the spinal cord, the anatomy suggests that the DDT may regulate mechanosensory, nociceptive, sympathetic, and locomotor functions via direct modulation of spinal targets. Germane to this inference, the DDT represents the exclusive source of DA in the spinal cord of both zebrafish and mammals (Doroshenko and Maĭskiĭ, 1987; Kastenhuber et al., 2010), so virtually all spinal DAergic signaling *in vivo* is likely to be supplied by the DDT. The strongest evidence of an *in vivo* function of the DDT acting directly in the spinal cord comes from adult murine models and unveils its key somatosensory and antinociceptive roles. *In vivo* whole-cell patch clamp recordings of rat substantia gelatinosa (SG) neurons, which are a first-order sensory spinal relay receiving direct input from dorsal root ganglia fibers, have revealed that these spinal targets: 1) are inhibited by local application of DA through D2-like (D2, D3, D4) DA receptor (DAR) signaling 2) have their responses to noxious and innocuous cutaneous stimulation directly inhibited by DA and 3) are strongly inhibited immediately following electrical stimulation of DDT neurons in the diencephalon (Taniguchi et al., 2011). All of these

manipulations suppress both the frequency and amplitude of glutamatergic spontaneous excitatory postsynaptic currents (EPSCs) in SG neurons, strongly suggesting that the DDT and DA exert presynaptic and postsynaptic inhibitory actions on these spinal targets.

Additional evidence for a mechanosensory, nociceptive, and even locomotor role of the DDT comes from clinical and translational studies of Restless Leg Syndrome (RLS), and Periodic Limb Movements during Sleep (PLMS), which are prevalent neurological disorders that affect over 10% of the U.S. and European population (Trenkwalder et al., 2009). RLS is characterized by abnormal limb sensations that are mitigated with motor activity, are exacerbated when the limbs are at rest, have a circadian profile in which these sensations are more severe at night, and often severely disrupt sleep and consequently induce cognitive deficits (Clemens et al., 2006). PLMS is considered a separate neurological disorder but occurs in over 80% of RLS patients (Ekbom and Ulfberg, 2009). The symptomatology of PLMS is more restrictive than that of RLS and is characterized by rhythmic bouts of involuntary movement of the lower limbs during non-REM stages of sleep. Whereas the role of the DDT in RLS likely involves nociceptive, sympathetic, circadian, and locomotor circuits, the role of the DDT in PLMS may be more exclusively involved with locomotor spinal circuits. Functional human neuroimaging studies suggest that PLMS is induced by either direct disinhibition of the spinal cord or by disinhibition of descending

reticulospinal tracts that may function to activate multiple segmental central pattern generators (CPGs) in lumbar portions of the spinal cord (Vetrugno et al., 2007). Interestingly, prescription D2-like DAR agonists ameliorate the symptoms of human RLS and PLMS and this efficacy has been attributed to the DDT and not nigrostriatal pathways (Lee et al., 1996; Tergau et al., 1999; Paulus et al., 2007a). Collectively, these circumstantial human clinical data suggest that pathophysiology of the DDT and concomitant insufficient inhibitory DAergic D2-like transmission in the spinal cord and/or hindbrain may induce the symptoms of RLS and PLMS, diseases which are ameliorated via therapeutic D2-like DAR activation of inhibitory input (Paulus et al., 2007a; 2007b).

Translational murine models provide even better evidence for a role of the DDT in the neural bases of RLS, but whether this role is exerted supraspinally or spinally, as well as which precise neural modalities (e.g. sensory, motor) are influenced, is unknown. Mouse models of RLS, in which the DDT is bilaterally abolished through 6- hydroxydopamine (6-OHDA), show increased locomotor activity and wakefulness across the sleep-wake cycle that is reversed by the D2/D3 agonist ropinirole (Qu et al., 2007; Zhao et al., 2007). Corroborating this phenomenon, D3 DAR knockout (D3KO) mice also exhibit this behavioral phenotype (Accili et al., 1996). Taken together, these studies suggest that the DDT may normally provide D3 receptor-mediated inhibition, namely during rest periods, to facilitate behavioral quiescence, but where this DAergic signaling

occurs and whether it acts specifically upon somatosensory and/or locomotor circuits is unclear.

In sum, the conserved vertebrate DDT *in vivo* has a clear and direct role on spinal sensory circuits, at least in adults, but whether it also has a direct spinal locomotor role is unknown. Furthermore, it is unknown what functions the DDT may serve in developing vertebrates *in vivo*, but *in vitro* and anatomical evidence suggests that the DDT may serve an early role in locomotor development (McEwen et al., 1997; Zhu et al., 2007; Tay et al., 2011). Compared to other animal models, including mammalian options, the zebrafish model represents a more promising approach to elucidating an *in vivo* role of the DDT in the locomotion of developing vertebrates. Since the central goal of this thesis is to investigate the DDT's neural bases of spinal locomotor influence, attention should be paid to what is known regarding the neuroethology of locomotion.

Neuroethology of Locomotion

Locomotion is essential for survival in most animals. The neural basis of locomotion lies in central pattern generators (CPGs), which are neural circuits with the intrinsic capacity to generate rhythmic patterns of activity. The locomotor CPG, which is contained within the spinal cord of vertebrates and the ventral nerve cord of cephalized invertebrates, does not require the brain or sensory

afferents to generate a coordinated motor pattern. This is a universal feature that has been demonstrated across invertebrate and vertebrate systems, including: leech, locust, lamprey, zebrafish, frog, mouse, rat, cat, dog, and monkey (Marder and Bucher, 2001). The ventromedial spinal cord is the locus of the mammalian locomotor CPG, as this region in isolation can produce coordinated locomotor output in mice; conversely, lateral or dorsal regions of the spinal cord in isolation are incapable of such locomotor rhythm generation (Kjaerulff and Kiehn, 1996).

The initial experiments that began elucidation of spinal locomotor CPGs were from several species of spinalized animals (i.e. transected at the hindbrain-spinal cord junction) capable of locomotor-like movements (Sherrington, 1910; Brown, 1913; Hinsey and Cutting, 1936; Fayein and Viala, 1976; Meisel and Rakerd, 1982) and even legitimate locomotion, insofar as the body received postural support (Grillner and Rossignol, 1978a). Sherrington and others posited that this spinalized phenomenon required a chained reflex involving constant sensory feedback. This idea was refuted by showing that a sensory-deafferented spinalized cat still locomotes (Grillner and Rossignol, 1978b). Mechanistically, electrophysiological neural recordings in reduced spinal cord preparations have demonstrated that the spinal cord has an intrinsic CPG or series of coupled segmental CPGs capable of producing rhythmic oscillatory patterns of activity that correspond to muscular activity patterns during locomotion in intact animals (Wallén and Williams, 1984; Cohen et al., 1990; Bonnot et al., 2002; McDearmid

and Drapeau, 2006). Activation of the intrinsic spinal CPG in the isolated spinal cord requires exogenous application of a neurotransmitter or neuromodulator to provide tonic excitatory drive (Dale and Roberts, 1984; Barry and O'Donovan, 1987; Barbeau and Rossignol, 1991; Noga et al., 1991; Douglas et al., 1993). This exogenous tonic excitation likely emulates descending glutamatergic command signals from the brain (Di Prisco et al., 1997; Chong and Drapeau, 2007). In the intact vertebrate, hindbrain command circuitry initiates locomotion via glutamatergic reticulospinal neurons that activate the spinal locomotor CPG (Garcia-Rill et al., 1983; Arrenberg et al., 2009; Hägglund et al., 2010).

The brain, in addition to providing excitatory drive to initiate locomotion, contains neuromodulatory systems that profoundly influence spinal locomotor circuitry, both indirectly and directly. Indirect spinal influences arise from local supraspinal processing within the brain that, after one or more outputs to relay centers, ultimately influences descending hindbrain command circuitry and/or the spinal cord itself, albeit polysynaptically. Direct spinal influences are achieved via supraspinal descending neuromodulatory systems that monosynaptically innervate the spinal cord (Swerdlow et al., 1986; Kjaerulff and Kiehn, 2001; Ball et al., 2003), and which are far more prevalent than local intraspinal neuromodulatory modules (Takada et al., 1988; McLean and Fetcho, 2004a; 2004b). Norepinephrine (NE), serotonin (5-HT) and dopamine (DA) are among the most prominent of vertebrate locomotor neuromodulators, where the latter

two also play large roles in modulating invertebrate locomotion. Since the focus of this thesis is to elucidate descending neuromodulation of spinal locomotor function via the conserved DDT, it is instructive to survey of what is known regarding spinal DAergic modulation of locomotion.

Dopaminergic Modulation of Locomotion

DA plays an important modulatory role for locomotion in invertebrates and vertebrates. One of the simplest cephalized invertebrates, the medicinal leech, exhibits swimming and crawling behaviors and DA is sufficient to selectively activate the motor pattern for crawling but not swimming, demonstrating that it is likely a strong determinant of the executed mode of locomotion in these animals (Puhl and Mesce, 2008; 2010; Puhl et al., 2012). Lamprey, among the simplest and most ancient of vertebrates, have an extensive DAergic system that modulates the cycle period of fictive swimming and alters the excitability of spinal motoneurons (Svensson et al., 2003). Lamprey possess DAergic neurons that reside within the spinal cord, as well as brain DAergic neurons in the diencephalon and rhombencephalon that project to other brain areas and to the spinal cord (Barreiro-Iglesias et al., 2008). Since studies of DAergic locomotor modulation in lamprey have been done using *in vitro* spinal cord preparations, it is unknown which source or sources of DA are important for spinal modulation of locomotion *in vivo* since all three disparate DAergic populations have potential to

directly signal in the spinal cord. Conversely, of these three DAergic somatic locations in lamprey (spinal cord, diencephalon, rhombencephalon), only the diencephalon of zebrafish and mammals contain DAergic neurons and the sole source of spinal DA originates from the DDT. This feature makes investigating the DDT's role in spinal modulation of locomotion much more tractable in zebrafish and mammals, especially in spinalized preparations *in vitro* or during local spinal application of DA.

Anatomical and electrophysiological murine studies *in vitro* indirectly suggest that the vertebrate DDT could play an early role in locomotor development *in vivo*. *In situ* hybridization studies have revealed that mRNA for the full complement of DAR genes (D1, D2, D3, D4, D5) is expressed across the dorsal-ventral axis of the neonatal mouse lumbhanar spinal cord, being expressed in the majority of motoneurons and ventromedial interneurons (Zhu et al., 2007). Functionally, studies from the *in vitro* neonatal mouse spinal cord demonstrate that, by postnatal day (P2), exogenous DA: 1) contributes to the initiation of the coordinated motor pattern during fictive locomotion (Jiang et al., 1999), 2) increases intrinsic excitability of motoneurons (Han et al., 2007) and augments their AMPA currents through D1-like DARs (Han and Whelan, 2009), 3) stabilizes rhythmic output of ventromedial premotor interneurons (Han et al., 2007) 4) modulates spinal reflexes, which are converted from depressive to facilitatory in D3KO mice (Clemens and Hochman, 2004) and 5) is necessary for coordinated

L-DOPA-induced air-stepping (McEwen et al., 1997). Before neonatal rodents can support their body weight to start walking, they are capable of coordinated locomotion in the form of L-DOPA-induced air-stepping that is dependent on DAR signaling (Sickles et al., 1992; McCrea et al., 1997) which is sufficient to act at the level of the spinal cord *in vitro* (McEwen et al., 1997). This early DAR-dependent signaling in the spinal cord may play a developmental role, since L-DOPA- induced air-stepping develops from being bipedal, at P0, to quadrupedal, by P5 (Van Hartesveldt et al., 1991). In disease states, for example, hypoxic–ischemic injury to the developing brain, DAergic cell populations are at risk and may contribute to the impaired motor development after these injuries (Bax et al., 2006). Hence, all of these mammalian data point to a role of the DDT in locomotor development, but answering whether this truly occurs *in vivo* is more tractable in the conserved zebrafish model of the DDT.

Zebrafish Model to Study Locomotor Function of Vertebrate DDT *In Vivo*

Compared to mammalian models in which detailed investigation of spinal circuitry is best accomplished *in vitro*, the larval zebrafish, which is both translucent and genetically tractable, is amenable to integrative investigation of the locomotor function of the vertebrate DDT at an organismal, systems, circuit, cellular, and subcellular level *in vivo*. However, the function of the zebrafish DDT is entirely unknown currently, although it is likely to be functional early since 7 of the 8

zebrafish DAR mRNAs are expressed in the spinal cord by only 2 days postfertilization (dpf) (Boehmler et al., 2004; 2007; Li et al., 2007b; Reimer et al., 2013). Furthermore, basic knowledge of DAergic modulation of zebrafish locomotion is lacking since it has been mostly limited to crude assessments of gross changes in the amount of locomotor activity, but not on specifically whether and how the pattern and/or coordination of locomotion changes.

Zebrafish exhibit a locomotor pattern of episodic beat-and-glide swimming, which consists of discrete swimming episodes interposed with passive gliding or quiescence (Fuiman and Webb, 1988). A developmental switch in the episodic locomotor pattern from long to short swimming episodes is observed between 3 and 4 dpf (Buss and Drapeau, 2001), which is concurrent with increased locomotion and the advent of hunting (Borla et al., 2002). Interestingly, the DDT does not yet exert a locomotor effect in the spinal cord at 3 dpf (Thirumalai and Cline, 2008), although, at this stage, the *otp* cells that comprise the DDT are positive for tyrosine hydroxylase (TH) and DA transporter mRNA (*dat; slc6a3*) and send robust projections across the entire rostrocaudal extent of the spinal cord (McLean and Fetcho, 2004a; Kastenhuber et al., 2010; Fujimoto et al., 2011) that, by 4 dpf, form putative synapses with spinal motor neurons (McLean and Fetcho, 2004b). This makes the DDT an auspicious potential player in mediating this locomotor developmental switch, especially since the other prominent descending neuromodulatory source in zebrafish, serotonin, reduces

quiescent periods but has no effect on active locomotor properties at 4 dpf (Brustein et al., 2003). Based on all of this information, this thesis postulates and investigates whether, by 4 dpf, the DDT directly modulates spinal locomotor circuits to confer the mature pattern of short swimming episodes that is observed into adulthood (Fuiman and Webb, 1988). Furthermore, this thesis hypothesizes that the DDT is integral, in addition to the advent of fine spontaneous motor control, to the conspicuously concurrent advent of execution of prey-tracking maneuvers during goal-directed hunting. Since this thesis will thus explore a role of the DDT in hunting, such an endeavor will be best leveraged by understanding the current state of the neuroethology of prey capture.

Neuroethology of Prey Capture and its Dopaminergic Influence

Prey capture is an integrative behavior that serves as a neuroethological platform for investigating its sensory, sensorimotor, motor, neuromodulatory, engrammic, attentional, and decision-making components (Ewert et al., 1999; 2001; Muto and Kawakami, 2013). Although the capture component is emphasized in the term, prey capture holistically consists of prey detection, pursuit, capture, and ingestion. While the neural bases of the sensory and sensorimotor components of prey capture have been well elucidated in genetically intractable organisms (Ewert et al., 1999; 2001; Olberg, 2012), as well as in the genetically tractable zebrafish (Gahtan, 2005; Smear et al., 2007; Del Bene et al., 2010; Muto et al.,

2013), the necessary locomotor and motor neural components for executing pursuit and capture maneuvers are not as well understood (Nishikawa, 1999). Interestingly, the neuromodulatory influence of systemic DAergic agonism in anurans strongly influences prey-catching motor strategies, inhibiting orienting maneuvers in favor of advancing snapping maneuvers (Glagow and Ewert, 1996; 1997a; 1997b; 1999). However, it remains unknown as to: 1) whether this exogenous DAergic phenomenon has a corresponding endogenous DAergic counterpart 2) which DAergic population may mediate state-dependent switching in prey-catching strategies and 3) the anatomical postsynaptic site of action of DAergic signaling for influencing prey-catching motor strategies.

Zebrafish Model to Study Prey Capture Function of Vertebrate DDT *In Vivo*

Zebrafish larvae- with their genetic tractability, translucency, and amenability to tethered virtual prey pursuit (Trivedi and Bollmann, 2013)- offer one of the best opportunities to comprehensively elucidate the many neural facets of prey capture. The goal of this thesis is to begin investigating the locomotor neural components of prey capture in the well-suited zebrafish model, with its extant knowledge base of the underlying germane spinal (McLean et al., 2007; 2008), hindbrain (Kinkhabwala et al., 2011; Koyama et al., 2011), and midbrain (Binder et al., 2014; Severi et al., 2014; Wang and McLean, 2014) locomotor networks and their neuromodulatory influences (Brustein et al., 2003; Lambert et al.,

2012). A developmental switch from a coarse (long, fast, erratic) to a fine (short, slow, directed) spontaneous locomotor repertoire (Buss and Drapeau, 2001) coincides with the advent of hunting behavior in zebrafish, at just 4 dpf. The newly acquired spontaneous locomotor repertoire conspicuously resembles much of the concurrently acquired hunting locomotor repertoire, with the exception of j-turns and capture swims, in that larvae track paramecia with short, slow and directed swimming episodes (Budick and O'Malley, 2000). This suggests that the neural circuitry dedicated to spontaneous swimming is employed during visually-guided hunting, which leads to two hypotheses: 1) the ontogenies of spontaneous swimming and prey capture performance will be correlated 2) perturbations compromising the spontaneous repertoire will concomitantly compromise the hunting repertoire and, ultimately, prey capture. This thesis hypothesizes that perturbing the DDT-spinal circuit will compromise both the spontaneous and hunting locomotor repertoire and, thus, execution of prey-catching strategies.

High-Throughput Analyses of the Role of the Vertebrate DDT in Zebrafish Locomotion and Prey Capture

Testing the hypothesis that the DDT is involved in locomotor development and goal-directed behavior will require many experimental conditions, necessitating a high-throughput approach to analyzing locomotor and prey capture behavior.

Such a high-throughput approach, which still enables sufficient spatial and temporal resolution for detailed kinematic analyses, is lacking in zebrafish. The only high-throughput approaches for locomotor analyses in zebrafish have poor spatial and temporal resolution and the employed arenas are too small to allow for unconstricted free-swimming (Kokel et al., 2010; Rihel et al., 2010; Peterson and Fishman, 2011; Tan and Zon, 2011), relegating assessments to crude measurements of changes in locomotor activity but without the acuity to examine fine locomotor kinematics (Ingebretson and Masino, 2013). In terms of the state of prey capture analyses in free-swimming zebrafish larvae, it has been limited to either 1) manually counting the number of prey remaining over time, but with no information about how the prey disappeared (Gahtan, 2005) 2) manually detecting and then recording ongoing hunting sequences and separately analyzing the kinematics of each of the videos of these brief, empirically-detected, putative prey encounters (Borla et al., 2002; McElligott and O'Malley, 2005; Bianco et al., 2011; Patterson et al., 2013). An overarching goal of this thesis is to develop and/or implement a novel method for high-throughput, automated detection and analyses of locomotion and hunting sequences in free-swimming zebrafish larvae. The locomotor analyses of this goal will be achieved via automated tracking of the body kinematics of multiple zebrafish larvae in the same large arena, akin to what has already been developed in drosophila (Branson et al., 2009). Concurrently, the hunting analyses of this goal will be attained via automated tracking of zebrafish eye convergences, which is a

reliable hallmark of prey detection and pursuit during the entire duration of each prey encounter (Bianco et al., 2011). Collectively, this novel methodology will enable detailed, automated, and unbiased assessments of the role of the DDT in zebrafish locomotor development and goal-directed hunting. Moreover, this versatile methodology may facilitate future studies within the rapidly growing zebrafish scientific community.

Chapter 1: The Conserved Dopaminergic Diencephalospinal Tract Mediates Vertebrate Locomotor Development In Zebrafish Larvae

Summary

The most conserved part of the vertebrate dopaminergic system is the orthopedia (*otp*)-expressing diencephalic neuronal population that constitutes the dopaminergic diencephalospinal tract (DDT). Although studies in the neonatal murine spinal cord *in vitro* suggest an early locomotor role of the DDT, the function of the DDT in developing vertebrates *in vivo* remains unknown. Here, we investigated the role of the DDT in the locomotor development of zebrafish larvae. To assess the development of the behavioral and neural locomotor pattern, we used high-throughput video tracking in combination with peripheral nerve recordings. We found a behavioral and neural correspondence in the developmental switch from an immature to mature locomotor pattern. Blocking endogenous dopamine receptor 4 (D_4R) signaling *in vivo* either before or after the developmental switch prevented or reversed the switch, respectively. Spinal transections of post-switch larvae reestablished the immature locomotor pattern, which was rescued to a mature-like pattern via spinal D_4R agonism. Selective chemogenetic ablation of *otp b* (*otpb*) neurons that contribute to the DDT perpetuated the immature locomotor pattern *in vivo*. This phenotype was

recapitulated by diencephalic transections that removed the dopaminergic *otpb* population and was rescued to a mature-like locomotor pattern by D_4R agonism. We conclude that the dopaminergic *otpb* population, via the DDT, is responsible for spinal D_4R signaling to mediate the developmental switch to the mature locomotor pattern of zebrafish. These results, integrated with the mammalian literature, suggest that the DDT represents an evolutionarily conserved neuromodulatory system that is necessary for normal vertebrate locomotor development.

Introduction

Noteworthy similarities and differences are present among the dopaminergic (DAergic) systems across vertebrates. Although midbrain DAergic neurons appear to be a more recent evolutionary development (Reiner et al., 1998; Smeets and González, 2000), the DAergic diencephalospinal tract (DDT), which provides the exclusive source of spinal dopamine (DA) in most vertebrates, is highly conserved and may represent an ancient neuromodulatory system of functional relevance to both zebrafish and mammals (Tay et al., 2011). The diencephalic DAergic neurons that comprise the DDT have a conserved somatic location, ascending and descending projections (Takada et al., 1988; Qu et al., 2005; Kastenhuber et al., 2010), and require the transcription factor orthopedia (*otp*) for the development of cellular identity in both zebrafish and mammals (Ryu et al., 2007). Although the function of the zebrafish DDT is unknown, the adult mammalian DDT is implicated in human restless leg syndrome (Qu et al., 2007; Zhao et al., 2007; Paulus et al., 2007a) and exerts direct antinociceptive actions in the rat spinal cord *in vivo* (Taniguchi et al., 2011). Conversely, the function of the DDT in developing vertebrates *in vivo* is unknown, but *in vitro* and anatomical evidence suggests that the DDT may serve an early role in locomotor development (McEwen et al., 1997; Zhu et al., 2007; Tay et al., 2011).

Zebrafish exhibit a locomotor pattern of episodic beat-and-glide swimming, which consists of discrete swimming episodes interposed with passive gliding. A developmental switch in the episodic locomotor pattern from long to short swimming episodes is observed between 3 and 4 days postfertilization (dpf) (Buss and Drapeau, 2001), which is concurrent with increased locomotion and the advent of foraging (Borla et al., 2002). Interestingly, the DDT does not yet exert a locomotor effect in the spinal cord at 3 dpf (Thirumalai and Cline, 2008), although, at this stage, the *otp* cells that comprise the DDT are positive for tyrosine hydroxylase (TH) and DA transporter mRNA (*dat*; *slc6a3*) and send robust projections across the entire rostrocaudal extent of the spinal cord (McLean and Fetcho, 2004a; Kastenhuber et al., 2010; Fujimoto et al., 2011) that, by 4 dpf, form putative synapses with spinal motor neurons (McLean and Fetcho, 2004b).

We postulated that the DDT becomes functional in the zebrafish spinal cord at 4 dpf to confer the mature locomotor pattern of short swimming episodes that is observed into adulthood (Fuiman and Webb, 1988). To assay the development of the episodic locomotor pattern, the present study introduces a novel adaptation of a high-throughput video-tracking algorithm (Ctrax; (Branson et al., 2009) to compare the free-swimming locomotor pattern with peripheral nerve recordings of the neural locomotor output of the spinal cord (Masino and Fetcho, 2005). Through pharmacological perturbations, demarcated transections, and selective

chemogenetic ablation of *otp* neurons, we demonstrate that the conserved DAergic *otp* neurons that comprise the DDT provide the impetus for spinal DA receptor 4 (D_4R) signaling to mediate the developmental switch to the mature episodic locomotor pattern. These findings suggest that the DDT may serve an evolutionarily conserved function in mediating vertebrate locomotor development.

Methods

Animals. All experiments were performed on zebrafish (*Danio rerio*) larvae between 1 and 7 dpf. Wild-type (WT) larvae were obtained from a laboratory stock (Segrest) of adults at the University of Minnesota. Embryos and larvae were raised in an incubator at 28.5°C under a 14/10 light/dark cycle (Lights On, 8:00 A.M.; Lights Off, 10:00 P.M.) until the start of behavioral or neural recordings between 3 and 7 dpf. Larvae were kept at room temperature during all manipulations and recording sessions and returned to the incubator during interims.

The Tg(*otpb.A:nfsB–egfp*)^{zc77} line was generated at the University of Utah. In the Tg(*otpb.A:nfsB–egfp*)^{zc77} line, the *otpb.A*promoter drives expression of the *nfsB* enzyme nitroreductase (Ntr). Specific plasmids used for cloning were as follows: p5E–*otpb.A* (Fujimoto et al., 2011), pME–*nsfB* (no stop codon) (kind gift from C. Seiler, University of Pennsylvania School of Medicine, Philadelphia, PA), p3E–*EGFPpA*, and pDestTol2pA2 (Kwan et al., 2007). Injection of DNA constructs and husbandry of stable transgenic lines were performed as described previously (Bonkowsky et al., 2008). All procedures were approved by the Institutional Animal Care and Use Committees at the University of Minnesota and the University of Utah.

Immunohistochemistry, in situ hybridization, and terminal deoxynucleotidyl transferase dUTP nick-end labeling staining. Whole-mount immunohistochemistry was performed as described previously (Bonkowsky et al., 2008; Fujimoto et al., 2011). Embryos were raised in phenylthiourea (0.003%) in E3 media to inhibit pigment formation beginning at 24 hours postfertilization (hpf). Antibodies used included the following: rabbit polyclonal anti-TH at 1:400 (Millipore), mouse monoclonal anti-GFP at 1:250 (Millipore), Cy3 anti-rabbit at 1:400 (Invitrogen), and Alexa Fluor 488 donkey anti-mouse at 1:400 (Invitrogen). Whole-mount *in situ* labeling for *dat* (Holzschuh et al., 2001) was performed as described previously (Bonkowsky and Chien, 2005; Fujimoto et al., 2011).

Terminal deoxynucleotidyl transferase dUTP nick-end labeling (TUNEL) was performed on whole-mount larvae (ApopTag Fluorescein *In Situ* Apoptosis Detection Kit; Millipore Bioscience Research Reagents). After standard fixation and dehydration of larvae in 100% methanol, larvae were rehydrated stepwise into PBS with 0.1% Tween 20 (PBST), permeabilized with 10 mg/ml Proteinase K in PBST at 28°C, washed twice with PBST, refixed for 20 min with 4% paraformaldehyde (PFA), and washed with PBST. Subsequently, 75 µl of equilibration buffer was added to the larvae for 1 h and then removed and replaced with 55 µl of “working-strength” (per Apoptosis Detection Kit instructions) terminal deoxynucleotidyl transferase enzyme overnight at 37°C. To avoid drying out the larvae, Eppendorf tubes were sealed with Parafilm. Before

use, the anti-digoxigenin conjugate was warmed to room temperature. The end-labeling reaction was stopped by washing the embryos three times for 15 min each with 2 ml of the stop/wash buffer, followed by three 1 min washes with PBS. Then 65 ml of working-strength sheep anti-digoxigenin rhodamine was added to the embryos overnight at 4°C. Double immunohistochemistry for GFP and TUNEL was performed by TUNEL staining; after washes with PBST, larvae were fixed for 20 min in 4% PFA at room temperature and washed again with PBST. Larvae were then permeabilized and antibody stained per our routine protocol (Bonkowsky et al., 2008; Fujimoto et al., 2011).

Microscopy and image analysis. Image acquisition and analysis were performed essentially as described previously (Fujimoto et al., 2011). Images of embryos/larvae processed for *in situ* or immunohistochemistry were taken using a confocal microscope or bright-field microscope. Embryos/larvae were taken stepwise into a solution of 80% glycerol/20% PBST and then mounted on a glass slide with a #0 coverslip fixed into place over a well made using electrical tape. NIH ImageJ software was used for image processing.

Metronidazole treatments. Tg(*otpb.A:nfsB–egfp*)^{zc77} embryos were dechorionated manually at 24 hpf and placed in 5 mM metronidazole (Mtz) (Vetranal from Sigma) dissolved in embryo media (0.03% Instant Ocean in dH_2O). These larvae were then transferred to fresh 10 mM Mtz and incubated

from 48 to 96 hpf, after which Mtz was removed through a series of washes in embryo media. Untreated siblings, also dechorionated at 24 hpf, remained in embryo media continuously, with fresh media being given at 24, 48, and 96 hpf. After Mtz washout at 96 hpf in Mtz-treated larvae, untreated and Mtz-treated larvae were given 1 d in embryo media before behavioral and neural locomotor activity was assessed at 5 dpf. Genotypes for untreated and Mtz-treated larvae were screened as Ntr-negative [Ntr^{-} ($egfp^{-}$)] or Ntr-positive [Ntr^{+} ($egfp^{+}$)] via an epifluorescent stereoscope (MZ16FA; Leica). Only larvae that exhibited an inflated swim bladder at 5 dpf were included in analyses for all experimental groups.

Pharmacology. All drug concentrations were determined in preliminary concentration–response experiments (data not shown). For each pharmacologic agent, we determined the lowest drug concentration that achieved a maximal locomotor effect rather than the IC_{50} or EC_{50} concentration that would only induce a half-maximal effect. As such, the lowest concentration for each drug that achieved a maximal locomotor effect was subsequently used for the reported experiments. For each DA receptor (DAR)-specific antagonist, for example, this concentration was determined to be 10 μM, which is consistent with the range of efficacious concentrations determined during high-throughput behavioral screening of 5280 (10–30 μM; (Rihel et al., 2010)) and 14,000 (10–100 μM; (Kokel et al., 2010) compounds in zebrafish larvae and embryos,

respectively. NMDA, dimethylsulfoxide (DMSO), DA, Mtz, DAR-specific antagonists (D_1R, SCH-23390 [*R*(+)-7-chloro-8-hydroxy-3-methyl-1-phenyl-2,3,4,5-tetrahydro-1*H*-3-benzazepine hydrochloride]; D_2/D_3R, raclopride [3,5-Dichloro-N-(1-ethylpyrrolidin-2-ylmethyl)-2-hydroxy-6-methoxybenzamide]; D_4R, L-745,870 (3-[[4-(4-chlorophenyl)piperazin-1-yl]methyl]-1*H*-pyrrolo[2,3-b]pyridine trihydrochloride)), and DAR-specific agonists (D_1-like, SKF-38393 [2,3,4,5-tetrahydro-7,8-dihydroxy-1-phenyl-1*H*-3-benazepine HCl]; D_2-like, quinpirole (trans-(-)-(4aR)-4,4a,5,6,7,8,8a,9-Octahydro-5-propyl-1H-pyrazolo[3,4-g]); D_4R, PD168,077 [*N*-[[4-(2-cyanophenyl)piperazin-1-yl]methyl]-3-methylbenzamide)] were obtained from Sigma.

Chronic drug incubations. For chronic incubations of DAR-specific antagonists to WT larvae, drugs were dissolved at stated concentrations in embryo media containing 0.1% DMSO; low concentrations of DMSO facilitate in aqueous drug delivery through the skin without affecting behavior (Rihel et al., 2010). Larvae subjected to embryo media containing 0.1% DMSO served as vehicle controls. Baseline free-swimming behavior of all groups was video recorded before the start of drug incubations and comprises the control data reported for 3 and 4 dpf larvae. Chronic drug incubations began at 7:00 P.M. for behavioral and neural assessments on the following day. All experimental groups remained in their respective drugs throughout the recording day, which spanned from 9:00 AM through 6:00 P.M. During all behavioral recording sessions, experimental groups

remained in their respective drugs. For neural recording sessions of pilot experiments, preparations were superfused in their respective drugs. It was determined that the effect of chronic drug incubations did not wash out after removal of the drug via superfusion in extracellular solution alone (see below, Electrophysiology) during the 30 min recording session. As such, neural recording sessions occurred in the presence of extracellular solution without drug. For each experimental condition, behavioral and neural recordings were each performed on a minimum of three different recording days, coming from a minimum of three different clutches. Behavioral and neural recordings for each experimental condition were equally sampled across the recording day and were pooled regardless of recording time.

Video acquisition. A group of 10 larvae in embryo media or embryo media containing drug were transferred to a 50 mm watch glass (Thermo Fisher Scientific) positioned atop a transmitted light stage (Schott TLS and MC-1500 LED Controller). The light intensity at the level of the arena was set to 15,000 lux to maximize contrast and facilitate tracking of dark targets on a light background. The aqueous depth was 10 mm at the center of the arena and became progressively shallower toward the periphery. The larvae acclimated to the recording arena for 5 min before the start of video recording. Spontaneous free-swimming was recorded for 10 min at 60 frames/s with a digital CMOS camera (Firefly MV; Point Gray Research) with an attached 50 mm macro lens (Sigma).

Videos were acquired, via Fview (open-source software; (Straw et al., 2011)), in uncompressed fly movie format (FMF).

Video analysis. The FMF files generated by Fview were imported into the California Institute of Technology Fly Tracker (Ctrax) (open-source software; (Branson et al., 2009) to obtain independent trajectories of each target within the arena. We used the open-source Fix Errors MATLAB Toolbox (FEMT), provided by the creators of Ctrax (Branson et al., 2009), to identify and fix tracking errors (such as swapping of target identities). The total number of errors per 10-minute video was 3.89 ± 0.38 (*n*= 100 videos), and all errors were corrected via the FEMT.

Subsequently, scripts from the open-source Behavioral Microarray MATLAB Toolbox, provided by the creators of Ctrax (Branson et al., 2009), were implemented to compute descriptive statistics of a suite of behavioral parameters for each of the individual targets from the fixed Ctrax trajectories. The target speed function, velmag, was extracted for each target to define and detect event onsets and offsets by thresholding the speed function at 1.5 mm/s. This threshold was sufficiently above most baseline noise, which was, on average, <0.15 mm/s. To filter out transient high-amplitude noise (i.e., >1.5 and <3.0 mm/s), only events that spanned at least four consecutive frames with an average speed of 3 mm/s or greater were classified as swimming episodes. Finally, 3 dpf-like swimming

consisted of long episodes characterized by continuous active undulations when viewing the video frame by frame, but larvae sometimes exhibited periods of the active swimming episode with little or no displacement. Consequently, such periods during an active swimming episode are not captured in the unfiltered speed function. To better capture the entire continuous swimming episode, events that occurred within an 18 frame (300 ms) interevent interval were concatenated into a single swimming episode. This classification system did not erroneously concatenate multiple individual swimming episodes because the shortest latencies between successive free-swimming episodes of zebrafish larvae between 3 and 9 dpf exceed 300 ms and on average exceed 800 ms (Fuiman and Webb, 1988; Muller et al., 2000; Farrell et al., 2011). Identical filters were applied for all videos across all ages and experimental groups.

Once all swimming episodes were identified, we quantified the total distance traveled per individual in centimeters (sum of instantaneous speeds during swimming episodes divided by the frame rate) and mean swimming episode duration per individual in milliseconds (mean duration from the onset to the offset of each individual episode) over the 10-minute recording period. Sample sizes were ultimately smaller for quantifying episode duration compared with total distance traveled because episode duration could not be obtained from animals that did not move during the recording session. Values for total distance traveled and episode duration are expressed as mean ± SD.

Electrophysiology. Neural recordings from paralyzed preparations (i.e., fictive swimming) were assessed via peripheral nerve recordings *in vivo* as described previously (Masino and Fetcho, 2005). Larvae were anesthetized with 0.02% Tricaine-S (Western Chemical) in extracellular recording solution that contained the following (in mM): 134 NaCl, 3 KCl, 1.2 $MgCl_2$, 2.1 $CaCl_2$, 10 HEPES buffer, and 10 glucose, adjusted to pH 7.8 with NaOH (osmolarity adjusted to 290 mOsm with sucrose). Larvae were transferred to Sylgard-lined dissecting dishes and pinned on their sides through the notochord using short pieces of fine tungsten wire (0.001 inch diameter). To access the peripheral motor nerves, the skin was removed between the tungsten pins using a sharp tungsten probe and fine forceps (Fine Science Tools). To prevent muscle contractions during recording, larvae were paralyzed using 5 µl of 0.1 mM α-bungarotoxin (Tocris Bioscience) added to the small amount (~15 µl) of extracellular solution in the dissection dish. Subsequently, larvae were transferred to the stage of an Olympus BX51 WI microscope, and extracellular recording solution was superfused at room temperature. Suction electrodes (6–15 µm tip diameter), filled with extracellular recording solution, were placed in an electrode holder and positioned over the peripheral nerves using micromanipulators (Siskiyou). All recordings were between midbody segments 10 and 20 and were acquired using a Multi-Clamp 700B amplifier (Molecular Devices), a Digidata series 1440A digitizer (Molecular Devices), and pClamp 10.2 software (Molecular Devices).

Extracellular voltage was monitored in current-clamp mode at a gain of 2000 (R_f = 50 MΩ) with the low- and high-frequency cutoff at 300 and 1000 Hz, respectively.

For all preparations in which spontaneous fictive swimming was assessed, spontaneous fictive activity was recorded for a minimum of 30 min. For acute drug administration (30 min) to fictive preparations, drugs were dissolved at stated concentrations in extracellular recording solution and superfused at 1 ml/min. NMDA (50 μM) was superfused for 15–20 min to elicit a baseline of NMDA-induced fictive swimming before application of DA or DAR agonists. DA or DAR agonists were superfused with NMDA for 10–15 min before returning to an NMDA solution (washout).

Analysis of peripheral nerve activity. A program written in MATLAB (MathWorks) was used to analyze extracellular peripheral nerve voltage recordings. The program detected the presence or absence of activity at each voltage sample [$v(n)$]. For each $v(n)$, the algorithm determined a voltage autocorrelation [$c_n(k)$] over a small window (3 ms) centered at $v(n)$. These "windowed" autocorrelations were computed as follows:

Equation 1:

$c_n(k) = \sum_{i=-N_0}^{i=N_0} v(n - i)v(n - i - k)$

where 3 ms windowing was implemented by setting N_0 = (3 ms × f_{sam})/2, where f_{sam} is the sampling frequency, and by setting $v(j) = 0$ for j outside the interval $[n - N_0, n + N_0]$.

A subset of the autocorrelation values (lags) from Equation 1 were used to compute a test statistic for each $v(n)$ with the same lags ($\vec{k_o} = [k_1, k_2, \ldots, k_m]$) used for all voltage samples. Building on Equation 1, for each $v(n)$, a test statistic c_n was computed as follows:

Equation 2:

$c_n = \sum_{k=k_1}^{k=k_m} \sum_{i=-N_0}^{i=N_0} v(n - i)v(n - i - k)$

where Equation 2 is the sum of the $c_n(k)$ from Equation 1 specified by $\vec{k}_o$. $\vec{k}_o$ was set at $\vec{k}_o = [1,2]$ to separate the distributions of the test statistics $\{c_n\}$ in the cases of noise versus activity.

Finally, activity was considered present at $v(n)$ only when c_n was greater than a detection threshold T. T was set as the maximum of a set of $\{c_n\}$ corresponding to the $\{v(n)\}$ in 1 contiguous second of the voltage recording in which activity was

absent (typically the first second of the recording) and was set this way for each individual voltage recording to account for differences in gain settings and/or baseline noise levels. Fictive locomotor bursts were detected, grouped into episodes, and the burst and episode properties (duration, frequency, and interburst or inter-episode intervals) for each voltage trace were determined as described previously (Masino and Fetcho, 2005). Values for episode duration are expressed as mean ± SD.

Transections of the nervous system. Transections at various levels of the nervous system were made with a fine razorblade (FA-10 Feather S; Ted Pella) held with a blade breaker and holder (10053-09; Fine Science Tools). Larvae were anesthetized and prepared for electrophysiological recordings as described above. Spinalized preparations were generated in both WT and Tg(*otpb.A:nfsB–egfp*)^{zc77} larvae between 4 and 7 dpf by transecting the nervous system between body segments 3 and 4, just caudal to the hindbrain–spinal cord junction (between body segments 2 and 3). Spinalization completely separated the brain from the spinal cord, ensuring that all descending inputs to the transected spinal cord were eliminated.

To target mid-diencephalic and caudal-diencephalic transections, Tg(*otpb.A:nfsB–egfp*)^{zc77} larvae between 4 and 7 dpf were used to visualize egfp^{+} *otpb* cell populations using an epifluorescent stereoscope (MZ16FA;

Leica). Following preparation for electrophysiological recordings as described above, larvae were reoriented dorsoventrally to visualize egfp^{+}*otpb* populations. Mid-diencephalic transections were made between rostral, non-DAergic and caudal, DAergic diencephalic *otpb* populations. Caudal diencephalic transections were made just posterior to the caudal DAergic diencephalic *otpb* population. Confirmation of successful transections was visually verified by the presence of only the egfp^{+} DAergic *otpb* population in mid-diencephalic-transected (MDT) preparations and the absence of all egfp^{+} *otpb* populations in caudal-diencephalic-transected (CDT) preparations.

Statistical analyses. Statistical analyses were performed with SigmaPlot 11.0 (Systat Software). Data were analyzed using Student's *t* tests (two conditions only), one-way ANOVAs (more than two conditions), or two-way ANOVAs [first factor: condition (either age or drug exposure) assayed by two different locomotor outputs (second factor: free swimming or fictive swimming)]. These statistical tests accounted for repeated measures when appropriate, namely when comparisons incorporated intra-animal baseline and postdrug datasets. For ANOVAs, *post hoc* (Holm–Sidak) pairwise multiple comparisons were performed to identify which groups were significantly different from one another. Significance was established using an α criterion of $p = 0.05$. In the figures, $*p < 0.05$, $**p < 0.01$, and $***p < 0.001$, respectively. In the text, reported sample sizes

denote the number of fish for each experimental group, which is also indicated by the numbers at the base of the bars in bar graphs within the figures.

Results

Behavioral and fictive correspondence in developmental switch of locomotor pattern

The developmental switch in the locomotor pattern from long to short swimming episodes has been demonstrated via peripheral nerve recordings in paralyzed larvae (Thirumalai and Cline, 2008), which is termed a fictive preparation. However, this switch has been characterized (Buss and Drapeau, 2001) but not quantified in free-swimming larvae. To this aim, we adapted open-source software, Ctrax (Branson et al., 2009), to individually track multiple zebrafish larvae in a group setting (Fig 1*A*). This high-throughput tracking algorithm allows for the assessment of a suite of behavioral classifications that include an array of locomotor parameters (Branson et al., 2009). We focused on two behavioral locomotor parameters for each individual larva: (1) total distance traveled (centimeters in 10 min), obtained from the sum of instantaneous speeds during swimming episodes divided by the frame rate (Fig 1*B*), to assess the amount of free-swimming activity (Fig 1*B*); and (2) mean swimming episode duration (milliseconds), obtained as the mean duration from the onset to offset of each swimming episode (Fig 1*C*, expansion of 5 s from * in *B*) across all identified swimming episodes (see Materials and Methods) in the speed function (Fig 1*B*), to assess the locomotor pattern during free-swimming activity (Fig 1*C*). The goal

of these behavioral assessments was to compare the developmental switch in the free-swimming episodic locomotor pattern (Buss and Drapeau, 2001) to that of neural activity during fictive swimming.

Free-swimming larvae at 3 dpf traveled significantly less distance (4.7 ± 11 cm, n = 210) than did 4 dpf larvae (38 ± 42 cm,n = 170; $t_{(378)} = -11.2$, $p < 0.001$). In terms of the locomotor pattern, we found a correspondence between behavioral (Beh) (Fig 1*C*) and fictive (Fic) (Fig 1*D*) episode durations in the developmental switch from long to short swimming episodes between 3 dpf (Beh, 1014 ± 684 ms, n = 56; Fic, 987 ± 364 ms, n = 10) and 4 dpf (Beh, 248 ± 59 ms, n = 120; Fic, 241 ± 57 ms, n = 11). A two-way ANOVA revealed a significant effect of age ($F_{(1,193)} = 74$, $p < 0.001$) but not preparation type (Beh vs Fic, $F_{(1,193)} = 0.03$, $p = 0.85$) (Fig 1*E*). This behavioral and fictive correspondence suggests that the difference in the episodic locomotor pattern between 3 and 4 dpf is attributable to an intrinsic development of the nervous system rather than a byproduct of extrinsic behavioral factors, which are not present in the fictive preparation.

The developmental switch from long to short swimming episodes did not begin over the time course of our recording sessions (9:00 A.M. to 6:00 P.M.) at 3 dpf, because the immature behavioral phenotype of long episode durations remained unchanged ($t_{(21)} = 0.78$, $p = 0.45$) from the morning (9:00 A.M. to 11:00 A.M.,

1228 ± 893 ms, *n* = 11) to early evening (4:00 P.M. to 6:00 P.M., 1024 ± 315 ms, *n* = 12). Strikingly, the switch occurred by the morning at 4 dpf, because the short episode durations at this time were not significantly different from those at the end of the recording day at 4 dpf (9:00 A.M. to 11:00 A.M., 270 ± 59 ms, *n* = 24; 4:00 P.M. to 6:00 P.M., 255 ± 55 ms, *n* = 30; $t_{(52)}$ = 0.97, *p* = 0.34). These data demonstrate that the developmental switch in the episodic locomotor pattern is rapid, occurring at some time window between the late evening at 3 dpf and the early morning at 4 dpf.

Blocking endogenous D_4R signaling prevents maturation of the locomotor pattern

To initially investigate whether the DDT is involved in conferring the mature episodic locomotor pattern, we tested the hypothesis that endogenous DAergic signaling is required to initiate the developmental switch to short swimming episodes. We systemically incubated larvae in specific DAR antagonists (D_1R, SCH-23390; D_2/D_3R, raclopride; D_4R, L-745,870) before and during the natural timing of the switch (3–4 dpf) and assessed resultant behavioral and fictive locomotor patterns at 4 dpf (Fig 2*A*). All DAR antagonists were administered at 10 μM, informed by initial concentration–response experiments (data not shown), in the presence of 0.1% DMSO to facilitate drug delivery (Rihel et al., 2010).

The DAR antagonists differentially affected the total distance traveled by 4 dpf larvae (one-way ANOVA; $F_{(3,256)} = 6.85$, $p < 0.001$) (Fig 2*B1*,*B2*). Compared with DMSO vehicles (38 ± 41 cm, $n = 60$), there was no change in the total distance traveled by blocking D_2/D_3Rs (37 ± 31 cm, $n = 70$; $p = 0.79$) (Fig 2*B1*,*B2*). Conversely, blocking either D_1Rs or D_4Rs reduced the total distanced traveled (D_1R, 24 ± 30 cm, $n = 60$, $p < 0.05$; D_4R, 17 ± 26 cm, $n = 70$, $p < 0.001$) (Fig 2*B1*,*B2*); note that both groups traveled significantly more than untreated 3 dpf larvae (D_1R, $p < 0.001$; D_4R, $p < 0.001$). This demonstrates that endogenous D_1R and D_4R signaling contribute to increased locomotion at 4 dpf but that other contributions, such as from serotonergic signaling (Brustein et al., 2003), likely contribute to the differences in the amount of free-swimming of 3 and 4 dpf larvae.

A two-way ANOVA revealed a significant effect on episode durations of 4 dpf larvae for DAR antagonist incubations ($F_{(3,216)} = 40$, $p < 0.001$) but not preparation type (Beh vs Fic, $F_{(3,216)} = 1.30$, $p = 0.26$) (Fig 2*C1*,*C2*). The episode durations produced by larvae incubated in D_1R antagonists (Beh, 470 ± 249 ms, $n = 43$; Fic, 348 ± 134 ms, $n = 8$) or D_2/D_3R antagonists (Beh, 298 ± 104 ms, $n = 62$; Fic, 268 ± 108 ms, $n = 7$) were not significantly different from DMSO vehicles (Beh, 253 ± 52 ms, $n = 44$; Fic, 264 ± 67 ms, $n = 7$; $p = 0.11$ and $p = 0.79$, respectively) (Fig 2*C1*,*C2*). In contrast, larvae incubated in D_4R antagonists produced significantly longer episode durations (Beh, 1199 ± 657 ms, $n = 52$; Fic,

1043 ± 294 ms, n = 8) than DMSO vehicles ($p < 0.001$) (Fig 2*C1*,*C2*). Moreover, the D_4R antagonist prevented the maturation of the locomotor pattern, because the induced long episode durations were indistinguishable ($p = 0.47$) from that of 3 dpf larvae (Fig 2*C2*). These results suggest that endogenous D_4R signaling mediates the advent of short swimming episodes.

Blocking endogenous D_4R signaling reverts the mature locomotor pattern to an immature pattern

We next examined whether endogenous D_4R signaling is required not only to initiate but also to maintain the mature locomotor pattern. To test this hypothesis, we systemically incubated larvae in specific DAR antagonists subsequent to the developmental switch (4–5 dpf) (Fig 3*A*), such that larvae were already exhibiting increased locomotion in the form of short and directed swimming episodes. Resultant behavioral and fictive locomotor patterns were assessed at 5 dpf (Fig 3*A*).

The DAR antagonists differentially affected the total distance traveled by 5 dpf larvae (one-way ANOVA, $F_{(3,246)} = 20$; $p < 0.001$) (Fig 3*B1*,*B2*). Compared with DMSO vehicles (36 ± 18 cm, n = 60), blocking D_2/D_3Rs after the switch increased the total distanced traveled (54 ± 27 cm, n = 60; $p < 0.001$) (Fig 3*B1*,*B2*), which was not observed when administered before the switch (Fig 2*B1*,*B2*).

Conversely, blocking either D_1Rs or D_4Rs reduced the total distanced traveled (D_1R, 26 ± 27 cm,n = 60, p < 0.05; D_4R, 24 ± 23 cm, n = 70, p < 0.01) (Fig 3*B1*,*B2*), similar to when the antagonists were given before the switch (Fig 2*B1*,*B2*). These data suggest that, at 5 dpf, endogenous D_1R and D_4R signaling contribute to increased locomotion, whereas endogenous D_2/D_3R signaling suppresses the initiation of locomotion.

A two-way ANOVA revealed an effect on episode durations of 5 dpf larvae for DAR antagonist incubations ($F_{(3,246)}$ = 31, p< 0.001) but not preparation type (Beh vs Fic, $F_{(3,246)}$ = 0.65, p = 0.42) (Fig 3*C1*,*C2*). The episode durations produced by larvae incubated in D_1R antagonists (Beh, 357 ± 286 ms, n = 46; Fic, 383 ± 256 ms, n = 7) or D_2/D_3R antagonists (Beh, 253 ± 114 ms, n = 59; Fic, 261 ± 57 ms, n = 7) were not significantly different from DMSO vehicles (Beh, 234 ± 60 ms, n = 59; Fic, 245 ± 53 ms, n = 6; p = 0.14 and p = 0.84, respectively) (Fig 3*C1*,*C2*). Conversely, larvae incubated in D_4R antagonists produced significantly longer episode durations (Beh, 871 ± 492 ms, n = 64; Fic, 1022 ± 493 ms, n = 7) than DMSO vehicles (p < 0.001) (Fig 3*C1*,*C2*). Moreover, the D_4R antagonist reversed the developmental switch in the locomotor pattern, relegating 5 dpf larvae to long episode durations that were not significantly different from that of 3 dpf larvae (p = 0.72) (Fig 3*C2*). These results demonstrate that D_4R signaling is necessary to maintain the mature locomotor pattern of short swimming episodes at 5 dpf.

D_4R signaling in the spinal cord is sufficient to induce the mature locomotor pattern of short swimming episodes

Having elucidated that systemic block of D_4R signaling can both prevent (Fig 2) and reverse (Fig 3) the developmental switch in the locomotor pattern, we next investigated whether the anatomical site of action is in the spinal cord. To test this, we compared the fictive locomotor pattern of intact animals at 4–7 dpf compared with those that were spinalized, in which the spinal cord was isolated from the brain to remove all descending inputs, including the DDT. Because fictive swimming in spinalized preparations does not occur spontaneously but can be elicited with NMDA (McDearmid and Drapeau, 2006), we added NMDA (50 μM) to induce fictive locomotor output and subsequently tested the effects of exogenous application of DAergic agonists. To more directly compare intact and spinalized fictive swimming, we assessed NMDA-induced, in addition to spontaneous, fictive swimming in intact animals.

There was a significant difference in episode durations among the experimental groups ($F_{(3,65)}$ = 23, p < 0.001). In intact preparations, episode durations were not significantly different (p = 0.61) between spontaneous (241 ± 57 ms, n = 11) and NMDA-induced (300 ± 186 ms, n = 21) fictive swimming (Fig 4*A*,*B*). Conversely, significantly longer episode durations were produced by spinalized preparations

(1871 ± 1285 ms, n = 30; p < 0.001) (Fig 4*A*,*B*), reminiscent of the immature locomotor pattern of intact 3 dpf larvae (Fig 1*D*,*E*). This demonstrates that some descending input from the brain is required to confer short NMDA-induced swimming episodes. Next, we tested whether supplying exogenous DA to the putatively DA-deprived transected spinal cord could sculpt NMDA-induced locomotor activity to better resemble that of the intact animal. Application of exogenous DA (1 μM) to spinalized preparations significantly shortened NMDA-induced episode durations (601 ± 251 ms, n = 7) when compared with NMDA application alone (p < 0.001) (Fig 4*A*,*B*). This result demonstrates that DA can act directly in the spinal cord to shorten fictive swimming episodes.

To determine whether DA acts via excitatory (D_1-like: D_1R, D_5R) or inhibitory (D_2-like: D_2R, D_3R, D_4R) DARs in the spinal cord to shorten NMDA-induced fictive episode durations, DAR-specific agonists (D_1-like, SKF-38393; D_2-like, quinpirole; or D_4R, PD168077) were applied to spinalized preparations of 4–7 dpf larvae. There was a significant difference among the pharmacological treatments ($F_{(4,55)}$ = 8.4, p < 0.001). Compared with NMDA alone, the D_1-like agonist (1 μM) had no effect on episode duration (1999 ± 750 ms, n = 7; p = 0.34), whereas the D_2-like agonist (1 μM) significantly shortened episode durations (475 ± 183 ms, n = 7; p < 0.001) (Fig 5*A*,*B*), similar to exogenous DA (Fig 5*B*). Moreover, application of a specific D_4R agonist (1 μM) was sufficient to significantly shorten episode durations (598 ± 234 ms, n = 9; p < 0.001) (Fig 5*A*,*B*), similar to that of

exogenous DA and the broad-spectrum D_2-like agonist (Fig 5*B*). This result demonstrates that D_4R signaling in the spinal cord is sufficient to shorten fictive episodes.

Selective chemogenetic ablation of *otpb* neurons

The evidence that DAergic signaling in the spinal cord is sufficient to shorten fictive swimming episodes (Fig 4, 5) suggests a critical role for *otp* neurons in sculpting the mature episodic locomotor pattern, because *otp* neurons provide the exclusive source of spinal DA (Kastenhuber et al., 2010; Tay et al., 2011). To explore this possibility, we used a transgenic line that drives expression in DAergic *otpb* neurons in the caudal ventral diencephalon, which coexpresses TH and *dat* and forms part of the DDT (Fujimoto et al., 2011). In addition, this transgenic line drives expression in a non-DAergic neurosecretory *otpb* population in the rostral diencephalon (Fujimoto et al., 2011). To test the hypothesis that *otpb* cells contribute to conferring the mature episodic locomotor pattern, we performed selective, cell-autonomous chemogenetic ablation of *otpb* cells in Tg(*otpb.A:nfsB–egfp*)^{zc77} larvae via the Ntr:Mtz system (Curado et al., 2008; Pisharath and Parsons, 2009).

Application of Mtz to the aqueous environment from 1 to 4 dpf (Fig 6*A*) induced selective cell death of *otpb* neurons in Tg(*otpb.A:nfsB–egfp*)^{zc77} larvae (Fig

6*B*,*C*). A marked increase of TUNEL staining in Mtz-treated Ntr^+ larvae (Ntr^+/Mtz^+) was observed when compared with untreated Ntr^+ siblings (Ntr^+/Mtz^-) or Mtz-treated WT larvae (WT/Mtz^+) (Fig 6*B*). Moreover, the increased TUNEL staining in Ntr^+/Mtz^+ larvae colocalized to both rostral non-DAergic and caudal DAergic diencephalic GFP^+ populations (Fig 6*C*). By 3 dpf, WT/Mtz^+ and Ntr^+/Mtz^- larvae showed robust *dat* mRNA expression in the ventral diencephalon (Fig 6*D*), which colocalizes with the DAergic *otpb* population (Fujimoto et al., 2011). Conversely, there was a marked absence of *dat* mRNA expression in the ventral diencephalon of Ntr^+/Mtz^+ larvae (Fig 6*D*), coincident spatially with the Ntr^+/Mtz^+ induced TUNEL staining (Fig 6*B*, arrows in right). This indicates an Ntr^+/Mtz^+-mediated loss of putatively functional DAergic *otpb* cells in the ventral diencephalon. Additionally, by 7 dpf, there was an absence of GFP^+cells in Ntr^+/Mtz^+ larvae when compared with Ntr^+/Mtz^- siblings (Fig 6*E*, left column), suggesting an Mtz-mediated loss of Ntr^+ cells. Many of the GFP^+ cells in the ventral diencephalon of Ntr^+/Mtz^- siblings colocalize with TH^+ cells in the ventral diencephalon (Fig 6*E*, top right), which suggests that Mtz treatment induced a loss of double-labeled TH^+ and Ntr^+ (GFP^+)*otpb* DAergic cells (Fig 6*E*). To determine the efficacy of Ntr^+/Mtz^+ mediated ablation of DAergic *otpb* cells, we counted the number of cells in the diencephalon that expressed both TH and GFP, in Ntr^+/Mtz^- compared with Ntr^+/Mtz^+ larvae. At 7dpf, Ntr^+/Mtz^- larvae had 26 ± 3 TH^+/GFP^+ DAergic *otpb* cells, which was significantly reduced to 3 ± 0.9 TH^+/GFP^+DAergic *otpb* cells in Ntr^+/Mtz^+ larvae ($p < 0.0001$; $n = 11$ larvae per

group; mean ± SEM). Together, these results demonstrate that the Mtz regimen was effective in selectively ablating *otpb* Ntr^+ cells in Tg(*otpb.A:nfsB–egfp*)^{zc77} larvae.

Loss of *otpb* neurons prevents maturation of the locomotor pattern

To test whether *otpb* neurons contribute to the developmental switch to the mature episodic locomotor pattern, we assessed the effect of ablating *otpb* neurons on the behavioral and fictive locomotor patterns at 5 dpf (Fig 7*A*). There was a significant difference in the total distance traveled among the experimental groups ($F_{(3,206)}$ = 15, $p < 0.001$). There were no significant differences among the total distance traveled by Ntr^-/Mtz^- (39 ± 32 cm, n = 50), Ntr^-/Mtz^+ (40 ± 32 cm, n = 40) and Ntr^+/Mtz^- (42 ± 25 cm, n = 50) larvae ($p > 0.76$ for all pairwise comparisons) (Fig 7*B1*,*B2*). Conversely, selective chemogenetic ablation of *otpb* cells in Ntr^+/Mtz^+ larvae significantly reduced the total distance traveled (14 ± 13 cm, n = 60) compared with all other groups ($p < 0.001$) (Fig 7*B1*,*B2*). In terms of the locomotor pattern, a two-way ANOVA revealed an effect on episode duration for treatment condition ($F_{(3,211)}$ = 15, $p < 0.001$) but not preparation type (Beh vs Fic, $F_{(3,211)}$ = 1.49, p = 0.22). The stage-appropriate expression of short episodes was observed in both behavioral and fictive preparations from Ntr^-/Mtz^- (Beh, 315 ± 82 ms, n = 47; Fic, 351 ± 112 ms, n = 7), Ntr^-/Mtz^+ (Beh, 317 ± 124 ms, n = 37; Fic, 379 ± 116 ms, n = 7) and

Ntr^+/Mtz^- (Beh, 298 ± 212 ms, *n* = 50; Fic, 349 ± 186 ms, *n* = 7) larvae (*p* > 0.75 for all pairwise comparisons) (Fig 7*C1*,*C2*). Conversely, a significant increase in the durations of behavioral and fictive episodes was observed in Ntr^+/Mtz^+ larvae (Beh, 738 ± 697 ms, *n* = 56; Fic, 897 ± 311 ms, *n* = 12) compared with all other groups (*p*< 0.001) (Fig 7*C1*,*C2*). These results indicate that *otpb* cells contribute to the mature locomotor pattern of short episodes because their specific ablation perpetuates long episodes in 5 dpf larvae.

Removal of the caudal diencephalon reverts the mature locomotor pattern to an immature pattern that is rescued by D_4R agonism

Specific chemogenetic ablation of *otpb* cells included the rostral non-DAergic and caudal DAergic *otpb* populations. To determine the relative contributions of DAergic and non-DAergic $otpb^+$ cells to the generation of short episodes, Tg(*otpb.A:nfsB–egfp*)^{zc77} larvae at 4–7 dpf were used to produce reduced preparations in which the nervous system was transected either just rostral to or just caudal to the DAergic *otpb* population. Mid-diencephalic-transected (MDT) (Fig 8*A*) preparations lack non-DAergic *otpb* cells and the ascending projections from DAergic *otpb* cells but retain DAergic *otpb* somata and their descending projections (i.e., including the DDT). Caudal-diencephalic-transected (CDT) (Fig 8*A*) preparations lack both DAergic and non-DAergic *otpb* neurons but retain

midbrain and hindbrain structures. The consequences of these transections were examined by measuring episode durations in fictive preparations.

Intact, MDT and CDT preparations exhibited spontaneous fictive swimming, but spinalized preparations did not (Fig 8*B*). Spontaneous episode durations were significantly different among the intact, MDT, and CDT groups ($F_{(2,23)} = 41$, $p < 0.001$). MDT preparations, which retain the DAergic *otpb* population and the DDT, produced short spontaneous episode durations (320 ± 187 ms, $n = 8$) that were not significantly different from intact larvae (333 ± 211 ms, $n = 8$; $p = 0.91$) (Fig 8*B*,*D*). CDT preparations, which lack DAergic *otpb* neurons, produced significantly longer spontaneous episode durations (1105 ± 231 ms, $n = 10$; $p < 0.001$) (Fig 8*B*,*D*) that were not significantly different ($p = 0.40$) from the episodes observed in 3 dpf WT larvae (Fig 1*D*). These results demonstrate that neither the non-DAergic *otpb* population nor the ascending projections of the DAergic *otpb* population are necessary for the generation of short spontaneous episodes. Only the caudal diencephalic region, in which DAergic *otpb* neurons reside, is necessary for the production of short spontaneous episodes.

Next, we tested the hypothesis that D_4R agonism would shorten the long episodes of CDT preparations to stage-appropriate short episodes and that this would be recapitulated at the level of the spinal cord via spinalized preparations. Because spinalized preparations do not exhibit spontaneous fictive swimming

(Fig 8*B*), we compared NMDA-induced locomotor activity from intact, MDT, CDT, and spinalized preparations in Tg(*otpb.A:nfsB–egfp*)^{zc77} larvae (Fig 8*C*). There was a significant difference in the NMDA-induced episode durations among these preparations ($F_{(5,36)}$ = 9.18, $p < 0.001$). The short NMDA-induced episode durations of intact (317 ± 250 ms, n = 4) and MDT (379 ± 172 ms, n = 7) preparations were not significantly different from one another (p = 0.82) or when compared with spontaneous episode durations of intact and MDT preparations (p = 0.91 and p = 0.53, respectively) (Fig 8*C*,*D*). Conversely, the duration of the NMDA-induced episodes generated by CDT (1355 ± 432 ms, n = 12) and spinalized (1310 ± 830 ms, n = 7) preparations were significantly longer ($p <$ 0.001 and $p < 0.001$, respectively) when compared with intact or MDT preparations (Fig 8*C*,*D*). However, the long NMDA-induced episodes of CDT and spinalized preparations were not significantly different from one another (p = 0.85) or when compared with spontaneous episodes of CDT preparations (p = 0.11 and p = 0.47, respectively) (Fig 8*D*). Subsequent to NMDA-induced locomotor activation, the D_4R agonist was exogenously applied and episode durations were measured in CDT and spinalized preparations (Fig 8*C*,*D*). A change in the locomotor pattern from long to short episode durations was observed in both preparations (CDT, 533 ± 172 ms, n = 6, $p < 0.001$; spinalized, 458 ± 117 ms, n = 5, $p < 0.001$). This result demonstrates that, in the absence of the caudal diencephalon, D_4R agonism is sufficient to produce short episodes

and suggests that the DAergic *otpb* population is the critical caudal diencephalic component for conferring the mature episodic locomotor pattern.

Discussion

We explored the function of the evolutionarily conserved vertebrate DDT and found that it mediates the progression of locomotor development in zebrafish larvae. The developmental switch to the mature episodic locomotor pattern requires spinal D_4R signaling that is driven by DAergic *otpb* cells comprising the DDT. Loss of DAergic input before the developmental switch led to a maintained immature locomotor pattern. Furthermore, continued DAergic input is necessary, because loss of D_4R signaling after the developmental switch led to a reversion to the immature pattern. Our findings demonstrate a tonic requirement for central sources of DAergic signaling that act in the spinal cord, with implications for understanding the normal development of locomotion in vertebrates or effects from disease states.

Behavioral and fictive correspondence in the locomotor pattern

Although a myriad of behavioral studies in zebrafish larvae have assayed the amount of free-swimming activity under an array of paradigms (for review, see (Tierney, 2011), only a few have assessed the actual locomotor pattern of swimming episodes during free-swimming (Fuiman and Webb, 1988; Muller et al., 2000; Buss and Drapeau, 2001). Of these, only Buss and Drapeau (2001) quantitatively compared free-swimming and fictive locomotor patterns and did so

just at 4 dpf, reporting a free-swimming and fictive correspondence that our study corroborates. Expanding on this, we found a strong correspondence between free-swimming and fictive locomotor patterns in the developmental switch from long to short swimming episodes between 3 and 4 dpf (Fig 1). Furthermore, there was correspondence between the altered free-swimming and fictive locomotor patterns resulting from blocking specific DARs (Fig 2, 3) or from chemogenetic ablation of *otpb* cells (Fig 7). Interestingly, behavioral and morphological factors in the free-swimming assay that could plausibly influence the locomotor pattern are not present in the immobilized fictive preparation. These factors include the following: (1) group interactions, because our assay tracked multiple larvae in the same arena; and (2) the absence or presence of an inflated swim bladder, which dramatically affect buoyancy and resultant free-swimming trajectories (Lindsey et al., 2010). Hence, the strong correspondence between the free-swimming and fictive locomotor patterns under all of our experimental conditions demonstrates that behavioral and morphological factors are not responsible for the developmental switch from the immature to mature episodic locomotor pattern, suggesting that the mechanisms underlying this switch are intrinsic to the nervous system.

Role for spinal D_4R signaling in sculpting mature locomotor pattern

We found that specifically D_4R signaling in the spinal cord is required for the advent and maintenance of the mature episodic locomotor pattern. Conversely, we demonstrate that all DAR subtypes play a role in influencing the amount of free-swimming activity. The specific DAR antagonists that we administered elicited unique locomotor phenotypes (Fig 2, 3), indicating that each drug concentration was sufficient to differentially modulate behavior. The D_4R antagonist group was hypoactive, which is consistent with other studies (Giacomini et al., 2006; Boehmler et al., 2007), and exhibited the immature pattern of long swimming episodes. The D_1R antagonist group was also hypoactive whereas the D_2/D_3R antagonist group was hyperactive, which is consistent with evidence for such opposing roles of these receptors (Souza et al., 2011), yet both of these groups exhibited the mature pattern of short swimming episodes. Therefore, we demonstrate that the amount of swimming activity is separable from the locomotor pattern during swimming activity, suggesting that non-overlapping neural mechanisms exist for these two phenomena. This interpretation is supported by evidence that, at 3 dpf, DAergic signaling in the brain influences the amount of swimming activity but not the locomotor pattern (Thirumalai and Cline, 2008), which also suggests that our results of systemic DAR-mediated changes in the amount of swimming activity may be attributable to blocking DARs in the brain.

We elucidated that the site of action of systemic D_4R-mediated changes in the locomotor pattern is likely in the spinal cord, because spinalization of 4–7 dpf larvae reverted the fictive locomotor pattern to immature-like long swimming episodes (Fig 4) that were transformed to mature-like short episodes via spinal D_4R agonism (Fig 5). The ability of D_4R antagonism to both prevent and reverse the developmental switch in the locomotor pattern suggests that the D_4R-dependent expression of short swimming episodes is not attributable to D_4R signaling simply providing a transient role in transforming neural circuit function. Rather, it indicates a requirement for ongoing D_4R-mediated maintenance of the swimming pattern, possibly in the form of providing neuromodulatory tone (Hauber, 2010) to spinal locomotor circuits.

Our functional evidence for spinal D_4R signaling is supported by previous *in situ* hybridization studies of DAR mRNA expression patterns and suggests a distinctive functional role for a specific D_4R subtype. Among D_2-like DARs, three D_2Rs (drd2a,b,c), one D_3R (drd3), and three D_4Rs (drd4a,b,c) have been identified in zebrafish larvae. Interestingly, all of these DAR mRNAs are expressed in the zebrafish spinal cord by 2 dpf (Boehmler et al., 2004; 2007) except drd4b, which is present at 5 dpf (Boehmler et al., 2007). Because these studies did not examine expression patterns at 3 and 4 dpf, it is possible that the advent of spinal drd4b expression correlates with, and may underlie, the developmental switch in the locomotor pattern between 3 and 4 dpf.

Role for DAergic *otpb* population, via the DDT, in driving spinal D_4R-mediated sculpting of mature locomotor pattern

Among the diencephalic DAergic populations in zebrafish (DC1–DC6), the *otp* populations comprise four of the six (DC2, DC4, DC5, and DC6) (Kastenhuber et al., 2010). Of these *otpb* populations, three of four (DC2, DC4, and DC5) exclusively comprise the DDT (Tay et al., 2011), and we hypothesized that some or all of these populations were involved in the spinal DAergic-mediated shortening of swimming episodes because the DDT provides the exclusive source of DA to the spinal cord (Kastenhuber et al., 2010). Because the Tg(*otpb.A:nfsB–egfp*)^{zc77} line that we used (Fig 6–8) drives expression in the majority of DC4, DC5, and DC6 populations (Fujimoto et al., 2011), we were able to selectively chemogenetically ablate two of the three (DC4 and DC5) *otp* neuronal populations that comprise the DDT. Because this chemogenetic ablation was sufficient to perpetuate the immature locomotor pattern, it suggests that DC4 and/or DC5 DAergic *otpb* populations are necessary for the developmental switch to short swimming episodes.

Conversely, we demonstrated that the non-DAergic *otpb* population is not necessary to confer the mature episodic locomotor pattern, which persisted after removal of these cells by way of mid-diencephalic transections (Fig 8).

Importantly, this transection also removed the majority of DAergic non-*otpb* populations, including a robust local subpallial DAergic system (Tay et al., 2011), as well as ascending subpallial projections of the DAergic *otpb* population (Tay et al., 2011), suggesting that these components are also not necessary for the expression of the mature episodic locomotor pattern. Removal of the DAergic *otpb* population by transecting at the caudal diencephalon reestablished the immature locomotor pattern (Fig 8), demonstrating that the caudal diencephalon, which distinguishes MDT from CDT preparations, plays a role in conferring the expression of the mature locomotor pattern. Because the hindbrain remains intact in CDT preparations and these larvae are unable to maintain short swimming episodes, it suggests that serotonergic and noradrenergic projections into the spinal cord, which exclusively originate in the hindbrain (McLean and Fetcho, 2004a; Kastenhuber et al., 2010), are not sufficient for or do not contribute to the mature pattern of short swimming episodes. This interpretation is consistent with a previous study that showed that serotonin reduces the quiescent periods between swimming episodes but does not influence the active properties of swimming episodes themselves, including episode duration (Brustein et al., 2003). Although the literature is lacking on any role for noradrenaline on the pattern of swimming episodes, the number of noradrenergic axonal projections to the spinal cord of zebrafish larvae is markedly small compared with that of DAergic axonal projections via the DDT, as demonstrated

by an essentially unaffected descending catecholaminergic tract after genetic knockdown of the noradrenaline system (Kastenhuber et al., 2010).

Although many cell populations and fibers of passage are contained within the caudal diencephalon, the physical removal of this region resulted in a similar locomotor phenotype as that induced from selective chemogenetic ablation of *otpb* cells, suggesting that DAergic *otpb* cells are the critical caudal diencephalic component. Consistent with this conclusion, in the absence of the caudal diencephalon, the reestablished immature locomotor pattern was rescued to a mature-like pattern via D_4R agonism (Fig 8). Moreover, the equitable efficacy of D_4R agonism to rescue the locomotor pattern in CDT and spinalized preparations (Fig 8) indicates the sufficiency of spinal D_4R signaling to confer the mature episodic locomotor pattern. This provides additional credence to the conclusion that caudal diencephalic DAergic *otpb* cells comprising the DDT act on D_4Rs in the spinal cord, rather than the brain, to confer the mature episodic locomotor pattern.

Conserved functional role of the vertebrate DDT

This study is the first to elucidate the role of the DDT in a developing vertebrate *in vivo*. The conserved transcriptional identity (Ryu et al., 2007), somatic location, morphology, and projection pattern (Takada et al., 1988; Tay et

al., 2011) of the DAergic *otp* population and DDT suggest that it has a conserved locomotor function across vertebrates. In support of this rationale in developing mammals, all DAR mRNAs are expressed across the dorsoventral axis of the neonatal mouse spinal cord and specifically in motor neurons (Zhu et al., 2007), which are modulated by DA during fictive locomotion *in vitro* as early as postnatal day 2 (P2) (Han et al., 2007). Moreover, before neonatal rodents can support their body weight to start walking, they are capable of coordinated locomotion in the form of L-DOPA-induced air-stepping that is dependent on DAR signaling (Sickles et al., 1992; McCrea et al., 1997). Spinalized *in vitro* preparations have demonstrated that this DAR signaling acts at the level of the spinal cord (McEwen et al., 1997). This early DAR-dependent signaling in the spinal cord may play a developmental role, since L-DOPA-induced air-stepping develops from being bipedal, at P0, to quadrupedal, by P5 (Van Hartesveldt et al., 1991). In disease states, for example, hypoxic–ischemic injury to the developing brain, DAergic cell populations are at risk and may contribute to the impaired motor development after these injuries (Bax et al., 2006). Hence, the evolutionarily conserved anatomical, genetic, and *in vitro* evidence suggests that, similar to our findings in zebrafish, the mammalian DDT may also contribute to locomotor development.

Figure Legends

Figure 1. Behavioral and fictive correspondence in developmental switch of locomotor pattern. ***A–E***, Comparison of behavioral (***A–C***) and fictive (***D***) swimming patterns between 3 dpf (left column) and 4 dpf (right column). ***A***, Free-swimming trajectory plots. Top row, Group trajectories from 10 larvae in the same 50 mm arena. Bottom row, Unique trajectory of an individual larva from the group trajectory above. ***B***, Speed function for an individual larva over the course of the 10 min record, from which total distance traveled and swimming episode durations were calculated. ***C***, Expansion of 5 s from * in ***B*** to show the locomotor pattern of discrete swimming episodes. Gray regions below *x*-axis represent episode durations detected from filter settings (see Materials and Methods). ***D***, Voltage traces of fictive swimming from extracellular peripheral nerve recordings. ***E***, Mean behavioral (light gray bars) and fictive (dark gray bars) swimming episode durations (milliseconds) at 3 and 4 dpf. Numbers at the base of bars in bar graph denote the sample sizes of fish for each experimental group. ***$p < 0.001$.

Figure 2. Blocking endogenous D_4R signaling prevents maturation of the locomotor pattern. ***A***, Timeline of experimental paradigm, in which larvae are incubated in DAR antagonists at 3 dpf, and behavioral and fictive locomotor patterns are assessed at 4 dpf.***B1***, Representative trajectory plot of an individual

larva (from a group of 10 larvae in the same arena) over 10 min, depicting total activity per individual for each experimental group (DMSO, D_1 antagonist, D_2/D_3 antagonist, D_4 antagonist). Labels for experimental groups also correspond to data in ***C1***. Circles surrounding trajectories denote the periphery of the 50-mm-diameter arena. ***B2***, Mean total distance traveled per individual (centimeters). ***C1***, Behavioral (top row) and fictive (bottom row) locomotor pattern of discrete swimming episodes. Top row, Speed function from individual in ***B1***. Gray regions below*x*-axis represent resultant episode durations detected from filter settings (see Materials and Methods). Bottom row, Voltage traces of fictive swimming from extracellular peripheral nerve recordings. ***C2***, Mean behavioral (lights gray bars) and fictive (dark gray bars) swimming episode durations (milliseconds) at 3 dpf and after pharmacological treatments at 4 dpf. Numbers at the base of bars in bar graphs denote the sample sizes of fish for each experimental group. *$p < 0.05$; ***$p < 0.001$.

Figure 3. Blocking endogenous D_4R signaling reverts the mature locomotor pattern to an immature pattern. ***A***, Timeline of experimental paradigm, in which larvae are incubated in DAR antagonists at 4 dpf, and resultant behavioral and fictive locomotor patterns are assessed at 5 dpf. ***B1***, Representative trajectory plot of an individual larva (from a group of 10 larvae in the same arena) over 10 min, depicting total activity per individual for each experimental group (DMSO, D_1 antagonist, D_2/D_3 antagonist, D_4 antagonist). Labels for experimental groups

also correspond to data in ***C1***. Circles surrounding trajectories denote the periphery of the 50-mm-diameter arena. ***B2***, Mean total distance traveled per individual (centimeters). ***C1***, Behavioral (top row) and fictive (bottom row) locomotor pattern of discrete swimming episodes. Top row, Speed function from individual in ***B1***. Gray regions below *x*-axis represent resultant episode durations detected from filter settings (see Materials and Methods). Bottom row, Voltage traces of fictive swimming from extracellular peripheral nerve recordings. ***C2***, Mean behavioral (lights gray bars) and fictive (dark gray bars) swimming episode durations (milliseconds) at 3 dpf, 4 dpf, and after pharmacological treatments at 5 dpf. Numbers at the base of bars in bar graphs denote the sample sizes of fish for each experimental group. *$p < 0.05$; **$p < 0.01$; ***$p < 0.001$.

Figure 4. DAergic signaling in the spinal cord is sufficient to induce the mature locomotor pattern of short swimming episodes. ***A***, Voltage traces of fictive swimming from extracellular peripheral nerve recordings from intact and spinalized preparations at 4–7 dpf. ***B***, Mean fictive swimming episode durations (milliseconds). Numbers at the base of bars in bar graph denote the sample sizes of fish for each experimental group. ***$p < 0.001$.

Figure 5. D_4R signaling in the spinal cord is sufficient to induce the mature locomotor pattern of short swimming episodes. ***A***, Voltage traces of fictive swimming from extracellular peripheral nerve recordings from spinalized

preparations at 4–7 dpf in NMDA alone (top traces) and NMDA + agonist (bottom traces). ***B***, Mean fictive swimming episode durations (milliseconds). Numbers at the base of bars in bar graph denote the sample sizes of fish for each experimental group. ****p* < 0.001.

Figure 6. Selective chemogenetic ablation of *otpb* neurons. ***A***, Timeline of experimental paradigm, in which larvae were incubated in 5 mMMtz from 24 to 48 hpf and 10 mM Mtz from 48 to 96 hpf; assessment of cell death was investigated from 1 to 7 dpf. ***B–E***, Ventral views in whole-mount Tg(*otpb.A:nfsB–egfp*)^{zc77} larvae; rostral is to the top. Scale bars, 50 μm. ***B***, TUNEL signal in confocal *z*-stacks; asterisk denotes region of rostral non-DAergic *otpb*$^{+}$ population, and arrows denote caudal DAergic *otpb*$^{+}$ population. ***C***, Confocal images showing colocalization of TUNEL signal and GFP in larvae treated with Mtz. First panel shows *z*-stack image; yellow box indicates caudal ventral diencephalon, which is magnified in subsequent panels as single confocal slices; arrow denotes a GFP^{+} and TUNEL stained cell. ***D***, Bright-field images of loss of *slc6a3* (*dat*) mRNA expression via *in situ* hybridization in whole-mount embryos. ***E***, Confocal *z*-stack images of double labeling for GFP and TH immunohistochemistry at 7 dpf.

Figure 7. Loss of *otpb* neurons prevents maturation of the locomotor pattern. ***A***, Timeline of experimental paradigm, in which *otpb*$^{+}$ cells are

chemogenetically ablated via Mtz treatment from 1 to 4 dpf in Tg(*otpb.A:nfsB–egfp*)^{zc77} larvae, and behavioral and fictive locomotor patterns are assessed at 5 dpf. ***B1***, Representative trajectory plot of an individual larva (from a group of 10 larvae in the same arena) over 10 min, depicting total activity per individual for each experimental group (Ntr^-/Mtz^-, Ntr^-/Mtz^+, Ntr^+/Mtz^-, Ntr^+/Mtz^+). Labels for experimental groups also correspond to data in ***C1***. Circles surrounding trajectories denote the periphery of the 50-mm-diameter arena. ***B2***, Mean total distance traveled per individual (centimeters). ***C1***, Behavioral (top row) and fictive (bottom row) locomotor pattern of discrete swimming episodes. Top row, Speed function from individual in ***B1***. Gray regions below *x*-axis represent resultant episode durations detected from filter settings (see Materials and Methods). Bottom row, Voltage traces of fictive swimming from extracellular peripheral nerve recordings. ***C2***, Mean behavioral (lights gray bars) and fictive (dark gray bars) swimming episode durations (milliseconds) at 5 dpf. Numbers at the base of bars in bar graphs denote the sample sizes of fish for each experimental group. ***$p < 0.001$.

Figure 8. Removal of the caudal diencephalon reverts the mature locomotor pattern to an immature pattern that is rescued by D_4R agonism. ***A***, Schematic of demarcated transections, denoted by dashed white lines, with respect to the rostral non-DAergic and caudal DAergic *otpb*$^+$ populations in Tg(*otpb.A:nfsB–egfp*)^{zc77}larvae. Repeated image is from a confocal *z*-stack

projection with a ventral view in whole-mount embryos; rostral is to the top.***B***, ***C***, Voltage traces from extracellular peripheral nerve recordings showing fictive swimming of 4–7 dpf larvae that is spontaneous in ***B*** and NMDA-induced in ***C***. ***D***, Mean fictive swimming episode durations (milliseconds) for spontaneous and NMDA-induced activity in intact, MDT, CDT, and spinalized-transected preparations. Numbers at the base of bars in bar graphs denote the sample sizes of fish for each experimental group. ***$p < 0.001$.

Figures

Figure 1

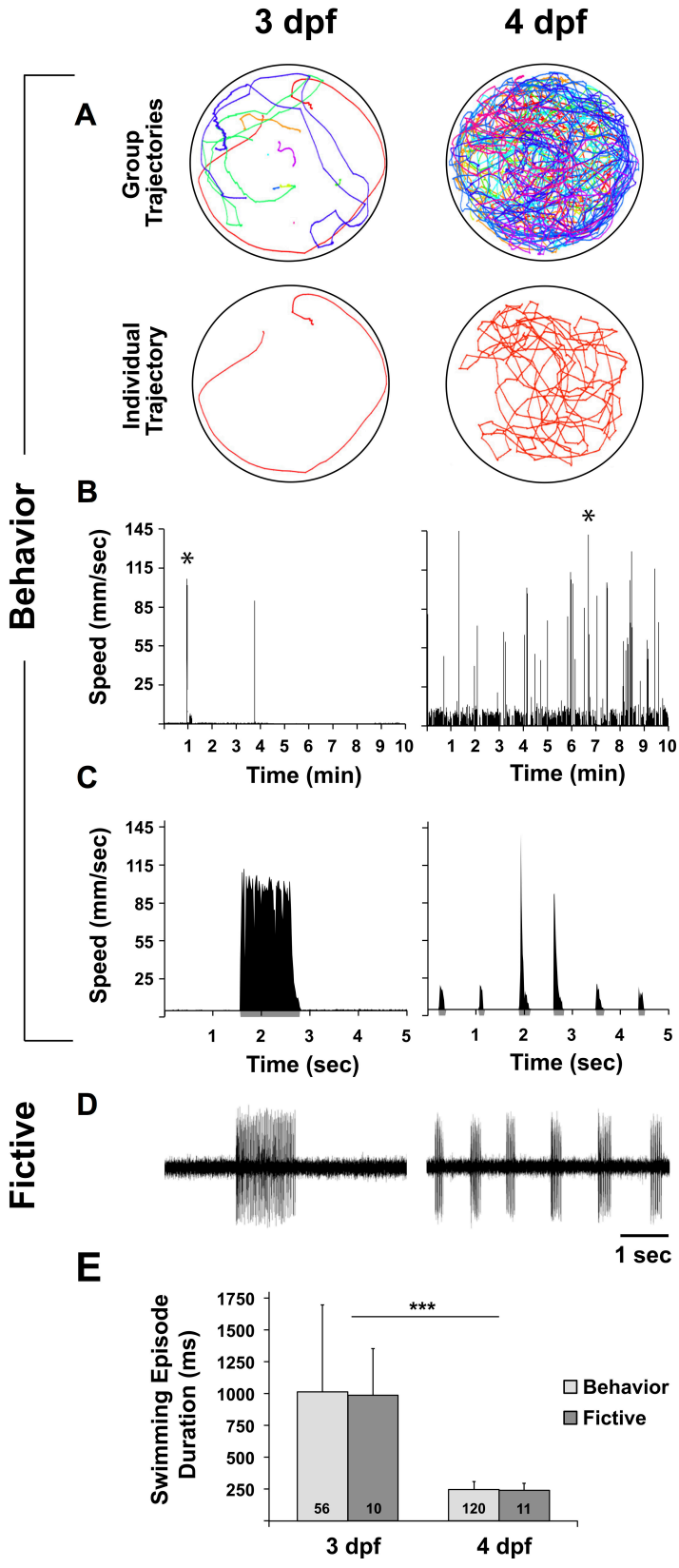

Figure 2

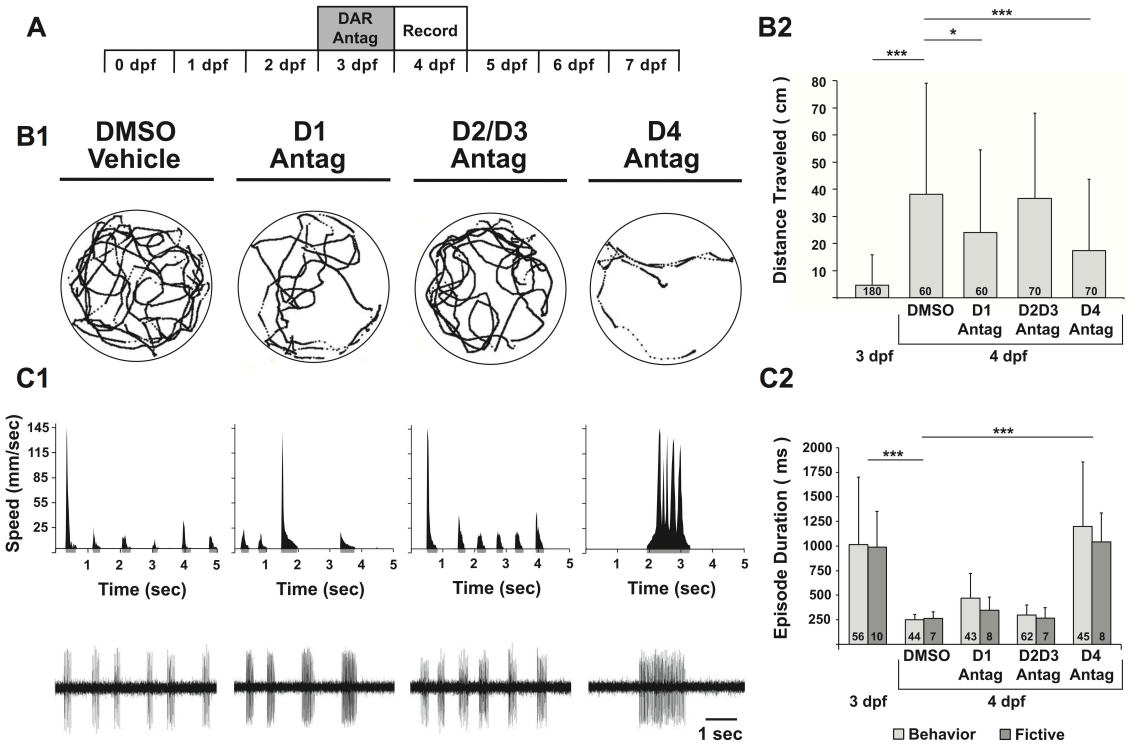
A
DAR Antag
Record
0 dpf
1 dpf
2 dpf
3 dpf
4 dpf
5 dpf
6 dpf
7 dpf
B1
DMSO Vehicle
D1 Antag
D2/D3 Antag
D4 Antag
B2
Distance Traveled (cm)
180
60
60
70
70
DMSO
D1 Antag
D2D3 Antag
D4 Antag
3 dpf
4 dpf
C1
Speed (mm/sec)
Time (sec)
1 sec
C2
Episode Duration (ms)
56
10
44
7
43
8
62
7
45
8
Behavior
Fictive

Figure 3

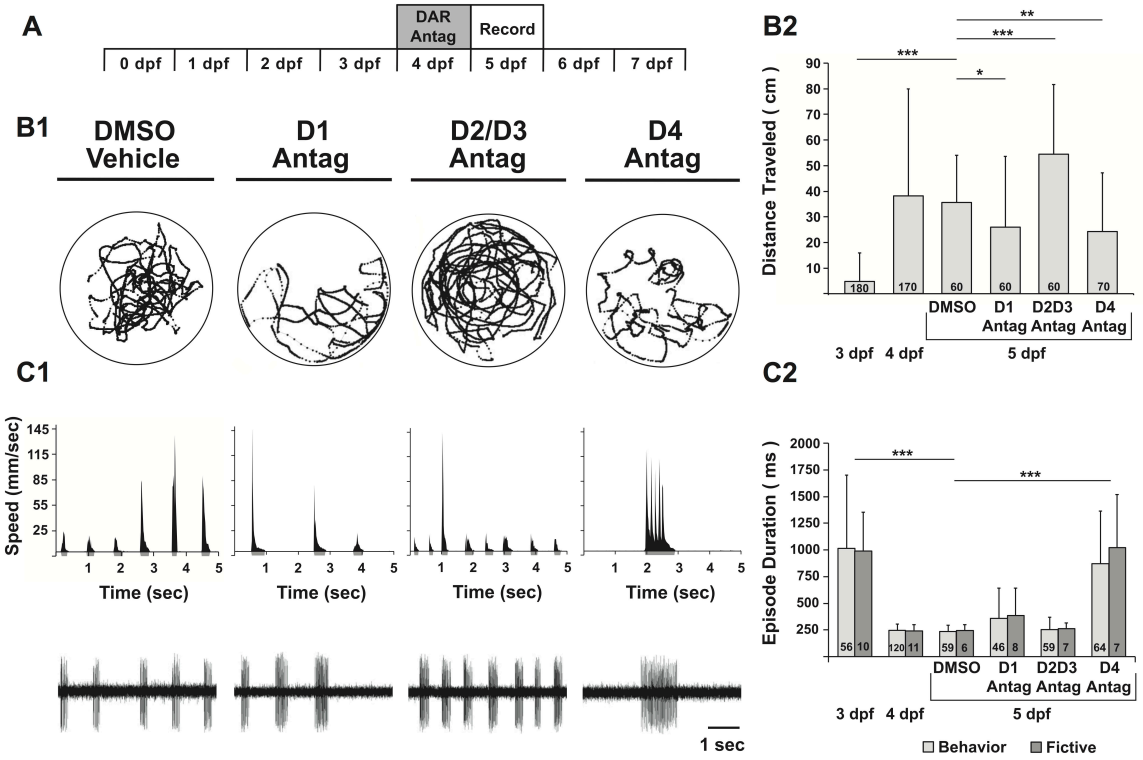
A
DAR Antag
Record
0 dpf
1 dpf
2 dpf
3 dpf
4 dpf
5 dpf
6 dpf
7 dpf
B1
DMSO Vehicle
D1 Antag
D2/D3 Antag
D4 Antag
B2
Distance Traveled (cm)
180
170
60
60
60
70
DMSO
D1 Antag
D2D3 Antag
D4 Antag
3 dpf
4 dpf
5 dpf
C1
Speed (mm/sec)
Time (sec)
1 sec
C2
Episode Duration (ms)
56
10
120
11
59
6
46
8
59
7
64
7
Behavior
Fictive

Figure 4

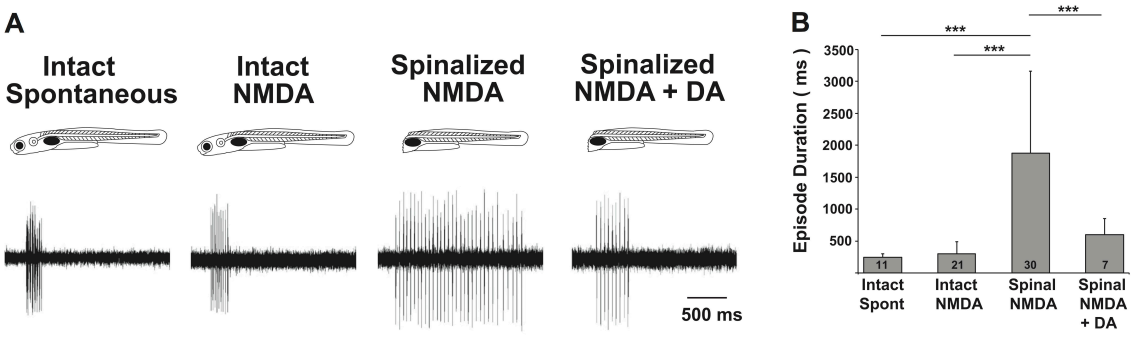
A
Intact Spontaneous
Intact NMDA
Spinalized NMDA
Spinalized NMDA + DA
500 ms
B
***
***
***
Episode Duration (ms)
3500
3000
2500
2000
1500
1000
500
11
21
30
7
Intact Spont
Intact NMDA
Spinal NMDA
Spinal NMDA + DA

Figure 5

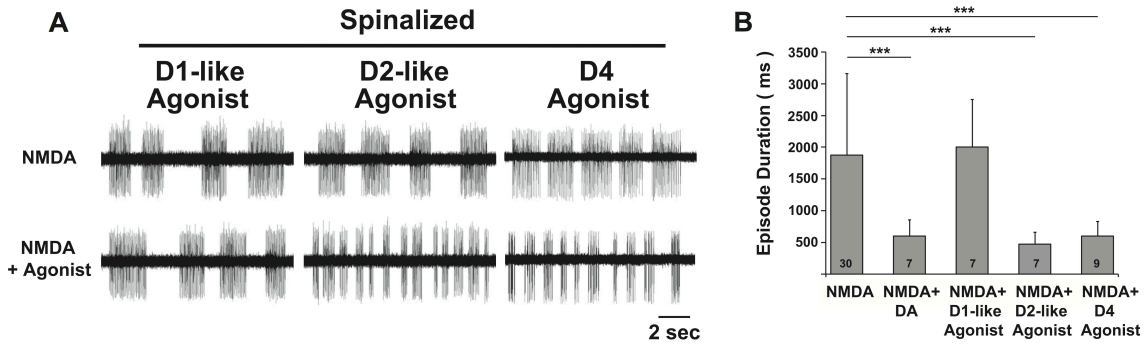
A
Spinalized
D1-like Agonist
D2-like Agonist
D4 Agonist
NMDA
NMDA + Agonist
2 sec
B
***
***
***
Episode Duration (ms)
3500
3000
2500
2000
1500
1000
500
30
7
7
7
9
NMDA
NMDA+ DA
NMDA+ D1-like Agonist
NMDA+ D2-like Agonist
NMDA+ D4 Agonist

Figure 6

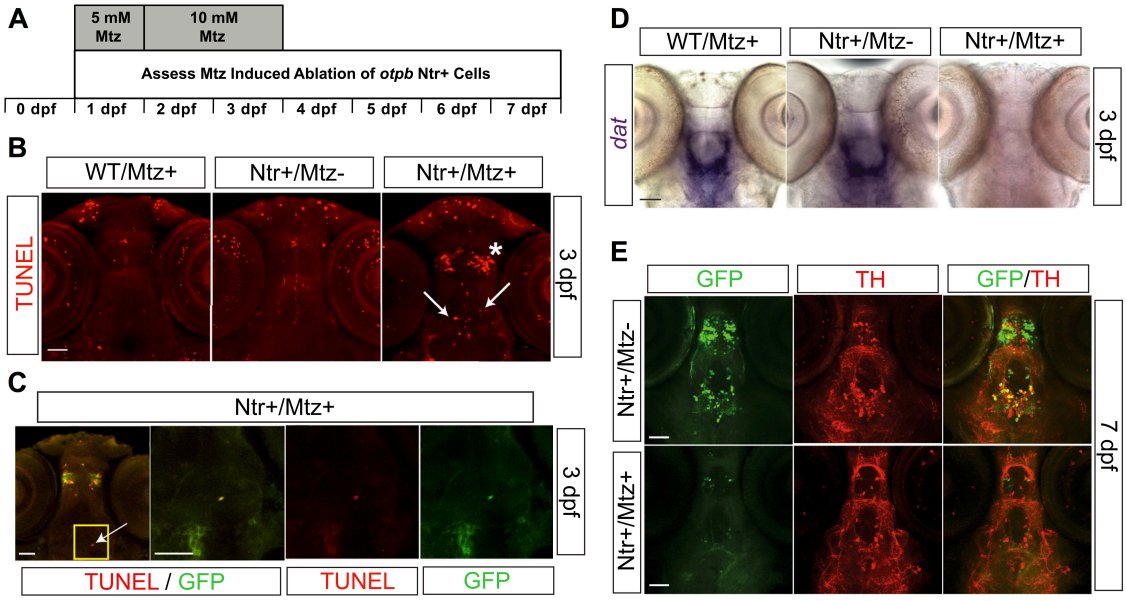
A
5 mM Mtz
10 mM Mtz
Assess Mtz Induced Ablation of otpb Ntr+ Cells
0 dpf
1 dpf
2 dpf
3 dpf
4 dpf
5 dpf
6 dpf
7 dpf
B
WT/Mtz+
Ntr+/Mtz-
Ntr+/Mtz+
TUNEL
3 dpf
C
Ntr+/Mtz+
3 dpf
TUNEL / GFP
TUNEL
GFP
D
WT/Mtz+
Ntr+/Mtz-
Ntr+/Mtz+
dat
3 dpf
E
GFP
TH
GFP/TH
Ntr+/Mtz-
Ntr+/Mtz+
7 dpf

Figure 7

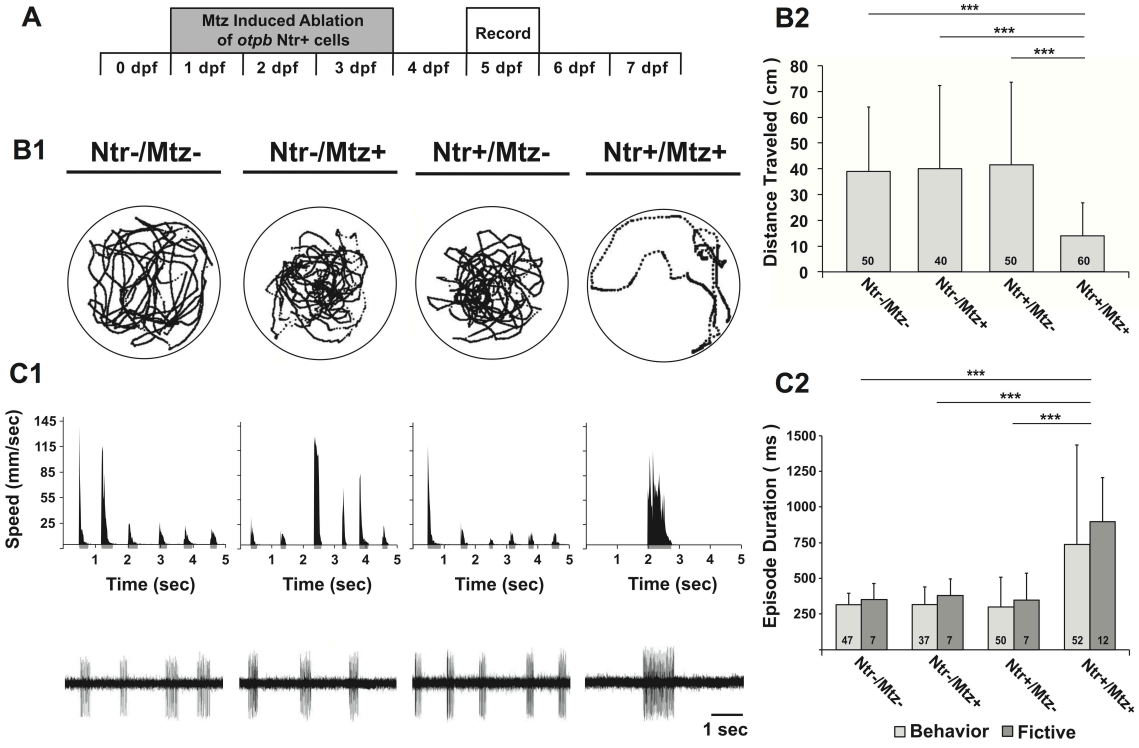
A
Mtz Induced Ablation of otpb Ntr+ cells
Record
0 dpf
1 dpf
2 dpf
3 dpf
4 dpf
5 dpf
6 dpf
7 dpf
B1
Ntr-/Mtz-
Ntr-/Mtz+
Ntr+/Mtz-
Ntr+/Mtz+
B2
Distance Traveled (cm)
50
40
50
60
C1
Speed (mm/sec)
Time (sec)
1 sec
C2
Episode Duration (ms)
47
7
37
7
50
7
52
12
Behavior
Fictive
***

Figure 8

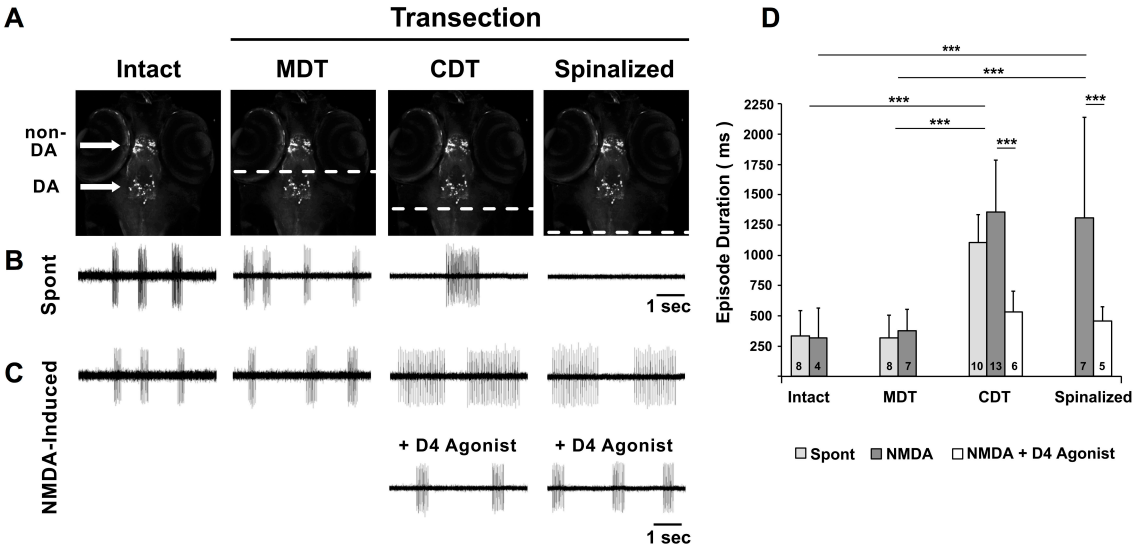
A
Transection
Intact
MDT
CDT
Spinalized
non-DA
DA
B
Spont
1 sec
C
NMDA-Induced
+ D4 Agonist
+ D4 Agonist
1 sec
D
***
***
***
***
***
***
Episode Duration (ms)
2250
2000
1750
1500
1250
1000
750
500
250
8
4
8
7
10
13
6
7
5
Intact
MDT
CDT
Spinalized
Spont
NMDA
NMDA + D4 Agonist

Chapter 2: A Widespread Conserved Dopaminergic System Exerts D4R-Mediated Meta-Locomotor Modulation and Specific Contributions To Goal-Directed Motor Strategies And Execution.

Summary

Prey capture is a compound ethologically-relevant behavior that can be broken up into its component elements to serve as a neuroethological platform for investigating its sensory, sensorimotor, motor, neuromodulatory, engrammic, attentional, and decision-making neural components. Despite a rich understanding of the underlying sensory and sensorimotor components, there is a dearth of studies on the explicit motor and locomotor neural components of prey capture. Here, we developed a novel high-throughput approach for investigating prey capture in zebrafish larvae. We revealed concurrent ontogenies of prey capture performance and refinement to a fine spontaneous locomotor repertoire, suggesting a relationship between the two. Relegation to a coarse spontaneous locomotor repertoire, via either blocking endogenous dopamine receptor 4 (D4R) signaling or chemogenetic ablation of *orthopedia*-specified diencephalic neurons and their conserved dopaminergic diencephalospinal tract (DDT), compromised prey capture performance. DDT-D4R perturbations modulated episodic patterning, turning, and swimming speeds in a dissociable manner, suggesting disparate D4R-mediated sites of action for

influencing each locomotor parameter. DDT-D4R perturbations increased swimming frequency, in addition to episodic patterning, in isolated and paralyzed preparations in a similar manner to free-swimming larvae. This suggested that the DDT-D4R network influences these locomotor parameters via motor-specific neuronal targeting, and DA or a D4R-specific agonist applied to the spinal cord was sufficient to slow neural correlates of locomotor frequencies in preparations transected at the hindbrain-spinal cord junction. Next, comprehensive automated analyses of eye convergence-defined hunting sequences following D4R antagonism revealed that prey-directed intact visual, oculomotor, visuomotor, and motor orienting functions were undermined by a bradykinesia-like loss of speed control during prey-advancing maneuvers. This deficit induced a compensatory shift to an orienting prey-catching strategy that nevertheless failed, specifically due to the inability to ultimately advance toward prey. Strikingly, the coarse and erratic spontaneous locomotor bias from D4R antagonism was invariably overridden during visually-guided hunting and replaced with fine attempts at motor control, albeit with a bradykinesia-like failure in execution. Hence, D4R-mediated speed control isolates as a critical determinant of prey capture success. Collectively, we posit a modular organization subserving a versatile locomotor network, wherein separate neural modules are recruited spontaneously and during hunting and that the hunting module is further subdivided into separable orienting and advancing regimes.

Introduction

Prey capture is an integrative behavior that serves as a neuroethological platform for investigating its sensory, sensorimotor, motor, neuromodulatory, engrammic, attentional, and decision-making components (Ewert et al., 1999; 2001; Muto and Kawakami, 2013). Although the capture component is emphasized in the term, prey capture holistically consists of prey detection, pursuit, capture, and ingestion. While the neural bases of the sensory and sensorimotor components of prey capture have been well elucidated in genetically intractable organisms (Ewert et al., 1999; 2001; Olberg, 2012), as well as in the genetically tractable zebrafish (Gahtan, 2005; Smear et al., 2007; Del Bene et al., 2010; Muto et al., 2013), the necessary locomotor and motor neural components for executing pursuit and capture maneuvers are not as well understood (Nishikawa, 1999). Zebrafish larvae- with their genetic tractability, translucency, and amenability to tethered virtual prey pursuit (Trivedi and Bollmann, 2013)- offer one of the best opportunities to comprehensively elucidate the many neural facets of prey capture. The goal of the present study is to begin investigating the locomotor neural components of prey capture in the well-suited zebrafish model, with its extant knowledge base of the underlying germane spinal (McLean et al., 2007; 2008), hindbrain (Kinkhabwala et al., 2011; Koyama et al., 2011), and midbrain (Binder et al., 2014; Severi et al., 2014; Wang and McLean, 2014) locomotor

networks and their neuromodulatory influences (Brustein et al., 2003; Lambert et al., 2012).

A developmental switch from coarse (long, fast, erratic) to fine (short, slow, directed) spontaneous locomotor episodes (Buss and Drapeau, 2001) coincides with the advent of hunting behavior in zebrafish, at just 4 days post fertilization (dpf). The newly acquired spontaneous locomotor repertoire conspicuously resembles much of the concurrently acquired hunting locomotor repertoire, with the exception of j-turns and capture swims, in that larvae track paramecia with short, slow and directed swimming episodes (Budick and O'Malley, 2000). This suggests that the neural circuitry dedicated to spontaneous swimming is employed during visually-guided hunting, which leads to two hypotheses: 1) the ontogenies of spontaneous swimming and prey capture performance will be correlated 2) perturbations compromising the spontaneous repertoire will concomitantly compromise the hunting repertoire and, ultimately, prey capture.

Our previous work provides a heuristic from which to perturb the spontaneous locomotor repertoire. We have shown that the conserved *orthopedia* (*otp*)-specified dopaminergic diencephalospinal tract (DDT) mediates the developmental switch in the episodic pattern from long to short swimming episodes by acting on D4 receptors (D4Rs) in the spinal cord *in vivo* (Lambert et al., 2012). Here, we hypothesized that blocking endogenous D4R signaling,

aside from affecting the duration of episodes, would also compromise other aspects of the spontaneous locomotor repertoire that have potential relevance to hunting, such as speed and turn angle, and that such perturbations would equatably contaminate the hunting repertoire and, consequently, impair prey capture performance.

Testing this hypothesis under many experimental conditions requires a high-throughput approach to prey capture analysis, which has been lacking in zebrafish. The state of prey capture analyses in free-swimming zebrafish larvae has been limited to either 1) manually counting the number of prey remaining over time, but with no information about how the prey disappeared (Gahtan, 2005) 2) manually detecting and then recording ongoing hunting sequences and separately analyzing the kinematics of each of the videos of these brief, empirically-detected, putative prey encounters (Borla et al., 2002; McElligott and O'Malley, 2005; Bianco et al., 2011; Patterson et al., 2013). Here, we developed a novel method for high-throughput, automated detection and analyses of hunting sequences in free-swimming zebrafish larvae via automated tracking of eye convergences, which is a reliable hallmark of prey detection and pursuit during the entire duration of each prey encounter (Bianco et al., 2011).

Through automated convergence-driven indexing of over 40 locomotor parameters to either non-hunting or hunting sequences, we found that

spontaneous and hunting locomotor repertoires were dissociable but that each were differentially influenced by endogenous D4R signaling. Blocking D4R signaling relegated larvae to an immature-like spontaneous repertoire of long, fast, erratic episodes, but this coarse bias was invariably overridden and replaced with attempts at finer motor control during convergence-defined hunting. Larvae under D4R antagonism still had functional vision and visuomotor initiation, respectively, to detect paramecia and attempt fine hunting locomotor elements toward them. However, their prey capture performance was impaired because they exhibited a specific bradykinesia-like deficit in advancing but not orienting maneuvers, resulting in an inability to reduce distance but not angular heading toward prey. Collectively, these results: 1) unveil a salient state-dependency of dopaminergic locomotor influence 2) suggest there are separate neural modules for executing spontaneous versus hunting locomotor repertoires 3) suggest the hunting locomotor repertoire is further subdivided into distinct neural modules for advancing versus orienting maneuvers.

Methods

Animals. All experiments were performed on zebrafish (*Danio rerio*) larvae between 1 and 7 dpf. Wild-type (WT) larvae were obtained from a laboratory stock (Segrest) of adults at the University of Minnesota. The Tg(*otpb.A:nfsB–egfp*)zc77 line, for prodrug-induced cell-autonomous chemogenetic ablation (Curado et al., 2008) of *otpb*+ neurons, was first described and used previously by our lab and collaborators (Lambert et al., 2012). Embryos and larvae were raised in an incubator at 28.5°C under a 14/10 light/dark cycle (Lights On, 8:00 A.M.; Lights Off, 10:00 P.M.) until the start of behavioral or neural recordings between 3 and 7 dpf. Larvae were kept at room temperature during all manipulations and recording sessions and returned to the incubator during interims. Paramecia cultures (*Paramecium caudatum*) were provided to larvae only during hunting kinematic or prey capture assays, and no experiments were performed on these fed larvae on subsequent days unless otherwise noted. Paramecia were obtained from the Zebrafish International Resource Center (ZIRC) and cultured by the staff at our zebrafish facility at the University of Minnesota. All procedures were approved by the Institutional Animal Care and Use Committee at the University of Minnesota.

Free-Swimming Behavior. Open-source software (Ctrax; (Branson et al., 2009)) was adapted to individually track the free-swimming of multiple zebrafish larvae

in a group setting, as we first implemented and described for zebrafish previously (Lambert et al., 2012). For spontaneous free-swimming experiments, 10 fish were simultaneously placed within a 50 mm watch glass (Thermo Fisher Scientific; 10 mm depth at center and progressively shallower toward periphery), allowed to acclimate 5 min, and were then video-recorded for either 10 min at 60 Hz or for 20 sec at 210 Hz. For hunting kinematic experiments, 3 or 4 fish were simultaneously placed in a custom 20 mm arena of shallow depth (1.5 mm) to facilitate visualization of fish and paramecia within the same focal plane. The fish were first placed in embryo media alone, given 5 min to acclimate, and 10 min of spontaneous free-swimming was video-recorded at 60 or 120 Hz. Subsequently, embryo media was replaced with paramecia culture containing ~30-60 paramecia to obtain a total volume of 600 µl within the arena. Video recording, at 60 Hz, began immediately after seeding paramecia and lasted for a minimum of 30 min. *Ad hoc* Matlab toolboxes, namely Fix Errors and Behavioral Microarray toolboxes provided by the creators of Ctrax (Branson et al., 2009), were used to fix tracking errors (such as fixing swapped fish identities, ensuring fidelity of tracking information from each fish in the arena) and extract descriptive statistics of a suite of parameters from each of the tracked zebrafish targets.

We wrote custom Matlab scripts to detect swimming, and subsequently compute over 40 locomotor parameters, from each fish's orientation and position and their respective derivatives, namely angular velocity, angular acceleration, and linear

velocity. Swimming was defined as a minimum of 3 consecutive frames (~50 ms at 60 Hz) in which the fish's absolute smoothed angular acceleration exceeded 0.9 mm/sec^2. For both spontaneous and hunting kinematic video recordings of fish in the 20 mm arena, nearby swimming events were only concatenated into a single swimming event if they occurred within 1 frame of one another (~17 ms at 60 Hz). It is important for this concatenation window to be short during hunting since inter-swim durations are routinely shorter than 300 ms during prey pursuit (Trivedi and Bollmann, 2013), whereas during spontaneous swimming they are over 300 ms and on average over 800 ms (Fuiman and Webb, 1988; Muller et al., 2000; Farrell et al., 2011; Lambert et al., 2012). For spontaneous video recordings in the 50 mm arena, the signal-to-noise ratio was smaller, compared to the 20 mm arena, due to fewer pixels representing each fish target. Consequently, swimming events occurring within a 9-frame window (~150 ms at 60 Hz) were concatenated into a single swimming event. Turn detection and computation was achieved via the fish's smoothed orientation (smoothed over 5 frames; ~83 ms at 60 Hz). Tail beat frequency and amplitude computations were achieved by identifying the local maxima and minima (or bursts) in a splined function of the fish's angular velocity. For 210 Hz recordings, a 5x spline was generated to interpolate 1050 Hz and was sufficient to resolve the fastest tail beat frequencies at ~80 Hz. For 60 Hz recordings, a 10x spline was generated to interpolate 600 Hz, which was sufficient to estimate slower but not faster tail beat frequencies. Although 60 Hz is not a high enough frame rate for the most

accurate quantification of tail beat frequencies, it was sufficient to establish a swim unilaterality index for differentiating unilaterally-biased from bilaterally-symmetric hunting maneuvers (see maneuver classifications in next section).

A digital CMOS camera (Firefly MV; Point Grey Research) with an attached 50 mm macro lens (Sigma) was used for all video recordings except for high-resolution, high-speed recordings (210 Hz), for which a digital CCD camera (Flea3; Point Grey Research) with an attached 12 mm lens was used. Videos using the Firefly camera were acquired, via Fview (open-source software; (Straw et al., 2011), in uncompressed fly movie format (FMF). Videos using the Flea3 camera were acquired as uncompressed AVIs in FlyCapture2 (Point Grey Research).

Automated Analyses Of Hunting Sequences. We developed a novel methodology for automated detection of hunting sequences in free-swimming larvae via automated tracking of eye convergences, which manual assessments have determined to be a specific and reliable hallmark of prey detection and pursuit during the entire duration of each prey encounter (Bianco et al., 2011). Custom Matlab scripts were written for all of the following procedures. The global orientations of tracked larvae (Fig 6A) were used to generate new videos in fish-centered reference frames for each fish, such that each global video frame was rotated with respect to the orientation of each fish in that frame. The

resultant fish-centered video frame was then padded with non-signal pixels and subsequently cropped about the head of the fish; the padding became important for fish-centered frames in which the fish's head was located near the periphery of the arena and padding pixels functioned to fill the remainder of the cropped image about the head. This procedure generated a fish-centered video wherein the position of the fish remained fixed over a moving background, which facilitated the tracking of each eye (Fig 6B) and computation of instantaneous eye angles (Fig 6C) over the entire video record. These fish-centered videos, if instead cropped about the entire fish body, could be used to skeletonize and segment the fish body for computing instantaneous body-segment angles and undulatory kinematics (data not shown), in a manner similar to previous studies (Trivedi and Bollmann, 2013). For computing the instantaneous difference in eye angles (i.e. eye convergence), we initially fed these fish-centered videos into Ctrax and confirmed that Ctrax could track the eyes and subsequently compute the instantaneous eye angles. However, tracking errors often occurred and had to be corrected *post hoc*.

Consequently, we instead integrated eye detection and angle computation within the same Matlab script that we wrote for generating fish-centered videos. Here, during the same iteration in which a video frame was transformed to a fish-centered reference frame, we thresholded this fish-centered frame such that only the dark eyes (and sometimes the swim bladder) remained as signal pixels. Only

signal objects that were within a bounding box encapsulating the full range of potential eye positions in the fish-centered frame were considered as potential eye objects. This effectively eliminated the swim bladder from being considered as an eye object since it was caudal to the eye-bounding box. Additionally, the eye convergence computation was only executed for fish-centered frames in which exactly 2 objects were detected within the eye-bounding box and for which the area of each of these objects was within 1 standard deviation (SD) of the mean eye area determined in initial videos. Instantaneous eye convergence angles exceeding 45 degrees were considered as a potential hunting event, and any other potential hunting events within a 300 ms window were concatenated as a single potential hunting event. Only potential hunting events lasting for a minimum of 250 ms and having a mean eye convergence angle exceeding 45 degrees were coded as hunting sequences (or eye convergence sequences) (Fig 6C). The duration and inter-duration of each hunting sequence was computed, as well as the number of hunting sequences and mean hunt duration per min, per 5 min, per 10 min, and throughout the entire record.

The timestamps of these hunting sequences were fed into our swim detection script in order to index the multivariable locomotor record into hunting and non-hunting sequences (Fig 6D), isolating the hunting and spontaneous locomotor repertoires, respectively. For hunting sequences, each locomotor maneuver executed during each hunt was indexed to: its hunt number, its sequential order

relative to the other maneuvers within the same hunt (e.g. 2nd maneuver within hunt), each of its computed locomotor parameters (e.g. turn angle, peak speed), and its maneuver type classification. Zebrafish larvae execute 5 different hunting maneuver types, which can be broadly dichotomized into orienting maneuvers, which function to reduce angular heading to prey, and advancing maneuvers, which function to reduce distance to prey (Budick and O'Malley, 2000; Borla et al., 2002; McElligott and O'Malley, 2005). The 3 orienting maneuver types are: 1) orienting swims: turning with bilateral undulations following initial turn cycle 2) j-turns: turning with unilaterally-biased undulations throughout episode 3) backups: backward velocity maneuver using synchronized bilateral pectoral fin abductions but without any needed axial motor output (Budick and O'Malley, 2000; Borla et al., 2002; McElligott and O'Malley, 2005). The 2 advancing maneuver types are: 1) forward swims: bilateral undulations with no turning component 2) capture swims: bilateral undulations with no turning component, a greater peak speed than forward swims, a late phasing of the peak speed within the swim, and an S-shaped body shape during the peak speed (Budick and O'Malley, 2000; Borla et al., 2002; McElligott and O'Malley, 2005). The indexed multivariable locomotor parameters per hunting maneuver were used to automate maneuver classification (Fig 6E) based on the above maneuver type definitions. Only hunting locomotor episodes (i.e. episodes occurring during a hunting sequence) were classified into maneuver types, so all of the following maneuver classification procedures were not employed for spontaneous swimming.

Backups were defined as 2 or more consecutive frames with a backward velocity exceeding 1 mm/sec, which often occurred in the absence of axial motor output but sometimes occurred concurrent with it. In both cases, close examination of the records revealed the same bilaterally synchronized fin abduction to effectively backup the fish. Consequently, both cases were classified as backups. A swim unilaterality index was computed for each maneuver, defined as the absolute value of the sum of all tail beat amplitudes in the maneuver aside from the initial swim cycle. Maneuvers with a swim unilaterality index greater than 0.5 and with a total turn angle greater than 4 degrees were classified as a j-turn, whereas they were classified as an orienting swim if only the turn angle threshold was satisfied. Maneuvers were classified as capture swims if the total turn angle was less than 4 degrees and the peak speed and peak acceleration occurred over midway into the maneuver and was greater than 10 mm/sec and 300 mm/sec^2, respectively. Otherwise, maneuvers with a total turn angle of less than 4 degrees were classified as forward swims. Finally, although the eyes deconverge coincident with either the final prey capture (Bianco et al., 2011) or the disengagement of a hunt (Westphal and O'Malley, 2013), we observed that larvae sometimes execute an abortive disengaging swim- consisting of a fast, large, and abrupt turn away from the current heading of pursued prey (Westphal and O'Malley, 2013)- just before deconvergence but which is not apart of prey pursuit. Consequently, maneuvers with a turn angle greater than 20 degrees, swim unilaterality index

less than 0.5, and peak speed greater than 10 mm/sec (which orienting swims were slower) were classified as disengaging swims and ultimately indexed as non-hunting maneuvers (but not included in spontaneous swimming).

Manual And Semi-Automated Analyses Of Hunting Sequences. Paramecia were too small and too numerous to track automatically, requiring their initial manual detection within our automatically detected hunting sequences. Undergraduate research assistants employed the Fix Errors GUI (Ctrax; (Branson et al., 2009)) to quickly enter in automatically-detected hunting sequence timestamps, manually and blindly assess several features of the fish-prey kinematics, and semi-automatically track pursued paramecia. For each hunting sequence, it was determined whether a paramecium was being pursued, whether it was clear which paramecium was being pursued in the event of multiple nearby paramecia, whether a capture attempt was executed and if it resulted in successful prey capture, the type of capture attempt (ram, suction, swim suction) executed, if the border of the arena interfered with a capture attempt, and whether a successful capture was successfully ingested or not. During some of these manual assessments, each hunting sequence was also empirically assessed as to whether the fish initiated a true eye convergence and manual classifications were made for each maneuver into one of the 5 maneuver types. This provided proof-of-principle of our automated detections and classifications, with automated eye convergences having a true eye convergence

rate of 96.88 ± 3.96% (*n* = 24 fish; 1117 out of 1153 total comparisons) and automated maneuver-type classifications matching 88.3% of manual classifications (76 out of 86 total comparisons).

For all hunting sequences involving a capture attempt, the Fix Errors GUI was used to manually place a target ellipse over the pursued paramecium just before the onset of the hunting sequence. Then the paramecium was able to either be automatically tracked throughout the duration of the hunting sequence, or semi-automatically tracked by a series of discrete ellipse placements and interposed trajectory interpolations throughout the sequence. A MAT-file containing all paramecium targets for each fish was then exported and the Behavioral Microarray toolbox was used to compute an inter-distance and inter-angle function for each fish-prey pair. Both functions were computed from the nose of the fish ellipse to the centroid of the paramecium ellipse. This updated MAT-file for each fish was fed into a custom-written Matlab script to iteratively place each structure of fish-prey kinematics in register with the automated hunting sequence and locomotor records. With this in hand, the fish-prey inter-distance and inter-angle at the precise start and end of the hunting sequence, as well as at the precise start and end of each locomotor maneuver within the sequence, was extracted and stored. These values were used to compute the distance-reduction and angle-reduction productivities of each locomotor maneuver, where

each was defined as the difference in either the inter-distance or inter-angle just after the maneuver compared to at the maneuver onset.

Prey Capture Assay. Quantification of prey capture performance was performed similar to that of previous studies in zebrafish (Gahtan, 2005), but with slight modifications. Approximately 200-300 paramecia, from ~1-5 mL paramecia culture, were seeded in 6 ml embryo media within a 60 mm petri dish, either alone or with 10 zebrafish larvae. A 200 frame video at 60 Hz was recorded each hour and was used to generate an SD z-projected time-lapse image in ImageJ (open-source, NIH), enabling individual paramecia to be counted by tracking their paths (as healthy paramecia remain in constant motion). Undergraduate research assistants blindly counted the number of paramecia in each encrypted image file; the percent of paramecia remaining each hour, compared to the initial seeding, was quantified for the 5-hour assay.

Electrophysiology. Neural recordings from paralyzed preparations (i.e., fictive swimming) were assessed via peripheral nerve recordings *in vivo* as established (Masino and Fetcho, 2005) and most germanely described previously (Lambert et al., 2012). Larvae were anesthetized with 0.02% Tricaine-S (Western Chemical) in extracellular recording solution, transferred to Sylgard-lined dissecting dishes, pinned on their sides through the notochord using short pieces of fine tungsten wire (0.001 inch diameter), the skin removed between the

tungsten pins, and paralyzed using 5 µL of 0.1 mM α-bungarotoxin (Tocris Bioscience) added to the small amount (~15 µl) of extracellular solution in the dissection dish. Subsequently, larvae were transferred to the stage of an Olympus BX51 WI microscope, and extracellular recording solution was superfused at room temperature. Suction electrodes (6 –15 µm tip diameter), filled with extracellular recording solution, were used to obtain peripheral nerve recordings between mid-body segments 10 and 20 and were acquired using a Multi-Clamp 700B amplifier (Molecular Devices), a Digidata series 1440A digitizer (Molecular Devices), and pClamp 10.2 software (Molecular Devices). Extracellular voltage was monitored in current-clamp mode at a gain of 2000 (R_f = 50 MΩ) with the low- and high-frequency cutoff at 300 and 1000 Hz, respectively. A custom Matlab script was written to analyze the extracellular peripheral nerve voltage recordings, which we have described previously (Lambert et al., 2012). Fictive locomotor bursts were detected, grouped into episodes, and the burst and episode properties (duration, frequency, and interburst or inter-episode intervals) for each voltage trace were determined.

For all preparations in which spontaneous fictive swimming was assessed, spontaneous fictive activity was recorded for a minimum of 30 min. For acute drug administration (~30 min) to fictive preparations, drugs were dissolved at stated concentrations in extracellular recording solution and superfused at 1 ml/min. NMDA (50 µM) was superfused for 15–20 min to elicit a baseline of

NMDA-induced fictive swimming before application of dopamine (DA) or DAR agonists. DA or DAR agonists were superfused with NMDA for 10–15 min before returning to an NMDA solution (washout).

Pharmacological and Prodrug Treatments. All pharmacological and prodrug treatments were determined and administered as we have described previously (Lambert et al., 2012), but with slight modifications. For chronic incubations of dopamine receptor (DAR)-specific antagonists to WT larvae, drugs were dissolved at stated concentrations in embryo media containing 0.1% dimethylsulfoxide (DMSO); low concentrations of DMSO facilitate in aqueous drug delivery through the skin without affecting behavior (Rihel et al., 2010). Larvae subjected to embryo media containing 0.1% DMSO served as vehicle controls. Chronic drug incubations began at 7:00 P.M. for behavioral and neural assessments on the following day. All chronic pharmacological groups remained in their respective drugs up until the start of behavioral or neural recordings. It was determined that some of the DAR antagonists alone would adversely affect paramecia viability over the 5-hour prey capture assay. However, we found that any altered locomotor effects from chronic DAR antagonism did not wash out over the course of 5 hours. Consequently, DAR antagonists were thoroughly washed out just prior to prey capture assays, as well as neural and behavioral recordings. Prodrug treatments of metronidazole (Mtz) to Tg(*otpb.A:nfsB*– *egfp*) zc77 embryos and larvae, in which nitroreductase expression (protein product of

nfsB transcription, under the control of the *otpb* promoter) converts Mtz to cytotoxic metabolites, was performed and evaluated as we have described previously (Lambert et al., 2012). Briefly, treatment of 5 mM Mtz from 24-48 hours post fertilization (hpf) and 10 mM Mtz from 48-96 hpf results in cell-autonomous chemogenetic ablation of *otpb*+ neurons (Lambert et al., 2012), after which we allowed larvae to recover for 1 day in embryo media alone before the start of prey capture assays, as well as neural and behavioral recordings, at 5 dpf.

NMDA, DMSO, DA, Mtz, DAR-specific antagonists (D_1R, SCH-23390 [R(+)-7-chloro-8-hydroxy-3-methyl-1-phenyl-2,3,4,5-tetrahydro-1H-3-benzazepine hydrochloride]; D_2/D_3R, raclopride [3,5-Dichloro-N-(1-ethylpyrroli- din-2-ylmethyl)-2-hydroxy-6-methoxybenzamide]; D_4R, L-745,870 (3- [[4-(4-chlorophenyl)piperazin-1-yl]methyl]-1 H-pyrrolo[2,3-b]pyridine trihydrochloride)), and DAR-specific agonists (D_1-like, SKF-38393 [2,3,4,5- tetrahydro-7,8-dihydroxy-1-phenyl-1 H-3-benazepine HCl]; D_2-like, quinpirole (trans-(-)-(4aR)-4,4a,5,6,7,8,8a,9-Octahydro-5-propyl-1H- pyrazolo[3,4-g]); D_4R, PD168,077 [N-[[4-(2-cyanophenyl)piperazin-1- yl]methyl]-3-methylbenzamide)] were obtained from Sigma.

Statistical analyses. Statistical analyses were performed with SigmaPlot 12.5 (Systat Software). Data were analyzed using Student's t tests (two conditions

only), one-way ANOVAs (more than two conditions), or two-way ANOVAs (more than 2 conditions and 2 output parameters). These statistical tests accounted for repeated measures when appropriate, namely when comparisons incorporated intra-animal baseline and postdrug datasets. For ANOVAs, post hoc (Holm–Sidak) pairwise multiple comparisons were performed to identify which groups were significantly different from one another. Significance was established using an α criterion of $p = 0.05$. In the figures, $*p = 0.05$, $**p = 0.01$, and $***p = 0.001$, respectively. In the text, reported sample sizes denote the number of fish for each experimental group, unless otherwise noted. All descriptive statistics are reported as either Mean ± SD or Mean ± SEM, as noted in the text.

Results

Concurrent Ontogenesis of the Spontaneous Locomotor Repertoire and Prey Capture Performance

If the neural substrates for spontaneous swimming are recruited during visually-guided hunting, then the ontogenies of the spontaneous locomotor repertoire and prey capture performance should be concomitant. To test this hypothesis, we examined both ontogenies from 3 to 7 dpf. Expanding upon our previous high-throughput behavioral analyses of free-swimming locomotion (Lambert et al., 2012), we used the angular velocity of tracked fish to detect swimming and the smoothed orientation to detect turning (Fig 1A1). Our refined kinematic procedure quantified 50 locomotor parameters (Table 1), with the three most putatively relevant parameters to hunting being: episode duration, peak swimming speed, and total turn angle.

From 3 to 7 dpf, there was a clear ontogeny from a coarse (long, fast, erratic) to a fine (short, slow, directed) spontaneous locomotor repertoire (Fig 1A2), with the magnitude of all 3 key locomotor parameters significantly decreasing from 3 to 4 dpf, but only peak speed decreasing further from 4 to 7 dpf (Table 1). Concomitantly, there was a strikingly similar ontogeny in prey capture performance (Fig 1B1) over the same developmental window (Fig 1B2),

quantified via a modified version of previous methods to count the percent of paramecia remaining over a 5 hour prey capture assay (Gahtan, 2005) (Fig 1B1). The final percent paramecia remaining in the absence of fish was not significantly different from when 3 dpf larvae were present ($p = 0.675$) (Fig 1B2). Conversely, there was a significant decrease in paramecia when 4 dpf larvae were present ($p < 0.001$), which was further decreased in the presence of 7 dpf larvae ($p < 0.001$) (Fig 1B2). Though purely correlational, these concurrent ontogenies suggest that a developmental switch and progression to finer spontaneous locomotor control, most notably in swimming speed, may subserve the advent of hunting prowess.

Blocking Endogenous D4R signaling or Chemogenetic Ablation of the DDT Relegates Larvae to an Immature Spontaneous Locomotor Repertoire and Impairs Prey Capture Performance

If precision of spontaneous swimming is a proxy to the level of recruitable precision during hunting, then perturbations of the spontaneous locomotor repertoire should equatably compromise prey capture performance. We have previously shown that blocking endogenous D4R signaling, as well as chemogenetically ablating *optb* neurons comprising the DDT, relegates 5 dpf larvae to immature-like long duration swimming episodes (Lambert et al., 2012). Empirical phenotypic observations suggested to us that these DDT-D4R perturbations might also compromise swimming speed and turning angles.

Employing our more comprehensive kinematic locomotor analyses in 5 dpf larvae systemically incubated overnight in a specific D4R antagonist (L-745,870; 10 μM) (Fig 2A1), a full relegation to an immature spontaneous locomotor repertoire of significantly longer, faster, and larger turn angle episodes was induced compared to DMSO vehicles (Fig 2A2; Table 2). Correspondingly, the final percent paramecia remaining in the presence of larvae under D4R antagonism was significantly higher than in the presence of DMSO vehicles ($p < 0.001$) (Fig 2B). Hence, disruption of the spontaneous locomotor repertoire via D4R antagonism also impairs prey capture performance, further suggesting that the former could influence the latter. These results also reveal that endogenous D4R signaling serves as a meta-locomotor modulator of episodic patterning, swimming speed, and turning.

To determine whether the full extent of D4R-driven meta-locomotor modulation is driven by *otpb* neurons comprising the DDT, we tested whether chemogenetic ablation of these neurons in Ntr+ Mtz+ larvae (Lambert et al., 2012), via the Ntr:Mtz system (Curado et al., 2008; Pisharath and Parsons, 2009) (Fig 2C1), recapitulates the phenotype of an immature spontaneous locomotor repertoire and, moreover, impairs prey capture performance at 5 dpf. This was indeed the case, but with a caveat. All three key locomotor parameters were significantly larger in DDT-ablated larvae (Ntr+ Mtz+) compared to Ntr-negative pro-drug Mtz-treated controls (Ntr- Mtz+) (Fig 2C2; Table 2), confirming a similar locomotor

relegation from DDT-ablation as under D4R antagonism. However, although the final percent paramecia remaining with DDT-ablated larvae was significantly greater than untreated controls ($p < 0.001$), the Mtz-treated controls also exhibited severe impairments in prey capture performance that were not significantly different from that of DDT-ablated larvae ($p = 0.311$) (Fig 2D). This non-specific effect of Mtz treatment early in development is only exploited after examination of prey capture performance, because there is no induced cell death (Lambert et al., 2012) from this Mtz treatment in Ntr- larvae and their subsequent spontaneous locomotor behavior is normal at 5 dpf (Fig 2C2; Table 2) (Lambert et al., 2012) .

It is possible that the high concentration (5-10 mM) of the Mtz antibiotic perturbs with the development of a functional digestive system for prey ingestion, which occurs between 1 and 4 dpf (Wallace and Pack, 2003) and exactly matches the time course of the aforementioned Mtz regimen. Not surprisingly, the advent of a fully functional digestive system at 4 dpf coincides precisely with the advent of prey capture, ingestion, and digestion (Borla et al., 2002; McElligott and O'Malley, 2005; Muto et al., 2013). Knowing this, the next strategy was to administer Mtz only subsequent to this critical gut and digestive development, this time from 4-6 dpf and then examine prey capture at 7 dpf (Fig 2E). This strategy circumvented the previous issues with Mtz, because these Mtz-treated controls, which again had a normal locomotor repertoire (Fig 2F), also had

excellent prey capture performance at 7 dpf that was not significantly different from untreated controls (Fig 2G). As for the chemogenetic ablation of the DDT from 4-6 dpf, it induced an immature locomotor repertoire of long, fast, erratic episodes (Fig 2F) and severely impaired prey capture performance compared to Mtz-treated or untreated controls (Fig 2G). As such, this effect is definitively from chemogenetic ablation of otpb neurons.

Unfortunately, chemogenetic ablation of otpb neurons at this later developmental time point, from 4-6 dpf, severely compromised health and was lethal to over 33% of larvae by 7dpf, none of which was observed in either control groups or from ablation of *otpb* neurons earlier in development (from 1-4 dpf). It is likely that the lethality from chemogenetic ablation of *otpb* neurons between 4-6 dpf is due to the loss of vital functions provided by the non-DAergic *otpb* population, because 4 dpf marks the advent of glucocorticoid stress responses (De Marco et al., 2013) and non-DAergic *otpb* neurosecretory neurons are critical for neuronal adaptation to stress (Amir-Zilberstein et al., 2012). Given these unfortunate caveats with chemogenetic ablation of all *otpb* neurons, we later restricted our more detailed investigations of hunting sequences to D4R antagonism.

Dissociable Meta-Locomotor Modulation by the DDT-D4R Network

Before investigating hunting any further, we first set out to gain inferences into whether the DDT-D4R network achieves meta-locomotor modulation via the same or distinct neuronal targets. If endogenous D4R signaling modulates all three key locomotor parameters via the same neuronal target, then these parameters should consistently covary. A coarse examination of the distribution of individual means following D4R antagonism (Fig 2A2) or DDT-ablation (2C2, F) would suggest a covarying scenario, especially for individual larvae that exhibited the largest mean episode durations, peak speeds, and turn angles. Interestingly examination of the distribution of all individual swimming episodes, comprising a total sample size of thousands to tens of thousands of locomotor events per experimental group, revealed that these three locomotor parameters do not often covary and , moreover, there can exist strikingly large disparities in their intra-episode magnitudes . Namely, we assessed scatter plots of episode duration as a function of speed or turning and quantified their corresponding goodness of fits following normal development (Fig 3A, B, C), D4R antagonism (Fig 3D, E, F) or DDT-ablation (Fig 3G, H, I).

There was a markedly low correlation coefficient and goodness of fit between the episode duration and peak speed of a given swimming episode; this held true whether looking at swimming episodes over natural development or following DDT-D4R perturbations (Fig 3C, F, H). This makes sense under normal conditions, since the putative spinal episode pattern generator is dissociable from

the spinal coordination generator (Wiggin et al., 2012), the latter of which is in register with dynamic tail beat frequencies and influences swimming speed (McLean et al., 2007; 2008; McLean and Fetcho, 2009). This alone reveals that spinal episodic patterning and CPG coordination/speed must be achieved through distinct spinal neuronal populations. Aside from the DDT-D4R perturbations separably increasing episode durations and peak speeds across swimming episodes, total turn angle was also not strongly correlated to episode duration. However, there was at least a marked increase in the goodness of fit between episode duration and turn angle for 3dpf larvae compared to older larvae (Fig 3C), following D4R antagonism compared to DMSO (Fig 3F), and following DDT-ablation in Ntr+ Mtz+ larvae compared to Ntr- Mtz+ controls (Fig 3I). This trend could at least partially be due to longer episode durations allotting more time to accrue total turning. Regardless, the distribution of individual swimming episodes reveals a variable locomotor space at 3 dpf that is recapitulated following DDT-D4R perturbations. This suggests that these three locomotor parameters are set and modulated by distinct neuronal targets, perhaps at disparate regions of the central nervous system.

Elevated Fictive and Free-Swimming Tailbeat Frequencies Following D4R Antagonism or *otpb* Chemogenetic Ablation

We have previously demonstrated that the DDT-D4R network's shortening of episodes is due intrinsically to nervous system development and not to any other factors such as: 1) behavioral influences from other fish in the same arena 2) whether or not the swim bladder is inflated 3) vision 4) posture 5) proprioception 6) muscle physiology or 7) swimming trajectories (Lambert et al., 2012). This is because none of these factors are present or used in fictive preparations in which larvae are isolated, paralyzed, and optionally placed in the dark (Masino and Fetcho, 2005), yet peripheral nerve recordings of the fictive neural locomotor pattern reveals that blocking endogenous D4R signaling or chemogenetic ablation of the DDT still results in immature-like long fictive swimming episodes compared to controls (Lambert et al., 2012). Since fictive tailbeat frequencies correspond well to free-swimming tailbeat frequencies that directly influence swimming speeds (McLean et al., 2007; 2008; McLean and Fetcho, 2009), we performed peripheral nerve recordings and examined the fine temporal structure within each fictive swimming episode (Fig 4A) to test the hypothesis that DDT-D4R perturbations increase fictive peak tailbeat frequencies (Fig 4B) equatably to the observed increase in free-swimming peak speeds (Fig 2A2, 2C2). Complementing these fictive experiments, we recording high-spatiotemporal video recordings, at 210 Hz, of free-swimming larvae at different developmental stages and under DDT-D4R perturbations and tracked the undulatory skeleton of each tracked larvae to readout its segmental angular velocities (Fig 4C) and quantify resultant peak free-swimming tailbeat frequencies (Fig 4D).

Developmentally, 3 dpf larvae exhibited significantly faster fictive ($p < 0.001$) (Fig 4A,B) and free-swimming ($p < 0.001$) (Fig 4C,D) tailbeat frequencies compared to at 4 dpf and beyond, which corroborates previous studies in both the absolute magnitude of these mean peak frequencies and their progressive slowing after the developmental switch (Buss and Drapeau, 2001). Strikingly, blocking endogenous D4R signaling also significantly increased fictive ($p < 0.001$) (Fig 4A,B) and free-swimming ($p < 0.001$) (Fig 4C,D) tailbeat frequencies compared to age-matched controls, and the same fictive ($p < 0.001$) (Fig 4A,B) and free-swimming ($p < 0.001$) (Fig 4C,D) increase occurred via chemogenetic ablation of the DDT in Ntr+ Mtz+ larvae compared to Ntr- Mtz+ controls. Collectively, these results reveal that the DDT-D4R network also acts to slow free-swimming and fictive tailbeat frequencies, and the latter indicates that it likely does so by modulating neuronal motor centers, just as it does for episode duration (Lambert et al., 2012), rather than from influencing any of the many factors absent in the isolated and paralyzed fictive preparation.

D4R Agonism in the Spinal Cord Slows Fictive Tailbeat Frequencies

Since the DDT-D4R network putatively affects both episodic locomotor patterning (Lambert et al., 2012) and tailbeat frequencies (Fig 4) ,via direct modulation of neural motor centers, and is sufficient to act on D4Rs directly in the spinal cord

for fictive episodic patterning (Lambert et al., 2012), we investigated whether the DDT-D4R influence on fictive tailbeat frequencies can also be achieved directly in the spinal cord. To test this, we examined peripheral nerve recordings of the fictive locomotor patterns of spinalized animals at 4–7 dpf (Fig 5A), in which the spinal cord was isolated from the brain to remove all descending inputs, including the DDT. Because fictive swimming in spinalized preparations does not occur spontaneously but can be elicited with NMDA (McDearmid and Drapeau, 2006), we added NMDA (50 μM) to induce fictive locomotor output and subsequently tested the effects of exogenous application of DAergic agonists, as we've previously described (Lambert et al., 2012).

There was a significant difference in the mean fictive tailbeat frequencies among the spinalized experimental groups ($p < 0.001$) (Fig 5B). Compared to the fictive tailbeat frequencies within coordinated long fictive swimming episodes in NMDA alone, application of exogenous DA, a broad-spectrum D2-like (D2R, D3R, D4R) agonist, or a specific D4R agonist significantly slowed the fictive tailbeat frequencies within coordinated DAergic-induced short fictive swimming episodes ($p < 0.001$ for each pairwise comparison of NMDA alone to the three DAR agonist treatments) (Fig 5A,B). Conversely, there were no significant differences among the mean fictive tailbeat frequencies of the three DAR agonist treatments ($p > 0.05$ for all pairwise comparisons) (Fig 5B). These results demonstrate that exogenous DA, which putatively emulates endogenous DAergic input from the

DDT in spinalized preparations, or specific D4R agonism is sufficient to act directly in the spinal cord to slow fictive swimming. This suggests that the endogenous DDT-D4R circuit can act in the spinal cord to slow free-swimming as well, perhaps by biasing the known spinal premotor and motor recruitment topographies to inhibit faster components in favor of slower ones (McLean et al., 2007; 2008).

High-Throughput Automated Detection and Analyses of Hunting Sequences in Free-Swimming Zebrafish Larvae

Many correspondences and experiments conspire to suggest that the neural circuits for spontaneous swimming are employed for execution of the hunting locomotor repertoire because: 1) the advent of hunting coincides with the advent of the newly acquired fine spontaneous locomotor repertoire (Borla et al., 2002) 2) fine spontaneous swimming conspicuously resembles much of the concurrently acquired hunting locomotor repertoire (Budick and O'Malley, 2000) 3) ontogenies of the spontaneous locomotor repertoire and prey capture performance coincide (Fig 1) and 4) DDT-D4R perturbations of the spontaneous locomotor repertoire concomitantly compromise prey capture performance (Fig 2). Consequently, we hypothesized that detailed kinematic analyses of fish-prey interactions during hunting sequences would reveal that D4R antagonism

induces more coarse and erratic hunting maneuvers, in which case this would be divulged as the mechanism for compromised prey capture performance (Fig 2D).

We decided to develop a new high-throughput, unbiased, automated methodology for prey capture kinematic analyses in free-swimming zebrafish larvae, since the current state of the field has been limited to manual and biased detections of multiple individual hunting sequences and subsequent laborious analysis of each individual hunting sequence separately (Borla et al., 2002; McElligott and O'Malley, 2005; Bianco et al., 2011; Patterson et al., 2013). The crux of our approach was in automating tracking of eye convergences, which manual assessments have determined to be a specific and reliable hallmark of prey detection and pursuit during the entire duration of each prey encounter (Bianco et al., 2011). This automation was achieved by the following. After individually tracking the body of each zebrafish larva within a group of four larvae in the same arena (Fig 6A), we used each larva's global orientation to generate a new video in a fish-centered reference frame for each fish, such that each global video frame was rotated with respect to the orientation of each fish and cropped about the head (Fig 6B). This facilitated the continuous automated tracking of each eye (Fig 6B) and computation of instantaneous differences in eye angles (Fig 6C) over the entire video record. Sequences of eye convergences that exceeded 45 degrees and lasted for a minimum of 250 ms were classified as hunting sequences (Fig 6B, bottom image; Fig 2C, e.g. of hunting sequence), as

this criteria is consistent with the eye convergence angle threshold and minimum hunting duration of manually detected hunting sequences (Bianco et al., 2011; Patterson et al., 2013; Trivedi and Bollmann, 2013).

The timestamps of these hunting sequences were fed into our swim detection script in order to index the multivariable locomotor record into hunting and non-hunting sequences (Fig 6D), isolating the hunting and spontaneous locomotor repertoires, respectively. For hunting sequences, each locomotor maneuver executed during each hunt was indexed to: its hunt number, its sequential order relative to the other maneuvers within the same hunt, each of its computed locomotor parameters, and its maneuver type classification. The indexed multivariable locomotor parameters per hunting maneuver were used to automate maneuver classification (Fig 6E; see Methods for maneuver definitions and classifications) based on characterizations of the five maneuver types (Budick and O'Malley, 2000; Borla et al., 2002; McElligott and O'Malley, 2005). Finally, to examine detailed fish-prey kinematics within our automatically detected hunting sequences, we semi-automated tracking of the pursued paramecium per hunt and then automated analyses of fish-prey kinematics (Fig 6F). Namely, we automated computation of the continuous fish-prey inter-distance and inter-angle throughout the hunting sequence and integrated these functions in registry with the previous automated eye convergence-defined hunting sequence and locomotor records (Fig 6F, right plot). This enabled

computation of the distance-reduction and angle-reduction productivities of each locomotor maneuver within a hunting sequence. Providing proof-of-principle of the fidelity of our various automated detections and classifications, blind manual assessments compared to our automated detections and classifications yielded automated eye convergences having a true eye convergence rate of 96.88 ± 3.96% (*n* = 24 fish; 1117 out of 1153 total comparisons) and automated maneuver-type classifications matching 88.3% of manual classifications (n = 3 fish; 76 out of 86 total comparisons). In sum, this new methodology for high-throughput automation of hunting kinematic analyses endows us with a powerful means to explore the role of endogenous D4R signaling in the many skilled facets of prey capture.

Intact Visual, Oculomotor and Visuomotor Responses to Prey are Undermined by Bradykinesia-Like Execution of Hunting Maneuvers Following D4R Antagonism

We implemented our newfound automated hunting kinematic analyses, in the presence of paramecia, to comprehensively assess the visual, oculomotor, visuomotor, and motor hunting performance of 7 dpf larvae under D4R antagonism compared to DMSO vehicles. Both DMSO vehicle and D4R antagonist groups exhibited a sharp increase in eye convergence angles, compared to non-hunting intervals, at the start of hunts that sustained throughout

the full duration of each hunt until its termination (Fig 7a). There were no significant differences between the magnitudes of eye convergences of the DMSO and D4R antagonist groups at baseline or at the start, middle, or end of hunting sequences ($p > 0.05$ for all pairwise comparisons) (Fig 7A). In terms of convergence frequency, there was no difference between the groups in the number of elicited convergence-defined hunts over the course of 30 minutes in the presence of paramecia ($p = 0.391$) (Fig 7B). Additionally, the mean duration of each convergence-defined hunting sequence was indistinguishable between groups ($p = 0.3893$) (Fig 7C), indicating that the D4 antagonist group remained engaged in each visual oculomotor prey-pursuit for a similar amount of time to controls. Importantly, these results indicate that the D4R antagonist group had similar visual function to detect and respond to prey with appropriate sustained oculomotor eye convergences. In the absence of prey, the number of convergence-defined hunts was extremely rare (DMSO: 6 ± 2, D4 Antag: 4 ± 3 convergences per 30 min). This marked specificity of increases in eye convergences critically depending on the presence of prey or prey-like stimuli and employable vision is well founded, as reported previously for prey-devoid conditions (Bianco et al., 2011), larvae in the presence of paramecia in the dark (Patterson et al., 2013), or blind larvae in the presence of paramecia in the light (Gahtan, 2005).

In terms of visuomotor performance, the mean number of elicited locomotor maneuvers per second of each hunt was not significantly different between groups ($p = 0.1012$) (Fig 7D), although there was a trend for fewer maneuvers from the D4R antagonist group. Of the elicited maneuvers, D4R antagonism induced a significant increase in the percentage of orienting maneuvers and decrease in the percentage of advancing maneuvers compared to DMSO vehicles ($p < 0.01$ and $p < 0.05$, respectively) (Fig 7E). This result divulges a salient D4R antagonist-induced shift in prey-catching motor strategies. Finally, examination of the percentage of execution of each of the five hunting maneuver types revealed further visuomotor insights. Of the orienting maneuver types, D4R antagonism induced a robust significant increase in the percentage of elicited j-turns ($p < 0.001$) at the expense of less orienting swims ($p < 0.05$), with no change in the small proportion of executed pectoral fin-driven backups $p = 0.7530$) (Fig 7F). Of the advancing maneuver types, D4R antagonism induced a significant decrease in the percentage of elicited capture swims ($p < 0.05$) but no significant change in the percentage of advancing swims ($p = 0.1025$), although there was a trend for a decrease (Fig 7F). These results indicate that D4R antagonism keeps visuomotor responses intact for a similar number of prey-induced maneuver initiations, but that the resultant prey-catching strategy is shifted to one of primarily orienting rather than advancing toward prey.

Despite most of the aforementioned metrics of visual, oculomotor, and visuomotor performance being similar between groups, there was a marked increase in the final percent of paramecia remaining in the presence of the D4 antagonist group at 7dpf compared to DMSO vehicle (Fig 7G), just as occurs at 5 dpf (Fig 2B). While D4 antagonism at 7 dpf induced an immature spontaneous non-hunting locomotor repertoire of long, fast, erratic episodes, similar to at 5 dpf (Fig 2C), isolating the specific convergence-defined hunting locomotor repertoire revealed that it surprisingly occupied an invariably fine locomotor regime similar to that of DMSO vehicles during hunting (Fig 7H; Table 3). All three key locomotor parameters were of significantly smaller magnitude for the D4R antagonist group during hunting compared to non-hunting (Fig 7H; Table 3). For the DMSO group, peak swimming speed and total turn angle, but not episode duration, were significantly smaller during hunting compared to non-hunting (Fig 7H; Table 3). Interestingly, D4R antagonism induced a significantly slower peak swimming speed ($p < 0.001$), but with no differences in episode duration ($p = 0.261$) or turning angle ($p = 0.767$), during hunting compared to that of DMSO vehicles during hunting (Fig 7I; Table 3). Collectively, these results reveal that blocking endogenous D4R signaling makes otherwise intact visual and oculomotor responses undermined by bradykinesia-like slow forward execution of hunting maneuvers, which could underlie poor prey capture performance. This putative failure in advancing toward prey could induce the observed compensatory shift to a primarily orienting visuomotor prey-catching strategy,

since the precision of fine turning maneuvers during hunting is still comparable to that of controls.

Inability to Reduce Distance but not Angular Heading Toward Prey Following D4R antagonism

To pinpoint the precise failure of prey capture following D4R antagonism, we semi-automatically tracked the pursued paramecium and subsequently automated fish-prey kinematic analyses of fish-prey inter-distances and inter-angles as a function of each maneuver within the hunt for DMSO vehicles (Fig 8A) and the D4R antagonist group (Fig 8B). The distance-reduction productivity per maneuver for the D4R antagonist group, compared to DMSO vehicles, was significantly worse for every maneuver within the hunting sequence except the first maneuver ($p < 0.001$ for 2nd, 3rd, and 4th maneuvers; $p = 0.451$ for 1st maneuver) (Fig 8C). Conversely, the angle-reduction productivity per maneuver for the D4R antagonist group, compared to DMSO vehicles, was just as good for every maneuver within the hunting sequence except the last maneuver in the sequences observed in the D4R antagonist group ($p > 0.3$ for 1st, 2nd, and 3rd maneuvers; $p < 0.01$ for 4th maneuver) (Fig 8D). The only reason the last maneuver in the sequence was unable to continue reducing fish-prey inter-angle was because the paramecium ultimately got away and obtained a large fish-prey inter-distance (data not shown), and zebrafish larvae can only detect and

maintain pursuit of paramecia within a ~ 4 mm half-circle about the head (Gahtan, 2005; McElligott and O'Malley, 2005; Patterson et al., 2013). Taken together, these fish-prey kinematics, compounded by our automated isolation and comprehensive hunting-specific visuomotor and locomotor assessments, reveal that D4R antagonism induces a bradykinesia-like advancing maneuver phenotype that results in an inability to reduce distance but not angular heading toward prey. Hence, this underscores the specificity in the deficit in hunting performance and suggests that there exist separate neural modules for execution of orienting and advancing maneuvers.

Intact Prey Capture Success Following D1R Antagonism, Despite a Perturbed Spontaneous Locomotor Repertoire and Aberrent Prey-Directed Episodic and Turning Patterns

Blocking endogenous D4R signaling differentially influenced spontaneous and hunting locomotor repertoires, inducing a perturbed coarse and erratic spontaneous locomotor phenotype that was powerfully and invariably overridden to attempts at fine and directed motor control during hunting (Fig 7H, I; Table 3), albeit these attempts failed due to being excessively slow (Fig 7I; Table 3). This suggests that there may exist separate neural modules for execution of spontaneous versus hunting locomotor repertoires. Further supporting this scenario, an initial screen of the effects of various DAR antagonists on prey

capture performance and spontaneous locomotion at 7dpf revealed that larvae subjected to D1R antagonism had just as good of final prey capture performance as DMSO vehicles (both groups consume 100% of paramecia by 5 hours) (Fig 9A) despite a dramatic relegation to a coarse and erratic spontaneous locomotor repertoire (Fig 9B; Table 4). Isolation of the convergence-defined hunting locomotor repertoire following D1R antagonism revealed significantly greater episode durations ($p < 0.05$) and turning angles ($p < 0.001$) compared to DMSO vehicles, but with no difference in the peak speed of executed hunting maneuvers ($p = 0.392$) (Fig 9C; Table 4). Hence, D1R antagonism induced an altered episodic and turning pattern during hunting but maintained similar pursuit speeds to controls, which still yielded normal prey capture success. Conversely, D4R antagonism did not alter episodic or turning patterns during hunting but did significantly reduce pursuit speeds (Fig 7I) and prey capture success (Fig 7G). Combinatorially, these results reveal that prey-directed patterning of episode durations and turn angles is flexible within a certain range to still yield hunting success and, chiefly, isolates that D4R-modulated pursuit speed is crucial for prey capture success.

Discussion

We developed a novel high-throughput approach to investigating prey capture in zebrafish and elucidated that endogenous D4R signaling specifically regulates goal-directed motor strategies and execution of the prey-advancing regime. The DDT-D4R network is a meta-locomotor modulator of spontaneous swimming that contributes to fine precision of episodic patterning, turning, and speed control. DDT-D4R perturbations relegate larvae to coarse and erratic spontaneous swimming that is invariably overridden to attempts at fine motor control during visually-guided hunting. Comprehensive, automated, hunting kinematic analyses unveil that normal prey-directed visual, oculomotor, visuomotor, and motor orienting functions following D4R antagonism are undermined by a bradykinesia-like loss of fine speed control during prey-advancing maneuvers. This deficit induces a compensatory shift to an orienting prey-catching strategy that nevertheless fails, specifically due to the inability to ultimately advance toward prey. Hence, D4R-mediated speed control isolates as a critical determinant of prey capture success. Collectively, we posit a modular organization subserving a versatile locomotor network, wherein separate neural modules are recruited spontaneously and during hunting and that the hunting module is further subdivided into separable orienting and advancing regimes.

Versatility of Automated Prey Capture Analyses for High-Throughput Pharmacological and Genomic Screens *In Vivo*

This is the first prey capture study to employ a high-throughput, unbiased, and automated means of detecting and analyzing hunting sequences in free-swimming zebrafish larvae. This approach will finally enable high-throughput unbiased pharmacological (Kokel et al., 2010; Rihel et al., 2010; Wolman et al., 2011) and genomic screens (Burgess and Granato, 2007a; Petzold et al., 2009; Wolman and Granato, 2012) for specific phenotypes exploited during goal-directed prey capture. Given the rich integrative nature of prey capture behavior, such screens will serve as a versatile and long-standing neuroethological platform for investigating its sensory, sensorimotor, motor, neuromodulatory, engrammic, attentional, and decision-making components (Ewert et al., 1999; 2001; Muto and Kawakami, 2013). Isolation of auspicious compounds and mutants following high-throughput prey capture screening can then be targeted for tethered virtual prey-pursuit (Trivedi and Bollmann, 2013; Preuss et al., 2014), during concurrent bidirectional optogenetic control (Douglass et al., 2008; Arrenberg et al., 2009; Wyart et al., 2009; De Marco et al., 2013; Kimura et al., 2013; Ljunggren et al., 2014) and whole-brain calcium/voltage imaging (Ahrens et al., 2012; 2013a; 2013b), to elucidate the causal mechanism of specific neural modules to elementary components of goal-directed behavior. Hence, our newly developed approach to high-throughput screening of prey capture will merge

investigations of goal-directed behavior in zebrafish to the more integrative recruitment and deployment that it deserves.

Endogenous D4R Signaling is Necessary for Prey Capture: Source DAergic Population and its D4R Site of Action

The crux of our findings significantly advances the elucidation of DAergic control of prey capture and suggests its conserved function from zebrafish to anurans. While exogenous DAergic agonism in anurans has been shown to inhibit orienting maneuvers in favor of advancing snapping maneuvers (Glasgow and Ewert, 1996; Glasgow and Ewert, 1997a; Glasgow and Ewert, 1997b; Glasgow and Ewert, 1999), it has remained unknown as to: 1) whether this exogenous DAergic phenomenon has a corresponding endogenous DAergic counterpart 2) which DAergic population may mediate state-dependent switching in prey-catching strategies 3) the specific DAR subtype through which this DAergic influence signals and 4) the anatomical postsynaptic site of action of this DAergic signaling. Our findings provide evidence that either answers or sheds more light on each of these questions.

Prey Capture Strategy, Execution, and Success Depends on Endogenous D4R Signaling. My study elucidates that endogenous DA, via D4R signaling, is necessary for determining prey-catching strategies in zebrafish and further

reveals a detailed kinematic analysis of the failed execution of advancing but not orienting maneuvers. Consistent with the exogenous effects in anurans, D4R antagonism in zebrafish shifts animals to an orienting prey-catching strategy while DAergic agonism in anurans shifts animals to an advancing (or snapping) prey-catching strategy (Glagow and Ewert, 1996; 1999). This suggests conversation in the DAergic role in prey capture. Our use of DAR pharmacology to reveal the specificity of D4R signaling to prey capture is well validated since the high fidelity of these compounds to acting specifically on the corresponding endogenous receptors *in vivo* has been confirmed in zebrafish (McLean et al., 2007; 2008). Most powerfully and germanely, a recent comprehensive study demonstrated that morpholino mRNA knockdown of a specific D4R transcript recapitulates specific physiological and anatomical outcomes of pharmacological D4R antagonism and, moreover, occludes D4R agonism rescue of local D4R-mediated changes in the spinal cord following multiple different methods of DDT ablation (Kinkhabwala et al., 2011; Koyama et al., 2011).

Corroborating the conclusion that the D4R antagonism phenotype during prey capture is not merely a general DAergic phenomenon, our blocking of endogenous D2D3R signaling had no effect on prey capture performance (data not shown) but does have marked physiological and behavioral consequences in other contexts in zebrafish (Binder et al., 2014; Severi et al., 2014; Wang and McLean, 2014). Furthermore, our blocking of endogenous D1R signaling

perturbed spontaneous swimming similar to that of D4R antagonism but, unlike D4R antagonism: 1) did not impair prey capture success 2) did not impair prey-directed fine speed control but 3) did alter prey-directed episodic and turning motor patterns. Beyond dissociating unique hunting phenotypes from D1R and D4R antagonism, the compounding conclusion is that prey-directed patterning of episode durations and turn angles is flexible within a certain range to still yield hunting success and, conversely, isolates that D4R-modulated pursuit speed is crucial for prey capture success.

DDT as a Putative DAergic Source Driving D4R-Modulation of Prey Capture. The DAergic *otpb* neurons and the DDT are already linked to D4R-mediated episodic locomotor patterning (Brustein et al., 2003; Lambert et al., 2012) and, here, chemogenetic ablation of the DDT recapitulated the D4R antagonism-induced relegation to the immature spontaneous locomotor repertoire. As such, the DDT network is likely involved in driving the D4R signaling crucial to motor-centric aspects of prey capture, but the caveats of the chemogenetic ablation employed (Buss and Drapeau, 2001) - only exploited by examining hunting at 5 dpf or by ablating the cells at a later time point that induces lethality - require an alternative strategy to investigating the germane role of the DDT in goal-directed hunting. Future studies that selectively ablate each *otpb* population separately *in vivo*, such as via targeted laser ablations (Budick and O'Malley, 2000), should clear this up and, moreover, potentially provide a means to selectively ablate the

DAergic *otpb* population and DDT and examine its consequences on locomotion and prey capture.

Postsynaptic Site of Action of D4R Influences on Prey Capture and Meta-Locomotor Modulation Via Laser Ablations of DDT Network. Even if the DAergic *otpb* neurons and DDT network were definitively confirmed to drive the D4R influences of prey capture, the postsynaptic site of action could still potentially occur anywhere across the rostral-caudal neuraxis, because the DDT fiber network spans continuously from telencephalon to spinal cord (Gahtan, 2005) (Fig 10A,B). Systematic visually-guided *in vivo* laser ablations (Borla et al., 2002; McElligott and O'Malley, 2005; Bianco et al., 2011; Patterson et al., 2013) at different points along the DDT fiber network (Fig 10A,B) would represent an excellent means to determine if the DDT network is truly involved in the specific D4R influences on prey capture and, if so, its anatomical site of action. Preliminary data of a unilateral DDT laser ablation at 6 dpf, at the level of the rostral spinal cord, has revealed a striking increase in episode durations post- versus pre-ablation (Fig 10C), which is promising for future experiments which will ablate the DDT to test its consequences on prey capture. Additionally, it provides more direct *in vivo* evidence for the DDT acting specifically in the spinal cord to shorten swimming episodes (Bianco et al., 2011). Importantly, although *otpb* diencephalospinal projections could potentially originate from both the tyrosine hydroxylase (TH)+ DAergic and TH- non-DAergic *otpb* populations (Fig

10D) (Rose and Moore, 2002; Kerman, 2008; Lohr et al., 2009; Lambert et al., 2012), we have evidence that virtually all *otpb:egfp-caax* fibers in the spinal cord are positive for TH (Fig 10E,F,G). This confirms that virtually all of the *otpb* diencephalospinal projections originate primarily or exclusively from the TH+ DAergic *otpb* population and, consequently, represent a specific fluorescent reporter to visualize and laser ablate the DDT. Complementary experiments that either laser ablate the DDT fibers at different rostro-caudal locations within the brain, or laser ablate the cell bodies themselves, will be instructive to the potentially multiple disparate sites of action that the DDT-D4R network acts upon to influence prey capture and meta-locomotor modulation, which could be located within the: 1) motor layers of the retinorecipient sensorimotor optic tectum within the midbrain that is necessary for prey capture (Gahtan, 2005; Smear et al., 2007; Del Bene et al., 2010; Fajardo et al., 2013; Muto et al., 2013) 2) tectal-recipient nucleus of the medial longitudinal fasiculus (nMLF), within the midbrain, implicated in forward swimming and prey capture (Gahtan, 2005; Sankrithi and O'Malley, 2010; Binder et al., 2014; Severi et al., 2014; Wang and McLean, 2014) 3) nMLF-recipient reticulospinal (RS) hindbrain neurons involved in driving forward swimming and with a topographic map of recruitment for swimming speed (Kinkhabwala et al., 2011; Koyama et al., 2011) 4) non-nMLF-recipient RS hindbrain “turn” neurons that drive optomotor turning (Orger et al., 2008; Huang et al., 2013) and 5) nMLF-, forward swimming RS-, and “turn” RS- recipient premotor interneurons and motor neurons within the speed-topographic spinal

cord (McLean et al., 2007; 2008; Orger et al., 2008; Koyama et al., 2011; Huang et al., 2013; Wang and McLean, 2014). The vast DDT fiber network comes in close proximity to all of these areas (McLean and Fetcho, 2004a; 2004b; Kastenhuber et al., 2010; Tay et al., 2011; Mu et al., 2012), making it plausible for it to induce such concurrent multisite modulation.

Cogent conjectures can be made as to the potential sites of action of DDT-D4R meta-locomotor modulation and prey capture influence. Our spinalized experiments show that spinal DAergic or D4R agonism is sufficient to slow fictive swimming frequencies, suggesting that the DDT can act directly in the spinal cord for swimming frequency modulation, in addition to episodic patterning (Lambert et al., 2012), since the DDT is the sole source of endogenous DA in the spinal cord (Kastenhuber et al., 2010; Tay et al., 2011; Reimer et al., 2013). This suggests that the DDT may slow swimming by preferentially providing tonic inhibitory D4R input to components of the spinal topographic map that are recruited for faster swimming frequencies, such as: primary motor neurons, dorsal secondary motor neurons, dorsal glutamatergic interneurons (e.g. V2as), or ventral glycinergic interneurons (e.g. circumferential descending interneurons (CiDs)) (McLean et al., 2007; 2008). However, it is quite possible that the DDT exerts a similar inhibitory D4R-induced bias onto the fast components of the hindbrain topographic recruitment pattern for swimming frequency (Kinkhabwala et al., 2011; Koyama et al., 2011). DDT-D4R modulation of spontaneous or prey-

directed turning, conversely, most likely acts at the level of RS “turn” cells in the hindbrain, although these have only been confirmed to be involved in visual grating-induced optomotor turning (Orger et al., 2008; Huang et al., 2013). Finally, advancing maneuvers during hunting could be controlled by the midbrain nMLF since it is involved in spontaneous forward swimming and exquisitely controls and modulates appropriate forward swimming speeds as a function of and in response to the grating speeds of optomotor response-inducing visual stimuli (Severi et al., 2014). If this is the case, the DDT-D4R network may interface with and provide D4R inhibition to the nMLF to facilitate sculpting of fine forward speed control; D4R antagonism may consequently disinhibit the nMLF and induce a loss of precision during attempts at subtle changes in speed gradation during prey pursuit.

Modular Organization of a Versatile Locomotor Network

The DAR antagonism-induced dissociation of spontaneous from hunting locomotor repertoires, as well as orienting from advancing maneuvers, suggests a modular organization subserving a versatile locomotor network. Indeed, the powerful zebrafish model has already dissected distinct neural modules dedicated to specific locomotor features and behaviors, and even for component elements of these behaviors, such as: 1) dorsal versus ventral muscle-innervating motor neurons for parallel and independent dorso-ventral motor

control (Bagnall and McLean, 2014) 2) spinal episodic patterning generators versus coordination generators (Wiggin et al., 2012) and 3) optomotor-induced turning (Orger et al., 2008; Huang et al., 2013) versus optomotor-induced forward swimming (Severi et al., 2014). However, it has been unknown if there are separate neural modules dedicated to spontaneous versus prey-directed swimming, as well as if there are distinct neural modules each dedicated to the different elementary components of prey capture. Our findings posit that this modular granularity is present at both levels and that endogenous D4R signaling, perhaps through a widespread integrative impetus at disparate regions via the extensive DDT network, differentially influences each module concurrently.

Figure Legends

Fig 1: Concurrent Ontogenesis of the Spontaneous Locomotor Repertoire and Prey Capture Performance. A1) angular velocity (black function) and smoothed orientation (red function) (both in degrees/sec) as a readout of body undulations and turning from an example larval swimming episode at 3, 4, and 7 dpf. Colored labels for each group correspond to and denote data groups in A2. **A2)** Multivariable plot of the distribution of individual means of episode duration (ms), peak speed (mm/sec), and total turn angle (degrees) for 3, 4, and 7 dpf groups, as denoted to the left in A1. **B1)** Time-lapse images from the z-stacks of the SD of pixel intensities from a 3-sec 60-Hz video-recording of 10 fish in a 60 mm petri dish at 0 and 5 hr post-incubation of paramecia. ImageJ was used to filter out the large zebrafish (top) from the small paramecia trajectories (bottom). **B2)** The percent paramecia remaining each hour for 5 hrs post-incubation with paramecia, in the presence of no fish and 3, 4, and 7 dpf fish.

Fig 2: Blocking Endogenous D4R signaling or Chemogenetic Ablation of the DDT Relegates Larvae to an Immature Spontaneous Locomotor Repertoire and Impairs Prey Capture Performance. A1) Angular velocity (black function) and smoothed orientation (red function) (both in degrees/sec) as a readout of body undulations and turning from an example larval swimming episode at 5 dpf in either DMSO or a D4R antagonist (D4 Antag). Colored labels

for each group correspond to and denote data groups in A2. **A2)** Multivariable plot of the distribution of individual means of episode duration (ms), peak speed (mm/sec), and total turn angle (degrees) for 5 dpf DMSO and D4 Antag groups, as denoted to the left in A1. **B)** The percent paramecia remaining each hour for 5 hrs post-incubation with paramecia, in the presence of DMSO or D4 antag fish. **C1)** Angular velocity (black function) and smoothed orientation (red function) (both in degrees/sec) as a readout of body undulations and turning from an example larval swimming episode at 5 dpf from either the Ntr- Mtz+ or Ntr+ Mtz+ group (latter is chemogenetic ablation of DDT). Colored labels for each group correspond to and denote data groups in A2. **C2)** Multivariable plot of the distribution of individual means of episode duration (ms), peak speed (mm/sec), and total turn angle (degrees) for 5 dpf Ntr- Mtz+ and Ntr+ Mtz+ groups, as denoted to the left in C1. **D)** The percent paramecia remaining each hour for 5 hrs post-incubation with paramecia, in the presence of untreated, Ntr- Mtz+, or Ntr+ Mtz+ antag fish. **E)** Experimental timeline for earlier (top) versus later (bottom) Mtz-induced chemogenetic ablation of *otpb* neurons and the DDT **F)** and **G)** Same as C2 and D but for 7 dpf Ntr- Mtz+ and Ntr+ Mtz+ groups subjected to later Mtz treatment (4-6 dpf instead of 1-4 dpf).

Fig 3: Dissociable Meta-Locomotor Modulation by the DDT-D4R Network. Scatter plots and linear regressions of the distribution of all individual swimming episodes across animals for episode duration as a function of **(A,D,G)** speed or

(B,E,H) turning and their **(C,F,I)** corresponding goodness of fits (R2) for (**A,B,C)** different aged groups (3, 4 and 7 dpf), (**D,E,F)** DMSO and D4 antag groups, and (**G,H,I)** Ntr- Mtz+ and Ntr+ Mtz+ groups. Numbers at the base of bars in bar graphs denote the total number of swimming events analyzed for each experimental group.

Fig 4: Elevated Fictive and Free-Swimming Tailbeat Frequencies Following D4R Antagonism or *otpb* Chemogenetic Ablation. A) Voltage traces of peripheral nerve recordings of intact spontaneous fictive swimming showing episodic patterning in left insets, with a bar denoting the time course expanded in the right traces. Right traces show bursting structure and frequency, which corresponds to free-swimming tailbeat frequencies, and the peak burst frequency within the entire episode is demarcated. **B)** Quantification of mean peak burst frequencies developmentally and following DAR antagonism or following Mtz- or Mtz+ for Ntr- or Ntr+ larvae. **C)** Angular velocity of the caudal-most segment of the tracked zebrafish skeleton for entire free-swimming episodes in left insets, with a bar denoting the time course expanded in the right traces. Right traces show free-swimming undulatory tailbeat structure and frequency, and the peak tailbeat frequency within the entire episode is demarcated. **D)** Quantification of mean peak tailbeat frequencies developmentally and following DAR antagonism or following Mtz- or Mtz+ for Ntr- or Ntr+ larvae. Numbers at the base of bars in bar graphs denote the number of fish for each experimental group.

Fig 5: D4R Agonism in the Spinal Cord Slows Fictive Tailbeat Frequencies. **A)** Voltage traces of peripheral nerve recordings of spinalized NMDA-induced fictive swimming showing episodic patterning in left insets, with a bar denoting the time course expanded in the right traces. Right traces show bursting structure and frequency **B)** Quantification of mean peak burst frequencies in NMDA alone and following various types of DAergic agonism. Numbers at the base of bars in bar graphs denote the number of fish for each experimental group.

Fig 6: High-Throughput Automated Detection and Analyses of Hunting Sequences in Free-Swimming Zebrafish Larvae. A) The bodies of 4 fish individually tracked in a 20 mm hunting arena. **B)** Frames from newly generated video in a fish-centered reference frame, obtained from iteratively rotating each frame to the global orientation of the fish and cropping about the head. This enables stable tracking of the left eye and angle (red ellipse and line) and right eye and angle (green ellipse and line) to detect an increase in eye convergences from non-hunting (top) to hunting (bottom). **C)** Unbiased eye convergence angle from automated eye tracking. A sustained increase in eye convergence angle specifically and invariably occurs during hunting (Bianco et al., 2011; Patterson et al., 2013; Trivedi and Bollmann, 2013). **D)** Convergence-defined indexing of hunting and non-hunting sequences in register with three key locomotor

parameters - angular velocity (degrees/sec), smoothed orientation (degrees/sec), and instantaneous speed (mm/sec) - from the multivariable locomotor record. **E)** Classification of hunting maneuvers via the kinematic features deduced from the multivariable locomotor record. **F)** Left: Semi-automated tracking of the pursued paramecium within an automated convergence-defined hunt, denoting the fish-prey inter-distance (d, red) and inter-angle (σ, blue), the continuous functions of which are plotted to the right in register with locomotor maneuvers during an example hunt.

Fig 7: Intact Visual, Oculomotor and Visuomotor Responses to Prey are Undermined by Bradykinesia-Like Execution of Hunting Maneuvers Following D4R Antagonism. Comparisons of the following for DMSO and D4 Antag groups at 7 dpf. **A)** Mean eye convergence angle (degrees) spontaneously (non-hunting) and at the start, middle, and end of hunts. **B)** Number of convergence-defined hunts in the presence of paramecia for 30 min. **C)** Mean eye convergence hunt duration (sec). **D)** Number of locomotor maneuvers per sec of hunt. **E)** Percent of orienting versus advancing maneuvers. **F)** Percent of each of the five automatically-classified hunting maneuvers. **G)** Percent paramecia remaining each hour for 5 hrs post-incubation with paramecia. **H)** Multivariable plot of the distribution of individual means of episode duration (ms), peak speed (mm/sec), and total turn angle (degrees), both spontaneously (non-hunting) and during convergence-defined hunting. **I)**

Expansion of bottom right portion of locomotor cube in H, showing similarities (episode duration and total turn angle) and differences (peak speed) in the hunting locomotor repertoires of DMSO and D4 antag larvae.

Fig 8: Inability to Reduce Distance but not Angular Heading Toward Prey Following D4R antagonism. Comparison of **A)** DMSO and **B)** D4 Antag larvae in terms of fish-prey inter-distance (red, mm) and inter-angle (blue, degrees) as a function of the sequence of locomotor maneuvers and their speeds. Quantification of the mean productivities of each locomotor maneuver to reduce **C)** fish-prey inter-distance or **D)** inter-angle.

Fig 9: Intact Prey Capture Success Following D1R Antagonism, Despite a Perturbed Spontaneous Locomotor Repertoire and Aberrant Prey-Directed Episodic and Turning Patterns. Comparisons of the following for DMSO and D1 Antag larvae at 7 dpf. **A)** Percent paramecia remaining each hour for 5 hrs post-incubation with paramecia. **B)** Multivariable plot of the distribution of individual means of episode duration (ms), peak speed (mm/sec), and total turn angle (degrees), both spontaneously (non-hunting) and during convergence-defined hunting. **I)** Expansion of bottom right portion of locomotor cube in B, showing similarities (peak speed) and differences (episode duration and total turn angle) in the hunting locomotor repertoires of DMSO and D1 antag larvae.

Fig 10: Laser Ablations of *otpb* DAergic DDT Network. A) Lateral and **B)** dorsal views of confocal z-stacks of the brain and spinal cord of a 5 dpf zebrafish larva expressing membrane-targeted GFP (egfp:caax) driven by the otpb.A enhancer line (Fujimoto et al., 2011), delineating ascending and descending projections from diencephalic *otpb* neurons. The lateral and dorsal stacks were pseudocolored in ImageJ and are 40 μm and 60 μm, respectively. Dashed boxes denote the approximate location of the DAergic optb population, as the Tg(*otpb.A:egfp-caax*) line labels the fibers well but not the source somata. Vertical dashed line represents the hindbrain-spinal cord junction between body segments 2 and 3. The prominent *otpb* DDT can be seen projecting well into the spinal cord to the right. **C)** Preliminary experiment from a 6 dpf larvae subjected to a unilateral DDT laser ablation in the rostral spinal cord, showing a marked increase in the distribution of free-swimming episode durations post- compare to pre-ablation. Post-ablation video-recording was made ~ 3 hrs post-ablation. **D)** Confocal z-stack of a dorsal view in a 7 dpf Tg(*otpb.A:nitroreductase-egfp*) larva to visualize the separable locations of the non-DAergic and DAergic *otpb* somata, making them amenable for individually targeted laser ablations. **E-G)** Lateral view in the spinal cord of **E)** a 3 dpf Tg(*otpb.A:egfp-caax*) larva with **F)** TH IHC showing **G)** strong co-localization of TH to *otpb* diencephalospinal projections in the spinal cord, confirming that these fibers originate from the DAergic *otpb* somata almost exclusively.

Tables 1, 2, 3, and 4. Multivariable locomotor record of the Mean ± SD of each computed locomotor parameter. Parameters which were targeted a priori for statistical analyses are highlighted in yellow. Statistically significant pairwise differences between a given group and its comparator (comparator denoted by a red box: Table 1 is 4dpf; Table 2 is 5 dpf DMSO; Table 3 is 7 dpf 20mm Spont; Table 4 is 7 dpf 20mm Spont) are highlighted in red where * = $p < 0.05$, ** = $p < 0.001$, and *** = $p < 0.001$. All data are representative of a 10 minute period of behavior unless otherwise noted. **All 50 parameter definitions are as follows:**

1) # episodes: total number of episodes in record

2) very_slow_episode_count: number of episodes with mean speed < 1.5 mm/sec

3) episode_duty_cycle: global episode duty cycle; proportion of sum of episode durations to the total record length

4) left_turn_count: number of left turns in entire record

5) right_turn_count: number of right turns in entire record

6) percent_episodes_turning (%): percent of episodes containing at least 1 turning event

7) total_distance_traveled (mm): total distance traveled in entire record

8) mean_dist2wall_all (mm): mean distance to wall over entire record

9) episode_duration (ms): duration from the start to end of an angular velocity episode for all episodes

10) displacement_episode_duration (ms): duration from the start to end of an angular velocity episode for episodes with a mean speed > 3 mm/sec

11) stationary_episode_duration (ms): duration from the start to end of an angular velocity episode for episodes with a mean speed < 1.5 mm/sec

12) speed_episode_duration (ms): duration from the start to end of an episode detected via swimming speed, as done previously in (Lambert et al., 2012)

13) episode_frequency (Hz): episodes per sec (Hz)

14) episode_mean_burst_frequency (Hz) * : mean tailbeat frequency in episode

15) episode_peak_burst_frequency (Hz) *: peak tailbeat frequency in episode

16) episode_num_tailbeats: number of full cycles of tailbeats in episode

17) episode_mean_speed (mm/sec): mean speed of an episode

18) episode_95th_speed (mm/sec): 95th percentile speed within an episode

19) episode_peak_speed (mm/sec): peak speed within an episode

20) displacement_episode_mean_speed (mm/sec): mean speed of episodes with a mean speed > 3 mm/sec

21) displacement_episode_95th_speed (mm/sec): 95th percentile speed of episodes with a mean speed of > 3 mm/sec

22) displacement_episode_peak_speed (mm/sec): peak speed of episodes with a mean speed of > 3 mm/sec

23) episode_burst_balance (rad; integrated dtheta): integrated angular velocity of entire episode

24) episode_burst_balance_last_50%_episode (rad): integrated angular velocity of last 50% of episode

25) left_turn_duration (ms): duration of individual left turn

26) left_turn_angle (degrees): angle of individual left turn

27) num_left_turns_in_episode: number of individual left turns in episode

28) total_left_turn_duration_in_episode (ms): total duration of all left turns in episode

29) total_left_turn_angle_in_episode (degrees): total angle of all left turns in episode

30) episode_phasing_of_left_turns (ms after start): phasing of individual left turn onsets relative to episode onset

31) right_turn_duration (ms): duration of individual right turn

32) right_turn_angle (degrees): angle of individual right turn

33) num_right_turns_in_episode: number of individual right turns in episode

34) total_right_turn_duration_in_episode (ms): total duration of all right turns in episode

35) total_right_turn_angle_in_episode (degrees): total angle of all right turns in episode

36) episode_phasing_of_right_turns (ms after start): phasing of individual right turn onsets relative to episode onset

37) total_num_turns_in_episode: total number of turns (left and right) in episode

38) total_turn_duration_in_episode (ms): total turning duration (left and right) in episode

39) total_turn_angle_in_episode (degrees): total turning angle (left and right) in episode

40) net_turn_angle_in_episode (degrees): net turning angle (left and right) in episode (such that equal left and right turn angles cancel; gives accurate terminal orientation relative to initial orientation)

41) abs_net_turn_angle_in_episode (degrees): magnitude of vector for net_turn_angle_in_episode

42) nonzero_total_num_turns_in_episode: total number of turns (left and right) for episodes containing at least 1 turn

43) nonzero_total_turn_duration_in_episode (ms): total turning duration (left and right turns) for episodes containing at least 1 turn

44) nonzero_total_turn_angle_in_episode (degrees): total turning angle (left and right turns) for episodes containing at least 1 turn

45) nonzero_net_turn_angle_in_episode (degrees): net turning angle (left and right) for episodes containing at least 1 turn

46) nonzero_abs_net_turn_angle_in_episode (degrees): magnitude of vector for nonzero_abs_net_turn_angle_in_episode

47) total_distance_traveled_episode (mm): total distance traveled per episode

48) dist2wall_episode_onset (mm): distance to wall at episode onset

49) dist2wall_episode_offset (mm): distance to wall at episode offset

50) delta_dist2wall_from_episode (mm): change in distance to wall as a function of episode

sample size (n): number of fish representing data for each experimental group

arena diameter (mm): 50 mm watch-glass was used exclusively for spontaneous free-swimming while 20 mm shallow (1.5 mm depth) arena was used for free-swimming both spontaneously and in the presence of paramecia (hunting).

*** 210 fps (n):** denotes if a high spatiotemporal spontaneous free-swimming recording was made at 210 Hz for the given experimental group, in which the parameters with an * were calculated

Figures

Figure 1

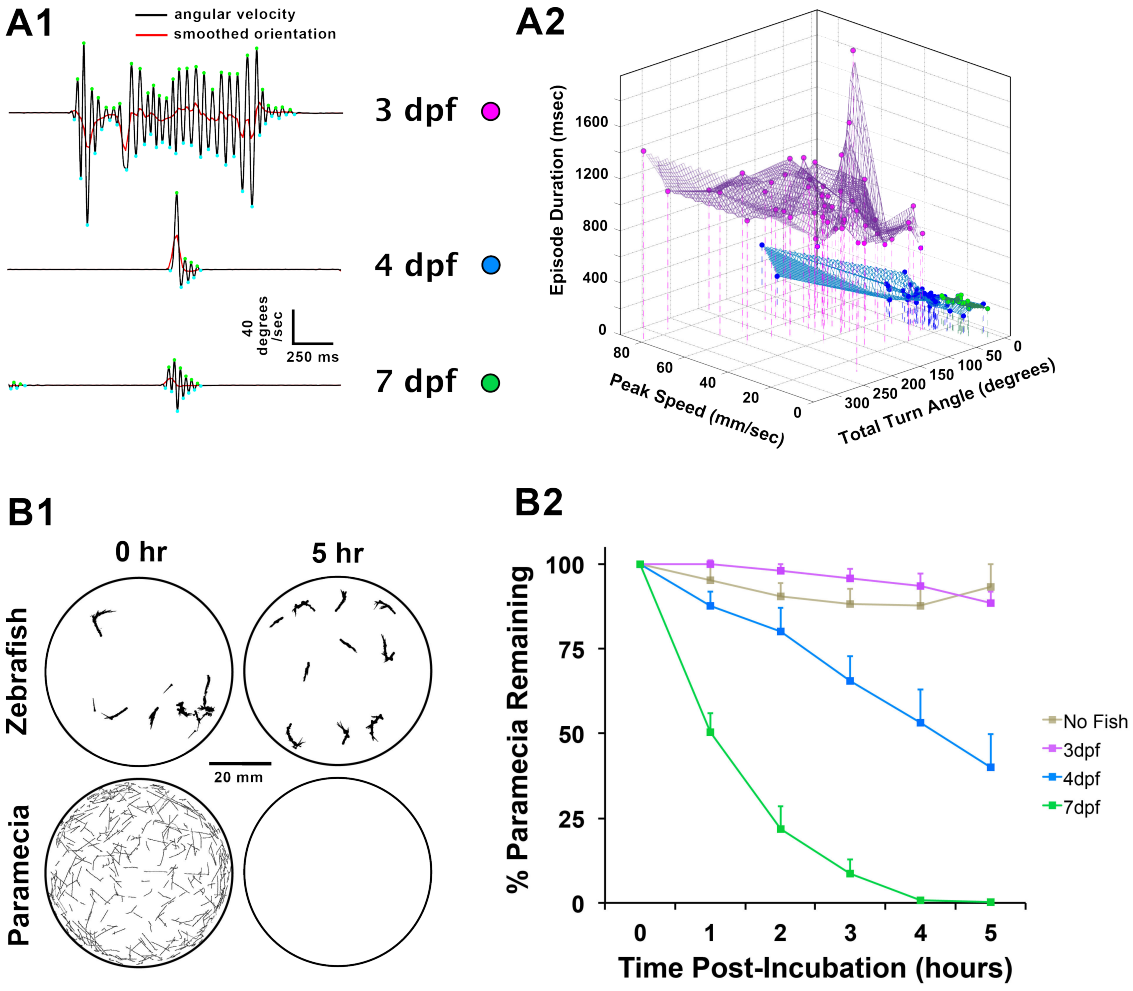

Figure 2

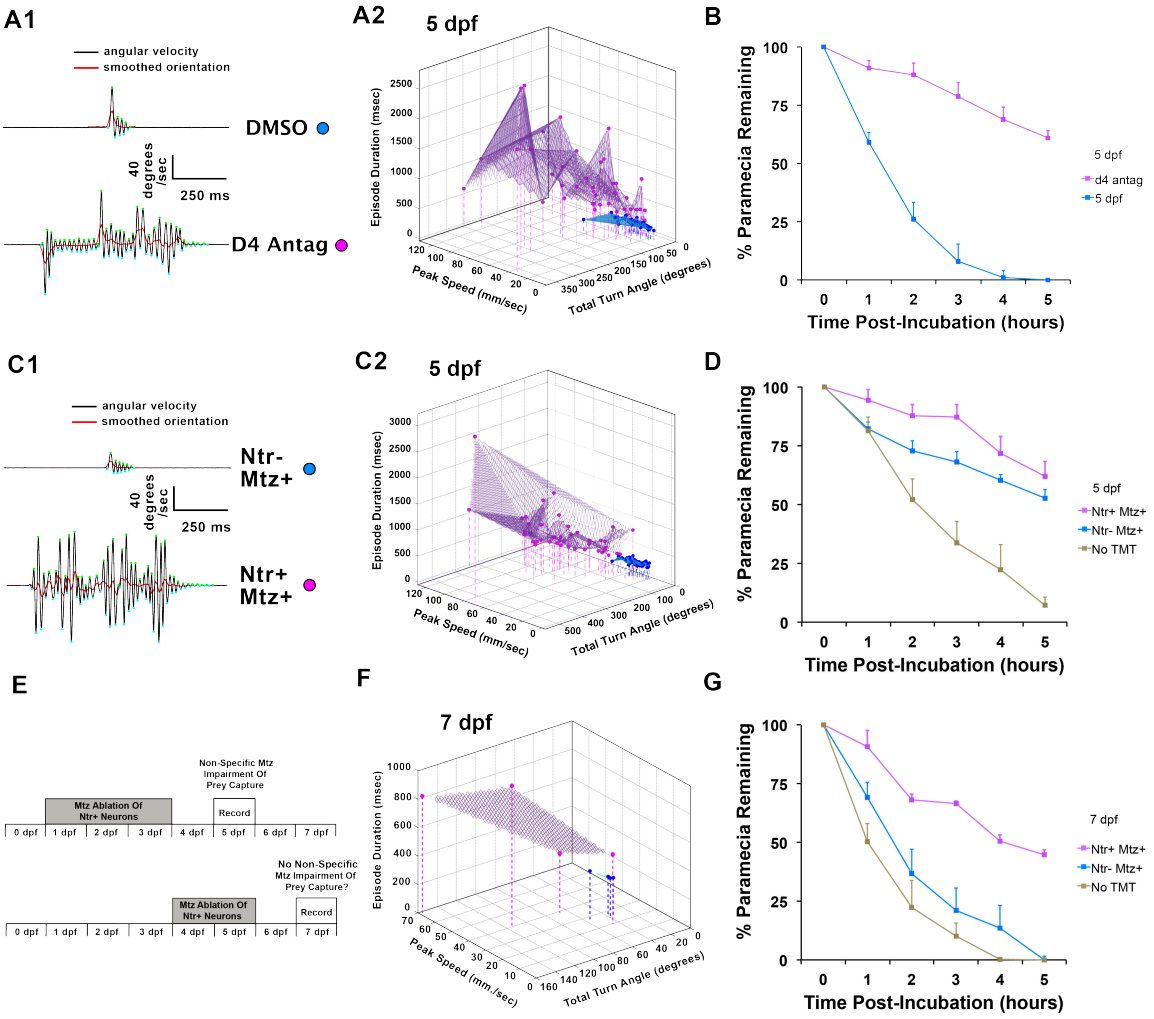
A1
angular velocity
smoothed orientation
DMSO
40 degrees /sec
250 ms
D4 Antag
A2
5 dpf
Episode Duration (msec)
Peak Speed (mm/sec)
Total Turn Angle (degrees)
B
% Paramecia Remaining
Time Post-Incubation (hours)
5 dpf
d4 antag
5 dpf
C1
angular velocity
smoothed orientation
Ntr- Mtz+
40 degrees /sec
250 ms
Ntr+ Mtz+
C2
5 dpf
Episode Duration (msec)
Peak Speed (mm/sec)
Total Turn Angle (degrees)
D
% Paramecia Remaining
Time Post-Incubation (hours)
5 dpf
Ntr+ Mtz+
Ntr- Mtz+
No TMT
E
Non-Specific Mtz Impairment Of Prey Capture
Mtz Ablation Of Ntr+ Neurons
Record
0 dpf
1 dpf
2 dpf
3 dpf
4 dpf
5 dpf
6 dpf
7 dpf
No Non-Specific Mtz Impairment Of Prey Capture?
Mtz Ablation Of Ntr+ Neurons
Record
F
7 dpf
Episode Duration (msec)
Peak Speed (mm./sec)
Total Turn Angle (degrees)
G
% Paramecia Remaining
Time Post-Incubation (hours)
7 dpf
Ntr+ Mtz+
Ntr- Mtz+
No TMT

Figure 3

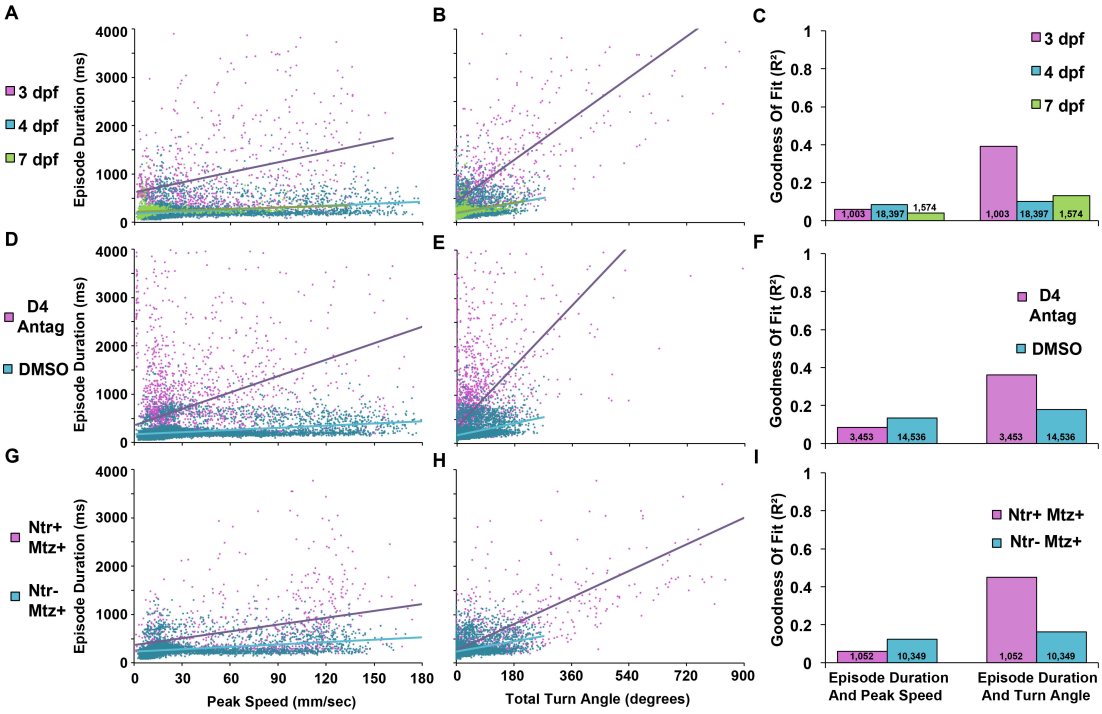
A
B
C
D
E
F
G
H
I
3 dpf
4 dpf
7 dpf
D4 Antag
DMSO
Ntr+ Mtz+
Ntr- Mtz+
Episode Duration (ms)
Goodness Of Fit (R²)
Peak Speed (mm/sec)
Total Turn Angle (degrees)
1,003
18,397
1,574
3,453
14,536
1,052
10,349
Episode Duration And Peak Speed
Episode Duration And Turn Angle

Figure 4

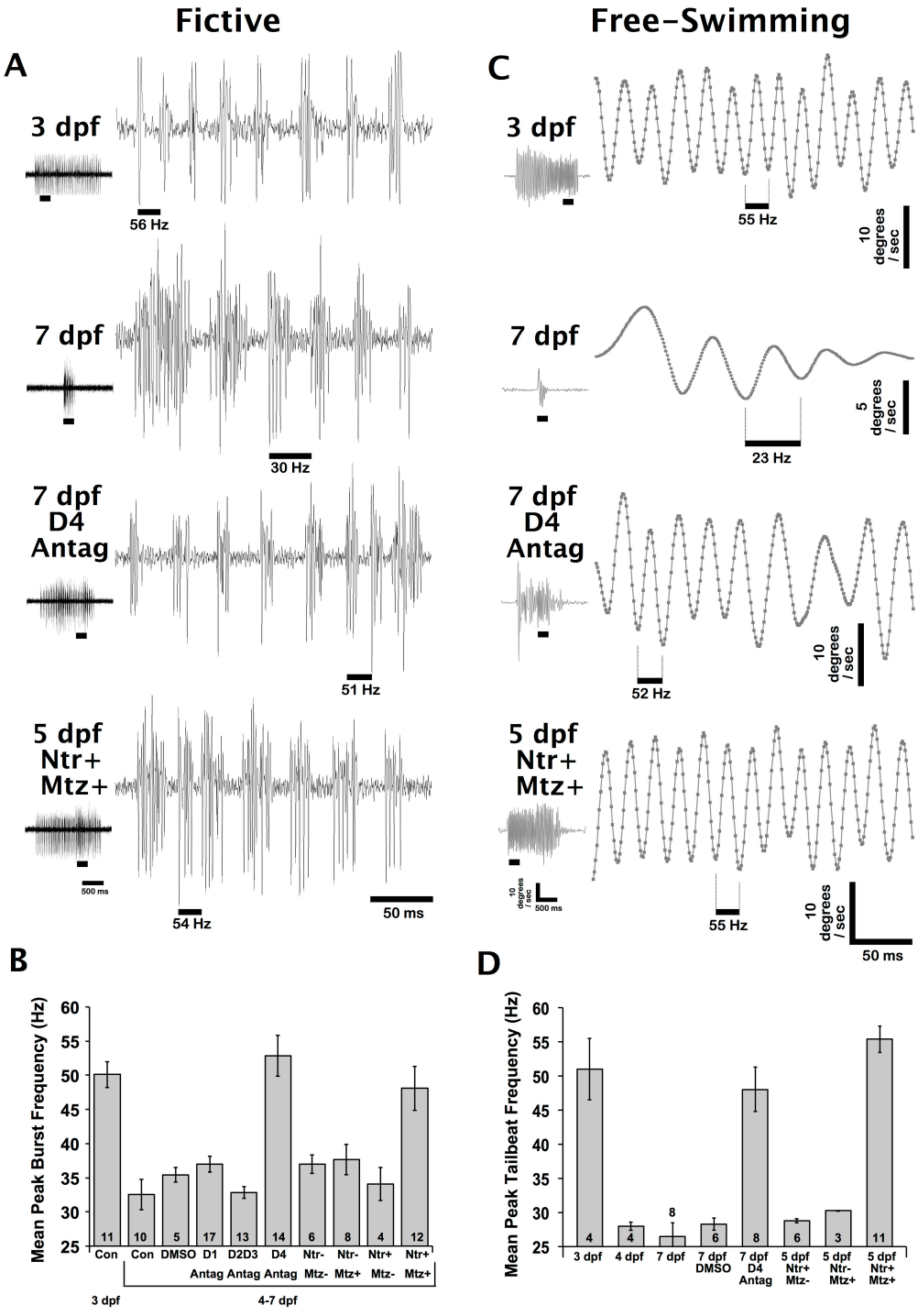
Fictive
Free-Swimming
A
3 dpf
56 Hz
7 dpf
30 Hz
7 dpf
D4
Antag
51 Hz
5 dpf
Ntr+
Mtz+
500 ms
54 Hz
50 ms
C
3 dpf
55 Hz
10
degrees
/ sec
7 dpf
23 Hz
5
degrees
/ sec
7 dpf
D4
Antag
52 Hz
10
degrees
/ sec
5 dpf
Ntr+
Mtz+
500 ms
55 Hz
10
degrees
/ sec
50 ms
B
Mean Peak Burst Frequency (Hz)
60
55
50
45
40
35
30
25
11
10
5
17
13
14
6
8
4
12
Con
Con
DMSO
D1
Antag
D2D3
Antag
D4
Antag
Ntr-
Mtz-
Ntr-
Mtz+
Ntr+
Mtz-
Ntr+
Mtz+
3 dpf
4-7 dpf
D
Mean Peak Tailbeat Frequency (Hz)
60
55
50
45
40
35
30
25
4
4
8
6
8
6
3
11
3 dpf
4 dpf
7 dpf
7 dpf
DMSO
7 dpf
D4
Antag
5 dpf
Ntr+
Mtz-
5 dpf
Ntr-
Mtz+
5 dpf
Ntr+
Mtz+

Figure 5

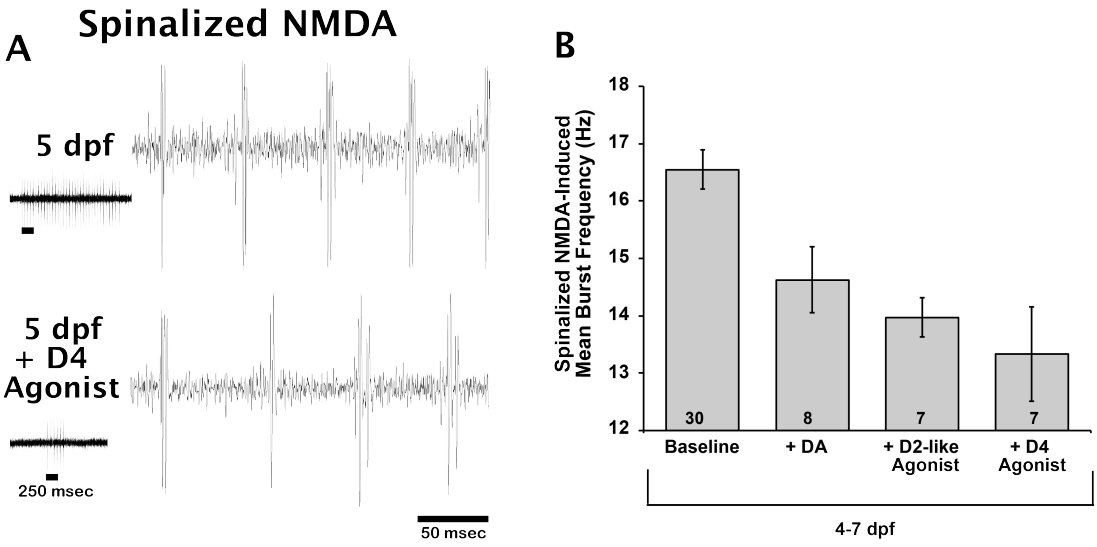
A
Spinalized NMDA
5 dpf
5 dpf
+ D4
Agonist
250 msec
50 msec
B
Spinalized NMDA-Induced
Mean Burst Frequency (Hz)
18
17
16
15
14
13
12
30
8
7
7
Baseline
+ DA
+ D2-like
Agonist
+ D4
Agonist
4-7 dpf

Figure 6

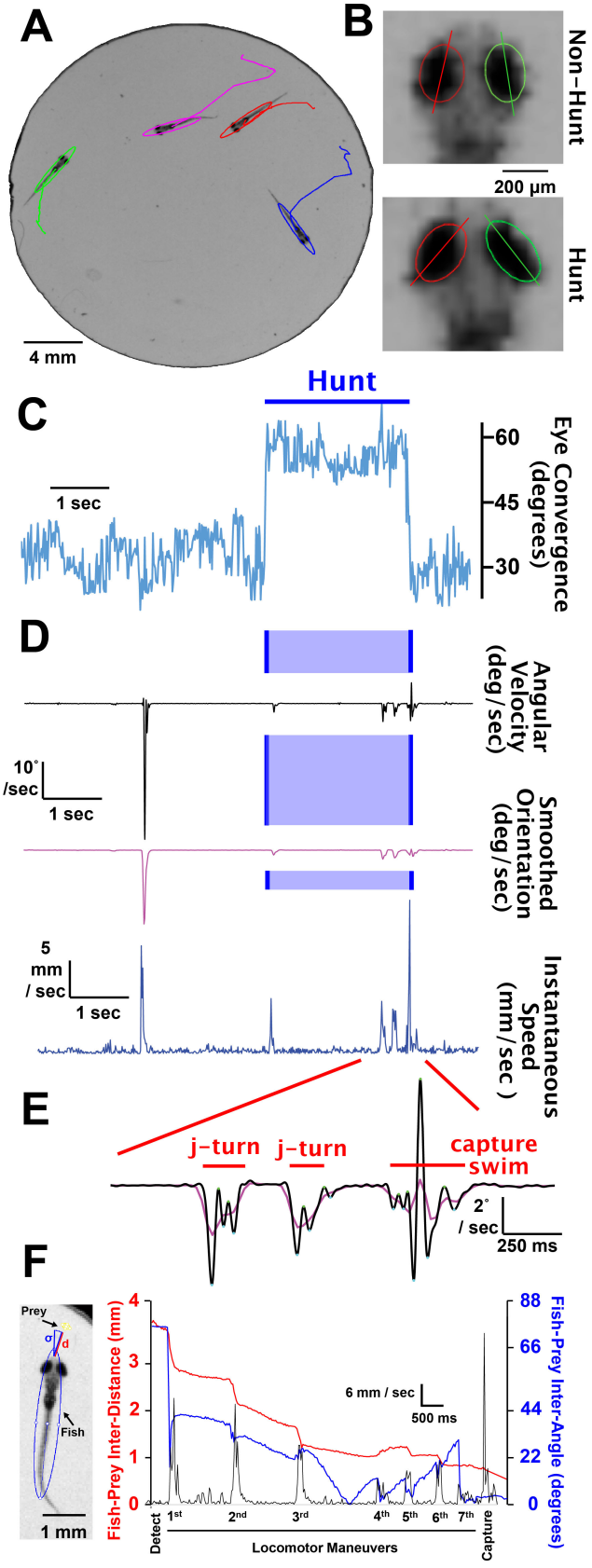
A
4 mm
B
Non-Hunt
200 µm
Hunt
C
Hunt
1 sec
60
45
30
Eye Convergence (degrees)
D
10°/sec
1 sec
Angular Velocity (deg/sec)
Smoothed Orientation (deg/sec)
5 mm / sec
1 sec
Instantaneous Speed (mm/sec)
E
j-turn
j-turn
capture swim
2° / sec
250 ms
F
Prey
Fish
1 mm
Fish-Prey Inter-Distance (mm)
6 mm / sec
500 ms
Fish-Prey Inter-Angle (degrees)
Detect
1st
2nd
3rd
4th
5th
6th
7th
Capture
Locomotor Maneuvers

Figure 7

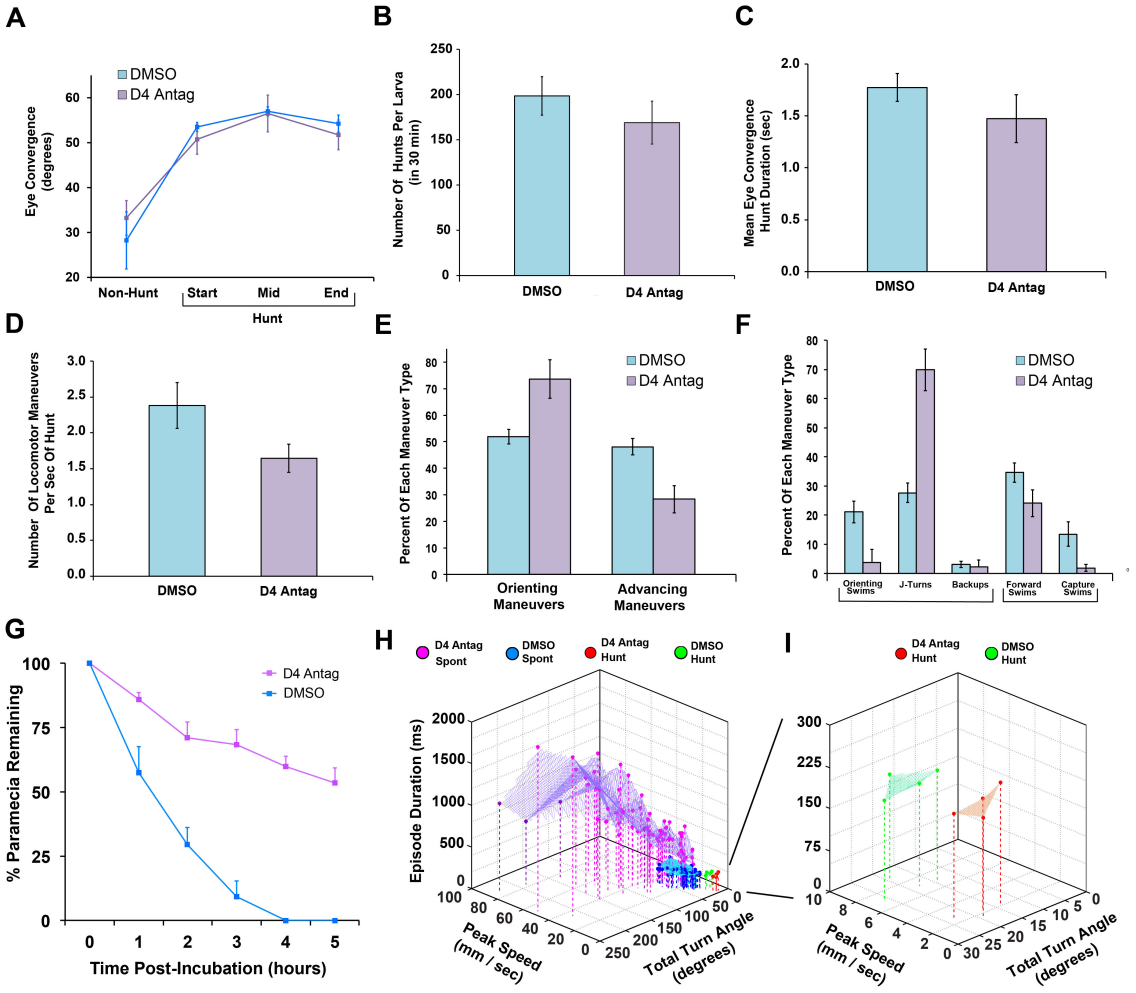
A
DMSO
D4 Antag
Eye Convergence (degrees)
Non-Hunt
Start
Mid
End
Hunt
B
Number Of Hunts Per Larva (in 30 min)
DMSO
D4 Antag
C
Mean Eye Convergence Hunt Duration (sec)
DMSO
D4 Antag
D
Number Of Locomotor Maneuvers Per Sec Of Hunt
DMSO
D4 Antag
E
Percent Of Each Maneuver Type
DMSO
D4 Antag
Orienting Maneuvers
Advancing Maneuvers
F
Percent Of Each Maneuver Type
DMSO
D4 Antag
Orienting Swims
J-Turns
Backups
Forward Swims
Capture Swims
G
% Paramecia Remaining
D4 Antag
DMSO
Time Post-Incubation (hours)
H
D4 Antag Spont
DMSO Spont
D4 Antag Hunt
DMSO Hunt
Episode Duration (ms)
Peak Speed (mm / sec)
Total Turn Angle (degrees)
I
D4 Antag Hunt
DMSO Hunt
Peak Speed (mm / sec)
Total Turn Angle (degrees)

Figure 8

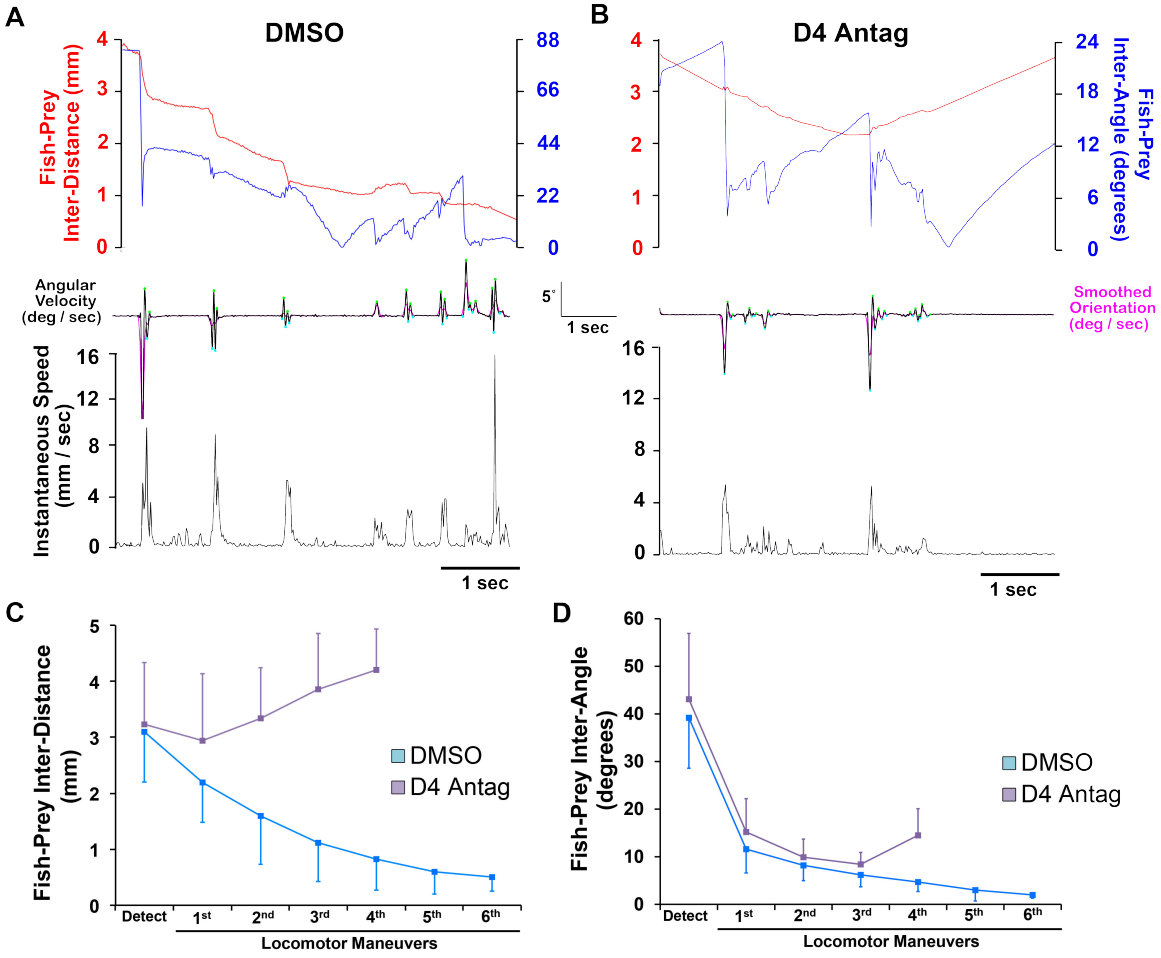
A
DMSO
B
D4 Antag
Fish-Prey Inter-Distance (mm)
Fish-Prey Inter-Angle (degrees)
Angular Velocity (deg / sec)
Smoothed Orientation (deg / sec)
5°
1 sec
Instantaneous Speed (mm / sec)
C
D
Fish-Prey Inter-Distance (mm)
Fish-Prey Inter-Angle (degrees)
DMSO
D4 Antag
Detect
1st
2nd
3rd
4th
5th
6th
Locomotor Maneuvers

Figure 9

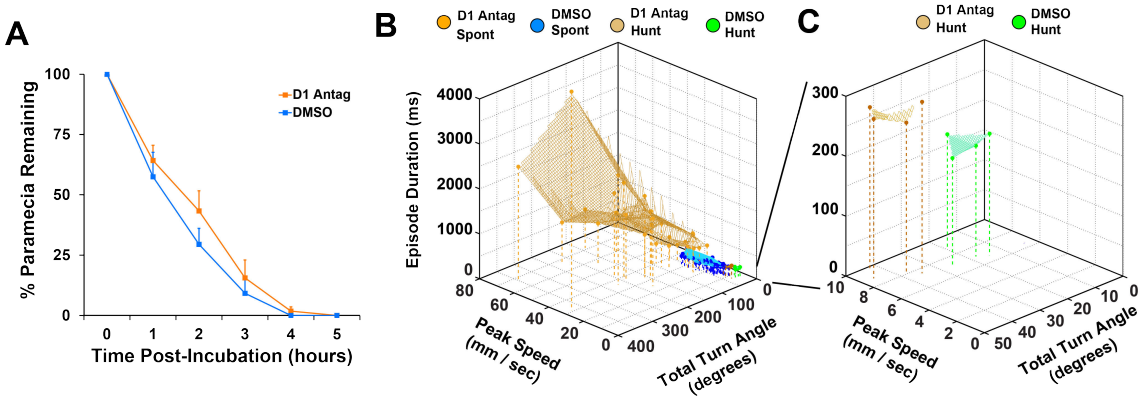
A
% Paramecia Remaining
100
75
50
25
0
0
1
2
3
4
5
Time Post-Incubation (hours)
D1 Antag
DMSO
B
D1 Antag Spont
DMSO Spont
D1 Antag Hunt
DMSO Hunt
Episode Duration (ms)
4000
3000
2000
1000
0
80
60
40
20
0
Peak Speed (mm / sec)
400
300
200
100
0
Total Turn Angle (degrees)
C
D1 Antag Hunt
DMSO Hunt
300
200
100
0
10
8
6
4
2
0
Peak Speed (mm / sec)
50
40
30
20
10
0
Total Turn Angle (degrees)

Figure 10

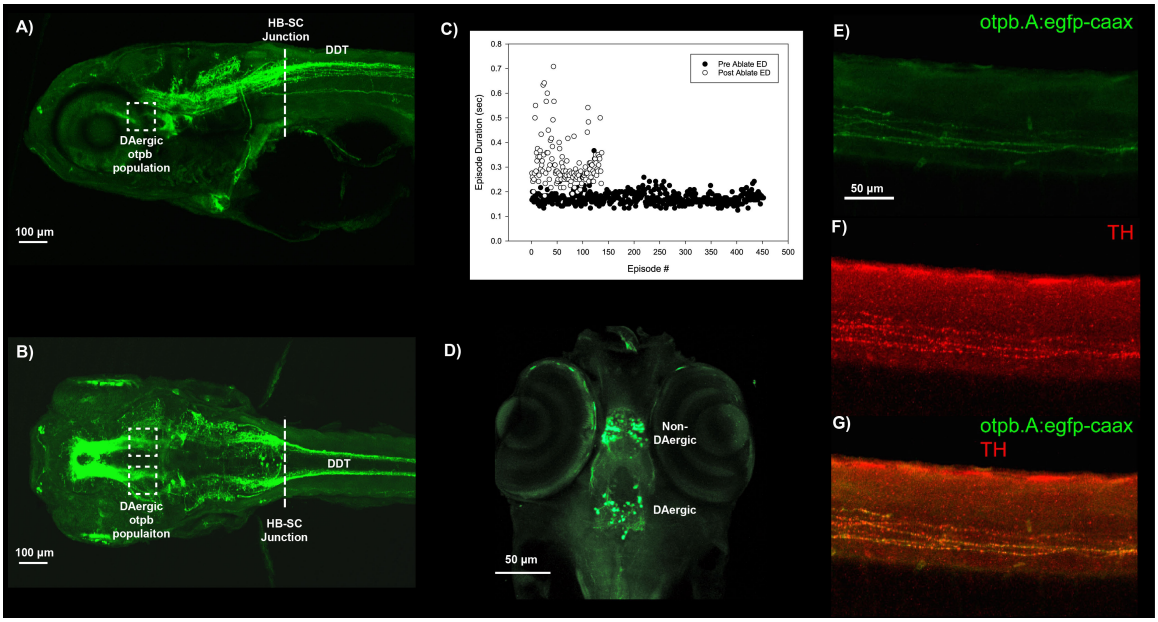
A)
HB-SC Junction
DDT
DAergic otpb population
100 µm
B)
DDT
DAergic otpb populaiton
HB-SC Junction
100 µm
C)
Pre Ablate ED
Post Ablate ED
Episode Duration (sec)
Episode #
D)
Non-DAergic
DAergic
50 µm
E)
otpb.A:egfp-caax
50 µm
F)
TH
G)
otpb.A:egfp-caax
TH

Table 1

Parameters	3 dpf	4 dpf	5 dpf	6 dpf	7 dpf
# episodes	9.860 +/- 14.304	266.870 +/- 198.031	127.200 +/- 108.503	137.800 +/- 176.390	101.820 +/- 78.032
vary_abse_episode_count	0.895 +/- 2.018	6.362 +/- 8.137	34.800 +/- 28.177	20.688 +/- 19.477	24.740 +/- 19.976
episode_duty_cycle	0.022 +/- 0.021	0.112 +/- 0.063	0.056 +/- 0.048	0.046 +/- 0.055	0.046 +/- 0.031
left_turn_count	29.922 +/- 32.253	146.333 +/- 73.726	52.500 +/- 30.493	29.800 +/- 32.437	64.286 +/- 43.642
right_turn_count	29.765 +/- 32.108	141.982 +/- 76.128	56.700 +/- 41.921	29.000 +/- 35.550	57.347 +/- 34.847
percent_episodes_turning (%)	87.732 +/- 16.499	72.498 +/- 11.425	79.968 +/- 18.524	37.044 +/- 18.334	85.925 +/- 9.774
total_distance_traveled (mm)	124.480 +/- 219.297	626.637 +/- 460.338	181.072 +/- 131.589	144.083 +/- 142.347	173.987 +/- 106.737
mean_dist2small_all (mm)	10.624 +/- 6.249	9.105 +/- 3.714	10.892 +/- 4.690	6.846 +/- 4.384	10.112 +/- 3.977
episode_duration (ms)	*** 0.875 +/- 0.302	0.218 +/- 0.036	0.287 +/- 0.029	0.215 +/- 0.042	0.289 +/- 0.033
displacement_episode_duration (ms)	0.967 +/- 0.327	0.219 +/- 0.038	0.287 +/- 0.028	0.215 +/- 0.042	0.289 +/- 0.039
stationary_episode_duration (ms)	0.760 +/- 0.137	0.195 +/- 0.164	0.303 +/- 0.119	0.215 +/- 0.042	0.268 +/- 0.094
speed_episode_duration (ms)	0.758 +/- 0.330	0.253 +/- 0.064	0.148 +/- 0.018	0.215 +/- 0.084	0.163 +/- 0.035
episode_frequency (Hz)	29.439 +/- 36.088	5.669 +/- 14.395	15.825 +/- 24.039	12.571 +/- 10.035	12.138 +/- 26.042
episode_mean_burst_frequency (Hz) *	30.446 +/- 1.788	24.264 +/- 1.462	N/A	N/A	21.492 +/- 3.029
episode_peak_burst_frequency (Hz) *	*** 51.035 +/- 9.383	27.949 +/- 1.181	N/A	N/A	26.522 +/- 5.477
episode_num_tailbeats	23.659 +/- 7.310	4.887 +/- 0.926	4.930 +/- 0.691	5.031 +/- 1.946	4.978 +/- 0.830
episode_mean_speed (mm/sec)	11.445 +/- 6.054	10.665 +/- 3.271	5.915 +/- 2.184	7.516 +/- 4.147	6.058 +/- 1.540
episode_95th_speed (mm/sec)	35.926 +/- 15.776	26.833 +/- 11.239	19.856 +/- 9.109	25.287 +/- 12.846	18.954 +/- 6.000
episode_peak_speed (mm/sec)	*** 47.309 +/- 17.379	28.284 +/- 12.257	22.125 +/- 10.297	* 20.168 +/- 11.567	* 20.807 +/- 6.831
displacement_episode_mean_speed (mm/sec)	13.322 +/- 8.234	10.810 +/- 3.134	5.925 +/- 2.175	7.516 +/- 4.147	6.210 +/- 1.557
displacement_episode_95th_speed (mm/sec)	37.412 +/- 14.963	27.165 +/- 11.048	19.856 +/- 9.109	18.433 +/- 10.223	18.954 +/- 6.000
displacement_episode_peak_speed (mm/sec)	49.012 +/- 15.915	28.284 +/- 12.257	22.125 +/- 10.297	20.168 +/- 11.567	20.807 +/- 6.831
episode_burst_balance (rad; integrated dtheta)	5.123 +/- 57.229	1.015 +/- 8.000	0.081 +/- 8.616	-2.647 +/- 6.713	0.480 +/- 8.998
episode_burst_balance_last_50%_episode (rad)	-0.236 +/- 29.441	0.525 +/- 4.192	-0.443 +/- 4.195	-1.257 +/- 3.501	0.160 +/- 4.921
left_turn_duration (ms)	0.080 +/- 0.023	0.067 +/- 0.010	0.064 +/- 0.007	0.070 +/- 0.006	0.064 +/- 0.009
left_turn_angle (degrees)	32.221 +/- 11.085	31.383 +/- 7.923	26.540 +/- 3.462	37.635 +/- 5.493	26.039 +/- 6.491

Table 1 (continued)

Parameters	3 dpf	4 dpf	5dpf	6 dpf	7 dpf
num_left_turns_in_episode	1.652 +/- 0.724	0.497 +/- 0.175	0.542 +/- 3.283	0.307 +/- 0.171	0.589 +/- 0.152
total_left_turn_duration_in_episode (ms)	0.140 +/- 0.092	0.034 +/- 0.012	0.034 +/- 0.015	0.022 +/- 0.013	0.041 +/- 0.016
total_left_turn_angle_in_episode (degrees)	58.799 +/- 39.667	15.896 +/- 8.716	15.657 +/- 7.873	11.568 +/- 6.712	17.387 +/- 8.998
episode_phasing_of_left_turns (ms after start)	0.622 +/- 0.356	0.063 +/- 0.034	0.068 +/- 0.049	0.119 +/- 0.114	0.077 +/- 0.060
right_turn_duration (ms)	0.079 +/- 0.019	0.068 +/- 0.012	0.068 +/- 0.007	0.066 +/- 0.012	0.066 +/- 0.013
right_turn_angle (degrees)	-34.129 +/- 14.687	-32.596 +/- 9.288	-32.486 +/- 8.576	-34.859 +/- 10.948	-27.986 +/- 15.371
num_right_turns_in_episode	1.614 +/- 0.637	0.457 +/- 0.128	0.596 +/- 0.331	0.247 +/- 0.142	0.578 +/- 0.184
total_right_turn_duration_in_episode (ms)	0.128 +/- 0.062	0.031 +/- 0.010	0.041 +/- 0.023	0.016 +/- 0.009	0.040 +/- 0.020
total_right_turn_angle_in_episode (degrees)	-57.805 +/- 34.597	-15.433 +/- 8.603	-21.682 +/- 17.426	-7.764 +/- 4.785	-18.727 +/- 20.757
episode_phasing_of_right_turns (ms after start)	0.609 +/- 0.352	0.064 +/- 0.035	0.068 +/- 0.045	0.112 +/- 0.075	0.078 +/- 0.051
total_num_turns_in_episode	3.266 +/- 1.159	0.953 +/- 0.281	1.138 +/- 0.556	0.554 +/- 0.301	1.168 +/- 0.241
total_turn_duration_in_episode (ms)	0.269 +/- 0.108	0.065 +/- 0.020	0.075 +/- 0.033	0.037 +/- 0.020	0.081 +/- 0.028
total_turn_angle_in_episode (degrees)	116.610 +/- 58.193	31.330 +/- 16.502	37.339 +/- 24.032	19.333 +/- 10.136	36.115 +/- 24.326
net_turn_angle_in_episode (degrees)	0.994 +/- 46.409	0.463 +/- 5.261	-6.026 +/- 12.402	3.804 +/- 5.759	-1.340 +/- 20.782
abs_net_turn_angle_in_episode (degrees)	57.616 +/- 30.075	25.584 +/- 11.803	28.579 +/- 14.720	13.923 +/- 7.410	27.672 +/- 17.868
nonzero_total_num_turns_in_episode	3.767 +/- 1.349	1.306 +/- 0.241	1.375 +/- 0.404	1.485 +/- 0.233	1.355 +/- 0.210
nonzero_total_turn_duration_in_episode (ms)	0.309 +/- 0.116	0.089 +/- 0.018	0.091 +/- 0.022	0.100 +/- 0.017	0.094 +/- 0.028
nonzero_total_turn_angle_in_episode (degrees)	*** 134.267 +/- 62.603	42.573 +/- 15.887	44.110 +/- 19.815	46.922 +/- 11.097	41.253 +/- 24.053
nonzero_net_turn_angle_in_episode (degrees)	1.656 +/- 54.266	0.656 +/- 7.007	-6.235 +/- 13.169	7.924 +/- 12.055	-1.062 +/- 21.238
nonzero_abs_net_turn_angle_in_episode (degrees)	67.710 +/- 35.067	34.897 +/- 11.359	34.176 +/- 10.869	37.889 +/- 8.150	31.604 +/- 17.256
total_distance_traveled_episode (mm)	8.074 +/- 10.533	2.062 +/- 1.424	1.994 +/- 1.161	1.680 +/- 1.130	2.128 +/- 1.228
dist2wall_episode_onset (mm)	412.059 +/- 489.935	239.351 +/- 421.004	10.758 +/- 4.354	7.575 +/- 4.048	426.505 +/- 492.984
dist2wall_episode_offset (mm)	411.992 +/- 489.992	239.336 +/- 421.013	10.627 +/- 4.427	7.519 +/- 4.096	426.432 +/- 493.046
delta_dist2wall_from_episode (mm)	0.113 +/- 0.924	0.020 +/- 0.052	0.130 +/- 0.256	0.056 +/- 0.132	0.125 +/- 0.122
sample size (n)	90	70	10	10	50
arena diameter (mm)	50	50	50	50	50
* 210 fps (n)	4	4	N/A	N/A	8

Table 2

Parameters	5 dpf DMSO	5 dpf D4 Antag	5 dpf Nic- Bitz*	5 dpf Nic+ Bitz+	7dpf Nic- Bitz+	7dpf Nic+ Bitz+
# episodes	253.411 +/- 226.922	57.426 +/- 110.032	261.932 +/- 166.837	23.111 +/- 14.979	326.567 +/- 211.300	29.253 +/- 13.883
very_slow_episode_count	10.714 +/- 28.838	1.309 +/- 2.593	31.333 +/- 34.426	0.467 +/- 0.991	N/A	N/A
episode_duty_cycle	0.105 +/- 0.073	0.054 +/- 0.062	0.126 +/- 0.069	0.026 +/- 0.019	0.168 +/- 0.059	0.028 +/- 0.014
left_turn_count	156.558 +/- 106.107	84.891 +/- 89.248	125.976 +/- 58.796	41.395 +/- 22.798	299.234 +/- 103.453	39.444 +/- 19.308
right_turn_count	161.535 +/- 119.324	76.000 +/- 75.816	131.756 +/- 60.147	42.442 +/- 24.751	266.444 +/- 96.453	44.902 +/- 26.673
percent_episodes_turning (%)	73.260 +/- 17.475	88.296 +/- 13.096	67.878 +/- 13.721	89.620 +/- 10.847	89.835 +/- 2.680	80.547 +/- 9.121
total_distance_traveled (mm)	589.624 +/- 599.373	238.069 +/- 340.647	695.546 +/- 369.493	324.799 +/- 231.348	705.140 +/- 265.657	269.888 +/- 170.362
mean_dist2wall_all (mm)	11.095 +/- 2.946	6.391 +/- 5.251	10.555 +/- 3.896	6.975 +/- 4.295	4.035 +/- 0.280	3.896 +/- 1.769
episode_duration (ms)	0.227 +/- 0.065	*** 0.856 +/- 0.778	0.287 +/- 0.142	*** 0.723 +/- 0.460	0.288 +/- 0.034	*** 0.712 +/- 0.329
displacement_episode_duration (ms)	0.214 +/- 0.032	0.871 +/- 0.603	0.288 +/- 0.041	0.701 +/- 0.452	0.288 +/- 0.034	0.712 +/- 0.329
stationary_episode_duration (ms)	0.439 +/- 0.742	2.753 +/- 4.477	0.209 +/- 0.045	2.802 +/- 4.763	0.288 +/- 0.034	0.712 +/- 0.329
speed_episode_duration (ms)	0.255 +/- 0.063	1.083 +/- 0.722	0.283 +/- 0.062	0.808 +/- 0.588	0.158 +/- 0.035	0.361 +/- 0.174
episode_frequency (Hz)	7.663 +/- 18.782	35.599 +/- 46.386	3.972 +/- 7.087	26.755 +/- 26.618	1.700 +/- 0.421	32.063 +/- 32.497
episode_mean_burst_frequency (Hz) *	N/A	N/A	24.194 +/- 2.054	34.868 +/- 4.815	N/A	N/A
episode_peak_burst_frequency (Hz) *	N/A	N/A	30.242 +/- 0.115	*** 50.361 +/- 6.395	N/A	N/A
episode_num_tailbeats	4.726 +/- 0.805	20.795 +/- 15.232	5.686 +/- 1.050	15.494 +/- 11.340	6.017 +/- 0.901	14.845 +/- 6.896
episode_mean_speed (mm/sec)	10.154 +/- 3.322	11.301 +/- 7.960	8.681 +/- 2.432	21.493 +/- 8.239	7.950 +/- 0.586	8.589 +/- 2.826
episode_95th_speed (mm/sec)	25.540 +/- 9.586	35.808 +/- 23.424	22.535 +/- 6.527	60.122 +/- 19.529	23.013 +/- 1.184	30.110 +/- 12.403
episode_peak_speed (mm/sec)	27.896 +/- 10.089	*** 45.899 +/- 26.969	24.519 +/- 6.927	*** 69.853 +/- 23.192	24.845 +/- 1.463	*** 41.968 +/- 20.224
displacement_episode_mean_speed (mm/sec)	10.747 +/- 2.899	11.954 +/- 8.081	8.737 +/- 2.425	21.752 +/- 8.147	7.950 +/- 0.586	8.589 +/- 2.826
displacement_episode_95th_speed (mm/sec)	26.499 +/- 8.806	36.753 +/- 23.695	22.537 +/- 6.526	60.378 +/- 19.313	21.345 +/- 1.123	29.887 +/- 15.180
displacement_episode_peak_speed (mm/sec)	27.891 +/- 9.591	50.191 +/- 26.957	24.522 +/- 6.926	69.797 +/- 23.039	26.045 +/- 1.463	41.965 +/- 20.224
episode_burst_balance (real; integrated diff+ita)	-1.389 +/- 8.145	5.265 +/- 64.130	0.048 +/- 2.794	-0.499 +/- 14.165	0.635 +/- 0.621	-1.807 +/- 6.480
episode_burst_balance_last_80%_episode (real)	-0.542 +/- 3.865	0.485 +/- 32.156	-0.016 +/- 1.608	0.546 +/- 9.018	0.290 +/- 0.417	2.609 +/- 7.454
left_turn_duration (ms)	0.071 +/- 0.011	0.070 +/- 0.022	0.074 +/- 0.010	0.078 +/- 0.013	0.070 +/- 0.002	0.061 +/- 0.009
left_turn_angle (degrees)	34.166 +/- 11.113	29.327 +/- 16.147	33.444 +/- 4.700	43.919 +/- 12.523	30.670 +/- 4.415	34.812 +/- 18.837

Table 2 (continued)

Parameters	5 dpf DMSO	5 dpf D4 Antag	5 dpf Nic- Bitc+	5 dpf Nic+ Bitc+	7dpf Nic- Bitc+	7dpf Nic+ Bitc+
num_left_turns_in_episode	0.449 +/- 0.127	1.483 +/- 1.077	0.457 +/- 0.117	1.800 +/- 0.949	0.597 +/- 0.075	1.022 +/- 0.519
total_left_turn_duration_in_episode (ms)	0.031 +/- 0.008	0.105 +/- 0.081	0.034 +/- 0.011	0.143 +/- 0.078	0.042 +/- 0.006	0.067 +/- 0.036
total_left_turn_angle_in_episode (degrees)	15.381 +/- 6.201	47.948 +/- 45.024	15.582 +/- 4.488	77.746 +/- 41.317	19.894 +/- 4.028	39.510 +/- 23.723
episode_phasing_of_left_turns (ms after start)	0.071 +/- 0.063	0.622 +/- 0.755	0.117 +/- 0.129	0.566 +/- 0.744	0.090 +/- 0.046	0.282 +/- 0.157
right_turn_duration (ms)	0.073 +/- 0.008	0.068 +/- 0.017	0.075 +/- 0.009	0.076 +/- 0.011	0.068 +/- 0.003	0.062 +/- 0.017
right_turn_angle (degrees)	-34.485 +/- 7.135	-31.068 +/- 15.813	-35.196 +/- 7.219	-43.780 +/- 10.176	-29.657 +/- 4.745	-30.969 +/- 18.036
num_right_turns_in_episode	0.477 +/- 0.179	1.441 +/- 0.952	0.478 +/- 0.125	1.833 +/- 1.007	0.584 +/- 0.049	1.065 +/- 0.419
total_right_turn_duration_in_episode (ms)	0.035 +/- 0.013	0.103 +/- 0.073	0.036 +/- 0.010	0.141 +/- 0.075	0.040 +/- 0.005	0.071 +/- 0.025
total_right_turn_angle_in_episode (degrees)	-17.011 +/- 9.003	-49.632 +/- 42.073	-17.425 +/- 6.296	-78.474 +/- 41.612	-18.342 +/- 3.912	-41.317 +/- 27.902
episode_phasing_of_right_turns (ms after start)	0.071 +/- 0.053	0.644 +/- 0.707	0.123 +/- 0.151	0.534 +/- 0.609	0.085 +/- 0.048	0.216 +/- 0.082
total_num_turns_in_episode	0.925 +/- 0.278	2.924 +/- 1.972	0.935 +/- 0.218	3.633 +/- 1.919	1.181 +/- 0.121	2.087 +/- 0.915
total_turn_duration_in_episode (ms)	0.066 +/- 0.018	0.207 +/- 0.143	0.070 +/- 0.017	0.284 +/- 0.145	0.082 +/- 0.010	0.138 +/- 0.058
total_turn_angle_in_episode (degrees)	32.394 +/- 13.983	97.639 +/- 77.761	33.009 +/- 9.212	156.220 +/- 80.006	38.237 +/- 7.777	80.915 +/- 50.030
net_turn_angle_in_episode (degrees)	-1.630 +/- 6.596	-1.684 +/- 39.367	-1.843 +/- 5.889	-0.728 +/- 21.826	1.551 +/- 1.610	-1.807 +/- 13.519
abs_net_turn_angle_in_episode (degrees)	27.852 +/- 13.007	47.353 +/- 31.024	25.685 +/- 7.156	64.417 +/- 21.858	33.401 +/- 5.477	47.935 +/- 25.507
nonzero_total_num_turns_in_episode	1.255 +/- 0.168	3.222 +/- 2.024	1.382 +/- 0.217	4.031 +/- 2.171	1.314 +/- 0.125	2.545 +/- 0.960
nonzero_total_turn_duration_in_episode (ms)	0.090 +/- 0.012	0.229 +/- 0.147	0.104 +/- 0.017	0.314 +/- 0.160	0.091 +/- 0.011	0.168 +/- 0.058
nonzero_total_turn_angle_in_episode (degrees)	43.781 +/- 13.367	*** 109.511 +/- 81.588	48.947 +/- 10.826	*** 173.846 +/- 89.953	42.569 +/- 8.587	*** 96.310 +/- 49.956
nonzero_net_turn_angle_in_episode (degrees)	-1.526 +/- 8.628	-2.682 +/- 41.818	-2.867 +/- 8.981	-0.489 +/- 23.882	1.689 +/- 1.784	-1.758 +/- 15.786
nonzero_abs_net_turn_angle_in_episode (degrees)	37.479 +/- 12.632	52.586 +/- 30.477	37.914 +/- 7.221	71.614 +/- 22.767	37.189 +/- 6.060	57.530 +/- 23.947
total_distance_traveled_episode (mm)	1.859 +/- 1.248	8.529 +/- 6.893	2.691 +/- 1.063	15.543 +/- 9.875	2.157 +/- 0.329	9.271 +/- 5.804
dist2wall_episode_onset (mm)	646.887 +/- 478.040	5.419 +/- 2.768	387.555 +/- 486.273	470.402 +/- 500.995	3.415 +/- 0.437	2.917 +/- 1.377
dist2wall_episode_offset (mm)	646.884 +/- 478.044	5.096 +/- 2.820	387.504 +/- 486.313	470.255 +/- 501.134	3.448 +/- 0.471	2.651 +/- 0.904
delta_dist2wall_from_episode (mm)	0.010 +/- 0.039	0.323 +/- 0.558	0.083 +/- 0.075	0.275 +/- 0.431	-0.032 +/- 0.057	0.266 +/- 0.526
sample size (n)		70	50	50	4	4
areva diameter (mm)		50	50	50	20	20
* 216 fps (n)	N/A	N/A	4	11	N/A	N/A

Table 3

Parameters	DMSO 30 mm Spont	DMSO 20 mm Spont	DMSO 20 mm Hunt	D4 Antag 30 mm Spont	D4 Antag 20 mm Spont	D4 Antag 20 mm Hunt
# episodes	144.750 +/- 114.370	197.250 +/- 140.763	193.703 +/- 123.421	35.318 +/- 27.520	38.500 +/- 11.091	74.000 +/- 55.154
very_slow_episode_count	32.250 +/- 30.951	N/A	N/A	6.000 +/- 9.832	N/A	N/A
episode_duty_cycle	0.062 +/- 0.045	0.052 +/- 0.037	0.058 +/- 0.017	0.034 +/- 0.021	0.054 +/- 0.019	0.002 +/- 0.001
left_turn_count	84.850 +/- 55.783	78.750 +/- 63.819	234.112 +/- 140.220	40.446 +/- 21.474	70.250 +/- 32.602	95.999 + /- 50.910
right_turn_count	72.850 +/- 40.421	54.250 +/- 43.813	231.003 +/- 109.321	41.723 +/- 24.142	54.250 +/- 26.513	88.396 +/- 41.298
percent_episodes_turning (%)	87.571 +/- 12.842	52.227 +/- 13.304	43.475 +/- 7.773	90.193 +/- 12.249	90.200 +/- 6.795	34.640 +/- 8.582
total_distance_traveled (mm)	248.934 +/- 151.491	205.108 +/- 151.853	94.442 +/- 44.909	183.210 +/- 135.713	501.919 +/- 299.435	20.612 +/- 16.159
mean_dist2wall_all (mm)	11.223 +/- 4.215	3.129 +/- 1.341	3.141 +/- 1.199	9.103 +/- 3.303	2.288 +/- 1.091	2.721 +/- 0.287
episode_duration (ms)	0.297 +/- 0.044	0.201 +/- 0.007	0.197 +/- 0.009	*** 0.746 +/- 0.381	*** 0.860 +/- 0.152	0.193 +/- 0.019
displacement_episode_duration (ms)	0.297 +/- 0.043	0.201 +/- 0.007	0.197 +/- 0.009	0.755 +/- 0.381	0.860 +/- 0.152	0.205 +/- 0.022
stationary_episode_duration (ms)	0.297 +/- 0.099	0.201 +/- 0.007	0.197 +/- 0.009	0.311 +/- 0.122	0.860 +/- 0.152	0.205 +/- 0.022
speed_episode_duration (ms)	0.165 +/- 0.045	0.133 +/- 0.005	0.088 +/- 0.004	0.424 +/- 0.200	0.314 +/- 0.068	0.116 +/- 0.023
episode_frequency (Hz)	10.067 +/- 15.151	6.074 +/- 4.202	6.490 +/- 3.990	26.989 +/- 28.433	16.692 +/- 6.808	26.613 +/- 24.158
episode_mean_burst_frequency (Hz) *	23.228 +/- 2.950	N/A	N/A	20.413 +/- 4.871	N/A	N/A
episode_peak_burst_frequency (Hz) *	28.316 +/-2.247	N/A	N/A	** 45.619 +/- 9.162	N/A	N/A
episode_num_tailbeats	5.474 +/- 1.068	4.008 +/- 0.085	4.144 +/- 0.313	15.450 +/- 8.354	18.766 +/- 3.929	4.088 +/- 0.490
episode_mean_speed (mm/sec)	7.038 +/- 3.299	4.671 +/- 0.678	2.452 +/- 0.365	7.560 +/- 2.585	11.510 +/- 3.977	1.267 +/- 0.057
episode_95th_speed (mm/sec)	23.199 +/- 11.652	15.711 +/- 2.834	7.273 +/- 0.841	26.715 +/- 10.437	47.010 +/- 17.963	2.125 +/- 0.650
episode_peak_speed (mm/sec)	25.958 +/- 12.906	15.462 +/- 2.470	*** 7.389 +/- 0.898	** 35.534 +/- 14.172	*** 69.423 +/- 25.447	*** 2.323 +/- 0.687
displacement_episode_mean_speed (mm/sec)	7.156 +/- 3.380	4.671 +/- 0.678	2.452 +/- 0.365	7.716 +/- 2.527	11.510 +/- 3.977	1.313 +/- 0.019
displacement_episode_95th_speed (mm/sec)	23.201 +/- 11.650	12.456 +/- 1.987	6.656 +/- 0.772	26.715 +/- 10.437	53.991 +/- 6.920	2.211 +/- 0.345
displacement_episode_peak_speed (mm/sec)	25.958 +/- 12.904	15.462 +/- 2.470	7.389 +/- 0.898	35.534 +/- 14.172	69.423 +/- 25.447	2.323 +/- 0.687
episode_burst_balance (rad; integrated dtheta)	0.004 +/- 10.365	1.507 +/- 3.844	-0.990 +/- 3.439	-0.626 +/- 23.345	2.738 +/- 14.027	2.727 +/- 7.581
episode_burst_balance_last_50%_episode (rad)	-0.034 +/- 5.213	0.830 +/- 2.013	-0.599 +/- 1.783	0.131 +/- 15.027	1.713 +/- 9.915	2.164 +/- 5.050
left_turn_duration (ms)	0.061 +/- 0.011	0.073 +/- 0.005	0.068 +/- 0.003	0.065 +/- 0.012	0.094 +/- 0.014	0.075 +/- 0.001
left_turn_angle (degrees)	26.318 +/- 8.006	31.628 +/- 3.699	31.452 +/- 2.513	25.436 +/- 9.040	48.925 +/- 13.851	32.849 +/- 3.169

Table 3 (continued)

Parameters	D4ISO 59 mm Spont	D4ISO 29 mm Spont	D4ISO 29 mm Hunt	D4 Antag 59 mm Spont	D4 Antag 29 mm Spont	D4 Antag 29 mm Hunt
num_left_turns_in_episode	0.621 +/- 0.221	0.369 +/- 0.102	0.229 +/- 0.028	1.151 +/- 0.791	1.677 +/- 0.672	0.114 +/- 0.040
total_left_turn_duration_in_episode (ms)	0.037 +/- 0.009	0.027 +/- 0.008	0.014 +/- 0.003	0.083 +/- 0.067	0.155 +/- 0.052	0.006 +/- 0.003
total_left_turn_angle_in_episode (degrees)	16.624 +/- 6.569	11.544 +/- 2.558	4.288 +/- 1.291	35.137 +/- 28.360	81.523 +/- 26.519	1.196 +/- 0.728
episode_phasing_of_left_turns (ms after start)	0.071 +/- 0.054	0.039 +/- 0.008	0.010 +/- 0.002	0.450 +/- 0.419	0.468 +/- 0.218	0.001 +/- 0.001
right_turn_duration (ms)	0.065 +/- 0.008	0.074 +/- 0.014	0.070 +/- 0.004	0.065 +/- 0.012	0.090 +/- 0.019	0.070 +/- 0.003
right_turn_angle (degrees)	-27.732 +/- 7.098	-36.303 +/- 6.831	-32.313 +/- 4.120	-23.356 +/- 7.295	-48.889 +/- 14.746	-31.293 +/- 0.139
num_right_turns_in_episode	0.598 +/- 0.220	0.250 +/- 0.068	0.225 +/- 0.068	1.092 +/- 0.601	1.279 +/- 0.593	0.247 +/- 0.026
total_right_turn_duration_in_episode (ms)	0.040 +/- 0.016	0.019 +/- 0.008	0.014 +/- 0.005	0.079 +/- 0.056	0.116 +/- 0.074	0.016 +/- 0.001
total_right_turn_angle_in_episode (degrees)	-17.373 +/- 8.301	-9.203 +/- 3.191	-4.625 +/- 2.248	-30.479 +/- 24.185	-62.924 +/- 38.617	-4.644 +/- 0.444
episode_phasing_of_right_turns (ms after start)	0.080 +/- 0.051	0.037 +/- 0.009	0.009 +/- 0.004	0.452 +/- 0.412	0.445 +/- 0.270	0.003 +/- 0.001
total_num_turns_in_episode	1.219 +/- 0.404	0.619 +/- 0.132	0.454 +/- 0.082	2.242 +/- 1.302	2.956 +/- 1.215	0.361 +/- 0.066
total_turn_duration_in_episode (ms)	0.077 +/- 0.020	0.046 +/- 0.013	0.028 +/- 0.007	0.162 +/- 0.106	0.271 +/- 0.106	0.022 +/- 0.002
total_turn_angle_in_episode (degrees)	33.998 +/- 12.153	20.751 +/- 3.081	8.913 +/- 3.346	65.616 +/- 45.466	144.491 +/- 58.910	5.840 +/- 0.284
net_turn_angle_in_episode (degrees)	-0.749 +/- 8.742	2.341 +/- 4.898	-0.336 +/- 1.499	4.659 +/- 26.670	18.599 +/- 30.276	-3.449 +/- 1.172
abs_net_turn_angle_in_episode (degrees)	27.640 +/- 8.917	17.375 +/- 2.726	8.634 +/- 3.241	41.728 +/- 26.249	101.399 +/- 36.713	5.840 +/- 0.284
nonzero_total_num_turns_in_episode	1.376 +/- 0.329	1.198 +/- 0.098	1.045 +/- 0.011	2.424 +/- 1.232	3.275 +/- 1.390	1.050 +/- 0.071
nonzero_total_turn_duration_in_episode (ms)	0.088 +/- 0.014	0.089 +/- 0.004	0.064 +/- 0.007	0.174 +/- 0.102	0.302 +/- 0.123	0.065 +/- 0.010
nonzero_total_turn_angle_in_episode (degrees)	30.490 +/- 10.991	40.978 +/- 7.579	** 19.567 +/- 4.459	** 79.166 +/- 43.553	*** 156.878 +/- 62.946	** 19.269 +/- 4.314
nonzero_net_turn_angle_in_episode (degrees)	-0.461 +/- 9.643	4.432 +/- 11.494	-0.398 +/- 3.466	4.815 +/- 27.494	19.954 +/- 32.775	-10.704 +/- 6.034
nonzero_abs_net_turn_angle_in_episode (degrees)	31.317 +/- 7.831	34.093 +/- 5.143	19.349 +/- 4.279	44.819 +/- 25.336	111.944 +/- 39.898	17.289 +/- 3.465
total_distance_traveled_episode (mm)	2.260 +/- 1.264	1.007 +/- 0.168	0.476 +/- 0.060	6.591 +/- 4.431	12.286 +/- 7.045	0.273 +/- 0.015
dist2wall_episode_onset (mm)	11.431 +/- 3.721	3.414 +/- 1.531	3.103 +/- 1.296	25.175 +/- 121.867	2.251 +/- 1.228	336.066 +/- 574.985
dist2wall_episode_offset (mm)	11.316 +/- 3.729	3.405 +/- 1.542	3.022 +/- 1.248	24.593 +/- 121.943	2.236 +/- 1.138	336.018 +/- 575.027
delta_dist2wall_from_episode (mm)	0.115 +/- 0.061	0.009 +/- 0.016	0.081 +/- 0.051	0.590 +/- 0.741	0.015 +/- 0.133	0.073 +/- 0.016
sample size (n)	40	4	4	70	4	4
arena diameter (mm)	50	20	20	50	20	20
* 210 fps (n)	6	N/A	N/A	8	N/A	N/A

Table 4

Parameters	DMSO 50 mm Spont	DMSO 20 mm Spont	DMSO 20 mm Hunt	D1 Antag 50 mm Spont	D1 Antag 20 mm Spont	D1 Antag 20 mm Hunt
# episodes	144.750 +/- 114.370	197.250 +/- 140.763	193.703 +/- 123.421	39.533 +/- 57.107	20.250 +/- 15.152	120.323 +/- 93.412
very_slow_episode_count	32.250 +/- 30.951	N/A	N/A	6.767 +/- 9.790	N/A	N/A
episode_duty_cycle	0.062 +/- 0.045	0.052 +/- 0.037	0.058 +/- 0.017	0.040 +/- 0.059	0.021 +/- 0.008	0.057 +/- 0.011
left_turn_count	84.850 +/- 55.783	78.750 +/- 63.819	234.112 +/- 140.220	66.724 +/- 136.831	17.667 +/- 8.083	123.456 +/- 66.432
right_turn_count	72.850 +/- 40.421	54.250 +/- 43.813	231.003 +/- 109.321	61.276 +/- 135.311	15.333 +/- 7.371	116.324 +/- 71.97
percent_episodes_turning (%)	87.571 +/- 12.842	52.227 +/- 13.304	43.475 +/- 7.773	87.184 +/- 15.616	57.886 +/- 8.568	42.435 +/- 0.350
total_distance_traveled (mm)	248.934 +/- 151.491	205.108 +/- 151.853	94.442 +/- 44.909	235.909 +/- 239.038	71.079 +/- 48.168	126.789 +/- 69.342
mean_dist2wall_all (mm)	11.223 +/- 4.215	3.129 +/- 1.341	3.141 +/- 1.199	8.359 +/- 4.112	4.014 +/- 2.971	2.419 +/- 0.109
episode_duration (ms)	0.297 +/- 0.044	0.201 +/- 0.007	0.197 +/- 0.009	*** 1.167 +/- 0.946	*** 0.531 +/- 0.220	0.260 +/- 0.015
displacement_episode_duration (ms)	0.297 +/- 0.043	0.201 +/- 0.007	0.197 +/- 0.009	1.211 +/- 1.022	0.531 +/- 0.220	0.260 +/- 0.015
stationary_episode_duration (ms)	0.297 +/- 0.099	0.201 +/- 0.007	0.197 +/- 0.009	0.438 +/- 0.330	0.531 +/- 0.220	0.260 +/- 0.015
speed_episode_duration (ms)	0.165 +/- 0.045	0.133 +/- 0.005	0.088 +/- 0.004	0.573 +/- 0.462	0.183 +/- 0.018	0.127 +/- 0.018
episode_frequency (Hz)	10.067 +/- 15.151	6.074 +/- 4.202	6.490 +/- 3.990	38.716 +/- 35.531	22.427 +/- 11.826	5.849 +/- 1.930
episode_mean_burst_frequency (Hz) *	23.228 +/- 2.950	N/A	N/A	N/A	N/A	N/A
episode_peak_burst_frequency (Hz) *	28.315 +/-2.247	N/A	N/A	N/A	N/A	N/A
episode_num_tailbeats	5.474 +/- 1.068	4.008 +/- 0.085	4.144 +/- 0.313	22.933 +/- 17.735	11.612 +/- 5.079	5.851 +/- 0.214
episode_mean_speed (mm/sec)	7.038 +/- 3.299	4.671 +/- 0.678	2.452 +/- 0.365	7.351 +/- 3.187	7.552 +/- 2.589	3.809 +/- 0.723
episode_95th_speed (mm/sec)	23.199 +/- 11.652	15.711 +/- 2.834	7.273 +/- 0.841	25.339 +/- 12.322	22.626 +/- 7.643	9.043 +/- 1.386
episode_peak_speed (mm/sec)	29.933 +/- 12.909	19.462 +/- 2.470	** 7.389 +/- 0.898	** 35.119 +/- 16.713	* 28.154 +/- 8.855	** 9.464 +/- 1.802
displacement_episode_mean_speed (mm/sec)	7.156 +/- 3.380	4.671 +/- 0.678	2.452 +/- 0.365	7.515 +/- 3.133	7.552 +/- 2.589	3.809 +/- 0.723
displacement_episode_95th_speed (mm/sec)	23.201 +/- 11.650	12.456 +/- 1.987	6.656 +/- 0.772	25.339 +/- 12.322	20.971 +/- 10.021	7.821 +/- 1.266
displacement_episode_peak_speed (mm/sec)	25.958 +/- 12.904	15.462 +/- 2.470	7.389 +/- 0.898	35.119 +/- 16.713	28.154 +/- 8.855	9.464 +/- 1.802
episode_burst_balance (rad; integrated dtheta)	0.004 +/- 10.365	1.507 +/- 3.844	-0.990 +/- 3.439	2.258 +/- 27.346	4.376 +/- 10.044	-0.291 +/- 0.416
episode_burst_balance_last_50%_episode (rad)	-0.034 +/- 5.213	0.830 +/- 2.013	-0.599 +/- 1.783	1.714 +/- 19.392	2.796 +/- 6.231	-0.460 +/- 0.862
left_turn_duration (ms)	0.061 +/- 0.011	0.073 +/- 0.005	0.068 +/- 0.003	0.089 +/- 0.023	0.091 +/- 0.018	0.079 +/- 0.001
left_turn_angle (degrees)	26.318 +/- 8.006	31.628 +/- 3.699	31.452 +/- 2.513	38.068 +/- 15.838	37.550 +/- 11.706	34.999 +/- 0.830

Table 4 (continued)

Parameters	D4ISO 56 mm Sprint	D4ISO 29 mm Sprint	D4ISO 29 mm Hunt	D1 Antag 90 mm Sprint	D1 Antag 29 mm Sprint	D1 Antag 29 mm Hunt
num_left_turns_in_episode	0.621 +/- 0.221	0.369 +/- 0.102	0.229 +/- 0.028	1.839 +/- 2.269	0.518 +/- 0.153	0.261 +/- 0.005
total_left_turn_duration_in_episode (ms)	0.037 +/- 0.009	0.027 +/- 0.008	0.014 +/- 0.003	0.160 +/- 0.153	0.045 +/- 0.007	0.024 +/- 0.004
total_left_turn_angle_in_episode (degrees)	16.624 +/- 6.569	11.544 +/- 2.558	4.288 +/- 1.291	65.867 +/- 60.391	17.276 +/- 5.751	9.603 +/- 1.966
episode_phasing_of_left_turns (ms after start)	0.071 +/- 0.054	0.039 +/- 0.008	0.010 +/- 0.002	0.745 +/- 0.700	0.656 +/- 0.770	0.009 +/- 0.000
right_turn_duration (ms)	0.065 +/- 0.008	0.074 +/- 0.014	0.070 +/- 0.004	0.083 +/- 0.026	0.124 +/- 0.072	0.076 +/- 0.003
right_turn_angle (degrees)	-27.732 +/- 7.098	-36.303 +/- 6.831	-32.313 +/- 4.120	-36.455 +/- 14.927	-76.712 +/- 43.796	-32.413 +/- 0.890
num_right_turns_in_episode	0.598 +/- 0.220	0.250 +/- 0.068	0.225 +/- 0.068	1.659 +/- 2.308	0.477 +/- 0.108	0.200 +/- 0.001
total_right_turn_duration_in_episode (ms)	0.040 +/- 0.016	0.019 +/- 0.008	0.014 +/- 0.005	0.142 +/- 0.158	0.059 +/- 0.030	0.019 +/- 0.000
total_right_turn_angle_in_episode (degrees)	-17.373 +/- 8.301	-9.203 +/- 3.191	-4.625 +/- 2.248	-64.389 +/- 72.488	-37.327 +/- 19.024	-7.350 +/- 0.202
episode_phasing_of_right_turns (ms after start)	0.080 +/- 0.051	0.037 +/- 0.009	0.009 +/- 0.004	0.745 +/- 0.709	0.306 +/- 0.366	0.011 +/- 0.001
total_num_turns_in_episode	1.219 +/- 0.404	0.619 +/- 0.132	0.454 +/- 0.082	3.498 +/- 4.559	0.996 +/- 0.250	0.461 +/- 0.004
total_turn_duration_in_episode (ms)	0.077 +/- 0.020	0.046 +/- 0.013	0.028 +/- 0.007	0.302 +/- 0.303	0.104 +/- 0.032	0.043 +/- 0.004
total_turn_angle_in_episode (degrees)	33.998 +/- 12.153	20.751 +/- 3.081	8.913 +/- 3.346	130.260 +/- 129.818	54.603 +/- 15.613	16.956 +/- 1.760
net_turn_angle_in_episode (degrees)	-0.749 +/- 8.742	2.341 +/- 4.898	-0.336 +/- 1.499	1.478 +/- 30.823	-20.051 +/- 23.370	2.254 +/- 2.168
abs_net_turn_angle_in_episode (degrees)	27.640 +/- 8.917	17.375 +/- 2.726	8.634 +/- 3.241	59.374 +/- 35.347	41.819 +/- 17.223	16.272 +/- 1.587
nonzero_total_num_turns_in_episode	1.376 +/- 0.329	1.198 +/- 0.098	1.045 +/- 0.011	3.812 +/- 4.489	1.794 +/- 0.758	1.086 +/- 0.000
nonzero_total_turn_duration_in_episode (ms)	0.088 +/- 0.014	0.089 +/- 0.004	0.064 +/- 0.007	0.328 +/- 0.298	0.183 +/- 0.061	0.101 +/- 0.008
nonzero_total_turn_angle_in_episode (degrees)	38.480 +/- 10.991	40.878 +/- 7.579	** 19.957 +/- 4.459	**** 141.811 +/- 126.737	**** 95.230 +/- 26.418	38.944 +/- 3.812
nonzero_net_turn_angle_in_episode (degrees)	-0.461 +/- 9.643	4.432 +/- 11.494	-0.398 +/- 3.466	3.857 +/- 34.337	-36.813 +/- 40.793	5.290 +/- 5.065
nonzero_abs_net_turn_angle_in_episode (degrees)	31.317 +/- 7.831	34.093 +/- 5.143	19.349 +/- 4.279	66.860 +/- 35.322	71.875 +/- 24.610	38.332 +/- 3.424
total_distance_traveled_episode (mm)	2.260 +/- 1.264	1.007 +/- 0.168	0.476 +/- 0.060	9.278 +/- 7.286	3.992 +/- 1.404	1.003 +/- 0.303
dist2wall_episode_onset (mm)	11.431 +/- 3.721	3.414 +/- 1.531	3.103 +/- 1.296	42.564 +/- 180.860	3.616 +/- 1.553	3.960 +/- 0.604
dist2wall_episode_offset (mm)	11.316 +/- 3.729	3.405 +/- 1.542	3.022 +/- 1.248	41.974 +/- 180.971	2.779 +/- 0.944	3.874 +/- 0.557
delta_dist2wall_from_episode (mm)	0.115 +/- 0.061	0.009 +/- 0.016	0.081 +/- 0.051	0.610 +/- 0.927	0.837 +/- 0.712	0.086 +/- 0.047
sample size (n)	40	4	4	30	4	4
arena diameter (mm)	50	20	20	50	20	20
* 210 fps (n)	6	N/A	N/A	N/A	N/A	N/A

General Discussion

This thesis provides new methodologies to automate high-throughput detection and analyses of locomotor and goal-directed behavior in zebrafish, and elucidates that both behaviors require the DDT and/or endogenous D4R signaling. The voluminous evidence for the vertebrate DDT's comprehensive conservation underscores the significance that our findings suggest an ancient and preserved role of the vertebrate DDT in locomotor development and goal-directed foraging. These methods and findings are guiding and facilitating current and future studies in zebrafish and other animal models, either in investigating the neuroethology of locomotion or the many components and neural modules underlying goal-directed behavior.

Role of the DDT-D4R Network in Locomotor Development (Ch1 & Ch2)

The crux of my locomotor findings is that the conserved *otpb* neurons comprising the DDT provide the impetus for endogenous D4R signaling, likely in the spinal cord, to initiate and maintain the developmental switch to the mature zebrafish locomotor pattern of short swimming episodes (Chapter 1) (Lambert et al., 2012). This conclusion is corroborated by three recent zebrafish studies (Tong and McDearmid, 2012; Reimer et al., 2013; Decker et al., 2014). Additionally, my further kinematic analyses reveal that the DDT and endogenous D4R signaling

powerfully influence other locomotor parameters that do not systemically covary with episode duration, revealing a DAergic meta-locomotor modulation that putatively influences different locomotor features via separable neural modules (Chapter 2).

Abnormal Differentiation of DDT and DA-Rescuable Locomotor Deficit in Trpm7 Mutants (Appendix 2b).

One of the studies corroborating a role for the DDT in locomotor development is a middle-authorship in this thesis (Appendix 2b); mutation of transient receptor potential, melastatin-like 7 (Trpm7), a combined ion channel and kinase implicated in the differentiation or function of many cell types, leads to abnormal differentiation of DAergic neurons and impairs locomotor development in zebrafish (Decker et al., 2014). This impaired behavioral and fictive motor phenotype is rescued by exogenous DA or L-Dopa (Decker et al., 2014). There are two abnormal DAergic populations in *trpm7* mutants, one in the hypothalamus and the other in the pretectum (Decker et al., 2014). This hypothalamic population corresponds to DC5 and DC6 populations in the diencephalon and contributes to the DDT (Kastenhuber et al., 2010; Tay et al., 2011). Interestingly, this population also represents two of the three *otpb* populations that were chemogenetically ablated and resulted in perpetuation of the immature locomotor pattern in my first study (Lambert et al., 2012). This cross-study overlap suggests that abnormal differentiation of DAergic neurons in

the hypothalamus, but not the pretectum, underlies the DAergic-rescuable motor impairment in *trpm7* mutants.

DDT-D4R Network as a Multifunctional Neuromodulator of Spinal Neuronal Differentiation and Locomotor Circuit Function.

A recent seminal and comprehensive study strongly validates my chief DDT-D4R circuit conclusion, definitively confirming that the zebrafish DDT functionally supplies DA to the spinal cord *in vivo* to induce endogenous spinal D4R signaling that influences early spinal neurogenesis and locomotor development (Reimer et al., 2013). The advent of detectable spinal levels of DA is at 33 hpf and corresponds to the initial invasion of DDT fibers into the rostral spinal cord, as far caudal as somite 8 (Reimer et al., 2013); the hindbrain-spinal cord junction is between somites 2/3 and the spinal cord consists of somites 3-33 (McDearmid and Drapeau, 2006; Chong and Drapeau, 2007). Concomitantly, the DDT signals through spinal D4Rs at this time, specifically in motor neural progenitor cells (pMNs), to promote neural differentiation of islet+ secondary motor neurons at the expense of Vsx1+ V2a premotor interneurons (Reimer et al., 2013). This voluminous evidence comes from: 1) blocking endogenous D4R signaling via 10 uM of L745870, the exact same antagonist and concentration that I have employed (Lambert et al., 2012) 2) obtaining the reverse effect (decreased motoneuron and increased V2A neurogenesis) via D4R agonism, and which is

specifically blocked by L745870 3) morpholino knockdown of D4R mRNA (specifically *drd4a*), validating the specificity and targeting efficacy of D4R pharmacology in zebrafish and my studies 4) morpholino knockdown of *tyrosine hydroxylase1* (*th1*) 5) toxic ablation of DAergic cells via 6-OHDA and 6) *otp* mutants, which genetically reduces DDT neurons and fibers (Ryu et al., 2007; Kastenhuber et al., 2010).

This DDT-D4R mechanism in shifting spinal motor neuronal differentiation occurs very early, between 33-72 hpf (Reimer et al., 2013), compared to the advent of the DDT-D4R induced developmental switch in the locomotor pattern at 96 hpf (4 dpf) that my study reveals (Lambert et al., 2012) and suggests separate spinal targets for each mechanism. The early differentiation mechanism is confirmed to be due to D4R signaling in pMNs but not differentiated motor neurons, and all 3 D4R mRNAs are greatly enriched in pMNs while only being minimally expressed in motor neurons at this time (Reimer et al., 2013). Also, blocking endogenous D4R signaling from 24-72 hpf, aside from affecting spinal neuronal differentiation, reduces total motility at 7dpf but does not affect expression of the mature locomotor pattern (Reimer et al., 2013) and unpublished observations). Conversely, the later locomotor pattern mechanism can be perturbed, via D4R antagonism or DDT chemogenetic ablation, at 5 dpf (Lambert et al., 2012) and even as late as 7 dpf (Chapter 2) and is reversible within a day (unpublished observations). If the later D4R antagonism-induced alteration in the locomotor

pattern was due to altering pMNs and ultimately differentiation of spinal motor and premotor pools, the perturbation would not be expected to be so quickly and completely reversible. Moreover, since the essential hindbrain and spinal locomotor CPGs are established by 4 dpf (McLean and Fetcho, 2004a) and is reflected in a mature-like episodic swimming pattern that remains consistently stable into adulthood (Fuiman and Webb, 1988), any influence on subsequent spinal neuronal differentiation would not be expected to overtly influence the already wired and established neural and behavioral locomotor patterns. Finally, the fact that the mature locomotor pattern at 4-7 dpf is immediately relegated to an immature pattern following spinal cord transection and is rescued by exogenous DA or D4R agonism within 5 to 10 minutes (Lambert et al., 2012) confirms that the DDT-D4R induced later mechanism of sculpting the locomotor pattern is from spinal neuronal signaling and not neuronal differentiation, since such a short time course is insufficient for the latter's plausibility. Hence, the zebrafish DDT is confirmed to be a versatile multifunctional neuromodulatory system that acts directly in the spinal cord to influence both neuronal differentiation and neuronal locomotor circuit function via distinct mechanisms and spinal targets, despite a common impetus through endogenous spinal D4R signaling.

DDT-D4R Network is Functional in Adults to Recapitulate Developmental Processes for Regeneration Following Spinal Cord Injury.

Reimer and colleagues (2013) went a step further in adult zebrafish to elucidate that spinal cord injury recruits the DDT to recapitulate D4R-mediated developmental processes and repurpose them for regeneration. Mirroring the same processes at the larval stage, the DDT drives D4R signaling in pMNs to promote new motor neuron generation rostral to the lesion site, where DDT fibers maintain innervation and even show compensatory new sprouting of arbors (Kuscha et al., 2012). Concomitantly, ISH and quantitative real-time PCR (qRT-PCR) for spinal D4Rs show that *drd4a* is upregulated in the ependymal progenitor zone, where pMNs reside, specifically rostral but not caudal to the lesion site. Moreover, 6-OHDA lesioning of DAergic neurons, which are exclusively in the brain and not the spinal cord even in adults (Kuscha et al., 2012), significantly decreases new motor neuron generation rostral to the lesion site, confirming that DDT axons are required. Conversely, significantly less regeneration occurs caudal to the lesion site, where DDT fibers are aberrantly absent and do not regrow into the caudal site until many weeks post-lesion (Kuscha et al., 2012). However, D4R agonist treatments locally administered to the caudal lesion site for several days significantly increases caudal drd4a expression and new motor neuron generation. This D4R agonism clearly emulates DAergic drive from the DDT, because the same treatment regimen administered rostral to the lesion site does not further enhance the already present new motor neuron generation rostrally that is dependent on its intact DDT innervation.

Collectively, spinal cord injury recruits the DDT to enhance arborizations and *drd4a* expression to facilitate new motor neuron generation rostral to the lesion site, and the caudal site is rescuable via a D4R agonist regimen. Although this study clearly demonstrates *in vivo* functionality of the adult DDT for regeneration, no data here or elsewhere in the literature exist to elucidate whether the adult DDT, or even DA for that matter, also influences normal adult locomotor patterns. Although this remains an open question, it appears that the putative spinal episode pattern generator in larvae (Lambert et al., 2012; Wiggin et al., 2012) may not be as hard-wired in adults (Gabriel et al., 2007), suggesting that the DDT-spinal D4R circuit to shorten swimming episodes in larvae may not be employed, or at least not replied upon as frequently, and that this task may be reallocated primarily to a hindbrain mechanism (Kimura et al., 2013).

DDT-D4R Network as a Multisite Meta-Locomotor Modulator.

My more exhaustive kinematic analyses reveal that the DDT-D4R circuit profoundly influences several distinct locomotor parameters in a separable fashion (Chapter 2). Namely, endogenous D4R antagonism or chemogenetic ablation of *otpb* neurons (and, hence, the DDT) relegates 4 to 7 dpf larvae to an immature locomotor repertoire of long, fast, and erratic (large turn angle) swimming episodes. Interestingly, examination of the distribution of all individual swimming episodes, comprising a total sample size of thousands to tens of

thousands of locomotor events per experimental group, reveals that there is no correlation between the episode duration and peak speed of a given swimming episode. This holds true whether looking at swimming episodes over natural development or following DDT-D4R perturbations. This makes sense under normal conditions, since the putative spinal episode pattern generator is dissociable from the spinal coordination generator (Wiggin et al., 2012), the latter of which is in regiser with dynamic tail beat frequencies and influences swimming speed (McLean et al., 2007; 2008; McLean and Fetcho, 2009). This alone reveals that spinal episodic patterning and CPG coordination/speed must be achieved through distinct spinal neuronal populations. Aside from the DDT-D4R perturbations separably increasing episode durations and peak speeds across swimming episodes, total turn angle is also not well correlated to episode duration but there is at least a mild correlative trend in this case; this could at least partially be due to more time to accrue total turning but suggests a separable neural mechanism as well. If all three of these locomotor parameters are set and modulated by the DDT-D4R circuit but at distinct sites, where might each of these sites be located and on which neuronal targets?

Episode Duration. The most comprehensive evidence exists for the site of action of DDT-D4R modulation of episode duration, which is quickly altered to an immature long episodic pattern upon removal of the brain and DA added directly to the spinal cord is sufficient to rescue spinalized preparations to sculpting short

mature-like episodes within minutes of application (Lambert et al., 2012). Chemogenetic ablation of *otpb* neurons and the DDT, the sole source of spinal DA, perpetuates immature long episodes *in vivo* and is consistent with the spinalized findings to conclude that the most likely *in vivo* site of action is in the spinal cord. Even though the DDT's extensive long-range morphology endows it with the potential to also modulate circuits in every major part of the brain (telencephalon, diencephalon, midbrain, and hindbrain), progressive transections that remove more and more parts of the brain reveal that the *otpb* neurons and DDT, in the absence of the more rostrally-located non-DAergic population, act caudal to the diencephalon to shorten swimming episodes, either in the hindbrain or spinal cord (Lambert et al., 2012). Moreover, the fact that larval spinalized preparations are hard-wired to continue generating episodic NMDA-induced locomotor activity (McDearmid and Drapeau, 2006; Eklöf-Ljunggren et al., 2012; Lambert et al., 2012; Wiggin et al., 2012), which is not seen in other major animal models upon spinal transection, definitively divulges a covert spinal mechanism for controlling episode duration. Taken together, the most parsimonious conclusion is that DAergic *otpb* neurons and the DDT act directly in the spinal cord *in vivo* to sufficiently shorten swimming episodes via endogenous spinal D4R signaling.

However, it has been shown that there is also a supraspinal locus for controlling episode generation and the DDT may also influence it; hindbrain reticulospinal

V2A neurons instantaneously shorten episode duration upon optogenetic inhibition in the middle of an ongoing locomotor episode at 3 dpf (Kimura et al., 2013). This makes sense since the reticulospinal neurons comprising the hindbrain swim command circuit provide the direct excitatory drive to the spinal cord to recruit the spinal CPG and initiate locomotion (Arrenberg et al., 2009), making for an intuitive locus to episodically gate the duration at which each swimming episode is elicited. Interestingly, the DDT traverses in close apposition to this hindbrain swim command circuit (McLean and Fetcho, 2004a; Kastenhuber et al., 2010; Tay et al., 2011), where some of the reticulospinal V2A neurons reside, so the DDT is poised to modulate hindbrain episode generators as well. Regardless, the type of neuron that controls episode duration and receives inhibitory modulation by D4R signaling likely has sustained activity throughout a swimming episode. As such, this activity pattern would be consistent with many glutamatergic reticulospinal neurons that provide sustained episodic excitatory drive to the spinal cord. In the spinal cord, this activity pattern would be consistent with a glutamatergic spinal source of sustained episodic excitatory drive to premotor CPG interneurons that putatively determine ongoing motoneuron output. Such a spinal neuron could hypothetically employ a persistent sodium current-driven plateau potential that gates the on-state of the spinal CPG and which direct D4R inhibition could sculpt shorter plateau potentials and, hence, shorter elicited swimming episodes.

Swimming Speed. It is plausible that the DDT-D4R circuit biases slower swimming speeds (Chapter 2) by influencing the basal recruitment of well-established topographic maps of swimming frequency in both the spinal cord (McLean et al., 2007; 2008) and hindbrain (Kinkhabwala et al., 2011; Koyama et al., 2011; Kimura et al., 2013), as well as via the higher order multifunctional nucleus of the medial longitudinal fasciculus (nMLF) in the midbrain (Severi et al., 2014). This is because all of these regions are established to exert exquisite control of swimming frequency and/or speed, and the DDT fibers and arborizations are positioned to putatively innervate and influence each area (McLean and Fetcho, 2004a; 2004b; Kastenhuber et al., 2010; Tay et al., 2011). My work shows that DA or D4R agonism in the spinal cord is sufficient to slow fictive swimming frequencies in spinalized preparations (Chapter 2), suggesting that the DDT may preferentially provide tonic inhibitory D4R input to components of the spinal topographic map that are recruited for faster swimming frequencies, such as: primary motor neurons, dorsal secondary motor neurons, dorsal glutamatergic interneurons (e.g. V2as), or ventral glycinergic interneurons (e.g. circumferential descending interneurons (CiDs)) (McLean et al., 2007; 2008). However, it is quite possible that the DDT exerts a similar inhibitory D4R-induced bias onto the fast components of the hindbrain topographic recruitment pattern for swimming frequency. Finally, the DDT longitudinal projection pattern and arborizations traversing the midbrain are in apposition to potentially inhibit the nMLF, which has been shown to be necessary for appropriate proportional

modulation of forward swimming speed as a function of the grating speeds of optomotor response-inducing visual stimuli (Severi et al., 2014).

Turning Angle. Larvae past 4 dpf consistently exhibit directed and fine spontaneous turning, at a mean total turning angle of ~40 degrees per episode (Chapter 2) (Mirat et al., 2013). Perturbation of the DDT-D4R circuitry induces significantly larger mean turn angles per spontaneous swimming episode, often inducing highly circuitous turning trajectories that exceed 360 degrees and sometimes exceed several circular turning revolutions (Chapter 2). Although there is a slight trend for this aberrant turning angle to be correlated to episode duration (Chapter 2), the DDT-D4R circuit could plausibly influence the highly specific and isolated small locus of turn cells in the hindbrain that are active during and necessary to control turning (Orger et al., 2008). Conversely, it is quite implausible that the DDT-D4R circuit could influence turning in the spinal cord, because this would require a unilaterally-biased modulation of much of the spinal locomotor circuit.

Future directions. Elucidating the specific putatively distinct sites of action of DDT-D4R modulation of these three locomotor parameters could be achieved via either *in vivo* targeted laser ablations (Gahtan and O'Malley, 2001) or spatiotemporal bidirectional optogenetic control (Douglass et al., 2008; Arrenberg et al., 2009; Wyart et al., 2009; De Marco et al., 2013; Kimura et al., 2013;

Ljunggren et al., 2014) of the DAergic *otpb* neurons and/or their ascending and descending projections. These experiments will be apart of my long-established project of exploring premature advancement of the locomotor developmental switch via pharmacological and ultimately optogenetic DAergic interventions, as well as elucidating the phenomenon's underlying pre- and post-synaptic mechanisms; see Appendix 1b for more details on significance, experimental design, and preliminary results. Additionally, this comprehensive project would greatly benefit from concurrently elucidating the spatiotemporal activity and specific sites of action of the DDT-D4R circuit's role in goal-directed hunting (Chapter 2). This could most powerfully be achieved via whole-brain calcium imaging (Ahrens et al., 2012; 2013b) and spatiotemporal bidirectional optogenetic control (Douglass et al., 2008; Arrenberg et al., 2009; Wyart et al., 2009; De Marco et al., 2013; Kimura et al., 2013; Ljunggren et al., 2014) during tethered virtual prey pursuit (Trivedi and Bollmann, 2013; Preuss et al., 2014) and fictive navigation (Ahrens et al., 2013a). The three primary locomotor parameters perturbed by DDT-D4R perturbations (Chapter 2)- episode duration, speed, and turn angle- are putatively critical to be executed with fine precision during free-swimming and virtual prey capture (Borla et al., 2002; McElligott and O'Malley, 2005; Trivedi and Bollmann, 2013; Preuss et al., 2014). My findings on the DDT-D4R role in prey capture reveals that precision of speed is critical for success, while the patterning of episodes and turning angles can deal with a broader modulatory range and still be efficacious for prey capture. What follows

is a critique of what my DAergic prey capture study (Chapter 2) elucidates and what remains to be investigated in future studies.

Role of the DDT-D4R Network in Goal-Directed Behavior (Ch2)

There is a rich literature on the neural bases of goal-directed locomotion in vertebrates (Grillner et al., 2008). However, studies on the specific goal-directed behavior of prey-directed hunting have primarily elucidated the underlying sensory and sensorimotor components (Ewert, 1970; Ewert and Ingle, 1971; Ewert and Siefert, 1974; Ewert et al., 1978; 1979; Ewert and Burghagen, 1979; Ewert, 1980; Sch rg-Pfeiffer and Ewert, 1981; Weerasuriya and Ewert, 1981; Ewert et al., 1983; Ewert, 1984; Ewert et al., 1985; Matsumoto et al., 1991; Glagow and Ewert, 1994; Wachowitz and Ewert, 1996; Gahtan, 2005; Smear et al., 2007; Del Bene et al., 2010; Ewert, 2010a; 2010b; Muto et al., 2013) but with a dearth of findings on the downstream motor and locomotor components (Nishikawa, 1999). My prey capture study reveals a powerful role of endogenous D4R signaling in biasing motor-planning prey-catching strategies and the execution of prey-directed maneuvers (Chapter 2). It also reveals that the spontaneous coarse erratic bias under D4R antagonism is powerfully overridden during visually-guided prey-pursuit, being invariably replaced with attempts at fine motor control that succeed in orienting but fail at advancing toward prey. On the presynaptic end, while chemogenetic ablation of the *otpb* neurons and the

DDT compromises the spontaneous locomotor repertoire and impairs prey capture, suggesting a pivotal role for the DDT network in prey capture and hunting maneuvers, the specific ablation methodology used (Curado et al., 2008; Pisharath and Parsons, 2009) induces caveats (Mathias et al., 2014) that preclude a sound investigation of the resultant DDT-perturbed alterations in prey capture (Chapter 2). Nevertheless, my prey capture study provides significant advancements in understanding the neural bases of prey capture and is explicitly instructive for future studies.

Endogenous D4R Signaling is Necessary For Prey Capture.

Although work in the classic anuran prey capture model has revealed that exogenous DAergic agonism influences prey-catching strategies (Glagow and Ewert, 1996; 1997a; 1997b; 1999), it is unknown whether there exists a true endogenous DAergic counterpart of this phenomenon and whether it would induce the opposite shift in motor strategies compared to exogenous agonism. My study elucidates that endogenous DAergic signaling in zebrafish is necessary for determining prey-catching strategies and further reveals a detailed kinematic analysis of the failed execution of advancing but not orienting maneuvers (Chapter 2). Consistent with the exogenous effects in anurans, D4R antagonism in zebrafish shifts animals to an orienting prey-catching strategy while DAergic agonism in anurans shifts animals to an advancing (or snapping) prey-catching

strategy ((Glagow and Ewert, 1996; 1999)). This suggests conversation in the DAergic role in prey capture.

Moreover, my study reveals that specifically endogenous D4R signaling, and not D1R or D2/D3R signaling, is responsible for this motor-centric role in prey capture (Chapter 2). The fidelity of DAR pharmacology in zebrafish has been definitively validated in several studies (Boehmler et al., 2004; Giacomini et al., 2006; Boehmler et al., 2007; Li et al., 2007b; Thirumalai and Cline, 2008; Souza et al., 2011; Lambert et al., 2012; Rihel and Schier, 2012; Irons et al., 2013; Reimer et al., 2013; Tran et al., 2014). Most powerfully, a recent study demonstrated that the effects of morpholino mRNA knockdown of the specific DAR gene products are equitably emulated by corresponding high-affinity DAR-specific antagonism; moreover, complementary experiments wherein the DDT is genetically or chemically ablated can be rescued by the specific high-affinity DAR agonist predicted from mRNA knockdown and, moreover, this rescue is occluded by the corresponding DAR mRNA knockdown or via DAR-specific antagonism (namely the *drd4a* mutant and D4R pharmacology, respectively) (Reimer et al., 2013).

The comprehensive high-throughout, automated, and unbiased analyses in my study reveal that the compromised prey capture performance following D4R antagonism is due to a specific motor-centric deficit in execution of a subset of

hunting maneuvers. Specifically, D4R antagonism impairs prey capture in zebrafish by inducing a bradykinesia-like phenotype specifically during execution of advancing maneuvers, inducing insufficient speed and negligible reduction in distance toward prey during either advancing or capture swims. Impressively, larvae under D4R antagonism still execute orienting maneuvers, used to reduce angular heading toward prey, equally as well as controls and, moreover, opt for a more dominant orienting prey-catching strategy compared to controls. It is unknown but provocative to consider whether this bias in orienting is due to 1) D4R signaling inducing an internal neural switch in prey-catching strategies, as suggested for exogenous DA in anurans (Ewert et al., 2001) and/or 2) an external stimulus-response shift to more orienting due to prey getting away more often and, consequently, increasing the frequency of larger fish-prey inter-angles.

Additionally, other analyses are consistent with the conclusion that visual, oculomotor, and visuomotor function are intact following D4R antagonism, underscoring a motor-specific deficit. Specifically, compared to controls, larvae under D4R antagonism: 1) visually detect and pursue prey at a similar frequency 2) exhibit the same oculomotor eye convergence angles at rest 3) exhibit the same increase in eye convergence angle upon prey detection 4) maintain the increased magnitude of eye convergence throughout each hunting sequence 5) engage in individual hunting sequences for the same duration 5) exhibit a similar latency to the first visuomotor initiation following the start of a hunting sequence

and 6) effectively execute visuomotor orienting maneuvers to similarly reduce angular heading toward dynamically motile prey. Collectively, my prey capture study convincingly shows that endogenous D4R signaling *in vivo* is necessary for specific advancing motor-centric strategies and their execution for effective prey capture (Chapter 2), but more evidence is needed to isolate the specific DAergic population involved and its ultimate anatomical postsynaptic site of action in driving the specific D4R signaling crucial to prey capture.

DAergic Population Necessary for the Endogenous D4R Influence on Prey Capture Strategy, Execution, and Success.

The DAergic *otpb* neurons and the DDT are likely involved in driving the D4R signaling crucial to motor-centric aspects of prey capture (Chapter 2), but the caveats of the chemogenetic ablation employed (Curado et al., 2008; Pisharath and Parsons, 2009; Mathias et al., 2014) require an alternative strategy to investigating the germane role of the DDT network in goal-directed hunting. Chemogenetic ablation of the DDT via the nitroreductase-metronidazole (Ntr-Mtz) system induces cell-autonomous specific cell death of *otpb* neurons with no collateral damage, as we have previously shown (Lambert et al., 2012). Examination of locomotor activity alone at 5 dpf reveals that ablation of the *otpb*+ DDT perpetuates the immature locomotor repertoire of long, fast, erratic episodes, while Mtz-treated controls are not different from untreated controls in terms of exhibiting short, slow, directed episodes and similar levels of total

distances traveled (Lambert et al., 2012), Chapter 2). From the known importance of these locomotor parameters to prey capture, namely precision of speed, it is hypothesized that chemogenetic ablation of the DDT will impair prey capture and motor strategies similar to systemic D4R antagonism. Indeed, prey capture is compromised following ablation of the DDT, compared to untreated controls (Chapter 2). Unfortunately, my prey capture study reveals that Mtz treatment alone from 1-4 dpf impairs prey capture performance at 5 dpf (Chapter 2), yet TUNEL staining confirms that there is definitively no specific or non-specific cell death from the Mtz prodrug alone (Lambert et al., 2012). Hence, there is a caveat to early Mtz treatment that is only exploited after examination of prey capture performance.

It is possible that the high concentration (5-10 mM) of the Mtz antibiotic perturbs with orexigenic satiety factors (Shimada et al., 2012) and/or with the development of a functional digestive system for prey ingestion, the latter of which occurs between 1 and 4 dpf (Wallace and Pack, 2003) and exactly matches the time course of the aforementioned Mtz regimen. The rostral digestive tract is fully functional by 3 dpf, when the lumen of the posterior pharynx is visible and the mouth is open, and posteriorly when the anus is open at the beginning of 4 dpf (Wallace and Pack, 2003). Not surprisingly, the advent of a fully functional digestive system at 4 dpf coincides precisely with the advent of prey capture, ingestion, and digestion (Borla et al., 2002; McElligott and

O'Malley, 2005; Muto et al., 2013). Knowing this, the next strategy was to administer Mtz only subsequent to this critical gut and digestive development, this time from 4-6 dpf and then examine prey capture at 7 dpf. This strategy circumvents the previous issues with Mtz, because these Mtz-treated controls have excellent prey capture performance at 7 dpf that is not significantly different from untreated controls (Chapter 2). As for the chemogenetic ablation of the DDT from 4-6 dpf, it induces an immature locomotor repertoire of long, fast, erratic episodes and severely impairs prey capture performance compared to Mtz-treated or untreated controls (Chapter 2). As such, this effect is definitively from chemogenetic ablation of *otpb* neurons.

Unfortunately, chemogenetic ablation of *otpb* neurons at this later developmental time point, from 4-6 dpf, severely impairs health and was lethal to over 33% of larvae by 7dpf (Chapter 2), none of which was observed in either control groups or from ablation of otpb neurons earlier in development (from 1-4 dpf). This result indicates that *otpb* neurons are vital to health in zebrafish, at some time point between 4-6 dpf, and could be do to either the caudal diencephalic DAergic population, and its DDT, or the rostral diencephalic non-DAergic population. The non-DAergic otpb population is a large heterogeneous cluster of neurosecretory neurons that are known to be critical for non-visual light seeking behavior in zebrafish (Fernandes et al., 2012), as well as neuronal adaptation to stress in both zebrafish and mouse (Amir-Zilberstein et al., 2012). The latter function

could be pivotal to early survival. Moreover, *otp*-deficient mice die shortly after birth (Acampora et al., 1999; Wang and Lufkin, 2000), confirming its lethality in a mammalian model with conserved *otp* populations and corresponding DDT (Ryu et al., 2007). Taken together, it is likely that the lethality from chemogenetic ablation of *otpb* neurons is due to the loss of vital functions provided by the non-DAergic *otpb* neurosecretory population between 4-7 dpf, which coincides with the advent of glucocorticoid-induced stress responses and other neuroendocrine functions in zebrafish (De Marco et al., 2013). Future studies that selectively ablate each *otpb* population separately *in vivo*, such as via targeted laser ablations (Gahtan and O'Malley, 2001), should clear this up and, moreover, potentially provide a means to selectively ablate the DAergic *otpb* population and DDT and examine its consequences on locomotion and prey capture.

Postsynaptic Site of Action of Endogenous D4R-Mediated Influence on Prey Capture Strategy, Execution, and Success.

Although my prey capture study reveals that endogenous D4R signaling is critical to specific motor aspects of prey capture and that the DDT could be involved, the anatomical site of action is currently unknown and could plausibly be located in several different neural domains.

Laser ablation of the entire DAergic *otpb* population, if it is the critical DAeric source for prey capture, should recapitulate the D4R antagonism-induced

impairments in prey capture. A corresponding control could be laser ablation of the non-DAergic population, although this may need to be performed and assessed before its potentially lethal effects discovered from late chemogenetic ablation (Chapter 2). Finally, it could be instructive to the anatomical site of action to laser ablate the DDT fibers at the level of the spinal cord. At the very least, spinal DDT fiber ablation would be expected to relegate 4-7 dpf larvae to long immature-like episodes since I have evidence that the DDT likely acts on spinal D4Rs to shorten swimming episodes (Lambert et al., 2012). Furthermore, if ablation of spinal DDT fibers impairs prey capture, it would suggest that endogenous D4R signaling directly in the spinal cord is responsible for some of the D4R influences on prey capture. This is a plausible anatomical scenario for simply influencing the execution of hunting maneuvers, although this task could also occur somewhere supraspinally. Conversely, a potential D4R-mediated shifting in visuomotor prey-catching strategies would most likely occur in the brain and not the spinal cord, such as in the zebrafish homolog of the striatum, the subpallium (Tay et al., 2011), or in visuomotor centers known to be critical for prey capture, namely the optic tectum and nMLF (Gahtan, 2005; Muto et al., 2013).

Finally, another exciting experimental avenue would be in exerting bidirectional optogenetic control (Douglass et al., 2008; Arrenberg et al., 2009; Wyart et al., 2009; De Marco et al., 2013; Kimura et al., 2013; Ljunggren et al., 2014) of

DAergic *otpb* neurons and the DDT during tethered virtual prey pursuit (Trivedi and Bollmann, 2013; Preuss et al., 2014) in controls and in larvae with D4R-specific knockdowns via artificial transcription activator-like effector nucleases (TALENS) (Bedell et al., 2012). Such an approach would provide exquisite control in systematically manipulating virtual prey parameters (Trivedi and Bollmann, 2013; Preuss et al., 2014) and comprehensively and definitively elucidating any graded prey-directed deficits in locomotion, prey catching strategy, or execution of specific hunting maneuvers. If any causal role of the DDT in locomotion and prey capture is found during optogenetic manipulations, then occlusion of this effect in specific TALEN D4R knockdowns would confirm a causal role of the specific D4R receptor involved (*drd4a*, *drd4b*, or *drd4c*). These experiments could concurrently help elucidate the putative distinct sites of action of the DDT-D4R network in modulating episode duration, speed, and turn angle. Furthermore, these experiments would fit well with my long-established ongoing project of premature advancement of the developmental switch (Appendix 1b).

Ancillary Publications, Current Projects, and Future Directions (Appendices)

My thesis and its novel methodologies in videography have spanned a total of eight primary research studies across five collaborations from six labs at five institutions, three studies of which are already published (Friedrich et al., 2012;

Lambert et al., 2012; Decker et al., 2014). Chapter 1 represents my published first-authorship (Lambert et al., 2012), which included a collaboration with the Bonkowsky lab (University of Utah). Appendices 2A (Friedrich et al., 2012) and 2B (Decker et al., 2014) represent my published middle-authorships, which included collaborations with the Downes (Boston University) and Cornell (University of Iowa) labs. Of the other five studies, three have been first-authorship projects (Chapter 2, Appendices 1A and 1B) and the other two middle-authorship projects (Appendices 2C and 2D). Additionally, I have two first-authorship review articles in preparation, both of which were greatly advanced from the writing of this dissertation. A synopsis of each project is given in the denoted sections of the thesis, and an abridged version of each, sans the two published middle-authorships (which are available in their entirety in Appendices 2A and 2B), is provided here for discussion.

Appendix 1A: Visuomotor Learning and Long-Term Memory of Goal-Directed Prey Capture.

I have employed my novel methodology for high-throughput automated detection and analyses of hunting sequences to elucidate that zebrafish larvae are capable of visuomotor learning and long-term memory of goal-directed prey capture performance. Larvae that are provided previous experience hunting either large paramecia (~ 200 μm) or small colpoda (~ 30 μm), 24 hours prior to testing, exhibit improved prey capture performance compared to naïve counterparts.

This effect is not simply due to obtained sustenance from prey, because colpoda feeding from 4 dpf onward did not improve the survival rate compared to unfed counterparts, although a regimen of paramecia or 5% egg yolk did. Several additional lines of evidence confirm that this enhancement is due to the visuomotor experience of chasing prey items and not due to any obtained sustenance resulting from prey capture. Compared to naïve counterparts, experienced larvae exhibit: 1) a shorter latency to increases in eye convergences and initiation of hunting sequences following exposure to prey 2) a shorter latency between execution of subsequent hunting maneuvers within a hunting sequence 3) a markedly better capture attempt success rate 4) consumption of all prey items in half the time course. Furthermore, this study reveals a strong negative correlation between capture attempt success rate and inter-maneuver durations, meaning that better precision of prey capture attempts correlates to shorter latencies between maneuvers. Interestingly, inhibition of protein synthesis, which is established to occlude many forms of long-term memory formation (Gerstner et al., 2009; Richter, 2010; Fioravante and Byrne, 2011; Konopka et al., 2011; Roberts et al., 2011; Wolman et al., 2011; Gal-Ben-Ari et al., 2012; Wolman and Granato, 2012; Aoki et al., 2013; Crystal and Glanzman, 2013; Glanzman, 2013; Hinz et al., 2013; Roberts et al., 2013), did not occlude the prey experience-dependent enhancements in prey capture performance. This could either be due to a protein synthesis-independent mechanism, which has been observed in drosophila (Gerstner et al., 2011; Chen et al., 2012a), or

from a lack of suboptimal phasing and/or duration of protein synthesis inhibition in relation to the prey training periods. Regardless, this study is the first to reveal the capacity of learning and long-term memory of goal-directed behavior in zebrafish larvae. Since this phenomenon occurs at a developmental time point when larvae are amenable to whole-brain calcium imaging (Ahrens et al., 2012; 2013a; 2013b) and bidirectional optogenetics (Douglass et al., 2008; Arrenberg et al., 2009; Wyart et al., 2009; De Marco et al., 2013; Kimura et al., 2013; Ljunggren et al., 2014), my work (Appendix 1a) will represent a landmark study that opens the doors to systematically and causally elucidating the neural mechanisms of goal-directed visuomotor learning and long-term memory *in vivo* at a brain-wide, systems, cellular, and subcellular level during virtual prey capture (Trivedi and Bollmann, 2013; Preuss et al., 2014).

Appendix 1B: Premature Advancement of Locomotor Development Via Spinal DAergic Agonism to Putatively Functional Spinal D4Rs.

While my published work on the role of the DDT-D4R network in locomotor development reveals that D4R antagonism can both prevent and reverse the developmental switch in the locomotor pattern at 4 and 5 dpf, respectively (Lambert et al., 2012), another important question is whether premature exposure of exogenous DA can advance the developmental switch at 3 dpf. That is, why don't 3 dpf larvae undergo this DDT/D4R-mediated switch, normally not

observed until 4 dpf, when both presynaptic and postsynaptic constituents of the DDT/spinal D4R circuit are already in place by or before 3 dpf (McLean and Fetcho, 2004a; Boehmler et al., 2007; Kastenhuber et al., 2010; Fujimoto et al., 2011; Reimer et al., 2013)? Although one might expect both DDT neuronal activity and spinal D4R expression to be low at 3 dpf, preliminary fictive experiments have led me to hypothesize that there is proper spatial expression of spinal D4Rs in premotor and/or motor neuron populations such that the spinal locomotor circuitry is primed for DAergic signaling from the DDT at 3 dpf. Systemic application of a D4R agonist transforms the spontaneous long-duration fictive swimming episodes of intact 3 dpf larvae to significantly shorter duration episodes. Moreover, either DA or a broad spectrum D2-like (D2R, D3R, D4R) agonist applied to the transected spinal cord of spinalized 3 dpf preparations transforms long-duration NMDA-induced fictive swimming episodes to a pattern of significantly shorter episodes, emulating a premature developmental switch via DAergic signaling in the spinal cord. These findings suggest that, at 3 dpf, the DDT does not provide sufficient endogenous spinal D4R signaling to the proper targets, but that spinal D4Rs are sufficiently expressed and primed to functionally modulate the spinal locomotor circuitry upon exogenous DAergic application to the spinal cord. This is consistent with previous studies that show that spinal motor neurons (which are definitively locomotor-related) express D4Rs before 3dpf, albeit at very low levels (Reimer et al., 2013). Also, a recent study exploring other phenomena demonstrated that systemic DAergic application at 2

dpf transforms otherwise long duration behavioral and fictive swimming episodes to become significantly shorter in duration; these investigators inadvertently and unknowingly induced a putative premature developmental switch to short swimming episodes, but with no evidence as to where in the nervous system this signaling is occurring (Tong and McDearmid, 2012). My DAergic spinalized studies at 3 dpf corroborate this finding and, moreover, further elucidate that the site of action to prematurely shorten episodes is sufficient to occur in the spinal cord. The fact that larvae at 3 dpf naturally continue to exhibit long immature-like episodes is consistent with another of my preliminary findings, which is that calcium activity of DDT neurons is markedly low at 3 dpf compared to 5 dpf. This, again, suggests that the 3 dpf DDT/spinal D4R circuitry is primed postsynaptically but without sufficient endogenous DAergic drive from the DDT. The continuation of this study will implement optogenetic control of DAergic *otpb* neurons and the DDT to investigate whether optogenetic activation of the DDT at 3 dpf causally initiates a premature advancement of locomotor development. In combination, these studies will be performed in controls and TALEN D4R mutants for *drd4a*, *drd4b*, and *drd4c*. An mutant-specific occlusion of any optogenetic DDT-driven advancement of locomotor development will causally isolate the necessary specific D4R subtype driven by the DDT.

Appendix 1C: An Ancient and Versatile Dopaminergic System: Evolutionary Conservation of the Dopaminergic Diencephalospinal Tract and Its Multifunctional Integration of the CNS. Review Article.

The contents of the General Introduction and General Discussion of this thesis comprise the precursor to one of my forthcoming first-author review articles, which will integrate these sections into a cogent review and positing of the DDT as a conserved multifunctional neuromodulatory network with putatively widespread influence on the CNS. Attention will be paid to collective conservational insights of the DDT network across vertebrates, ranging from genetic, topological, somatic, morphological, projectional, physiological, developmental, and behavioral components. The range of the DDT's known functions and the level of understanding of the neural mechanistic bases underlying these functions will be discussed. Other potential functions of the DDT network, based on its known projections and innervations, will be posited for future investigations. Finally, a proposal will be made for using the zebrafish model to best exploit the neural bases of the DDT's multiple functions *in vivo*, with an explicit roadmap delineated to employing integrative experimental designs to best achieve this collective goal.

Appendix 1D: Zebrafish Prey Capture as a Premiere Model to Elucidate Visuomotor Transformations, Learning, and Long-Term Memory of Goal-Directed Behavior. Review Article.

The precursor of another one of my forthcoming first-author review articles comes from the new methodology that I developed for this thesis, its implementation in two different studies of goal-directed prey capture (Chapter 2, Appendix 1A), and my proposal on how to best integrate this new methodology into the existing powerful germane repertoire of experimental approaches in zebrafish *in vivo*. The new methodology I developed in this thesis is the first to employ a high-throughput, unbiased, and automated means of detecting and analyzing hunting sequences in free-swimming zebrafish larvae. This approach will finally enable high-throughput unbiased pharmacological (Kokel et al., 2010; Rihel et al., 2010; Wolman et al., 2011) and genomic screens (Burgess and Granato, 2007a; Petzold et al., 2009; Wolman and Granato, 2012) for specific phenotypes exploited during goal-directed prey capture. Given the rich integrative nature of prey capture behavior, such screens will serve as a versatile and long-standing neuroethological platform for investigating its sensory, sensorimotor, motor, neuromodulatory, engrammic, attentional, and decision-making components (Ewert et al., 1999; 2001; Muto and Kawakami, 2013). Isolation of auspicious compounds and mutants following high-throughput prey capture screening can then be targeted for tethered virtual prey-pursuit (Trivedi and Bollmann, 2013; Preuss et al., 2014), during concurrent bidirectional optogenetic control (Douglass et al., 2008; Arrenberg et al., 2009; Wyart et al., 2009; De Marco et al., 2013; Kimura et al., 2013; Ljunggren et al., 2014) and whole-brain calcium/voltage imaging (Ahrens et al., 2012; 2013a; 2013b), to

elucidate the causal mechanism of specific neural modules to elementary components of goal-directed behavior. Hence, my newly developed approach to high-throughput screening of prey capture will merge investigations of goal-directed behavior in zebrafish to the more integrative recruitment and deployment that it deserves.

Appendix 2C: High-throughput Pharmacological and Genomic Therapeutic Interventions For Auditory and Vestibular Dysfunction In Myo7a Mutants.

I am sharing my novel methodologies and expertise for videography in zebrafish in a joint zebrafish collaboration with the Schimmenti lab (University of Minnesota- Twin Cities) and the Ekker lab (Mayo Clinic). The goal of the study is to explore pharmacological and genomic therapies in a zebrafish model of hearing loss, called the mariner mutant (Ernest, 2000). This mutant exhibits a phenotype very distinguishable from a wild-type fish. The mariner mutants are deaf and demonstrate abnormal circular swimming. The current study (Appendix 2c) is performing a calcium-driven drug screen and TALEN knockdown screen (Bedell et al., 2012) for potential pharmacological and genomic interventions that ameliorate the observed hearing deficiency and abnormal swimming during development of the mariner mutants. The intentional hypothesis is to modulate the function of the mechanotransducer (MET) channel in order to compensate for the loss of tension on the tip link typically generated by tethering of the tip link to Myosin 7a, a motor protein specific to hair cells of the inner ear. The drugs and

genome-editing will be chosen based on their putative ability to modulate the MET channel as well as those that target the voltage-gated calcium channel at the lower periphery of the cell. The efficacy of each drug will be evaluated through a series of behavioral, imaging, and hearing assays. The behavioral assays will employ my adaptation of high-throughput behavioral analyses (Branson et al., 2009) in zebrafish (Lambert et al., 2012), with additional novel kinematic assessments that I have developed but have yet to be published. Finally, this study has translational potential, because any auspicious candidates from this chemical screen would be potential lead compounds for downstream clinical applications for the prevention of genetic-based newborn hearing loss.

Appendix 2D: High-throughput Genomic and Pharmacological Inhibition of Regeneration in Flatworms.

I have also employed my adaptation of high-throughput videography for a collaboration with the Marchant lab (University of Minnesota- Twin Cities). This project is investigating the effects of bioaminergic ligands on the locomotion of planarians. These are aquatic, free-living flatworms that are a classic model for developmental biologists to study the process of regeneration. Worms maintain an adult population of multipotent stem cells that allows regeneration of missing body parts with correct size and polarity. The Marchant group is interested in studying the effects of genetic (by RNAi) and pharmacological inhibition of gene products involved in regeneration, and assessment of locomotor phenotypes

provides a good way for screening the efficacy of these interventions as planarian polarity genes are expressed in muscle.

Major Findings of this Thesis:

This thesis elucidates, in zebrafish larvae, that the vertebrate DDT-D4R network is a multifunctional modulator of locomotor function, goal-directed motor strategies, and execution of specific prey-directed maneuvers. The DAergic *otpb* neurons and the DDT provide the impetus for endogenous spinal D4R signaling *in vivo* to initiate and maintain the developmental switch to a mature locomotor pattern of short swimming episodes (Lambert et al., 2012) (this is also Chapter 1). This seminal finding is corroborated by another one of my studies that shows that abnormal differentiation of putative DDT neurons underlies the DAergic-rescuable locomotor impairment of episode duration and swimming speed in *trpm7* mutants (Decker et al., 2014) (this is also Appendix 2b). My more detailed kinematic analyses elucidates that the DDT-D4R network is a multifunctional locomotor modulator that exerts separable and dissociable modulation of multiple locomotor parameters (e.g. episode duration, swimming speed, turning angle, undulation frequency) via putatively distinct sites of action within the brain and spinal cord (Chapter 2). Since many of these DDT-D4R modulated locomotor parameters are putatively important for prey capture (Borla et al., 2002; McElligott and O'Malley, 2005; Trivedi and Bollmann, 2013), this lead to my

hypothesis that the DDT-D4R network instrumentally influences prey capture. To thoroughly test this hypothesis, I have developed a novel methodology for high-throughout, unbiased, automated detection and analyses of hunting sequences in free-swimming larvae (Chapter 2 and Appendix 1a). My DAergic prey capture study definitively reveals that endogenous D4R signaling *in vivo*, and perhaps *otpb* neurons and the DDT, are necessary for specific motor-centric strategies and their execution for effective prey capture; specifically, D4R antagonism induces bradykinesia-like execution of advancing but not orienting maneuvers, inducing insufficient speed and negligible reduction in distance toward prey and, ultimately, poor prey capture performance (Chapter 2). I also employed my novel high-throughput analyses of hunting sequences to reveal that zebrafish larvae are capable of goal-directed visuomotor learning and long-term memory of prey capture performance (Appendix 1a), which should serve as a landmark study to investigate this phenomenon's underlying engrams *in vivo* via a combination of whole-brain calcium and voltage imaging, bidirectional optogenetics, and tethered virtual prey capture. In terms of continuing investigations of the DDT-D4R network, one of my ongoing studies suggests that, at 3 dpf, prior to the locomotor developmental switch, the DDT-D4R network is D4R-primed and integrated into the spinal locomotor circuitry postsynaptically but without sufficient endogenous DAergic drive from the DDT (Appendix 1b). This finding is instructive to further elucidating developmental presynaptic and/or postsynaptic mechanisms conferring locomotor functionality of DDT axons onto D4R-positive

spinal neurons, ideally using bidirectional optogenetics combined with separate targeted genomic knockdowns of the three D4R genes: *drd4a*, *drd4b*, and *drd4c*. I also have two additional ongoing studies that employ my videography methods, developed for the crux of my thesis, to explore therapies for zebrafish deaf mutants (Appendix 2c) and targets for regeneration in flatworms (Appendix 2d). In retrospect, my thesis provides both significant advancements in our understanding of the conserved vertebrate multifunctional DDT and new methodological tools for high-throughout automated analyses of locomotor and/or goal-directed behavior for future studies in zebrafish and other animal models.

Bibliography

Aarts M, **Iihara K**, **Wei W-L**, **Xiong Z-G**, **Arundine M**, **Cerwinski W**, **MacDonald JF**, **Tymianski M**. A key role for TRPM7 channels in anoxic neuronal death. *Cell* 115: 863–877, 2003.

Abrams EW, **Mullins MC**. Early zebrafish development: It's in the maternal genes. *Current opinion in genetics & development* 19: 396–403, 2009.

Acampora D, **Postiglione MP**, **Avantaggiato V**, **Di Bonito M**, **Vaccarino FM**, **Michaud J**, **Simeone A**. Progressive impairment of developing neuroendocrine cell lineages in the hypothalamus of mice lacking the Orthopedia gene. *Genes Dev.* 13: 2787–2800, 1999.

Accili D, **Fishburn CS**, **Drago J**, **Steiner H**, **Lachowicz JE**, **Park BH**, **Gauda EB**, **Lee EJ**, **Cool MH**, **Sibley DR**, **Gerfen CR**, **Westphal H**, **Fuchs S**. A targeted mutation of the D3 dopamine receptor gene is associated with hyperactivity in mice. *Proc. Natl. Acad. Sci. U.S.A.* 93: 1945–1949, 1996.

Ahrens MB, **Huang K-H**, **Narayan S**, **Mensh BD**, **Engert F**. Two-photon calcium imaging during fictive navigation in virtual environments. *Front. Neural Circuits* 7: 104, 2013a.

Ahrens MB, **Li JM**, **Orger MB**, **Robson DN**, **Schier AF**, **Engert F**, **Portugues R**. Brain-wide neuronal dynamics during motor adaptation in zebrafish. *Nature* (May 9, 2012). doi: 10.1038/nature11057.

Ahrens MB, **Orger MB**, **Robson DN**, **Li JM**, **Keller PJ**. Whole-brain functional imaging at cellular resolution using light-sheet microscopy. *Nat Meth* (March 18, 2013b). doi: 10.1038/nmeth.2434.

Amir-Zilberstein L, **Blechman J**, **Sztainberg Y**, **Norton WHJ**, **Reuveny A**, **Borodovsky N**, **Tahor M**, **Bonkowsky JL**, **Bally-Cuif L**, **Chen A**, **Levkowitz G**. Homeodomain Protein Otp and Activity-Dependent Splicing Modulate Neuronal Adaptation to Stress. *Neuron* 73: 279–291, 2012.

Aoki T, **Kinoshita M**, **Aoki R**, **Agetsuma M**, **Aizawa H**, **Yamazaki M**, **Takahoko M**, **Amo R**, **Arata A**, **Higashijima S-I**, **Tsuboi T**, **Okamoto H**. Imaging of neural ensemble for the retrieval of a learned behavioral program. *Neuron* 78: 881–894, 2013.

Arduini BL, **Henion PD**. Melanophore sublineage-specific requirement for zebrafish touchtone during neural crest development. *Mechanisms of Development* 121: 1353–1364, 2004.

Arrenberg AB, **Del Bene F**, **Baier H**. Optical control of zebrafish behavior with

halorhodopsin. *Proc. Natl. Acad. Sci. U.S.A.* 106: 17968–17973, 2009.

Badakov R, **Jaźwińska A**. Efficient transfection of primary zebrafish fibroblasts by nucleofection. *Cytotechnology* 51: 105–110, 2006.

Bagnall MW, **McLean DL**. Modular organization of axial microcircuits in zebrafish. *Science* 343: 197–200, 2014.

Ball KT, **Budreau D**, **Rebec GV**. Acute effects of 3,4-methylenedioxymethamphetamine on striatal single-unit activity and behavior in freely moving rats: differential involvement of dopamine D1 and D2 receptors. *Brain Research* 994: 203–215, 2003.

Banack SA, **Cox PA**. Biomagnification of cycad neurotoxins in flying foxes: implications for ALS-PDC in Guam. *Neurology* 61: 387–389, 2003.

Barbeau H, **Rossignol S**. Initiation and modulation of the locomotor pattern in the adult chronic spinal cat by noradrenergic, serotonergic and dopaminergic drugs. *Brain Research* 546: 250–260, 1991.

Barreiro-Iglesias A, **Villar-Cerviño V**, **Anadón R**, **Rodicio MC**. Descending brain-spinal cord projections in a primitive vertebrate, the lamprey: Cerebrospinal fluid-contacting and dopaminergic neurons. *J. Comp. Neurol.* 511: 711–723, 2008.

Barry MJ, **O'Donovan MJ**. The effects of excitatory amino acids and their antagonists on the generation of motor activity in the isolated chick spinal cord. *Brain Research* 433: 271–276, 1987.

Bax JJ, **Poldermans D**, **Schuijf JD**, **Scholte AJHA**, **Elhendy A**, **van der Wall EE**. Imaging to Differentiate Between Ischemic and Nonischemic Cardiomyopathy. *Heart Failure Clinics* 2: 205–214, 2006.

Bedell VM, **Wang Y**, **Campbell JM**, **Poshusta TL**, **Starker CG**, **Krug RG**, **Tan W**, **Penheiter SG**, **Ma AC**, **Leung AYH**, **Fahrenkrug SC**, **Carlson DF**, **Voytas DF**, **Clark KJ**, **Essner JJ**, **Ekker SC**. In vivo genome editing using a high-efficiency TALEN system. *Nature* 491: 114–118, 2012.

Ben-Shachar D, **Eshel G**, **Riederer P**, **Youdim MB**. Role of iron and iron chelation in dopaminergic-induced neurodegeneration: implication for Parkinson's disease. *Ann. Neurol.* 32 Suppl: S105–10, 1992.

Bianco IH, **Kampff AR**, **Engert F**. Prey Capture Behavior Evoked by Simple Visual Stimuli in Larval Zebrafish. *Front. Syst. Neurosci.* 5, 2011.

Bill BR, **Petzold AM**, **Clark KJ**, **Schimmenti LA**, **Ekker SC**. A Primer for

Morpholino Use in Zebrafish. *Zebrafish* 6: 69–77, 2009.

Binder P-M, **Thiele TR**, **Donovan JC**, **Pipes RM**, **Baier H**. Descending Control of Swim Posture by a Midbrain Nucleus in Zebrafish. *Neuron* (July 23, 2014). doi: 10.1016/j.neuron.2014.04.018.

Boehmler W, **Carr T**, **Thisse C**, **Thisse B**, **Canfield VA**, **Levenson R**. D4 Dopamine receptor genes of zebrafish and effects of the antipsychotic clozapine on larval swimming behaviour. *Genes, Brain and Behavior* 6: 155–166, 2007.

Boehmler W, **Obrecht-Pflumio S**, **Canfield V**, **Thisse C**, **Thisse B**, **Levenson R**. Evolution and expression of D2 and D3 dopamine receptor genes in zebrafish. *Dev. Dyn.* 230: 481–493, 2004.

Bonkowsky JL, **Chien C-B**. Molecular cloning and developmental expression of foxP2in zebrafish. *Dev. Dyn.* 234: 740–746, 2005.

Bonkowsky JL, **Wang X**, **Fujimoto E**, **Lee JE**, **Chien C-B**, **Dorsky RI**. Domain-specific regulation of foxP2 CNS expression by lef1. *BMC Dev Biol* 8: 103, 2008.

Bonnot A, **Whelan PJ**, **Mentis GZ**, **O'Donovan MJ**. Locomotor-like activity generated by the neonatal mouse spinal cord. *Brain Res. Brain Res. Rev.* 40: 141–151, 2002.

Borla MA, **Palecek B**, **Budick S**, **O rsquo Malley DM**. Prey Capture by Larval Zebrafish: Evidence for Fine Axial Motor Control. *Brain Behav Evol* 60: 207–229, 2002.

Branson K, **Robie AA**, **Bender J**, **Perona P**, **Dickinson MH**. High-throughput ethomics in large groups of Drosophila. *Nat Meth* 6: 451–457, 2009.

Brauchi S, **Krapivinsky G**, **Krapivinsky L**, **Clapham DE**. TRPM7 facilitates cholinergic vesicle fusion with the plasma membrane. *Proc. Natl. Acad. Sci. U.S.A.* 105: 8304–8308, 2008.

Brown TG. The phenomenon of“ narcosis progression” in mammals. *Proceedings of the Royal Society of London. Series B, Containing Papers of a Biological Character* 86: 140–164, 1913.

Brustein E, **Chong M**, **Holmqvist B**, **Drapeau P**. Serotonin patterns locomotor network activity in the developing zebrafish by modulating quiescent periods. *J. Neurobiol.* 57: 303–322, 2003.

Budick SA, **O'Malley DM**. Locomotor repertoire of the larval zebrafish: swimming, turning and prey capture. *Journal of Experimental Biology* 203: 2565–2579, 2000.

Burgess HA, **Granato M**. Sensorimotor Gating in Larval Zebrafish. *J. Neurosci.* 27: 4984–4994, 2007a.

Burgess HA, **Granato M**. Modulation of locomotor activity in larval zebrafish during light adaptation. *Journal of Experimental Biology* 210: 2526–2539, 2007b.

Burns RS, **Chiueh CC**, **Markey SP**, **Ebert MH**, **Jacobowitz DM**, **Kopin IJ**. A primate model of parkinsonism: selective destruction of dopaminergic neurons in the pars compacta of the substantia nigra by N-methyl-4-phenyl-1,2,3,6-tetrahydropyridine. *Proc. Natl. Acad. Sci. U.S.A.* 80: 4546–4550, 1983.

Buss RR, **Drapeau P**. Synaptic drive to motoneurons during fictive swimming in the developing zebrafish. *J. Neurophysiol.* 86: 197–210, 2001.

Chen CC, **Wu JK**, **Lin HW**, **Pai TP**, **Fu TF**, **Wu CL**, **Tully T**, **Chiang AS**. Visualizing Long-Term Memory Formation in Two Neurons of the Drosophila Brain. *Science* 335: 678–685, 2012a.

Chen H-C, **Su L-T**, **González-Pagán O**, **Overton JD**, **Runnels LW**. A key role for Mg(2+) in TRPM7's control of ROS levels during cell stress. *Biochem. J.* 445: 441–448, 2012b.

Chen Y-C, **Priyadarshini M**, **Panula P**. Complementary developmental expression of the two tyrosine hydroxylase transcripts in zebrafish. *Histochem. Cell Biol.* 132: 375–381, 2009.

Cheung Y-T, **Lau WK-W**, **Yu M-S**, **Lai CS-W**, **Yeung S-C**, **So K-F**, **Chang RC-C**. Effects of all-trans-retinoic acid on human SH-SY5Y neuroblastoma as in vitro model in neurotoxicity research. *Neurotoxicology* 30: 127–135, 2009.

Chong M, **Drapeau P**. Interaction between hindbrain and spinal networks during the development of locomotion in zebrafish. *Devel Neurobio* 67: 933–947, 2007.

Chuang DT, **Chuang JL**, **Wynn RM**. Lessons from genetic disorders of branched-chain amino acid metabolism. *J. Nutr.* 136: 243S–9S, 2006.

Chubanov V, **Waldegger S**, **Schnitzler MMY**, **Vitzthum H**, **Sassen MC**, **Seyberth HW**, **Konrad M**, **Gudermann T**. Disruption of TRPM6/TRPM7 complex formation by a mutation in the TRPM6 gene causes hypomagnesemia with secondary hypocalcemia. *Proc. Natl. Acad. Sci. U.S.A.* 101: 2894–2899, 2004.

Clemens S, **Hochman S**. Conversion of the modulatory actions of dopamine on spinal reflexes from depression to facilitation in D3 receptor knock-out mice. *J. Neurosci.* 24: 11337–11345, 2004.

Clemens S, **Rye D**, **Hochman S**. Restless legs syndrome: Revisiting the

dopamine hypothesis from the spinal cord perspective. *Neurology* 67: 125–130, 2006.

Cohen AH, **Dobrov TA**, **Li G**, **Kiemel T**, **Baker MT**. The development of the lamprey pattern generator for locomotion. *J. Neurobiol.* 21: 958–969, 1990.

Coitinho AS, **de Mello CF**, **Lima TT**, **de Bastiani J**, **Fighera MR**, **Wajner M**. Pharmacological evidence that alpha-ketoisovaleric acid induces convulsions through GABAergic and glutamatergic mechanisms in rats. *Brain Research* 894: 68–73, 2001.

Cornell RA, **Yemm E**, **Bonde G**, **Li W**, **d'Alençon C**, **Wegman L**, **Eisen J**, **Zahs A**. Touchtone promotes survival of embryonic melanophores in zebrafish. *Mechanisms of Development* 121: 1365–1376, 2004.

Crystal JD, **Glanzman DL**. A biological perspective on memory. *Curr. Biol.* 23: R728–31, 2013.

Curado S, **Stainier DYR**, **Anderson RM**. Nitroreductase-mediated cell/tissue ablation in zebrafish: a spatially and temporally controlled ablation method with applications in developmental and regeneration studies. *Nature Protocols* 3: 948–954, 2008.

Dale N, **Roberts A**. Excitatory amino acid receptors in Xenopus embryo spinal cord and their role in the activation of swimming. *The Journal of Physiology* 348: 527–543, 1984.

De Marco RJ, **Groneberg AH**, **Yeh C-M**, **Castillo Ramírez LA**, **Ryu S**. Optogenetic elevation of endogenous glucocorticoid level in larval zebrafish. *Front. Neural Circuits* 7: 82, 2013.

Decker AR, **Decker AR**, **McNeill MS**, **Lambert AM**, **Overton JD**, **Overton JD**, **Chen Y-C**, **Lorca RA**, **Lorca RA**, **Johnson NA**, **Johnson NA**, **Brockerhoff SE**, **Mohapatra DP**, **Mohapatra DP**, **MacArthur H**, **MacArthur H**, **Panula P**, **Masino MA**, **Runnels LW**, **Runnels LW**, **Cornell RA**. Abnormal differentiation of dopaminergic neurons in zebrafish trpm7 mutant larvae impairs development of the motor pattern. *Developmental Biology* 386: 428–439, 2014.

Del Bene F, **Wyart C**, **Robles E**, **Tran A**, **Looger L**, **Scott EK**, **Isacoff EY**, **Baier H**. Filtering of visual information in the tectum by an identified neural circuit. *Science* 330: 669–673, 2010.

Di Prisco GV, **Pearlstein E**, **Robitaille R**, **Dubuc R**. Role of sensory-evoked NMDA plateau potentials in the initiation of locomotion. *Science* 278: 1122–1125, 1997.

Doroshenko NZ, **Maĭskiĭ VA**. [Distribution in the diencephalon of the rat of retrogradely primuline-labelled dopamine-containing neurons forming spinal projections]. *Neirofiziologiia* 19: 771–779, 1987.

Douglas JR, **Noga BR**, **Dai X**, **Jordan LM**. The effects of intrathecal administration of excitatory amino acid agonists and antagonists on the initiation of locomotion in the adult cat. *J. Neurosci.* 13: 990–1000, 1993.

Douglass AD, **Kraves S**, **Deisseroth K**, **Schier AF**, **Engert F**. Escape behavior elicited by single, channelrhodopsin-2-evoked spikes in zebrafish somatosensory neurons. *Curr Biol* 18: 1133–1137, 2008.

Downes GB, **Granato M**. Acetylcholinesterase function is dispensable for sensory neurite growth but is critical for neuromuscular synapse stability. *Developmental Biology* 270: 232–245, 2004.

Downes GB, **Granato M**. Supraspinal input is dispensable to generate glycine-mediated locomotive behaviors in the zebrafish embryo. *J. Neurobiol.* 66: 437–451, 2006.

Doyle CA. Relationships between spinocervical tract neurons and descending catecholamine-containing axons in the cat. *Neuroscience Letters* 171: 217–220, 1994.

Drapeau P, **Ali DW**, **Buss RR**, **Saint-Amant L**. In vivo recording from identifiable neurons of the locomotor network in the developing zebrafish. *Journal of Neuroscience Methods* 88: 1–13, 1999.

Eaton RC, **Farley RD**, **Kimmel CB**, **Schabtach E**. Functional development in the Mauthner cell system of embryos and larvae of the zebra fish. *J. Neurobiol.* 8: 151–172, 1977.

Ekbom K, **Ulfberg J**. Restless legs syndrome. *Journal of Internal Medicine* 266: 419–431, 2009.

Ekker SC. Zinc finger-based knockout punches for zebrafish genes. *Zebrafish* 5: 121–123, 2008.

Eklöf-Ljunggren E, **Haupt S**, **Ausborn J**, **Dehnisch I**, **Uhlén P**, **Higashijima S**, **Manira El A**. Origin of excitation underlying locomotion in the spinal circuit of zebrafish. *Proc. Natl. Acad. Sci. U.S.A.* 109: 5511–5516, 2012.

Elizondo MR, **Arduini BL**, **Paulsen J**, **MacDonald EL**, **Sabel JL**, **Henion PD**, **Cornell RA**, **Parichy DM**. Defective skeletogenesis with kidney stone formation in dwarf zebrafish mutant for trpm7. *Curr Biol* 15: 667–671, 2005.

Elizondo MR, **Budi EH**, **Parichy DM**. trpm7 regulation of in vivo cation homeostasis and kidney function involves stanniocalcin 1 and fgf23. *Endocrinology* 151: 5700–5709, 2010.

Emran F, **Rihel J**, **Dowling JE**. A Behavioral Assay to Measure Responsiveness of Zebrafish to Changes in Light Intensities. *JoVE*, 2008.

Encinas M, **Iglesias M**, **Liu Y**, **Wang H**, **Muhaisen A**, **Ceña V**, **Gallego C**, **Comella JX**. Sequential treatment of SH-SY5Y cells with retinoic acid and brain-derived neurotrophic factor gives rise to fully differentiated, neurotrophic factor-dependent, human neuron-like cells. *Journal of Neurochemistry* 75: 991–1003, 2000.

Ernest S. Mariner is defective in myosin VIIA: a zebrafish model for human hereditary deafness. *Human Molecular Genetics* 9: 2189–2196, 2000.

Ewert J-P, **Burghagen H**, **Schürg-Pfeiffer E**. Neuroethological Analysis of the Innate Releasing Mechanism for Prey-Catching Behavior in Toads. In: *Advances in Vertebrate Neuroethology*. Boston, MA: Springer US, 1983, p. 413–475.

Ewert J-P. Neurobiological Basis for the Recognition and Localization of Environmental Signals: How Does a Toad Brain Recognize Prey and Enemy? In: *Neuroethology*. Berlin, Heidelberg: Springer Berlin Heidelberg, 1980, p. 69–128.

Ewert J-P. Tectal Mechanisms That Underlie Prey-Catching and Avoidance Behaviors in Toads. In: *Comparative Neurology of the Optic Tectum*. Boston, MA: Springer US, 1984, p. 247–416.

Ewert J-P. Toad's prey-catching: A complex system with heuristic value. *Behav Brain Sci* 10: 389, 2010a.

Ewert J-P. Neuroethology of releasing mechanisms: Prey-catching in toads. *Behav Brain Sci* 10: 337, 2010b.

Ewert JP, **Arend B**, **Becker V**, **Borchers HW**. Invariants in Configurational Prey Selection by Bufo bufo (L.). *Brain Behav Evol* 16: 38–51, 1979.

Ewert JP, **Borchers HW**, **Wietersheim AV**. Question of prey feature detectors in the toad'sBufo bufo (L.) visual system: A correlation analysis. *J. Comp. Physiol. A Neuroethol. Sens. Neural. Behav. Physiol.* 126: 43–47, 1978.

Ewert JP, **Burghagen H**. Configurational Prey Selection by Bufo, Alytes, Bombina and Hyla. *Brain Behav Evol* 16: 157–175, 1979.

Ewert JP, **Buxbaum-Conradi H**, **Dreisvogt F**, **Glagow M**, **Merkel-Harff C**, **Röttgen A**, **Schürg-Pfeiffer E**, **Schwippert WW**. Neural modulation of

visuomotor functions underlying prey-catching behaviour in anurans: perception, attention, motor performance, learning. *Comp. Biochem. Physiol., Part A Mol. Integr. Physiol.* 128: 417–461, 2001.

Ewert JP, **Buxbaum-Conradi H**, **Glagow M**, **Röttgen A**, **Schürg-Pfeiffer E**, **Schwippert WW**. Forebrain and midbrain structures involved in prey-catching behaviour of toads: stimulus-response mediating circuits and their modulating loops. *Eur J Morphol* 37: 172–176, 1999.

Ewert JP, **Ingle D**. Excitatory effects following habituation of prey-catching activity in frogs and toads. *Journal of Comparative and Physiological Psychology* 77: 369–374, 1971.

Ewert JP, **Matsumoto N**, **Schwippert WW**. Morphological identification of prey-selective neurons in the grass frog's optic tectum. *Naturwissenschaften* 72: 661–663, 1985.

Ewert JP, **Siefert G**. Neuronal correlates of seasonal changes in contrast-detection of prey catching behaviour in toads (bufo bufo L.). *Vision Research* 14: 431–432, 1974.

Ewert JP. Neural Mechanisms of Prey-catching and Avoidance Behavior in the Toad (Bufo bufo L.). *Brain Behav Evol* 3: 36–56, 1970.

Fajardo O, **Zhu P**, **Friedrich RW**. Control of a specific motor program by a small brain area in zebrafish. *Front. Neural Circuits* 7: 67, 2013.

Farrell TC, **Cario CL**, **Milanese C**, **Vogt A**, **Jeong J-H**, **Burton EA**. Evaluation of spontaneous propulsive movement as a screening tool to detect rescue of Parkinsonism phenotypes in zebrafish models. *Neurobiology of Disease* 44: 9–18, 2011.

Fayein NA, **Viala D**. Development of locomotor activities in young chronic spinal rabbits. *Neuroscience Letters* 3: 329–333, 1976.

Fernandes AM, **Fero K**, **Arrenberg AB**, **Bergeron SA**, **Driever W**, **Burgess HA**. Deep brain photoreceptors control light-seeking behavior in zebrafish larvae. *Curr. Biol.* 22: 2042–2047, 2012.

Filippi A, **Mahler J**, **Schweitzer J**, **Driever W**. Expression of the paralogous tyrosine hydroxylase encoding genes th1 and th2 reveals the full complement of dopaminergic and noradrenergic neurons in zebrafish larval and juvenile brain. *J. Comp. Neurol.* 518: 423–438, 2010.

Fioravante D, **Byrne JH**. Protein degradation and memory formation. *Brain Res. Bull.* 85: 14–20, 2011.

Friedrich T, **Lambert AM**, **Masino MA**, **Downes GB**. Mutation of zebrafish dihydrolipoamide branched-chain transacylase E2 results in motor dysfunction and models maple syrup urine disease. *Dis Model Mech* 5: 248–258, 2012.

Fuiman LA, **Webb PW**. Ontogeny of routine swimming activity and performance in zebra danios (Teleostei: Cyprinidae). *Animal Behaviour* 36: 250–261, 1988.

Fujimoto E, **Stevenson TJ**, **Chien C-B**, **Bonkowsky JL**. Identification of a dopaminergic enhancer indicates complexity in vertebrate dopamine neuron phenotype specification. *Developmental Biology* 352: 393–404, 2011.

Gabriel JP, **Mahmood R**, **Walter AM**, **Kyriakatos A**, **Hauptmann G**, **Calabrese RL**, **Manira El A**. Locomotor Pattern in the Adult Zebrafish Spinal Cord In Vitro. *J. Neurophysiol.* 99: 37–48, 2007.

Gahtan E, **O'Malley DM**. Rapid lesioning of large numbers of identified vertebrate neurons: applications in zebrafish. *Journal of Neuroscience Methods* 108: 97–110, 2001.

Gahtan E. Visual Prey Capture in Larval Zebrafish Is Controlled by Identified Reticulospinal Neurons Downstream of the Tectum. *J. Neurosci.* 25: 9294–9303, 2005.

Gal-Ben-Ari S, **Kenney JW**, **Ounalla-Saad H**, **Taha E**, **David O**, **Levitan D**, **Gildish I**, **Panja D**, **Pai B**, **Wibrand K**, **Simpson TI**, **Proud CG**, **Bramham CR**, **Armstrong JD**, **Rosenblum K**. Consolidation and translation regulation. *Learn. Mem.* 19: 410–422, 2012.

Garcia-Rill E, **Skinner RD**, **Fitzgerald JA**. Activity in the mesencephalic locomotor region during locomotion. *Exp. Neurol.* 82: 609–622, 1983.

Geisler R, **Rauch G-J**, **Geiger-Rudolph S**, **Albrecht A**, **van Bebber F**, **Berger A**, **Busch-Nentwich E**, **Dahm R**, **Dekens MPS**, **Dooley C**, **Elli AF**, **Gehring I**, **Geiger H**, **Geisler M**, **Glaser S**, **Holley S**, **Huber M**, **Kerr A**, **Kirn A**, **Knirsch M**, **Konantz M**, **Küchler AM**, **Maderspacher F**, **Neuhauss SC**, **Nicolson T**, **Ober EA**, **Praeg E**, **Ray R**, **Rentzsch B**, **Rick JM**, **Rief E**, **Schauerte HE**, **Schepp CP**, **Schönberger U**, **Schonthaler HB**, **Seiler C**, **Sidi S**, **Söllner C**, **Wehner A**, **Weiler C**, **Nüsslein-Volhard C**. Large-scale mapping of mutations affecting zebrafish development. *BMC Genomics* 8: 11, 2007.

Gerstner JR, **Lyons LC**, **Wright KP**, **Loh DH**, **Rawashdeh O**, **Eckel-Mahan KL**, **Roman GW**. Cycling Behavior and Memory Formation. *J. Neurosci.* 29: 12824–12830, 2009.

Gerstner JR, **Vanderheyden WM**, **Shaw PJ**, **Landry CF**, **Yin JC**. Cytoplasmic to nuclear localization of fatty-acid binding protein correlates with specific forms

of long-term memory in Drosophila. *Commun Integr Biol* 4: 623–626, 2011.

Giacomini NJ, **Rose B**, **Kobayashi K**, **Guo S**. Antipsychotics produce locomotor impairment in larval zebrafish. *Neurotoxicology and Teratology* 28: 245–250, 2006.

Glagow M, **Ewert JP**. Increases of excitatory receptive fields of retinal ganglion cells in common toads under apomorphine are not associated with size preference in prey-snapping. *Neuroscience Letters* 173: 83–86, 1994.

Glagow M, **Ewert JP**. Apomorphine-induced suppression of prey oriented turning in toads is correlated with activity changes in pretectum and tectum: [14C]2DG studies and single cell recordings. *Neuroscience Letters* 220: 215–218, 1996.

Glagow M, **Ewert JP**. Dopaminergic modulation of visual responses in toads. I. Apomorphine-induced effects on visually directed appetitive and consummatory prey-catching behavior. *J Comp Physiol A* 180: 1–9, 1997a.

Glagow M, **Ewert JP**. Dopaminergic modulation of visual responses in toads. II. Influences of apomorphine on retinal ganglion cells and tectal cells. *J Comp Physiol A* 180: 11–18, 1997b.

Glagow M, **Ewert JP**. Apomorphine Alters Prey-Catching Patterns in the Common Toad: Behavioral Experiments and ¹⁴C-2-Deoxyglucose Brain Mapping Studies. *Brain Behav Evol* 54: 223–242, 1999.

Glanzman DL. PKM and the maintenance of memory. *F1000 Biol Rep* 5: 4, 2013.

Gleason MR, **Armisen R**, **Verdecia MA**, **Sirotkin H**, **Brehm P**, **Mandel G**. A mutation in serca underlies motility dysfunction in accordion zebrafish. *Developmental Biology* 276: 441–451, 2004.

Granato M, **Nüsslein-Volhard C**. Fishing for genes controlling development. *Current opinion in genetics & development* 6: 461–468, 1996.

Granato M, **van Eeden FJ**, **Schach U**, **Trowe T**, **Brand M**, **Furutani-Seiki M**, **Haffter P**, **Hammerschmidt M**, **Heisenberg CP**, **Jiang YJ**, **Kane DA**, **Kelsh RN**, **Mullins MC**, **Odenthal J**, **Nüsslein-Volhard C**. Genes controlling and mediating locomotion behavior of the zebrafish embryo and larva. *Development* 123: 399–413, 1996.

Grillner S, **Rossignol S**. Contralateral reflex reversal controlled by limb position in the acute spinal cat injected with clonidine i.v. *Brain Research* 144: 411–414, 1978a.

Grillner S, **Rossignol S**. On the initiation of the swing phase of locomotion in chronic spinal cats. *Brain Research* 146: 269–277, 1978b.

Grillner S, **Wallén P**, **Saitoh K**, **Kozlov A**, **Robertson B**. Neural bases of goal-directed locomotion in vertebrates—An overview. *Brain Research Reviews* 57: 2–12, 2008.

Han P, **Nakanishi ST**, **Tran MA**, **Whelan PJ**. Dopaminergic Modulation of Spinal Neuronal Excitability. *J. Neurosci.* 27: 13192–13204, 2007.

Han P, **Whelan PJ**. Modulation of AMPA currents by D1-like but not D2-like receptors in spinal motoneurons. *Neuroscience* 158: 1699–1707, 2009.

Hanano T, **Hara Y**, **Shi J**, **Morita H**, **Umebayashi C**, **Mori E**, **Sumimoto H**, **Ito Y**, **Mori Y**, **Inoue R**. Involvement of TRPM7 in cell growth as a spontaneously activated Ca2+ entry pathway in human retinoblastoma cells. *J. Pharmacol. Sci.* 95: 403–419, 2004.

Hara K, **Kokubo Y**, **Ishiura H**, **Fukuda Y**, **Miyashita A**, **Kuwano R**, **Sasaki R**, **Goto J**, **Nishizawa M**, **Kuzuhara S**, **Tsuji S**. TRPM7 is not associated with amyotrophic lateral sclerosis-parkinsonism dementia complex in the Kii peninsula of Japan. *Am. J. Med. Genet. B Neuropsychiatr. Genet.* 153B: 310–313, 2010.

Hauber W. Dopamine release in the prefrontal cortex and striatum: temporal and behavioural aspects. *Pharmacopsychiatry* 43 Suppl 1: S32–41, 2010.

Hägglund M, **Borgius L**, **Dougherty KJ**, **Kiehn O**. Activation of groups of excitatory neurons in the mammalian spinal cord or hindbrain evokes locomotion. *Nat Neurosci* 13: 246–252, 2010.

Hegarty SV, **Sullivan AM**, **O'Keeffe GW**. Midbrain dopaminergic neurons: a review of the molecular circuitry that regulates their development. *Developmental Biology* 379: 123–138, 2013.

Hermosura MC, **Nayakanti H**, **Dorovkov MV**, **Calderon FR**, **Ryazanov AG**, **Haymer DS**, **Garruto RM**. A TRPM7 variant shows altered sensitivity to magnesium that may contribute to the pathogenesis of two Guamanian neurodegenerative disorders. *Proc. Natl. Acad. Sci. U.S.A.* 102: 11510–11515, 2005.

Herrero Hernández E. Pigmentation genes link Parkinson's disease to melanoma, opening a window on both etiologies. *Medical Hypotheses* 72: 280–284, 2009.

Herring WJ, **McKean M**, **Dracopoli N**, **Danner DJ**. Branched chain acyltransferase absence due to an Alu-based genomic deletion allele and an

exon skipping allele in a compound heterozygote proband expressing maple syrup urine disease. *Biochim. Biophys. Acta* 1138: 236–242, 1992.

Hinsey JC, **Cutting CC**. Reflexes in the spinal opossum. *J. Comp. Neurol.* 64: 375–387, 1936.

Hinz FI, **Aizenberg M**, **Tushev G**, **Schuman EM**. Protein synthesis-dependent associative long-term memory in larval zebrafish. *J. Neurosci.* 33: 15382–15387, 2013.

Hirata H, **Saint-Amant L**, **Downes GB**, **Cui WW**, **Zhou W**, **Granato M**, **Kuwada JY**. Zebrafish bandoneon mutants display behavioral defects due to a mutation in the glycine receptor beta-subunit. *Proc. Natl. Acad. Sci. U.S.A.* 102: 8345–8350, 2005.

Hirata H, **Saint-Amant L**, **Waterbury J**, **Cui W**, **Zhou W**, **Li Q**, **Goldman D**, **Granato M**, **Kuwada JY**. accordion, a zebrafish behavioral mutant, has a muscle relaxation defect due to a mutation in the ATPase Ca2+ pump SERCA1. *Development* 131: 5457–5468, 2004.

HOCHSTEIN P, **COHEN G**. The cytotoxicity of melanin precursors. *Annals of the New York Academy of Sciences* 100: 876–886, 1963.

Hochstein P, **Cohen G**. THE CYTOTOXICITY OF MELANIN PRECURSORS*. *Annals of the New York Academy of Sciences* 100: 876–886, 2006.

Holstege JC, **Dijken HV**, **Buijs RM**, **Goedknegt H**, **Gosens T**, **Bongers CMH**. Distribution of dopamine immunoreactivity in the rat, cat, and monkey spinal cord. *J. Comp. Neurol.* 376: 631–652, 1996.

Holzschuh J, **Ryu S**, **Aberger F**, **Driever W**. Dopamine transporter expression distinguishes dopaminergic neurons from other catecholaminergic neurons in the developing zebrafish embryo. *Mechanisms of Development* 101: 237–243, 2001.

Homanics GE, **Skvorak K**, **Ferguson C**, **Watkins S**, **Paul HS**. Production and characterization of murine models of classic and intermediate maple syrup urine disease. *BMC Med. Genet.* 7: 33, 2006.

Huang K-H, **Ahrens MB**, **Dunn TW**, **Engert F**. Spinal Projection Neurons Control Turning Behaviors in Zebrafish. *Current Biology* (August 2013). doi: 10.1016/j.cub.2013.06.044.

Ingebretson JJ, **Masino MA**. Quantification of locomotor activity in larval zebrafish: considerations for the design of high-throughput behavioral studies. *Front. Neural Circuits* 7: 109, 2013.

Inoue K, **Branigan D**, **Xiong Z-G**. Zinc-induced neurotoxicity mediated by transient receptor potential melastatin 7 channels. *Journal of Biological Chemistry* 285: 7430–7439, 2010.

Irons TD, **Kelly PE**, **Hunter DL**, **MacPhail RC**, **Padilla S**. Acute administration of dopaminergic drugs has differential effects on locomotion in larval zebrafish. *Pharmacology Biochemistry and Behavior* 103: 792–813, 2013.

Jiang Z, **Carlin KP**, **Brownstone RM**. An in vitro functionally mature mouse spinal cord preparation for the study of spinal motor networks. *Brain Research* 816: 493–499, 1999.

Jin J, **Desai BN**, **Navarro B**, **Donovan A**, **Andrews NC**, **Clapham DE**. Deletion of Trpm7 disrupts embryonic development and thymopoiesis without altering Mg2+ homeostasis. *Science* 322: 756–760, 2008.

Jin J, **Wu L-J**, **Jun J**, **Cheng X**, **Xu H**, **Andrews NC**, **Clapham DE**. The channel kinase, TRPM7, is required for early embryonic development. *Proc. Natl. Acad. Sci. U.S.A.* 109: E225–33, 2012.

Kania BF. Neurochemical changes in the brain and spinal cord of sheep: a basis for the immobilizing action of etorphine. *J S Afr Vet Assoc* 56: 89–92, 1985.

Kastenhuber E, **Kratochwil CF**, **Ryu S**, **Schweitzer J**, **Driever W**. Genetic dissection of dopaminergic and noradrenergic contributions to catecholaminergic tracts in early larval zebrafish. *J. Comp. Neurol.* 518: 439–458, 2010.

Kelsh RN, **Brand M**, **Jiang YJ**, **Heisenberg CP**, **Lin S**, **Haffter P**, **Odenthal J**, **Mullins MC**, **van Eeden FJ**, **Furutani-Seiki M**, **Granato M**, **Hammerschmidt M**, **Kane DA**, **Warga RM**, **Beuchle D**, **Vogelsang L**, **Nüsslein-Volhard C**. Zebrafish pigmentation mutations and the processes of neural crest development. *Development* 123: 369–389, 1996.

Kerman IA. Organization of brain somatomotor-sympathetic circuits. *Exp Brain Res* 187: 1–16, 2008.

Kim BJ, **Park EJ**, **Lee JH**, **Jeon J-H**, **Kim SJ**, **So I**. Suppression of transient receptor potential melastatin 7 channel induces cell death in gastric cancer. *Cancer Sci.* 99: 2502–2509, 2008.

Kimmel CB, **Ballard WW**, **Kimmel SR**, **Ullmann B**, **Schilling TF**. Stages of embryonic development of the zebrafish. *Dev. Dyn.* 203: 253–310, 1995.

Kimmel CB, **Patterson J**, **Kimmel RO**. The development and behavioral characteristics of the startle response in the zebra fish. *Dev. Psychobiol.* 7: 47–60, 1974.

Kimura Y, **Satou C**, **Fujioka S**, **Shoji W**, **Umeda K**, **Ishizuka T**, **Yawo H**, **Higashijima S-I**. Hindbrain V2a Neurons in the Excitation of Spinal Locomotor Circuits during Zebrafish Swimming. *Current Biology* (April 2013). doi: 10.1016/j.cub.2013.03.066.

Kinkhabwala A, **Riley M**, **Koyama M**, **Monen J**, **Satou C**, **Kimura Y**, **Higashijima S-I**, **Fetcho J**. A structural and functional ground plan for neurons in the hindbrain of zebrafish. *Proc. Natl. Acad. Sci. U.S.A.* 108: 1164–1169, 2011.

Kjaerulff O, **Kiehn O**. Distribution of networks generating and coordinating locomotor activity in the neonatal rat spinal cord in vitro: a lesion study. *J. Neurosci.* 16: 5777–5794, 1996.

Kjaerulff O, **Kiehn O**. 5-HT modulation of multiple inward rectifiers in motoneurons in intact preparations of the neonatal rat spinal cord. *J. Neurophysiol.* 85: 580–593, 2001.

Kokel D, **Bryan J**, **Laggner C**, **White R**, **Cheung CYJ**, **Mateus R**, **Healey D**, **Kim S**, **Werdich AA**, **Haggarty SJ**, **MacRae CA**, **Shoichet B**, **Peterson RT**. Rapid behavior-based identification of neuroactive small molecules in the zebrafish. *Nat Meth* 6: 231–237, 2010.

Kolisek M, **Sponder G**, **Mastrototaro L**, **Smorodchenko A**, **Launay P**, **Vormann J**, **Schweigel-Röntgen M**. Substitution p.A350V in Na^{+}/Mg^{2+} exchanger SLC41A1, potentially associated with Parkinson's disease, is a gain-of-function mutation. *PLoS ONE* 8: e71096, 2013.

Koller WC, **Cochran JW**, **Klawans HL**. Calcification of the basal ganglia: computerized tomography and clinical correlation. *Neurology* 29: 328–333, 1979.

Konopka W, **Schütz G**, **Kaczmarek L**. The microRNA contribution to learning and memory. *neuroscientist* 17: 468–474, 2011.

Koyama M, **Kinkhabwala A**, **Satou C**, **Higashijima S-I**, **Fetcho J**. Mapping a sensory-motor network onto a structural and functional ground plan in the hindbrain. *Proc. Natl. Acad. Sci. U.S.A.* 108: 1170–1175, 2011.

Krapivinsky G, **Mochida S**, **Krapivinsky L**, **Cibulsky SM**, **Clapham DE**. The TRPM7 ion channel functions in cholinergic synaptic vesicles and affects transmitter release. *Neuron* 52: 485–496, 2006.

Kuscha V, **Barreiro-Iglesias A**, **Becker CG**, **Becker T**. Plasticity of tyrosine hydroxylase and serotonergic systems in the regenerating spinal cord of adult zebrafish. *J. Comp. Neurol.* 520: 933–951, 2012.

Kwan KM, **Fujimoto E**, **Grabher C**, **Mangum BD**, **Hardy ME**, **Campbell DS**,

Parant JM, **Yost HJ**, **Kanki JP**, **Chien C-B**. The Tol2kit: A multisite gateway-based construction kit for Tol2 transposon transgenesis constructs. *Dev. Dyn.* 236: 3088–3099, 2007.

Lambert AM, **Bonkowsky JL**, **Masino MA**. The Conserved Dopaminergic Diencephalospinal Tract Mediates Vertebrate Locomotor Development in Zebrafish Larvae. *J Neurosci* 32: 13488–13500, 2012.

Lan J, **Jiang DH**. Desferrioxamine and vitamin E protect against iron and MPTP-induced neurodegeneration in mice. *J. Neural Transm.* 104: 469–481, 1997.

Lee TH, **Gee KR**, **Ellinwood EH**, **Seidler FJ**. Combining “caged-dopamine” photolysis with fast-scan cyclic voltammetry to assess dopamine clearance and release autoinhibition in vitro. *Journal of Neuroscience Methods* 67: 221–231, 1996.

Legendre P, **Korn H**. Glycinergic Inhibitory Synaptic Currents and Related Receptor Channels in the Zebrafish Brain. *European Journal of Neuroscience* 6: 1544–1557, 1994.

Lewis A, **Wilson N**, **Stearns G**, **Johnson N**, **Nelson R**, **Brockerhoff SE**. Celsr3 is required for normal development of GABA circuits in the inner retina. *PLoS Genet.* 7: e1002239, 2011.

Li M, **Du J**, **Jiang J**, **Ratzan W**, **Su LT**, **Runnels LW**, **Yue L**. Molecular Determinants of Mg2+ and Ca2+ Permeability and pH Sensitivity in TRPM6 and TRPM7. *J. Biol. Chem.* 282: 25817–25830, 2007a.

Li P, **Shah S**, **Huang L**, **Carr AL**, **Gao Y**, **Thisse C**, **Thisse B**, **Li L**. Cloning and spatial and temporal expression of the zebrafish dopamine D1 receptor. *Dev. Dyn.* 236: 1339–1346, 2007b.

Lindsey BW, **Smith FM**, **Croll RP**. From inflation to flotation: contribution of the swimbladder to whole-body density and swimming depth during development of the zebrafish (Danio rerio). *Zebrafish* 7: 85–96, 2010.

Link V, **Shevchenko A**, **Heisenberg C-P**. Proteomics of early zebrafish embryos. *BMC Dev Biol* 6: 1, 2006.

Lister JA, **Robertson CP**, **Lepage T**, **Johnson SL**, **Raible DW**. nacre encodes a zebrafish microphthalmia-related protein that regulates neural-crest-derived pigment cell fate. *Development* 126: 3757–3767, 1999.

Liu W, **Su L-T**, **Khadka DK**, **Mezzacappa C**, **Komiya Y**, **Sato A**, **Habas R**, **Runnels LW**. TRPM7 regulates gastrulation during vertebrate embryogenesis. *Developmental Biology* 350: 348–357, 2011.

Ljunggren EE, **Haupt S**, **Ausborn J**, **Ampatzis K**, **Manira El A**. Optogenetic activation of excitatory premotor interneurons is sufficient to generate coordinated locomotor activity in larval zebrafish. *J. Neurosci.* 34: 134–139, 2014.

Lohr H, **Ryu S**, **Driever W**. Zebrafish diencephalic A11-related dopaminergic neurons share a conserved transcriptional network with neuroendocrine cell lineages. *Development* 136: 1007–1017, 2009.

Low SE, **Amburgey K**, **Horstick E**, **Linsley J**, **Sprague SM**, **Cui WW**, **Zhou W**, **Hirata H**, **Saint-Amant L**, **Hume RI**, **Kuwada JY**. TRPM7 Is Required within Zebrafish Sensory Neurons for the Activation of Touch-Evoked Escape Behaviors. *J. Neurosci.* 31: 11633–11644, 2011.

Marder E, **Bucher D**. Central pattern generators and the control of rhythmic movements. *Current Biology* 11: R986–96, 2001.

Masino MA, **Fetcho JR**. Fictive swimming motor patterns in wild type and mutant larval zebrafish. *J. Neurophysiol.* 93: 3177–3188, 2005.

Mathias JR, **Zhang Z**, **Saxena MT**, **Mumm JS**. Enhanced Cell-Specific Ablation in Zebrafish Using a Triple Mutant of Escherichia Coli Nitroreductase. *Zebrafish* (January 15, 2014). doi: 10.1089/zeb.2013.0937.

Matsumoto N, **Schwippert WW**, **Beneke TW**, **Ewert JP**. Forebrain-mediated control of visually guided prey-catching in toads: investigation of striato-pretectal connections with intracellular recording/labeling methods. *Behavioural Processes* 25: 27–40, 1991.

McCrea AE, **Stehouwer DJ**, **Van Hartesveldt C**. Dopamine D1 and D2 antagonists block l-DOPA-induced air-stepping in decerebrate neonatal rats. *Developmental Brain Research* 100: 130–132, 1997.

McDearmid JR, **Drapeau P**. Rhythmic motor activity evoked by NMDA in the spinal zebrafish larva. *J. Neurophysiol.* 95: 401–417, 2006.

McElligott MB, **O'Malley DM**. Prey tracking by larval zebrafish: axial kinematics and visual control. *Brain Behav Evol* 66: 177–196, 2005.

McEwen ML, **Van Hartesveldt C**, **Stehouwer DJ**. L-DOPA and quipazine elicit air-stepping in neonatal rats with spinal cord transections. *Behavioral Neuroscience* 111: 825–833, 1997.

McKeown KA, **Downes GB**, **Hutson LD**. Modular Laboratory Exercises to Analyze the Development of Zebrafish Motor Behavior. *Zebrafish* 6: 179–185, 2009.

McLean DL, **Fan J**, **Higashijima S-I**, **Hale ME**, **Fetcho JR**. A topographic map of recruitment in spinal cord. *Nature* 446: 71–75, 2007.

McLean DL, **Fetcho JR**. Ontogeny and innervation patterns of dopaminergic, noradrenergic, and serotonergic neurons in larval zebrafish. *J. Comp. Neurol.* 480: 38–56, 2004a.

McLean DL, **Fetcho JR**. Relationship of tyrosine hydroxylase and serotonin immunoreactivity to sensorimotor circuitry in larval zebrafish. *J. Comp. Neurol.* 480: 57–71, 2004b.

McLean DL, **Fetcho JR**. Spinal Interneurons Differentiate Sequentially from Those Driving the Fastest Swimming Movements in Larval Zebrafish to Those Driving the Slowest Ones. *J. Neurosci.* 29: 13566–13577, 2009.

McLean DL, **Masino MA**, **Koh IYY**, **Lindquist WB**, **Fetcho JR**. Continuous shifts in the active set of spinal interneurons during changes in locomotor speed. *Nat Neurosci* 11: 1419–1429, 2008.

McNeill MS, **Paulsen J**, **Bonde G**, **Burnight E**, **Hsu M-Y**, **Cornell RA**. Cell death of melanophores in zebrafish trpm7 mutant embryos depends on melanin synthesis. *J Investig Dermatol* 127: 2020–2030, 2007.

Meisel RL, **Rakerd B**. Induction of hindlimb stepping movements in rats spinally transected as adults or as neonates. *Brain Research* 240: 353–356, 1982.

Menasche P, **Grousset C**, **Gauduel Y**, **Mouas C**, **Piwnica A**. Prevention of hydroxyl radical formation: a critical concept for improving cardioplegia. Protective effects of deferoxamine. *Circulation* 76: V180–5, 1987.

Mendelsohn BA, **Gitlin JD**. Coordination of development and metabolism in the pre-midblastula transition zebrafish embryo. *Dev. Dyn.* 237: 1789–1798, 2008.

Mirat O, **Sternberg JR**, **Severi KE**, **Wyart C**. ZebraZoom: an automated program for high-throughput behavioral analysis and categorization. *Front. Neural Circuits* 7: 107, 2013.

Morton DH, **Strauss KA**, **Robinson DL**, **Puffenberger EG**, **Kelley RI**. Diagnosis and treatment of maple syrup disease: a study of 36 patients. *PEDIATRICS* 109: 999–1008, 2002.

Mu Y, **Li X-Q**, **Zhang B**, **Du J-L**. Visual Input Modulates Audiomotor Function via Hypothalamic Dopaminergic Neurons through a Cooperative Mechanism. *Neuron* 75: 688–699, 2012.

Muller UK, **Stamhuis EJ**, **Videler JJ**. Hydrodynamics of unsteady fish swimming

and the effects of body size: comparing the flow fields of fish larvae and adults. *Journal of Experimental Biology* 203: 193–206, 2000.

Muto A, **Kawakami K**. Prey capture in zebrafish larvae serves as a model to study cognitive functions. *Front. Neural Circuits* 7: 110, 2013.

Muto A, **Ohkura M**, **Abe G**, **Nakai J**, **Kawakami K**. Real-Time Visualization of Neuronal Activity during Perception. *Current Biology* (January 2013). doi: 10.1016/j.cub.2012.12.040.

Nadler MJ, **Hermosura MC**, **Inabe K**, **Perraud AL**, **Zhu Q**, **Stokes AJ**, **Kurosaki T**, **Kinet JP**, **Penner R**, **Scharenberg AM**, **Fleig A**. LTRPC7 is a Mg.ATP-regulated divalent cation channel required for cell viability. *Nature* 411: 590–595, 2001.

Nishikawa KC. Neuromuscular control of prey capture in frogs. *Philos. Trans. R. Soc. Lond., B, Biol. Sci.* 354: 941–954, 1999.

Noga BR, **Kriellaars DJ**, **Jordan LM**. The effect of selective brainstem or spinal cord lesions on treadmill locomotion evoked by stimulation of the mesencephalic or pontomedullary locomotor regions. *J. Neurosci.* 11: 1691–1700, 1991.

Olberg RM. Visual control of prey-capture flight in dragonflies. *Current Opinion in Neurobiology* 22: 267–271, 2012.

Olson BD, **Sgourdou P**, **Downes GB**. Analysis of a zebrafish behavioral mutant reveals a dominant mutation in atp2a1/SERCA1. *Genesis* 48: 354–361, 2010.

Orger MB, **Kampff AR**, **Severi KE**, **Bollmann JH**, **Engert F**. Control of visually guided behavior by distinct populations of spinal projection neurons. *Nat Neurosci* 11: 327–333, 2008.

Pan T, **Li X**, **Jankovic J**. The association between Parkinson's disease and melanoma. *Int. J. Cancer* 128: 2251–2260, 2011.

Parichy DM, **Elizondo MR**, **Mills MG**, **Gordon TN**, **Engeszer RE**. Normal table of postembryonic zebrafish development: staging by externally visible anatomy of the living fish. *Dev. Dyn.* 238: 2975–3015, 2009.

Patterson BW, **Abraham AO**, **Maciver MA**, **McLean DL**. Visually guided gradation of prey capture movements in larval zebrafish. *J. Exp. Biol.* 216: 3071–3083, 2013.

Paulus W, **Dowling P**, **Rijsman R**, **Stiasny-Kolster K**, **Trenkwalder C**, **de Weerd A**. Pathophysiological concepts of restless legs syndrome. *Mov Disord.* 22: 1451–1456, 2007a.

Paulus W, **Dowling P**, **Rijsman R**, **Stiasny-Kolster K**, **Trenkwalder C**. Update of the pathophysiology of the Restless-Legs-Syndrome. *Mov Disord.* 22: S431–S439, 2007b.

Pei W, **Kratz LE**, **Bernardini I**, **Sood R**, **Yokogawa T**, **Dorward H**, **Ciccone C**, **Kelley RI**, **Anikster Y**, **Burgess HA**, **Huizing M**, **Feldman B**. A model of Costeff Syndrome reveals metabolic and protective functions of mitochondrial OPA3. *Development* 137: 2587–2596, 2010.

Peterson RT, **Fishman MC**. Designing Zebrafish Chemical Screens. In: *The Zebrafish: Disease Models and Chemical Screens*. Elsevier, 2011, p. 525–541.

Petzold AM, **Balciunas D**, **Sivasubbu S**, **Clark KJ**, **Bedell VM**, **Westcot SE**, **Myers SR**, **Moulder GL**, **Thomas MJ**, **Ekker SC**. Nicotine response genetics in the zebrafish. *Proc. Natl. Acad. Sci. U.S.A.* 106: 18662–18667, 2009.

Pisharath H, **Parsons MJ**. Nitroreductase-mediated cell ablation in transgenic zebrafish embryos. *Methods Mol. Biol.* 546: 133–143, 2009.

Preuss SJ, **Trivedi CA**, **Berg-Maurer Vom CM**, **Ryu S**, **Bollmann JH**. Classification of Object Size in Retinotectal Microcircuits. *Curr. Biol.* (September 16, 2014). doi: 10.1016/j.cub.2014.09.012.

Puhl JG, **Masino MA**, **Mesce KA**. Necessary, Sufficient and Permissive: A Single Locomotor Command Neuron Important for Intersegmental Coordination. *J Neurosci* 32: 17646–17657, 2012.

Puhl JG, **Mesce KA**. Dopamine Activates the Motor Pattern for Crawling in the Medicinal Leech. *J Neurosci* 28: 4192–4200, 2008.

Puhl JG, **Mesce KA**. Keeping It Together: Mechanisms of Intersegmental Coordination for a Flexible Locomotor Behavior. *J Neurosci* 30: 2373–2383, 2010.

Qu S, **Le W**, **Zhang X**, **Xie W**, **Zhang A**, **Ondo WG**. Locomotion is increased in a11-lesioned mice with iron deprivation: a possible animal model for restless legs syndrome. *J. Neuropathol. Exp. Neurol.* 66: 383–388, 2007.

Qu S, **Ondo WG**, **Zhang X**, **Xie WJ**, **Pan TH**, **Le WD**. Projections of diencephalic dopamine neurons into the spinal cord in mice. *Exp Brain Res* 168: 152–156, 2005.

Reimer MM, **Norris A**, **Ohnmacht J**, **Patani R**, **Zhong Z**, **Dias TB**, **Kuscha V**, **Scott AL**, **Chen Y-C**, **Rozov S**, **Frazer SL**, **Wyatt C**, **Higashijima S-I**, **Patton EE**, **Panula P**, **Chandran S**, **Becker T**, **Becker CG**. Dopamine from the Brain Promotes Spinal Motor Neuron Generation during Development and Adult

Regeneration. *Dev. Cell* 25: 478–491, 2013.

Reiner A, **Medina L**, **Veenman CL**. Structural and functional evolution of the basal ganglia in vertebrates. *Brain Res. Brain Res. Rev.* 28: 235–285, 1998.

Ren G, **Li S**, **Zhong H**, **Lin S**. Zebrafish tyrosine hydroxylase 2 gene encodes tryptophan hydroxylase. *Journal of Biological Chemistry* 288: 22451–22459, 2013.

Richter JD. Translational control of synaptic plasticity. *Biochem. Soc. Trans.* 38: 1527–1530, 2010.

Ridet JL, **Sandillon F**, **Rajaofetra N**, **Geffard M**, **Privat A**. Spinal dopaminergic system of the rat: light and electron microscopic study using an antiserum against dopamine, with particular emphasis on synaptic incidence. *Brain Research* 598: 233–241, 1992.

Rihel J, **Prober DA**, **Arvanites A**, **Lam K**, **Zimmerman S**, **Jang S**, **Haggarty SJ**, **Kokel D**, **Rubin LL**, **Peterson RT**, **Schier AF**. Zebrafish Behavioral Profiling Links Drugs to Biological Targets and Rest/Wake Regulation. *Science* 327: 348–351, 2010.

Rihel J, **Schier AF**. Behavioral screening for neuroactive drugs in zebrafish. *Devel Neurobio* 72: 373–385, 2012.

Rink E, **Wullimann MF**. Development of the catecholaminergic system in the early zebrafish brain: an immunohistochemical study. *Brain Res. Dev. Brain Res.* 137: 89–100, 2002.

Roberts AC, **Bill BR**, **Glanzman DL**. Learning and memory in zebrafish larvae. *Front. Neural Circuits* 7: 126, 2013.

Roberts AC, **Reichl J**, **Song MY**, **Dearinger AD**, **Moridzadeh N**, **Lu ED**, **Pearce K**, **Esdin J**, **Glanzman DL**. Habituation of the C-start response in larval zebrafish exhibits several distinct phases and sensitivity to NMDA receptor blockade. *PLoS ONE* 6: e29132, 2011.

Rose JD, **Moore FL**. Behavioral neuroendocrinology of vasotocin and vasopressin and the sensorimotor processing hypothesis. *Front Neuroendocrinol* 23: 317–341, 2002.

Ryazanova LV, **Rondon LJ**, **Zierler S**, **Hu Z**, **Galli J**, **Yamaguchi TP**, **Mazur A**, **Fleig A**, **Ryazanov AG**. TRPM7 is essential for Mg2+ homeostasis in mammals. *Nat Commun* 1: 109, 2010.

Ryu S, **Mahler J**, **Acampora D**, **Holzschuh J**, **Erhardt S**, **Omodei D**, **Simeone**

A, **Driever W**. Orthopedia homeodomain protein is essential for diencephalic dopaminergic neuron development. *Current Biology* 17: 873–880, 2007.

Sah R, **Mesirca P**, **Van den Boogert M**, **Rosen J**, **Mably J**, **Mangoni ME**, **Clapham DE**. Ion channel-kinase TRPM7 is required for maintaining cardiac automaticity. *Proc. Natl. Acad. Sci. U.S.A.* 110: E3037–46, 2013.

Saint-Amant L, **Drapeau P**. Time course of the development of motor behaviors in the zebrafish embryo. *J. Neurobiol.* 37: 622–632, 1998.

Sallinen V, **Kolehmainen J**, **Priyadarshini M**, **Toleikyte G**, **Chen Y-C**, **Panula P**. Dopaminergic cell damage and vulnerability to MPTP in Pink1 knockdown zebrafish. *Neurobiology of Disease* 40: 93–101, 2010.

Sallinen V, **Torkko V**, **Sundvik M**, **Reenilä I**, **Khrustalyov D**, **Kaslin J**, **Panula P**. MPTP and MPP+ target specific aminergic cell populations in larval zebrafish. *Journal of Neurochemistry* 108: 719–731, 2009.

Sankrithi NS, **O'Malley DM**. Activation of a multisensory, multifunctional nucleus in the zebrafish midbrain during diverse locomotor behaviors. *Neuroscience* 166: 970–993, 2010.

Sánchez Camacho C, **Marín O**, **Smeets WJAJ**, **Donkelaar Ten HJ**, **González A**. Descending supraspinal pathways in amphibians. II. Distribution and origin of the catecholaminergic innervation of the spinal cord. *J. Comp. Neurol.* 434: 209–232, 2001.

Sch rg-Pfeiffer E, **Ewert JP**. Investigation of neurons involved in the analysis of gestalt prey features in the frogRana temporaria. *J. Comp. Physiol. A Neuroethol. Sens. Neural. Behav. Physiol.* 141: 139–152, 1981.

Segura Aguilar J, **Kostrzewa RM**. Neurotoxins and neurotoxic species implicated in neurodegeneration. *Neurotox Res* 6: 615–630, 2004.

Severi KE, **Portugues R**, **Marques JC**, **Marques JC**, **O'Malley DM**, **Orger MB**, **Engert F**. Neural control and modulation of swimming speed in the larval zebrafish. *Neuron* 83: 692–707, 2014.

Sherrington CS. Flexion-reflex of the limb, crossed extension-reflex, and reflex stepping and standing. *The Journal of Physiology* 40: 28–121, 1910.

Shimada Y, **Hirano M**, **Nishimura Y**, **Tanaka T**. A High-Throughput Fluorescence-Based Assay System for Appetite-Regulating Gene and Drug Screening. *PLoS ONE* 7: e52549, 2012.

Sickles AE, **Stehouwer DJ**, **Van Hartesveldt C**. Dopamine D1 and D2

antagonists block L-dopa-elicited air-stepping in neonatal rats. *Brain Res. Dev. Brain Res.* 68: 17–22, 1992.

SILBERMAN J, **DANCIS J**, **FEIGIN I**. Neuropathological observations in maple syrup urine disease: branched-chain ketoaciduria. *Arch. Neurol.* 5: 351–363, 1961.

Skagerberg G, **Björklund A**, **Lindvall O**, **Schmidt RH**. Origin and termination of the diencephalo-spinal dopamine system in the rat. *Brain Res. Bull.* 9: 237–244, 1982.

Skvorak KJ, **Hager EJ**, **Arning E**, **Bottiglieri T**, **Paul HS**, **Strom SC**, **Homanics GE**, **Sun Q**, **Jansen EEW**, **Jakobs C**, **Zinnanti WJ**, **Gibson KM**. Hepatocyte transplantation (HTx) corrects selected neurometabolic abnormalities in murine intermediate maple syrup urine disease (iMSUD). *Biochim. Biophys. Acta* 1792: 1004–1010, 2009a.

Skvorak KJ, **Paul HS**, **Dorko K**, **Marongiu F**, **Ellis E**, **Chace D**, **Ferguson C**, **Gibson KM**, **Homanics GE**, **Strom SC**. Hepatocyte transplantation improves phenotype and extends survival in a murine model of intermediate maple syrup urine disease. *Mol. Ther.* 17: 1266–1273, 2009b.

Smear MC, **Tao HW**, **Staub W**, **Orger MB**, **Gosse NJ**, **Liu Y**, **Takahashi K**, **Poo M-M**, **Baier H**. Vesicular glutamate transport at a central synapse limits the acuity of visual perception in zebrafish. *Neuron* 53: 65–77, 2007.

Smeets WJ, **Lopez JM**, **González A**. Immunohistochemical localization of DARPP-32 in the brain of the lizard, Gekko gecko: co-occurrence with tyrosine hydroxylase. *J. Comp. Neurol.* 435: 194–210, 2001.

Smeets WJAJ, **González A**. Catecholamine systems in the brain of vertebrates: new perspectives through a comparative approach. *Brain Research Reviews* 33: 308–379, 2000.

Souza BR, **Romano-Silva MA**, **Tropepe V**. Dopamine D2 Receptor Activity Modulates Akt Signaling and Alters GABAergic Neuron Development and Motor Behavior in Zebrafish Larvae. *J. Neurosci.* 31: 5512–5525, 2011.

Strauss KA, **Mazariegos GV**, **Sindhi R**, **Squires R**, **Finegold DN**, **Vockley G**, **Robinson DL**, **Hendrickson C**, **Virji M**, **Cropcho L**, **Puffenberger EG**, **McGhee W**, **Seward LM**, **Morton DH**. Elective liver transplantation for the treatment of classical maple syrup urine disease. *Am. J. Transplant.* 6: 557–564, 2006.

Strauss KA, **Morton DH**. Branched-chain Ketoacyl Dehydrogenase Deficiency: Maple Syrup Disease. *Curr Treat Options Neurol* 5: 329–341, 2003.

Strauss KA, **Wardley B**, **Robinson D**, **Hendrickson C**, **Rider NL**, **Puffenberger EG**, **Shellmer D**, **Shelmer D**, **Moser AB**, **Morton DH**. Classical maple syrup urine disease and brain development: principles of management and formula design. *Mol. Genet. Metab.* 99: 333–345, 2010.

Straw AD, **Branson K**, **Neumann TR**, **Dickinson MH**. Multi-camera real-time three-dimensional tracking of multiple flying animals. *Journal of The Royal Society Interface* 8: 395–409, 2011.

Su L-T, **Agapito MA**, **Li M**, **Simonson WTN**, **Huttenlocher A**, **Habas R**, **Yue L**, **Runnels LW**. TRPM7 regulates cell adhesion by controlling the calcium-dependent protease calpain. *J. Biol. Chem.* 281: 11260–11270, 2006.

Su L-T, **Liu W**, **Chen H-C**, **González-Pagán O**, **Habas R**, **Runnels LW**. TRPM7 regulates polarized cell movements. *Biochem. J.* 434: 513–521, 2011.

Sun H-S, **Jackson MF**, **Martin LJ**, **Jansen K**, **Teves L**, **Cui H**, **Kiyonaka S**, **Mori Y**, **Jones M**, **Forder JP**, **Golde TE**, **Orser BA**, **MacDonald JF**, **Tymianski M**. Suppression of hippocampal TRPM7 protein prevents delayed neuronal death in brain ischemia. *Nat Neurosci* 12: 1300–1307, 2009.

Svensson E, **Woolley J**, **Wikström M**, **Grillner S**. Endogenous dopaminergic modulation of the lamprey spinal locomotor network. *Brain Research* 970: 1–8, 2003.

Swerdlow NR, **Vaccarino FJ**, **Amalric M**, **Koob GF**. The neural substrates for the motor-activating properties of psychostimulants: a review of recent findings. *Pharmacology Biochemistry and Behavior* 25: 233–248, 1986.

Takada M, **Li ZK**, **Hattori T**. Single thalamic dopaminergic neurons project to both the neocortex and spinal cord. *Brain Research* 455: 346–352, 1988.

Takada M. Widespread dopaminergic projections of the subparafascicular thalamic nucleus in the rat. *Brain Res. Bull.* 32: 301–309, 1993.

Tan JL, **Zon LI**. Chemical Screening in Zebrafish for Novel Biological and Therapeutic Discovery. In: *The Zebrafish: Disease Models and Chemical Screens*. Elsevier, 2011, p. 491–516.

Taniguchi W, **Nakatsuka T**, **Miyazaki N**, **Yamada H**, **Takeda D**, **Fujita T**, **Kumamoto E**, **Yoshida M**. In vivo patch-clamp analysis of dopaminergic antinociceptive actions on substantia gelatinosa neurons in the spinal cord. *PAIN* 152: 95–105, 2011.

Tay TL, **Lin Q**, **Seow TK**, **Tan KH**, **Hew CL**, **Gong Z**. Proteomic analysis of protein profiles during early development of the zebrafish, Danio rerio.

Proteomics 6: 3176–3188, 2006.

Tay TL, **Ronneberger O**, **Ryu S**, **Nitschke R**, **Driever W**. Comprehensive catecholaminergic projectome analysis reveals single-neuron integration of zebrafish ascending and descending dopaminergic systems. *Nat Commun* 2: 171, 2011.

Tergau F, **Wischer S**, **Paulus W**. Motor system excitability in patients with restless legs syndrome. *Neurology* 52: 1060–1063, 1999.

Terland O, **Flatmark T**. Drug-induced parkinsonism: cinnarizine and flunarizine are potent uncouplers of the vacuolar H+-ATPase in catecholamine storage vesicles. *Neuropharmacology* 38: 879–882, 1999.

Thirumalai V, **Cline HT**. Endogenous dopamine suppresses initiation of swimming in prefeeding zebrafish larvae. *J. Neurophysiol.* 100: 1635–1648, 2008.

Thisse C, **Thisse B**. High-resolution in situ hybridization to whole-mount zebrafish embryos. *Nature Protocols* 3: 59–69, 2008.

Tierney KB. Behavioural assessments of neurotoxic effects and neurodegeneration in zebrafish. *Biochimica et Biophysica Acta (BBA) - Molecular Basis of Disease* 1812: 381–389, 2011.

Tillet Y, **Kitahama K**. Distribution of central catecholaminergic neurons: a comparison between ungulates, humans and other species. *Histol. Histopathol.* 13: 1163–1177, 1998.

Tong H, **McDearmid JR**. Pacemaker and plateau potentials shape output of a developing locomotor network. *Curr. Biol.* 22: 2285–2293, 2012.

Tran S, **Nowicki M**, **Muraleetharan A**, **Gerlai R**. Differential effects of dopamine D1 and D 2/3 receptor antagonism on motor responses. *Psychopharmacology (Berl.)* (August 20, 2014). doi: 10.1007/s00213-014-3713-0.

Trenkwalder C, **Högl B**, **Winkelmann J**. Recent advances in the diagnosis, genetics and treatment of restless legs syndrome. *J Neurol* 256: 539–553, 2009.

Trivedi CA, **Bollmann JH**. Visually driven chaining of elementary swim patterns into a goal-directed motor sequence: a virtual reality study of zebrafish prey capture. *Front. Neural Circuits* 7: 86, 2013.

Van Epps HA, **Yim CM**, **Hurley JB**, **Brockerhoff SE**. Investigations of photoreceptor synaptic transmission and light adaptation in the zebrafish visual mutant nrc. *Invest. Ophthalmol. Vis. Sci.* 42: 868–874, 2001.

Van Hartesveldt C, **Sickles AE**, **Porter JD**, **Stehouwer DJ**. L-dopa-induced air-stepping in developing rats. *Brain Res. Dev. Brain Res.* 58: 251–255, 1991.

Vetrugno R, **D'Angelo R**, **Montagna P**. Periodic limb movements in sleep and periodic limb movement disorder. *Neurol Sci* 28: S9–S14, 2007.

Wachowitz S, **Ewert JP**. A key by which the toad's visual system gets access to the domain of prey. *Physiology & Behavior* 60: 877–887, 1996.

Wallace KN, **Pack M**. Unique and conserved aspects of gut development in zebrafish. *Developmental Biology* 255: 12–29, 2003.

Wallén P, **Williams TL**. Fictive locomotion in the lamprey spinal cord in vitro compared with swimming in the intact and spinal animal. *The Journal of Physiology* 347: 225–239, 1984.

Wang M, **Wen H**, **Brehm P**. Function of neuromuscular synapses in the zebrafish choline-acetyltransferase mutant bajan. *J. Neurophysiol.* 100: 1995–2004, 2008.

Wang W, **Lufkin T**. The murine Otp homeobox gene plays an essential role in the specification of neuronal cell lineages in the developing hypothalamus. *Developmental Biology* 227: 432–449, 2000.

Wang W-C, **McLean DL**. Selective Responses to Tonic Descending Commands by Temporal Summation in a Spinal Motor Pool. *Neuron* (July 23, 2014). doi: 10.1016/j.neuron.2014.06.021.

Weerasuriya A, **Ewert JP**. Prey-selective neurons in the toad's optic tectum and sensorimotor interfacing: HRP studies and recording experiments. *J. Comp. Physiol. A Neuroethol. Sens. Neural. Behav. Physiol.* 144: 429–434, 1981.

Wei W-L, **Sun H-S**, **Olah ME**, **Sun X**, **Czerwinska E**, **Czerwinski W**, **Mori Y**, **Orser BA**, **Xiong Z-G**, **Jackson MF**, **Tymianski M**, **MacDonald JF**. TRPM7 channels in hippocampal neurons detect levels of extracellular divalent cations. *Proc. Natl. Acad. Sci. U.S.A.* 104: 16323–16328, 2007.

Westerfield M. *The Zebrafish Book*. 2007.

Westphal RE, **O'Malley DM**. Fusion of locomotor maneuvers, and improving sensory capabilities, give rise to the flexible homing strikes of juvenile zebrafish. *Front. Neural Circuits* 7: 108, 2013.

Wiggin TD, **Anderson TM**, **Eian J**, **Peck JH**, **Masino MA**. Episodic swimming in the larval zebrafish is generated by a spatially distributed spinal network with modular functional organization. *J. Neurophysiol.* 108: 925–934, 2012.

Wolman M, **Granato M**. Behavioral genetics in larval zebrafish: learning from the young. *Devel Neurobio* 72: 366–372, 2012.

Wolman MA, **Jain RA**, **Liss L**, **Granato M**. Chemical modulation of memory formation in larval zebrafish. *Proc. Natl. Acad. Sci. U.S.A.* 108: 15468–15473, 2011.

Wyart C, **Del Bene F**, **Warp E**, **Scott EK**, **Trauner D**, **Baier H**, **Isacoff EY**. Optogenetic dissection of a behavioural module in the vertebrate spinal cord. *Nature* 461: 407–410, 2009.

Xi Y, **Yu M**, **Godoy R**, **Hatch G**, **Poitras L**, **Ekker M**. Transgenic zebrafish expressing green fluorescent protein in dopaminergic neurons of the ventral diencephalon. *Dev. Dyn.* 240: 2539–2547, 2011.

Yamamoto K, **Ruuskanen JO**, **Wullimann MF**, **Vernier P**. Two tyrosine hydroxylase genes in vertebrates New dopaminergic territories revealed in the zebrafish brain. *Mol. Cell. Neurosci.* 43: 394–402, 2010.

Yamamoto K, **Ruuskanen JO**, **Wullimann MF**, **Vernier P**. Differential expression of dopaminergic cell markers in the adult zebrafish forebrain. *J. Comp. Neurol.* 519: 576–598, 2011.

Zhang Y-Z, **Ouyang Y-C**, **Hou Y**, **Schatten H**, **Chen D-Y**, **Sun Q-Y**. Mitochondrial behavior during oogenesis in zebrafish: a confocal microscopy analysis. *Development, Growth & Differentiation* 50: 189–201, 2008.

Zhao H, **Zhu W**, **Pan T**, **Xie W**, **Zhang A**, **Ondo WG**, **Le W**. Spinal cord dopamine receptor expression and function in mice with 6-OHDA lesion of the A11 nucleus and dietary iron deprivation. *J. Neurosci. Res.* 85: 1065–1076, 2007.

Zhu H, **Clemens S**, **Sawchuk M**, **Hochman S**. Expression and distribution of all dopamine receptor subtypes (D1–D5) in the mouse lumbar spinal cord: A real-time polymerase chain reaction and non-autoradiographic in situ hybridization study. *Neuroscience* 149: 885–897, 2007.

Zinnanti WJ, **Lazovic J**, **Griffin K**, **Skvorak KJ**, **Paul HS**, **Homanics GE**, **Bewley MC**, **Cheng KC**, **LaNoue KF**, **Flanagan JM**. Dual mechanism of brain injury and novel treatment strategy in maple syrup urine disease. *Brain* 132: 903–918, 2008.

Zottoli SJ, **Faber DS**. Review : The Mauthner Cell: What Has it Taught us? *neuroscientist* 6: 26–38, 2000.

Appendix

Appendix List:

First-Author Projects:

1A) Lambert AM and Masino MA (In Preparation). High-throughput automated detection and analyses of hunting sequences unveil goal-directed visuomotor learning and long-term memory in zebrafish larvae.

2A) Lambert AM, Montgomery JE, Peck JH, Masino MA (Work In Progress). Optogenetic and pharmacological advancement of vertebrate locomotor development via the dopaminergic diencephalospinal tract.

3A) Lambert AM and Masino MA (In Preparation). An ancient dopaminergic system: evolutionary conservation of the dopaminergic diencephalospinal tract and its multifunctional integration of the CNS . **Review article**.

4A) Lambert AM and Masino MA (In Preparation). Zebrafish prey capture as a premiere model to elucidate visuomotor transformations, learning, and long-term memory of goal-directed behavior. **Review article**.

Middle-Author Projects:

2A) Friedrich T, **Lambert AM**, Masino MA, Downes GB (2012). Mutation of zebrafish dihydrolipoamide branched chain transacylase E2 results in motor dysfunction and models maple syrup urine disease. Dis Model Mech 5(2):248-58.

2B) Decker AR*, McNeill MS*, **Lambert AM**, Overton JD, Chen YC, Lorca RA, Johnson NA, Brockerhoff S, Mohapatra DP, MacArthur H, Panula P, Masino MA, Runnels LW, Cornell RA (2014). Abnormal differentiation of dopaminergic neurons in zebrafish *trpm7* mutant larvae impairs development of the motor pattern. Dev Biol 386(2):428-39.

2C) Koleilat A, **Lambert AM**, Masino MA, Ekker SC, Schimmenti, LA (Work In Progress). Amelioration of vestibular and auditory deficits in Myo7a mutants via high-throughput genomic and pharmacological interventions.

2D) Chan JD, Grab T, **Lambert AM**, Masino MA, Marchant JS (Work In Progress). High-throughput genomic and pharmacological targeting of bioaminergic targets for regeneraton in the planarian Dugesia japonica.

Appendix 1A: High-throughput automated detection and analyses of hunting sequences unveil goal-directed visuomotor learning and long-term memory in zebrafish larvae.

I have employed my novel methodology for high-throughput automated detection and analyses of hunting sequences to elucidate that zebrafish larvae are capable of visuomotor learning and long-term memory of goal-directed prey capture performance. Larvae that are provided previous experience hunting either large paramecia (~ 200 µm) (para-PF) (Fig 1,B,C) or small colpoda (~ 30 µm) (Fig 1B,C), 24 hours prior to testing, exhibit improved prey capture performance at 7 dpf, compared to naïve or yolk sac-depleted (YD) counterparts (Fig 1A,C). The dramatic size difference between the two motile microbes can be seen In Fig 1B, which shows one comparatively large paramecium surrounded by multiple colpoda. This experience-dependent potentiation of prey capture is not simply due to obtained sustenance from prey, because colpoda feeding from 4 dpf onward does not improve the survival rate compared to unfed counterparts, although a regimen of paramecia or 5% egg yolk does (Fig 1D). Several additional lines of evidence confirm that this enhancement is due to the visuomotor experience of chasing prey items and not due to any obtained sustenance resulting from prey capture. Compared to naïve counterparts, experienced larvae exhibit: 1) a shorter latency to increases in eye convergences and initiation of hunting sequences following exposure to prey (Fig 2) 2) a shorter

latency between execution of subsequent hunting maneuvers within a hunting sequence (Fig 3) 3) a markedly better capture attempt success rate (Fig 3C) 4) consumption of all prey items in half the time course (Fig 1A,C). Furthermore, this study reveals a strong negative correlation between capture attempt success rate and inter-maneuver durations (Fig 3C), meaning that better precision of prey capture attempts correlates to shorter latencies between maneuvers. Several additional experiments to the ones delineated here provide further insights into the experience-dependent nature of these long-term behavioral enhancements. For example, larvae provided with experience in the presence of artemia, an aquatic crustacean that is much larger (~ 450 μm) than paramecia but which zebrafish nevertheless hunt within weeks of development, induces 5 to 6 dpf larvae to hunt artemia but with an inability to ingest them due to their large size (data not shown). This exclusive visuomotor experience, in the absence of any sustenance, recapitulates, at 7 dpf, many of the long-term enhancements in hunting performance gained from either paramecia or colpoda exposure. Interestingly, inhibition of protein synthesis, which is established to occlude many forms of long-term memory formation (Gerstner et al., 2009; Richter, 2010; Fioravante and Byrne, 2011; Konopka et al., 2011; Roberts et al., 2011; Wolman et al., 2011; Gal-Ben-Ari et al., 2012; Wolman and Granato, 2012; Aoki et al., 2013; Crystal and Glanzman, 2013; Glanzman, 2013; Hinz et al., 2013; Roberts et al., 2013), did not occlude the prey experience-dependent enhancements in prey capture performance (Fig 4). This could either be due to a protein

synthesis-independent mechanism, which has been observed in drosophila (Gerstner et al., 2011; Chen et al., 2012a), or from a lack of suboptimal phasing and/or duration of protein synthesis inhibition in relation to the prey training periods. However, we confirmed that our primary protein-synthesis inhibitor, cycloheximide, inhibited protein-synthesis of heat shock-induced GFP in *hsp70:GFP* larvae *in vivo* (Fig 4A,B). Regardless, this study is the first to reveal the capacity of learning and long-term memory of goal-directed behavior in zebrafish larvae. Since this phenomenon occurs at a developmental time point when larvae are amenable to whole-brain calcium imaging (Ahrens et al., 2012; 2013a; 2013b) and bidirectional optogenetics (Douglass et al., 2008; Arrenberg et al., 2009; Wyart et al., 2009; De Marco et al., 2013; Kimura et al., 2013; Ljunggren et al., 2014), this work will represent a landmark study that opens the doors to systematically and causally elucidating the neural mechanisms of goal-directed visuomotor learning and long-term memory *in vivo* at a brain-wide, systems, cellular, and subcellular level during virtual prey capture (Trivedi and Bollmann, 2013; Preuss et al., 2014). All experiments for this project are completed and will comprise a full 8 to 10 figures in a manuscript that will be drafted and submitted for publication in the coming months, just after submission of the manuscript comprising Chapter 2 of this thesis.

Figure 1

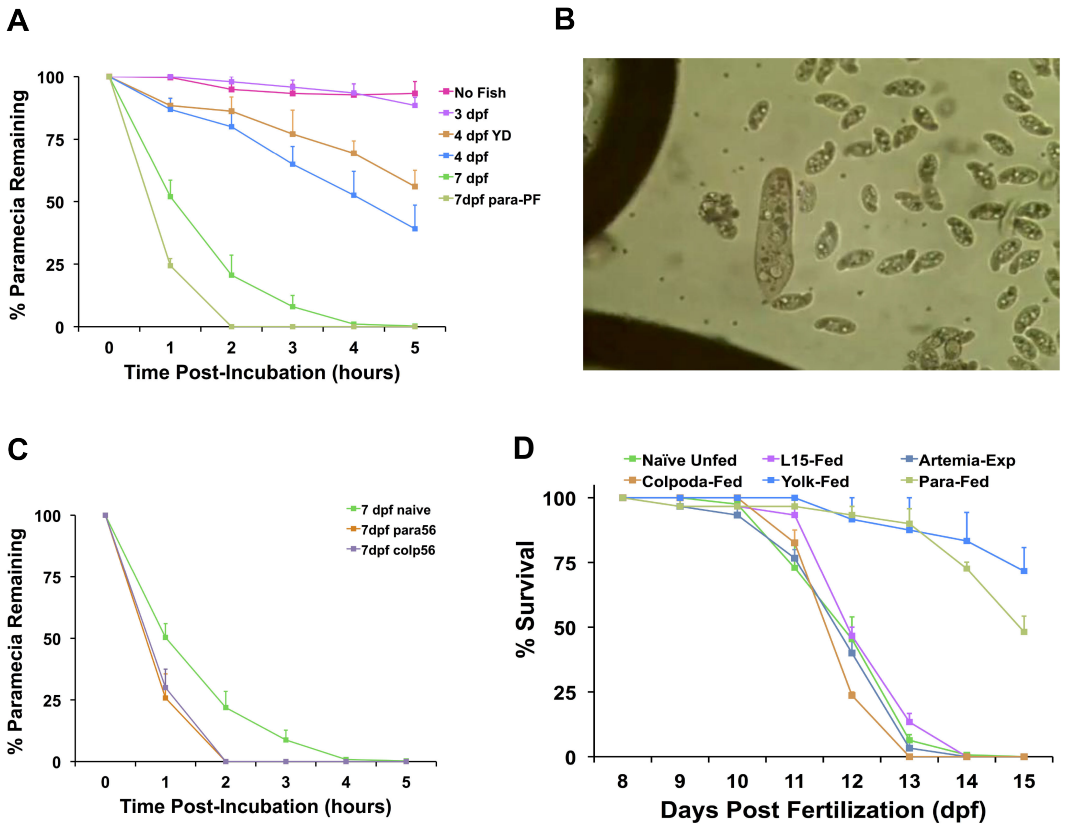
A
B
C
D
% Paramecia Remaining
Time Post-Incubation (hours)
No Fish
3 dpf
4 dpf YD
4 dpf
7 dpf
7dpf para-PF
7 dpf naive
7dpf para56
7dpf colp56
% Survival
Days Post Fertilization (dpf)
Naïve Unfed
L15-Fed
Artemia-Exp
Colpoda-Fed
Yolk-Fed
Para-Fed

Figure 2

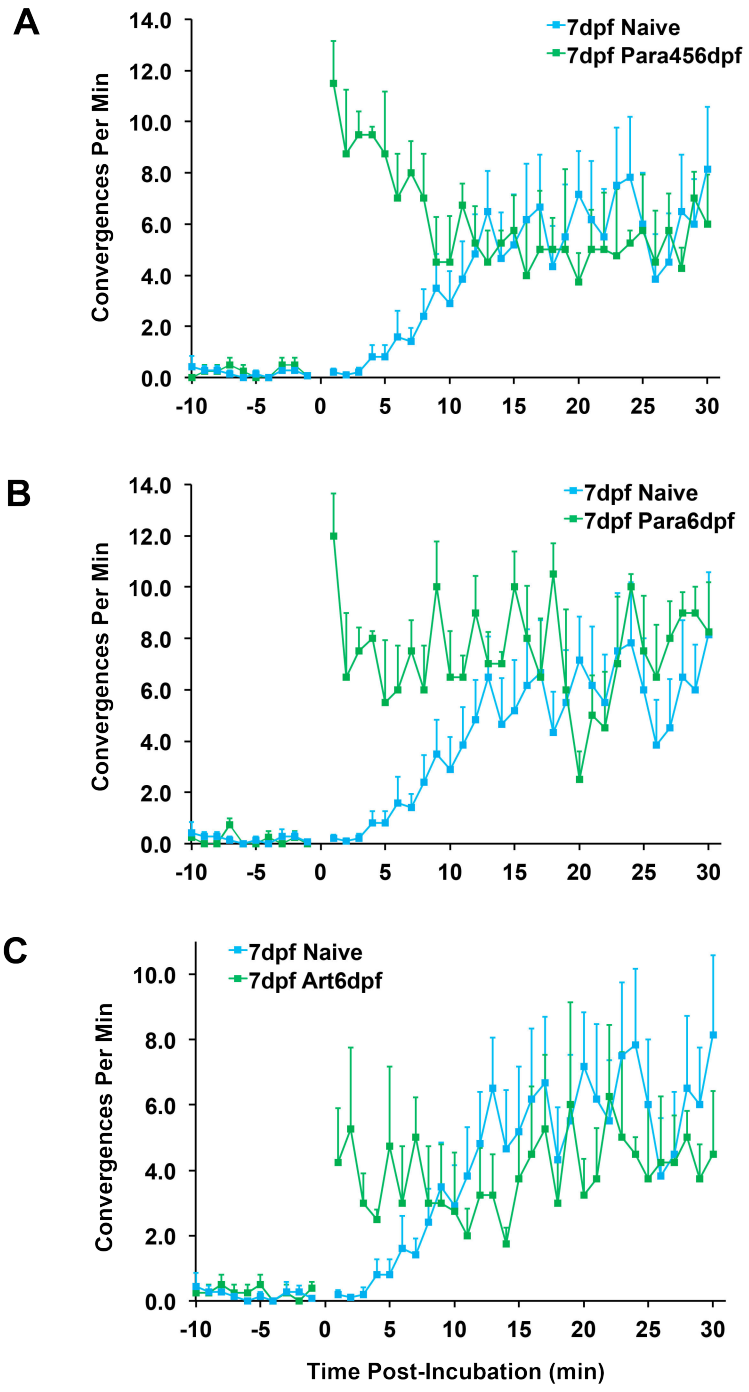
A
7dpf Naive
7dpf Para456dpf
Convergences Per Min
14.0
12.0
10.0
8.0
6.0
4.0
2.0
0.0
-10
-5
0
5
10
15
20
25
30
B
7dpf Naive
7dpf Para6dpf
Convergences Per Min
C
7dpf Naive
7dpf Art6dpf
Convergences Per Min
Time Post-Incubation (min)

Figure 3

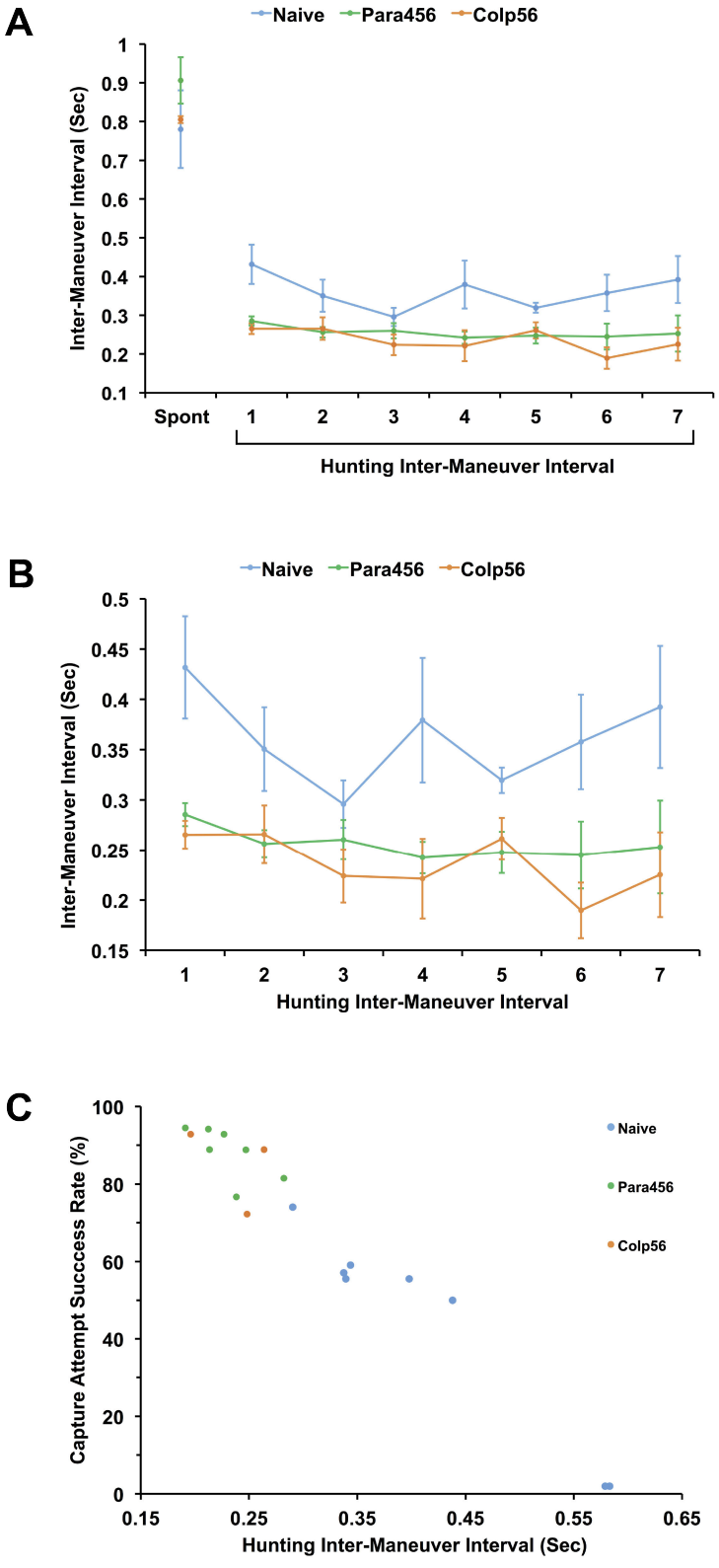
A
Naive
Para456
Colp56
Inter-Maneuver Interval (Sec)
1
0.9
0.8
0.7
0.6
0.5
0.4
0.3
0.2
0.1
Spont
1
2
3
4
5
6
7
Hunting Inter-Maneuver Interval
B
Naive
Para456
Colp56
Inter-Maneuver Interval (Sec)
0.5
0.45
0.4
0.35
0.3
0.25
0.2
0.15
1
2
3
4
5
6
7
Hunting Inter-Maneuver Interval
C
Capture Attempt Succcess Rate (%)
100
80
60
40
20
0
0.15
0.25
0.35
0.45
0.55
0.65
Hunting Inter-Maneuver Interval (Sec)
Naive
Para456
Colp56

Figure 4

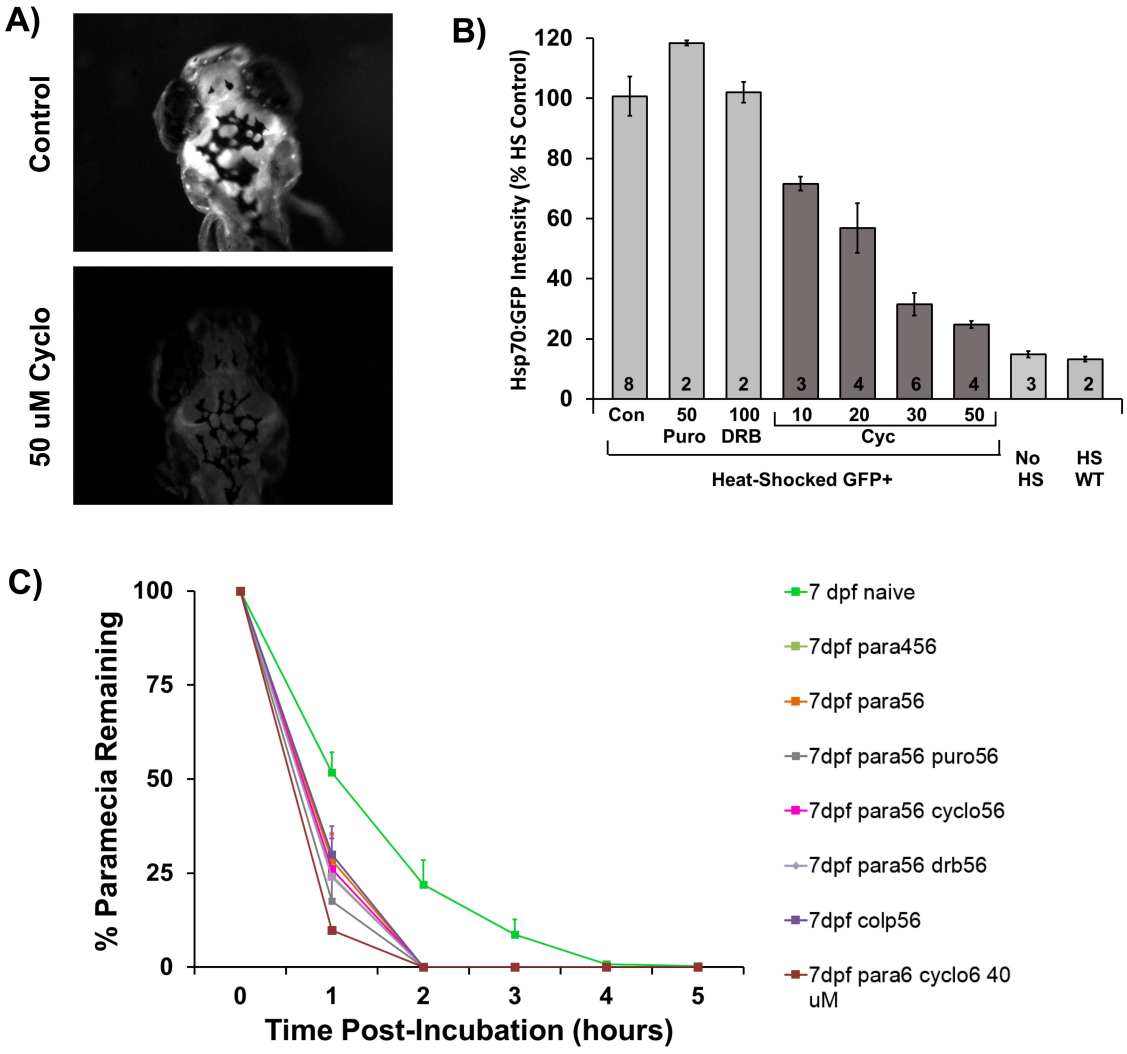
A)
Control
50 uM Cyclo
B)
Hsp70:GFP Intensity (% HS Control)
120
100
80
60
40
20
0
8
2
2
3
4
6
4
3
2
Con
50 Puro
100 DRB
10
20
30
50
Cyc
Heat-Shocked GFP+
No HS
HS WT
C)
% Paramecia Remaining
100
75
50
25
0
0
1
2
3
4
5
Time Post-Incubation (hours)
7 dpf naive
7dpf para456
7dpf para56
7dpf para56 puro56
7dpf para56 cyclo56
7dpf para56 drb56
7dpf colp56
7dpf para6 cyclo6 40 uM

Appendix 1B: Optogenetic and pharmacological advancement of vertebrate locomotor development via the dopaminergic diencephalospinal tract.

While my published work on the role of the DDT-D4R network in locomotor development reveals that D4R antagonism can both prevent and reverse the developmental switch in the locomotor pattern at 4 and 5 dpf, respectively (Lambert et al., 2012), another important question is whether premature exposure of exogenous DA can advance the developmental switch at 3 dpf. That is, why don't 3 dpf larvae undergo this DDT/D4R-mediated switch, normally not observed until 4 dpf, when both presynaptic and postsynaptic constituents of the DDT/spinal D4R circuit are already in place by or before 3 dpf (McLean and Fetcho, 2004a; Boehmler et al., 2007; Kastenhuber et al., 2010; Fujimoto et al., 2011; Reimer et al., 2013)? Although one might expect both DDT neuronal activity and spinal D4R expression to be low at 3 dpf, preliminary fictive experiments have led me to hypothesize that there is proper spatial expression of spinal D4Rs in premotor and/or motor neuron populations such that the spinal locomotor circuitry is primed for DAergic signaling from the DDT at 3 dpf. Systemic application of a D4R agonist transforms the spontaneous long-duration fictive swimming episodes of intact 3 dpf larvae to significantly shorter duration episodes (Fig 1A,B). Moreover, either DA or a broad spectrum D2-like (D2R, D3R, D4R) agonist applied to the transected spinal cord of spinalized 3 dpf

preparations transforms long-duration NMDA-induced fictive swimming episodes to a pattern of significantly shorter episodes, emulating a premature developmental switch via DAergic signaling in the spinal cord (Fig 1C,D). These findings suggest that, at 3 dpf, the DDT does not provide sufficient endogenous spinal D4R signaling to the proper targets, but that spinal D4Rs are sufficiently expressed and primed to functionally modulate the spinal locomotor circuitry upon exogenous DAergic application to the spinal cord. This is consistent with previous studies that show that spinal motor neurons (which are definitively locomotor-related) express D4Rs before 3dpf, albeit at very low levels (Reimer et al., 2013). Also, a recent study exploring other phenomena demonstrated that systemic DAergic application at 2 dpf transforms otherwise long duration behavioral and fictive swimming episodes to become significantly shorter in duration; these investigators inadvertently and unknowingly induced a putative premature developmental switch to short swimming episodes, but with no evidence as to where in the nervous system this signaling is occurring (Tong and McDearmid, 2012). My DAergic spinalized studies at 3 dpf corroborate this finding and, moreover, further elucidate that the site of action to prematurely shorten episodes is sufficient to occur in the spinal cord. The fact that larvae at 3 dpf naturally continue to exhibit long immature-like episodes is consistent with another of my preliminary findings, which is that calcium activity of DDT neurons is markedly low at 3 dpf compared to 5 dpf (Fig 2). This, again, suggests that the 3 dpf DDT/spinal D4R circuitry is primed postsynaptically but without sufficient

endogenous DAergic drive from the DDT. Finally, supporting my fictive and calcium imaging findings of the capacity for a spinal DAergic pharmacological advancement of the locomotor switch, quantitative real-time PCR (qRT-PCR) of the *drd4b* gene reveals that it is expressed in the brain and spinal cord as high or higher than at 5dpf (Fig 3). The continuation of this study will implement optogenetic control of DAergic *otpb* neurons and the DDT to investigate whether optogenetic activation of the DDT at 3 dpf causally initiates a premature advancement of locomotor development. In combination, these studies will be performed in controls and TALEN D4R mutants for *drd4a*, *drd4b*, and *drd4c*. An mutant-specific occlusion of any optogenetic or pharmacological DDT-driven advancement of locomotor development will causally isolate the necessary specific D4R subtype driven by the DDT.

Figure 1

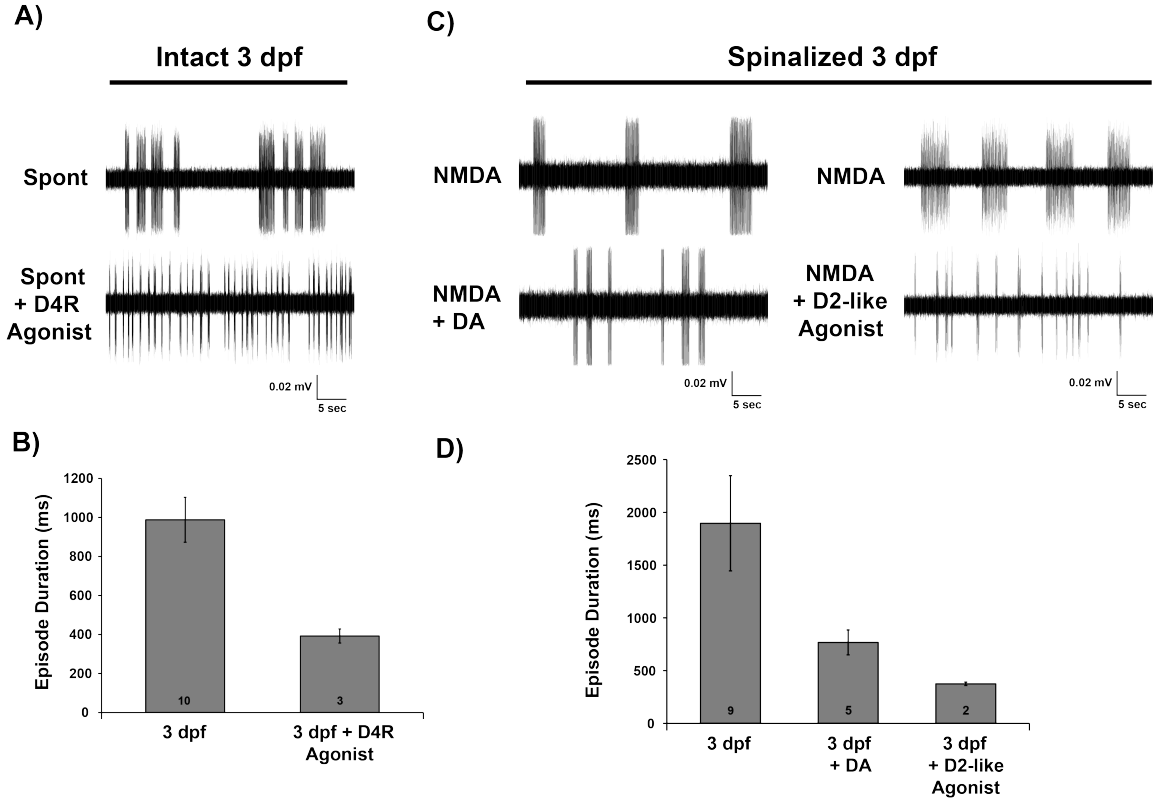
A)
Intact 3 dpf
Spont
Spont + D4R Agonist
0.02 mV
5 sec
C)
Spinalized 3 dpf
NMDA
NMDA + DA
NMDA
NMDA + D2-like Agonist
0.02 mV
5 sec
0.02 mV
5 sec
B)
Episode Duration (ms)
1200
1000
800
600
400
200
0
10
3
3 dpf
3 dpf + D4R Agonist
D)
Episode Duration (ms)
2500
2000
1500
1000
500
0
9
5
2
3 dpf
3 dpf + DA
3 dpf + D2-like Agonist

Figure 2

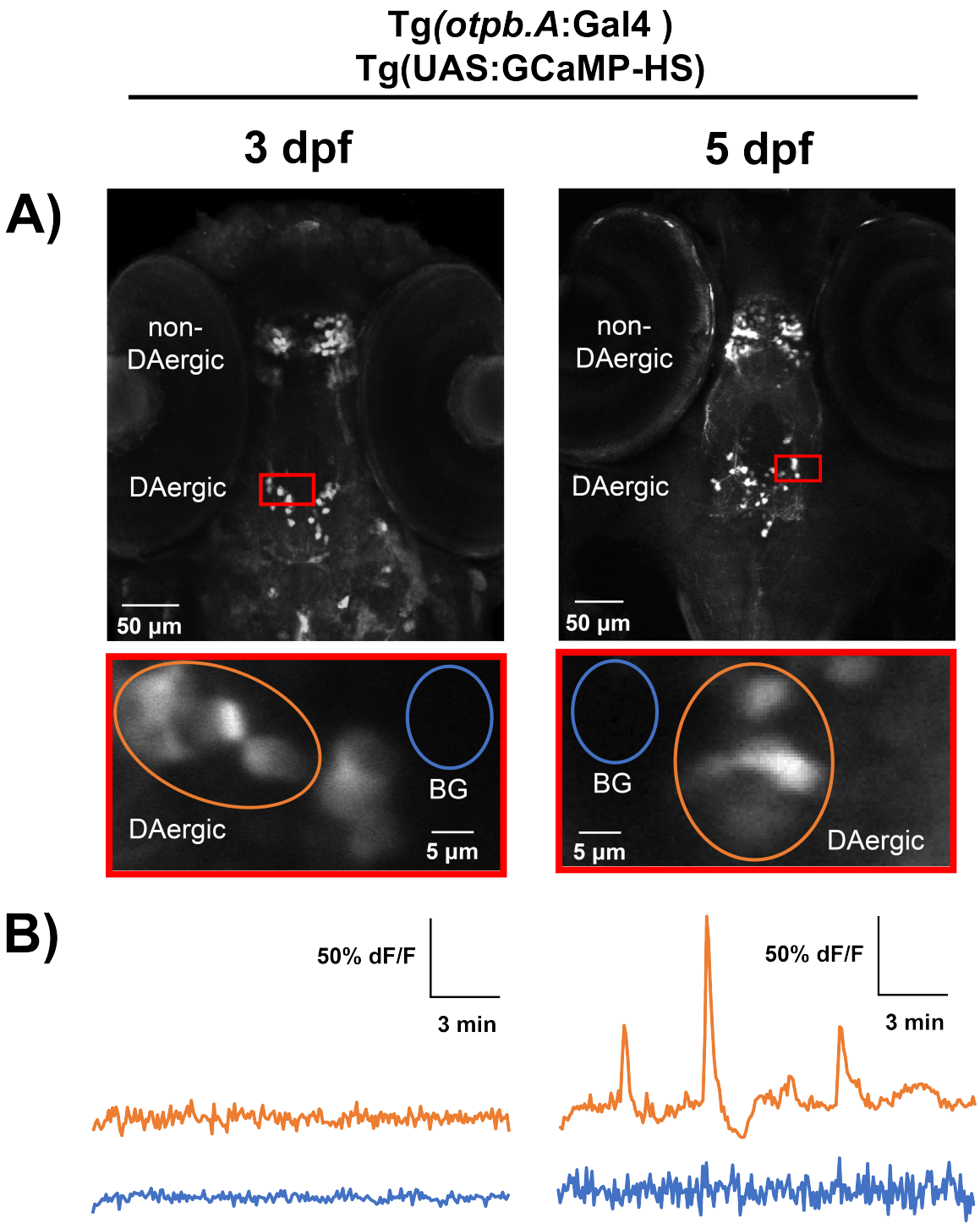
Tg(otpb.A:Gal4)
Tg(UAS:GCaMP-HS)
3 dpf
5 dpf
A)
non-
DAergic
DAergic
50 µm
non-
DAergic
DAergic
50 µm
BG
DAergic
5 µm
BG
5 µm
DAergic
B)
50% dF/F
3 min
50% dF/F
3 min

Figure 3

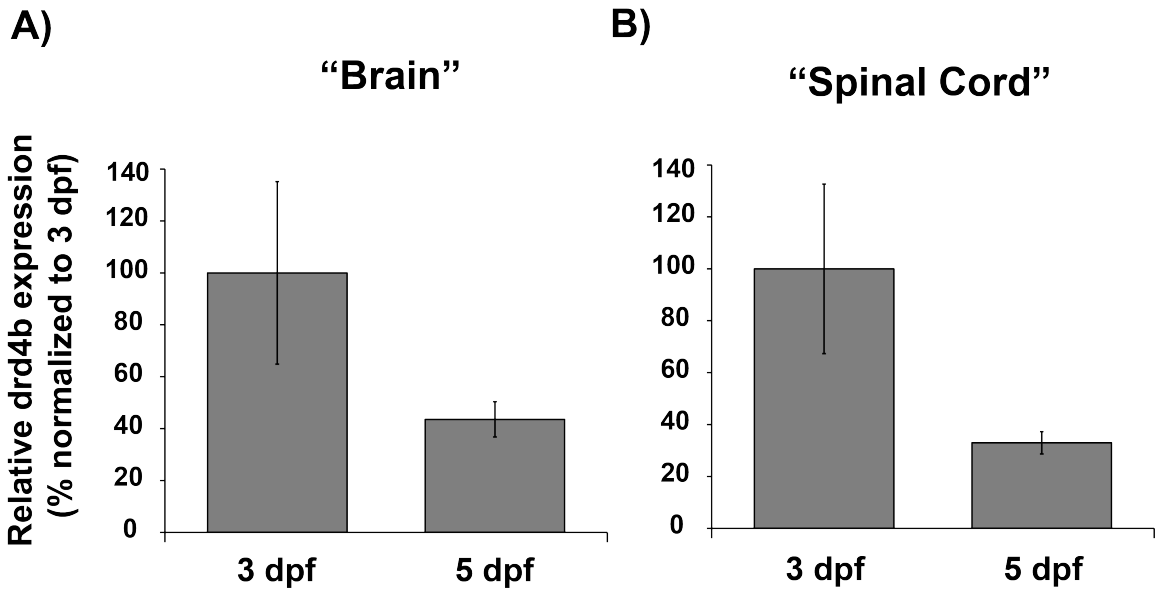
A)
"Brain"
Relative drd4b expression
(% normalized to 3 dpf)
140
120
100
80
60
40
20
0
3 dpf
5 dpf
B)
"Spinal Cord"
140
120
100
80
60
40
20
0
3 dpf
5 dpf

Appendix 1C: An ancient and versatile dopaminergic system: evolutionary conservation of the dopaminergic diencephalospinal tract and its multifunctional integration of the CNS. Review article.

The contents of the General Introduction and General Discussion of this thesis comprise the precursor to one of my forthcoming first-author review articles, which will integrate these sections into a cogent review and positing of the DDT as a conserved multifunctional neuromodulatory network with putatively widespread influence on the CNS. Attention will be paid to collective conservational insights of the DDT network across vertebrates, ranging from genetic, topological, somatic, morphological, projectional, physiological, developmental, and behavioral components. The range of the DDT's known functions and the level of understanding of the neural mechanistic bases underlying these functions will be discussed. Other potential functions of the DDT network, based on its known projections and innervations, will be posited for future investigations. Finally, a proposal will be made for using the zebrafish model to best exploit the neural bases of the DDT's multiple functions *in vivo*, with an explicit roadmap delineated to employing integrative experimental designs to best achieve this collective goal.

Appendix 1D: Zebrafish prey capture as a premiere model to elucidate visuomotor transformations, learning, and long-term memory of goal-directed behavior. Review article

The precursor of another one of my forthcoming first-author review articles comes from the new methodology that I developed for this thesis, its implementation in two different studies of goal-directed prey capture (Chapter 2, Appendix 1A), and my proposal on how to best integrate this new methodology into the existing powerful germane repertoire of experimental approaches in zebrafish *in vivo*. The new methodology I developed in this thesis is the first to employ a high-throughput, unbiased, and automated means of detecting and analyzing hunting sequences in free-swimming zebrafish larvae. This approach will finally enable high-throughput unbiased pharmacological (Kokel et al., 2010; Rihel et al., 2010; Wolman et al., 2011) and genomic screens (Burgess and Granato, 2007a; Petzold et al., 2009; Wolman and Granato, 2012) for specific phenotypes exploited during goal-directed prey capture. Given the rich integrative nature of prey capture behavior, such screens will serve as a versatile and long-standing neuroethological platform for investigating its sensory, sensorimotor, motor, neuromodulatory, engrammic, attentional, and decision-making components (Ewert et al., 1999; 2001; Muto and Kawakami, 2013). Isolation of auspicious compounds and mutants following high-throughput prey capture screening can then be targeted for tethered virtual prey-pursuit (Trivedi and Bollmann, 2013; Preuss et al., 2014), during concurrent bidirectional

optogenetic control (Douglass et al., 2008; Arrenberg et al., 2009; Wyart et al., 2009; De Marco et al., 2013; Kimura et al., 2013; Ljunggren et al., 2014) and whole-brain calcium/voltage imaging (Ahrens et al., 2012; 2013a; 2013b), to elucidate the causal mechanism of specific neural modules to elementary components of goal-directed behavior. Hence, my newly developed approach to high-throughput screening of prey capture will merge investigations of goal-directed behavior in zebrafish to the more integrative recruitment and deployment that it deserves.

Appendix 2A: Mutation of zebrafish dihydrolipoamide branched chain transacylase E2 results in motor dysfunction and models maple syrup urine disease.

Summary

Analysis of zebrafish mutants that demonstrate abnormal locomotive behavior can elucidate the molecular requirements for neural network function and provide new models of human disease. Here, we show that zebrafish *quetschkommode* (*que*) mutant larvae exhibit a progressive locomotor defect that culminates in unusual nose-to-tail compressions and an inability to swim. Correspondingly, extracellular peripheral nerve recordings show that *que* mutants demonstrate abnormal locomotor output to the axial muscles used for swimming. Using positional cloning and candidate gene analysis, we reveal that a point mutation disrupts the gene encoding dihydrolipoamide branched-chain transacylase E2 (Dbt), a component of a mitochondrial enzyme complex, to generate the *que* phenotype. In humans, mutation of the *DBT* gene causes maple syrup urine disease (MSUD), a disorder of branched-chain amino acid metabolism that can result in mental retardation, severe dystonia, profound neurological damage and death. *que*mutants harbor abnormal amino acid levels, similar to MSUD patients and consistent with an error in branched-chain amino acid metabolism. *que* mutants also contain markedly reduced levels of the

neurotransmitter glutamate within the brain and spinal cord, which probably contributes to their abnormal spinal cord locomotor output and aberrant motility behavior, a trait that probably represents severe dystonia in larval zebrafish. Taken together, these data illustrate how defects in branched-chain amino acid metabolism can disrupt nervous system development and/or function, and establish zebrafish *que* mutants as a model to better understand MSUD.

Introduction

Maple syrup urine disease (MSUD) is an inherited metabolic disorder of branched-chain amino acids (BCAA): isoleucine, leucine and valine (Strauss and Morton, 2003; Chuang et al., 2006). It demonstrates an autosomal recessive pattern of inheritance, and affects ~1 in every 185,000 children worldwide. However, much higher incidence rates are observed in Old Order Mennonite communities, with a ratio of 1:200 children, owing to founder effects. The first step of BCAA metabolism consists of a reversible transamination reaction to yield α-keto acids. The second step is oxidative decarboxylation of the α-keto acids by the mitochondrial branched-chain α-keto acid dehydrogenase (BCKD) complex. Mutation in any of the four genes encoding the three catalytic components of the BCKD complex has been shown to cause MSUD. Affected individuals accumulate BCAAs and α-keto acids in tissues and plasma, which cause the urine and bodily secretions to smell like maple syrup (burned sugar), hence the name of the disorder. In the most severe or 'classic' form of MSUD, the elevated BCAAs and α-keto acids can have a devastating impact on the central nervous system (CNS). If not treated, toxic build up of BCAAs and α-keto acids cause severe dystonia, coma, cerebral edema, dysmyelination and death within a couple weeks after birth. Treatment for MSUD typically consists of severe dietary restriction of BCAAs (Strauss et al., 2010). However, even with a carefully monitored diet, secondary illnesses can lead to metabolic crisis and neurological

damage, which is thought to generate the mental retardation and psychiatric problems that are often observed. An alternative treatment for MSUD is elective liver transplantation, which reduces plasma levels of BCAAs and α-keto acids and spares the CNS from severe injury (Strauss et al., 2006). Unfortunately, the scarcity of livers for transplantation, surgical risks and lifetime usage of immunosuppressants limit this treatment option. A better understanding of the mechanisms that cause the neuropathology of MSUD and development of new therapeutic drugs could greatly benefit affected individuals as well as yield new insight into CNS metabolism.

To investigate the pathophysiology of MSUD, a mouse model of the classic form of the disease was created by deleting the gene encoding the E2 subunit of the BCKD complex (Homanics et al., 2006). A model of a less severe form of the disease, intermediate MSUD, was also developed. These mice recapitulate several aspects of MSUD, including elevated levels of BCAAs and α-keto acids in tissues and plasma, severe neurological impairment, and decreased phenotypic severity in response to liver cell transplantation (Zinnanti et al., 2008; Skvorak et al., 2009a; 2009b). However, the neuropathological mechanisms of MSUD remain poorly understood. Additional animal models could provide a complementary tool to study the mechanisms of this disease that generate CNS injury.

Developing zebrafish provide an excellent system to investigate the cellular and molecular mechanisms of MSUD. Although BCAA metabolism has yet to be described in this system, larval zebrafish offer several advantageous features, including small size, rapid development external to the mother, optical transparency, large clutch sizes and organ systems that are broadly similar to those in mammals. These features make zebrafish larvae readily amenable to a wide variety of behavioral, genetic, imaging, physiological and pharmacological approaches. The identification of zebrafish mutants with impaired BCKD complex function hold promise as a particularly useful tool to investigate the effects of disrupted BCAA metabolism.

Zebrafish perform a characteristic sequence of motor behaviors during development, which reflects different stages of locomotor network formation (Kimmel et al., 1974; Saint-Amant and Drapeau, 1998; Downes and Granato, 2006; McKeown et al., 2009). These behaviors were used as the basis for extensive mutagenesis screens to identify mutants with specific defects in embryonic motility (Granato et al., 1996). Mutants that demonstrated similar, abnormal behavior were grouped into phenotypic classes, including the accordion class. Starting around 21 hours post-fertilization (hpf), wild-type embryos demonstrate smooth, alternating tail coils. By contrast, accordion class mutants compress along the rostro-caudal axis and relax, like an accordion. *Quetschkommode* (*que*) mutants were grouped into the accordion

class but, outside of the initial study identifying these mutants, it has not been characterized nor has the identity of the mutated gene been reported.

In this study, we reveal that *que* mutants contain a mutation that disrupts the E2 subunit of the BCKD complex. Correspondingly, we present evidence that *que*mutants accumulate high concentrations of BCAAs. *que* larvae also contain reduced levels of the neurotransmitter glutamate, which probably contributes to the aberrant CNS function and abnormal behavior observed in this mutant. Combined, these data identify the *que* mutant as a vertebrate model of MSUD, which holds promise as a powerful tool to better understand this disease and identify therapeutic compounds.

Methods

Zebrafish maintenance and breeding. All animal protocols were approved by the Institutional Animal Care and Use Committees (IACUC) at the University of Massachusetts and the University of Minnesota. Zebrafish were raised and maintained according to standard procedures. Developing zebrafish were kept at 28.5°C in E3 media and staged according to morphological criteria (Kimmel et al., 1995; Parichy et al., 2009). Experiments were performed using *que*^{ti274}, *beo*^{ap21} and *acc*^{tq206} mutant alleles maintained on a mixed Tübingen (Tü) or tub longfin (TLF) genetic background.

Behavioral analysis. To characterize swimming behavior, light-touch stimuli were applied to the head of larvae using a 1 mm insect pin. The response was recorded using a high-speed video camera (Fastec Imaging, San Diego, CA), recording 500–1000 frames per second, mounted to a 35 mm lens (Nikon, Melville, NY). The head-to-tail angle for each frame was measured using automated software developed by G.B.D.'s laboratory (Kelly Anne McKeown and Sandy Whittlesey, unpublished). Briefly, pixel density analysis was used to identify three landmarks along the larval body: the tip of the nose, the border between the yolk ball and yolk extension, and the tip of the tail. These three points form an angle, and these angles were plotted over time using Microsoft Excel.

Electrophysiological recordings. Zebrafish larvae at 4 dpf were anesthetized with 0.02% Tricaine-S (Western Chemical) in extracellular recording solution (Legendre and Korn, 1994; Drapeau et al., 1999; Masino and Fetcho, 2005) and paralyzed with 0.1% (w/v) α-bungatoxoin (Sigma), which significantly reduced or abolished postsynaptic muscle activity based on patch recordings from muscle fibers (Masino and Fetcho, 2005). The extracellular solution was superfused continuously at 22–26°C. Larvae were pinned in a dorsoventral position to a Sylgard-lined glass-bottom Petri dish and the skin was removed. Extracellular suction electrode recording techniques were used to monitor the activity of peripheral nerves during fictive behavior (Masino and Fetcho, 2005). Activity occurred spontaneously but was also initiated by gently applying a touch stimulus to the head with a tungsten pin controlled and positioned by a manual micromanipulator (MX130, Siskiyou, Grants Pass, OR). The tip of the extracellular suction electrode (~15 μm tip diameter) was positioned at the dorsoventral midline of a myotomal cleft where the skin had been removed. All extracellular recordings were restricted to between body segments 7 and 15. A MultiClamp 700B (Molecular Devices, Sunnyvale, CA) amplifier was used to monitor extracellular voltage in current-clamp mode at a gain of 1000 (R_f=50 MO) with the low- and high-frequency cut-off at 100 and 4000 Hz, respectively. Recordings were sampled at 10 kHz. Extracellular recordings were digitized

using a digitizing board (DigiData series 1440A, Molecular Devices, Sunnyvale, CA) acquired using pClamp 10 software and rectified offline.

Analysis of peripheral nerve activity. A program written in MATLAB (Mathworks, Natick, MA) was used to analyze the data. Estimates of mean burst frequency were determined from a Fourier transform, such that the initial estimate of mean burst frequency was the frequency at which the Fourier transform magnitude peaked over a frequency band from 0.1 to 5 Hz. The rectified voltage recordings were smoothed with a Gaussian-weighted moving average with 99% of the weight concentrated over an interval whose width was one-quarter of the reciprocal of the estimated burst frequency ('quarter-width').

The occurrence times of rhythmic bursts in the smoothed voltages were determined with an algorithm that searched for local peaks and troughs over quarter-width intervals while forcing adjacent peaks and troughs to be separated by at least quarter-width, and furthermore forcing peaks and troughs to alternate. With the peaks and troughs defined, the individual 'burst sections' were then defined as the interval between adjacent troughs. To determine the start of individual bursts, the burst-onset was defined as the time at which the smoothed waveform rose from the first trough to 10% of the way to the next peak. Similarly, burst-termination was defined as the time at which the smoothed waveform fell from the peak by 90% of the vertical distance to the next trough. Next, the

analysis program was used to determine the bout and burst properties for each voltage trace in a manner similar to that used by Masino and Fetcho (2005). Finally, the amount of overlap in activity between alternating (left-right) bursts was measured as the proportion of the total burst time occupied by the simultaneous activity in the paired (left-right) extracellular recordings (Fig 2C,D, overlap indicated by gray bars). The means and standard deviations for each parameter were then determined.

Chromosomal mapping and sequence analysis. Crosses between fish heterozygous for the *que* allele and WIK fish were used to generate a three-generation map cross panel. F2 *que* mutant embryos and wild-type siblings were collected, sorted based upon the 96 hpf phenotype and stored in methanol at −20°C. DNA was extracted from more than 833 mutant larvae, and SSLP markers and SNP markers were obtained and generated against genes to refine the mapping interval. Exons and intron-exon boundaries of candidate genes were sequenced (Genewiz, South Plainfield, NY) from wild type, *que* siblings and homozygous mutants.

Morpholino analysis. Wild-type zebrafish embryos were pressure injected at the one- to four-cell stage with 12 ng of morpholino designed to block translation of *dbt* or the standard control morpholino (Gene Tools, Phinomath, OR). This amount of morpholino was selected based upon dose-response experiments in

which higher doses were found to generate morphological defects and/or lethality. The sequence of the translation-blocking morpholino was 5′-CGCACAG-TAATGACCGCCGCCATCT-3′. Underlined residues indicate the start codon. The control morpholino sequence was 5′-CCTCTTAC-CTCAGTTACAATTTATA-3′. The embryos were raised at 28.5°C, and locomotive behavior was examined across development. Kinematic analysis, as described above, was performed at 96 hpf.

RT-PCR. RT-PCR was used to analyze mRNA splicing in mutants as well as examine expression during development. Primers designed against *dbt* protein-coding exon 6 (5′-ATCAAACTAAGCGAAG-TTGTCGG-3′) and exon 7 (5′-GCGCAACCGGACCAAC-3′) were used to amplify cDNA from wild-type and homozygous *que* mutant larvae. The primers used to amplify β-actin were 5′-CACACCGTGCCCATCTATGA-3′ and 5′ -AGGATCTTCATCAGGTAGTCTGTCAG-3′. The RNAs were reverse transcribed using the Omniscript kit (Qiagen, Venlo, The Netherlands). The *dbt* PCR products were sequenced for confirmation (Genewiz, South Plainfield, NY). RT-PCR reactions were performed multiple times to decrease the likelihood of amplification artifacts.

Whole-mount in situ hybridization. Antisense digoxigenin probes were generated against *dbt* using cDNA (Genbank IDBC090917) acquired from Open

Biosystems (Huntsville, AL). Whole-mount, colorimetric in situ hybridization was performed using established protocols (Thisse and Thisse, 2008) and examined using a compound microscope (Zeiss, Thornwood, NY) attached to a digital camera (Zeiss, Thornwood, NY). Cross-sections were generated by hand sectioning in situ hybridization stained embryos with a razor blade attached to a surgical blade holder. To generate sagittal sections, in situ hybridization stained embryos were embedded in 1.5% Agar and 5% sucrose. Blocks were kept in 30% sucrose solution overnight. The next day blocks were cut into 20 mm sections using a cryostat (Leica, Buffalo Grove, IL).

Amino acid quantification. For each amino acid quantification experiment 50 96-hpf larvae were sorted based upon the locomotor phenotype, were flash frozen in liquid nitrogen and stored at −80°C. The samples were homogenized and precipitated with 0.1 M lithium citrate, 3.3% 5-sulphosalicylic acid. The samples were sonicated for 10 minutes, then centrifuged at 4600 *g* for 20 minutes. The supernatant was then applied to VivaSpin500 size exclusion columns (Sartorium, Germany) and centrifuged at 15,000 *g* for 4 hours. The flow-through was stored at −80°C then sent to the University of California Davis California Genome and Proteomics Center to resolve free amino acid concentrations.

Antibody staining. The tissue was prepared by embedding 96 hpf larvae as described for in situ hybridization. Double immunostaining was performed using standard protocols (similar to Downes and Granato) (Downes and Granato, 2004). The primary antibodies were rabbit anti-L-glutamate (1:100 dilution, ab9440; Abcam, Cambridge, MA) and mouse anti-acetylated tubulin (1:200 dilution, T6793; Sigma, St Louis, MO). Secondary antibodies were Alexa Fluor 488 goat anti rabbit (1:1000 dilution, A11034; Molecular Probes/Sigma, St Louis, MO) and Alexa Fluor 594 goat anti mouse (1:1000 dilution, A11005; Molecular Probes, Sigma, St Louis, MO). Images were acquired using a confocal microscope (Nikon, Melville, NY).

The fluorescent intensity for acetylated tubulin and L-glutamate antibody staining was quantified using the EZ Viewer program (Nikon, Melville, NY) by collecting entire frames (10,1283 μm^2) or selecting a region of interest above the notochord (3060 μm^2) for both channels. The numbers used for quantification are the analog-to-digital converter (ADC) values of L-glutamate normalized to acetylated tubulin.

Results

que mutants exhibit abnormal rostro-caudal compressions in response to touch

A single allele of *que* (*ti274*) was identified from a previously performed mutagenesis screen (Granato and Nüsslein-Volhard, 1996; Zottoli and Faber, 2000). The mutation is recessive, and homozygous mutants first demonstrate abnormal rostro-caudal compressions at around 72 hpf (data not shown). The abnormal behavior becomes more robust by 96 hpf. At this time point, high-speed video analysis shows that wild-type larvae respond to touch by first performing a large-amplitude body bend in which the nose touches the tip of the tail, a so-called C-start or C-bend (defined here as greater than 110°), followed by lower-amplitude body undulations to swim away (Fig 1A; supplementary material Movie 1) (Eaton et al., 1977; Zottoli and Faber, 2000). By contrast, *que* mutants do not perform the initial C-bend or lower-amplitude body undulations, and instead demonstrate rostro-caudal shortening (Fig 1B; supplementary material Movie 2). This behavior, called accordion behavior (Granato et al., 1996), is due to abnormal coordination of axial left-right muscle contractions. Other mutants have been shown to demonstrate accordion behavior due to defects in either CNS function, such as *bandoneon* (*beo*), or muscle relaxation, such as *accordion* (*acc*) (Gleason et al., 2004; Hirata et al., 2004; 2005; Olson et al., 2010). We used kinematic analysis to compare the

swimming behavior of wild-type, *beo*, *acc* and *que* larvae to each other to determine whether we could distinguish defects in CNS function from defects in muscle relaxation and classify *que* mutants. No clear trend emerged; however, *que* mutants consistently show the most dramatic disruption of swimming behavior compared with *acc* or *beo* mutants. Although *acc* and *beo* mutants demonstrate abnormal swimming behavior, C-bends are often observed (Fig 1C–E). By contrast, *que* mutants very rarely execute large-amplitude body bends (Fig 1F). *que* mutants continue to perform accordion behavior 5–6 days post-fertilization (dpf). They fail to inflate the swim bladder, which would enable them to feed, and eventually die around 7 dpf.

que mutants demonstrate abnormal motor output

To better examine whether *que* mutants harbor a defect in CNS function as opposed to a defect in muscle relaxation, we analyzed fictive locomotor output from the spinal cord by performing extracellular peripheral nerve recordings. Zebrafish larvae demonstrate bouts of motor output in response to touch (Fig 2A,B). These bouts are composed of tightly coordinated bursts that alternate rapidly between the left and right sides and orchestrate the axial muscle contractions that constitute swimming. In wild-type larvae, we observed rapid alternations in locomotor output between the left and right sides, with little overlap in bursting activity (6.5±6%, n=5; Fig 2C), as described previously

(Masino and Fetcho, 2005). In *que* mutants, although the coordination of left-right locomotor activity was similar to wild-type siblings (compare Fig 2C with 2D), the amount of overlap between left-right bursting activity was significantly increased (19.1±11.3%, n=7, t=−2.3, P<0.05). This increase in activity overlap is consistent with the abnormal coordination of left-right muscle contractions performed by *que*mutants. These data do not rule out the possibility that *que* mutants contain a defect in muscle relaxation; however, they do indicate that abnormal motor output from the CNS at least contributes to the behavior of this mutant.

To further characterize potential differences in locomotor output between wild-type and *que* mutant siblings, we examined a range of bout and burst properties related to rhythmic locomotor activity during fictive swimming (Masino and Fetcho, 2005). Although most of these properties were not significantly different between wild-type and mutant larvae (Table 1), *que* mutants generated a significantly greater number of bouts following touch stimulus applied to the head than did wild-type larvae [11.6±6.2 bouts and 1.9±0.9 bouts, respectively (t=3.5, P<0.01,n=5)]. These results suggest that, compared with wild type, there are subtle, yet significant, changes in the locomotor circuit that underlie swimming in *que* mutant larvae and participate in generating the mutant behavioral phenotype.

The *que* gene encodes dihydrolipoamide branched-chain transacylase E2 (Dbt)

To determine the molecular identity of the *que* gene, we used a positional cloning strategy. Using a three-generation map cross panel, we screened pools of genomic DNA from wild-type siblings and homozygous mutants with a panel of simple sequence length polymorphism (SSLP) markers. *que* mapped to chromosome 22, which confirmed previous low-resolution mapping results (Geisler et al., 2007). We then used DNA extracted from single embryos and single nucleotide polymorphism (SNP) markers to refine the map position to a 0.36 cM interval between the markers ENSDART109865 and wu:f63d09 (Fig 3A). Extensive genome database analysis and sequencing of nearby candidate genes led us to *dihydrolipoamide branched chain transacylase E2* (*dbt*), which encodes a subunit of the BCKD complex, which is required for BCAA metabolism. Zebrafish Dbt is a predicted 493 amino acids in length, and it is ~78.2% identical to the human protein (data not shown). Mutations in the human *DBT* gene are known to cause MSUD, which can result in severe dystonia and death if not treated. Given that *que* mutants demonstrate abnormal behavior and nervous system function consistent with the severe dystonia observed in humans, we sequenced the *dbt* gene. Sequence analysis of the *dbt* gene from *que* homozygotes revealed a single nucleotide substitution in the splice donor site of exon 6 compared with wild type. The guanine of the intron side of this splice site is changed to an adenine (Fig 3B). To determine whether

this change affects the splicing of intron 6, as would be predicted, we performed reverse transcriptase (RT)-PCR using one primer in exon 6 and one primer in exon 7 (Fig 3C). We found that RNA extracts from wild-type larvae were spliced according to prediction; however, RNA extracts from homozygous mutants revealed a larger transcript that contained the entire 86 base pairs of intron 6, indicating that it was spliced incorrectly (data not shown). This intron alters the sequence downstream of Lys268 and contains four stop codons, which would prematurely truncate the Dbt protein by 224 amino acids. *dbt* contains an acetyl transferase domain, essential for its function, which would be largely absent from the *que* mutant protein. Interestingly, in humans, a mutation that prematurely truncates the DBT protein at the orthologous position (Lys257) was reported in an individual with the most severe or 'classic' form of MSUD (Herring et al., 1992). These data indicate that the *que* mutation is a loss-of-function allele that diminishes or abolishes BCKD complex function.

To further confirm the molecular identity of *que*, we injected wild-type embryos with either a standard control morpholino or a morpholino designed to block translation of *dbt*. Embryos were injected at the one- to four-cell stage and monitored over the course of development. Embryos injected with the standard control morpholino exhibited mostly normal behavior throughout the course of development (97.2% of surviving larvae, *n*=107; Fig 3D). Notably, 37.5% (*n*=144) of surviving larvae injected with the morpholino designed to

demonstrated clear rostro-caudal compressions and fewer large-amplitude body bends at 96 hpf, similar to *que* mutants (Fig 3E). It is important to note that morpholinos are known to lose effectiveness at ~4–5 dpf owing to turnover, which probably explains why not all embryos injected with the *dbt* morpholino demonstrated the robust accordion behavior performed by *que* mutants (Bill et al., 2009). We also attempted to perform rescue experiments in mutant embryos by injecting mRNA encoding *dbt* at the one- to four-cell stage and analyzing motility behavior at 4 dpf. We did not observe rescue (data not shown); however, mRNA is known to lose effectiveness ~2 dpf owing to turnover.

The *que* behavioral phenotype is not apparent until 3–4 dpf, which indicates that Dbt is required at this stage of development and precludes mRNA rescue. Regardless, the mapping data, nature of the *que* mutation, aberrant mRNA splicing observed in mutants, and morpholino phenocopy all argue that the *que* gene encodes Dbt.

dbt mRNA becomes enriched in the brain and gut organs during development

We next examined the spatial and temporal expression of *dbt* in developing zebrafish. RT-PCR revealed that *dbt* mRNA was present at all time points examined from 6 hpf to 120 hpf (Fig 4A). In situ hybridization also confirmed early expression. *dbt* was detected at the two-cell stage, indicating it is a maternally deposited mRNA (Fig 4B). The spatial expression of *dbt* is initially

widespread through 24 hpf (Fig 4C,D); however, its expression pattern over the next few days of development becomes enriched in the brain and organs in the gut, such as liver and intestine (Fig 4E–H). These data suggest that *dbt* plays an important role in BCAA metabolism through function in these tissues. The prominent expression within the brain, in particular, suggests that *dbt* is important for CNS function. Intriguingly, the expression pattern of *dbt*, with progressive enrichment in the brain and gut organs over the course of development, is reminiscent of another mitochondrial protein that is important for CNS function, Opa3 (Pei et al., 2010).

que mutants harbor elevated levels of BCAAs

In mammalian systems, impaired *DBT* function, as demonstrated by MSUD-affected individuals, results in elevated levels of BCAAs (Strauss and Morton, 2003; Chuang et al., 2006). Because *dbt* is disrupted in *que* mutants, we investigated their free amino acid profiles. Owing to the small size of larval zebrafish, a homogenate of 50 whole animals was used for each assay. We compared the free amino acid levels of wild-type and *que* mutant larvae at 96 hpf. Strikingly, *que* larvae harbor elevated levels of BCAAs (Fig 5A,B). Isoleucine, leucine and valine concentrations were 788%, 1006% and 688% (n=3, P<0.01) of those of wild type, respectively. *que* mutants also showed a marked decrease in free glutamine levels, at 24% of wild-type (n=3, P<0.01). In addition, statistically significant decreases were observed in the levels of a wide

variety of free amino acids, including aspartate (16%), GABA (32%) and serine (28% of wild type; all n=3,P<0.01); and alanine (44%), glutamate (38%), glycine (41%), methionine (49%) and threonine (60% of wild type; all n=3, P<0.05). To rule out the possibility that abnormal motor behavior itself alters free amino acid levels, we examined *beo* mutants, which contain a mutation in the glycine receptor β2 subunit and exhibit abnormal behavior similar to *que* mutants (Fig 5C) (Hirata et al., 2005). The free amino acid levels in *beo* mutants (n=1) were similar to that of wild-type controls, indicating that accordion behavior alone does not substantially alter free amino acid concentrations. Combined, these data provide strong evidence that mutation of the *que* gene results in an error in amino acid metabolism, yielding a prominent accumulation of BCAAs.

Glutamate levels are reduced in the brain of *que* mutant larvae

Although the neuropathology of MSUD is not well understood, reduced concentrations of neurotransmitters, including glutamate, were observed in the intermediate MSUD mouse model (Zinnanti et al., 2008). Neurotransmitter depletion was found to correlate with abnormal motor behavior and a highly abnormal posture consisting of recumbency and stiff, extended limbs. Given that our analysis of the free amino acids levels in *que* mutants showed decreased concentrations of free glutamate and these mutants demonstrate abnormal CNS function and motor behavior, we examined the distribution of glutamate using an antibody. As a control for antibody penetration and overall tissue morphology, we

also stained using an acetylated tubulin antibody. Antibody penetration and general morphology of the brain of *que* mutants seemed similar to wild type at 96 hpf (compare Fig 6A with 6D). By contrast, glutamate levels were markedly reduced in *que* mutant larvae (n=5 embryos, 12 sections, P<0.01; compare Fig 6B with 6E, Fig 6G), which probably contributes to the abnormal nervous system function and behavior observed by this stage of development.

Discussion

In this study, we revealed that the *dbt* gene plays an essential role in developing zebrafish. The molecular nature of the *que* mutation, phenocopy through antisense morpholino injection, and the profile of free amino acid concentrations indicate that loss of *dbt* function result in abnormal amino acid metabolism and a dramatic accumulation of BCAAs. We determined that the *dbt* gene becomes enriched in the brain and organs in the gut during zebrafish development, and that impaired *dbt* function results in reduced levels of glutamate in the brain. Because glutamate is crucial for CNS function, the reduced levels of this neurotransmitter probably promote the abnormal spinal cord output and accordion behavior demonstrated by *que* mutants.

dbt is required for brain function in zebrafish

The findings from this study, as well as observations in rodent and human systems, suggest a model for how mutation of the zebrafish *dbt* gene leads to abnormal swimming. In mammalian systems, *dbt* is required for the second step of BCAA metabolism, and its impairment leads to elevated levels of BCAAs and α-keto acids in plasma and tissue (Chuang et al., 2006). Elevated BCAAs in the plasma, in particular leucine, are thought to out-compete other amino acids at the blood-brain barrier, which results in neurotransmitter deficiencies, growth restrictions, cytotoxic edema, myelin disruption, and impaired energy metabolism

throughout the CNS (Zinnanti et al., 2008). α-keto acid toxicity has also been proposed to directly disrupt CNS function. Intracranial injection of α-ketovaleric acid, which is derived from valine, has been shown to elicit seizures in rats, whereas administration of other α-keto acids had no behavioral effect (Coitinho et al., 2001). In individuals with MSUD, reducing the concentrations of BCAAs and α-keto acids in the plasma by liver transplantation can protect CNS function and development (Strauss et al., 2006).

We propose that very similar mechanisms regulate BCAA metabolism in zebrafish (Fig 7). Throughout the first 5 days of zebrafish development, the embryo consumes the presumptive equivalent of a high-protein diet in mammals by absorbing BCAA-containing proteins from the yolk (Link et al., 2006; Tay et al., 2006). During the earliest stages of development, within the first few hours post-fertilization, the metabolic needs of the embryo are largely met by maternally derived mitochondria and mRNA (Mendelsohn and Gitlin, 2008; Zhang et al., 2008; Abrams and Mullins, 2009). However, as embryogenesis proceeds, BCAA metabolism increasingly relies upon zygotic transcription. In wild-type embryos, BCKD complex function in the liver, other gut organs and the brain itself, protect the CNS from BCAA toxicity, similar to mammalian systems. According to this model, BCKD complex function supports appropriate import of amino acids into the CNS, robust metabolic generation of neurotransmitters, which are essential to support the coordinated CNS output that generates

vigorous swimming behavior. In *que* mutants, our data indicate that mutation of *dbt* disrupts BCKD complex function to cause the toxic accumulation of BCAAs and, probably, α-keto acids. This error probably causes abnormal retention, metabolism and import of amino acids into the CNS, reduced levels of glutamate and other neurotransmitters, abnormal CNS function, and accordion behavior (Fig 7). It will be interesting to use transgenic approaches to determine whether restoring gene function in the liver of *que* mutants preserves normal CNS function, as shown in mammals (Strauss et al., 2006; Skvorak et al., 2009a; 2009b). Driving gene expression in other organs not yet explored in mammals can also be investigated, which might indicate new therapeutic options for individuals with MSUD.

que mutants are a new animal model of MSUD

que larvae harbor a mutation in zebrafish *dbt*, which results in elevated BCAA levels, similar to both the mouse models of MSUD and affected humans. In the mouse model of intermediate MSUD, elevated levels of BCAAs have been shown to correlate with progressive disruption of CNS function and concomitant defects in motor behavior that culminate in severe dystonia (SILBERMAN et al., 1961; Morton et al., 2002; Zinnanti et al., 2008). Similarly, severe dystonia has been reported in MSUD-affected individuals during acute metabolic decompensation (SILBERMAN et al., 1961; Morton et al., 2002; Zinnanti et al., 2008). *que* mutants demonstrate a progressive defect in motor behavior that

culminates in abnormal CNS function and accordion behavior. Accordion behavior is probably the expression of severe dystonia in developing zebrafish. We and others have previously shown that zebrafish mutants that exhibit accordion behavior contain mutations in genes known to control movement and muscle tone in mammalian systems (Downes and Granato, 2004; Gleason et al., 2004; Hirata et al., 2004; 2005; Wang et al., 2008; Olson et al., 2010).

The findings from this study indicate that *que* mutants are a new animal model of MSUD. One aspect of MSUD is the distinct, maple syrup smell of bodily secretions of affected individuals. We did not detect any distinct odor of *que* mutants (data not shown); however, this is probably due to the small size and minute amounts of secretions produced by larval zebrafish. Nevertheless, *que* larvae seem to recapitulate molecular, biochemical, cellular and behavioral aspects of MSUD. Because larval zebrafish contain a smaller nervous system than do mammalian systems, with fewer numbers of cells, *que* mutants provide a promising system to better characterize the progression of CNS injury in response to BCAA toxicity. Moreover, the small size, aquatic nature, development that is external to the mother and the ability to obtain large numbers of zebrafish embryos make them amenable to small-molecule screens (Zon and Peterson, 2010). The behavioral phenotype of *que* mutants is robust and easily quantifiable; therefore, *que* mutants could be developed into a high-throughput system to screen libraries of compounds to

identify small molecules that improve swimming behavior. Compounds that improve the behavioral phenotype of *que* mutants could be candidate therapeutics for individuals with MSUD.

Other aspects of MSUD can also be investigated using larval zebrafish. Gene targeting approaches can be readily employed, such as morpholino injection or zinc-finger nuclease technology, to model MSUD caused by disruption of other BCKD complex subunits (Ekker, 2008; Bill et al., 2009). These technologies can also be used to examine the in vivo role of BCKD regulatory proteins, such as the BCKD phosphatase or kinase. Genetic modifier screens can also be performed using the *que* mutant to search for genes that can compensate for disruptions in BCAA metabolism. Taken together, these approaches can provide a promising platform to better understand CNS metabolism and develop new therapies to combat MSUD.

Figure Legends

Fig 1: que mutants exhibit abnormal swimming behavior at 96 hpf. (A,B) Selected frames from high-speed video recordings are shown with times indicated in milliseconds. (A) A wild-type larva demonstrates a normal C-bend (A4, asterisk) in response to a touch stimulus, followed by smaller-amplitude body undulations to clear the field (A5-A12). (B) A *que* mutant demonstrates abnormal rostro-caudal shortening and it fails to escape. (C–F) Kinematic traces are shown, with zero degrees indicating a straight body and positive and negative angles representing body bends in opposite directions. Time is shown in seconds. Ten representative traces are shown for each phenotype. (C) Wild-type embryos typically perform a C-bend (defined here as greater than 110°; asterisks) followed by smaller-amplitude body undulations. (D) *bandoneon* (*beo*) mutants, which contain a CNS defect and demonstrate behavior similar to *que*, sometimes perform a C-bend followed by abnormal body bends.
(E) *accordion* (*acc*) mutants, which contain a muscle relaxation defect and also demonstrate behavior similar to *que*, sometimes perform a C-bend but fail to perform smaller-amplitude body bends. (F) *que* mutants rarely perform a C-bend and demonstrate few smaller-amplitude body undulations.

Table 1: Comparison of bout and burst properties related to fictive locomotor activity in wild type and *que* mutants

Fig 2: The spinal locomotor output is altered in *que* mutants. (A,B) Representative single extracellular peripheral nerve recordings from (A) wild type and (B) a *que* mutant. *que* mutants produce a greater number of bouts following a gentle tap to the head (arrow) than do wild type. (C,D) Representative paired (left-right) extracellular peripheral nerve recordings in which (C) wild type fish demonstrate tightly coordinated bursting activity with little overlap. By contrast, (D) *que* mutants generate greater bursting overlap. Gray bars denote burst activity in the top trace and extend to the bottom trace for ease of comparison.

Fig 3: The *que* gene encodes dihydrolipoamide branched-chain transacylase E2 (Dbt), a subunit of the BCKD complex. (A) *que* maps to a 0.36 cM interval on chromosome 22. Molecular markers are shown at the top and the number of recombinants out of the number of meiotic events are shown at bottom. *dbt* was positioned within the zero recombinant interval. (B) Chromatogram sequence traces of *dbt* from wild-type, hetero-and homozygous mutant larvae. The nucleotide substitution at the exon-intron boundary (G to A) can be observed in hetero- and homozygotes. (C) A schematic of the *dbt* protein is shown with the boundaries between exons indicated as vertical lines. Protein domains, including the acetyl transferase domain, are also shown. Below, the wild-type splice pattern is illustrated, with protein-coding exon 6, the sequence at the splice site, the intervening intron, and protein-coding exon 7 depicted.

The *que* mutant splicing pattern is also illustrated, including the nucleotide substitution, which results in a failure to remove the intron. The intron contains four stop codons (asterisks). RT-PCR results using mRNA from wild type, *que* mutants and –RT controls are also shown using primers targeted towards exon 6 and exon 7. A larger DNA product, containing intron sequence, can be observed using mRNA isolated from *que* mutants. (D,E) Ten kinematic traces are shown for embryos injected with (D) the control morpholino or (E) a *dbt* translation-blocking morpholino. Embryos injected with the control morpholino perform C-bends (asterisk) and normal swimming behavior. *dbt* morphant embryos demonstrate abnormal swimming behavior and few large amplitude body bends, similar to *que* mutants.

Fig 4: *dbt* becomes enriched in the brain and organs in the gut across development. (A) RT-PCR results are shown using mRNA isolated at different time points during zebrafish development. *dbt* was detected at all stages examined. –RT and β-actin controls are also shown. (B–H) In situ hybridization shows broad *dbt* expression at (B) the two-cell stage, (C) 12 hpf and (D) 24 hpf. The inset of a cross-section (the black bracket indicates the approximate level of the cross-section) reveals robust *dbt* expression in muscle. *dbt* expression become enriched in the brain and gut at (E) 48 hpf and (F) 96 hpf. (G) Sagittal sections of stained 96 hpf embryos illustrate expression in the brain (arrowhead) and gut. The white bracket indicates a portion of the region shown at higher

magnification in H. Above the left edge of the white bracket, *dbt* expression in the liver can be observed, whereas above the right edge of the white bracket, *dbt* expression in the intestine is revealed.

Fig 5: The free amino acid profile of *que* mutants shows elevated levels of BCAAs at 96 hpf. The amino acids are referred to by their three-letter code, except for GABA. Each experiment contained a homogenate of 50 larvae. The error bars indicate standard error. (A) The free amino acid profile for wild-type larvae (n=3). (B) The free amino acid profile of *que* mutant larvae reveals a dramatic accumulation of BCAAs: isoleucine, leucine and valine. Other amino acid levels were reduced. * Significant difference from wild-type at P<0.05; ** significant difference from wild-type at P<0.01 (n=3). (C) The free amino acid profile of *beo,* a zebrafish mutant that demonstrates abnormal behavior owing to a CNS defect, indicates that abnormal behavior alone does not markedly alter free amino acid levels (n=1).

Fig 6: *que* mutants contain a reduced concentration of glutamate in the brain.(A–F) Cross-sectional views of the hindbrain of 96 hpf larvae are shown. Immunohistochemistry using antibodies against acetylated tubulin, which predominantly labels axon tracts, reveals the overall structure of the brain and demonstrates tissue penetration of the antibodies. Staining using an antibody against L-glutamate illustrates the distribution of this neurotransmitter. (A)

Labeling with the anti-acetylated tubulin reveals the axon tracts and overall structure of the hindbrain of wild-type larvae. (B) The hindbrain of wild-type larvae contains a broad distribution of L-glutamate. (C) The merged images show several L-glutamate-positive cells surrounded by anti-acetylated tubulin labeling. (D) The overall structure of the hindbrain of *que* mutants revealed by anti-acetylated tubulin appears similar to the hindbrain wild-type larvae. (E) The fluorescence intensity of labeling with the L-glutamate antibody is greatly reduced compared with wild type when imaged using the same microscope settings. However, increasing the gain of the confocal microscope shows more faint L-glutamate staining (inset). (F) The merged images show little L-glutamate staining compared with acetylated tubulin labeling. (G) The graph shows a significant reduction in L-glutamate staining intensity in *que* mutants normalized to acetylated tubulin staining. The fluorescent intensity values are the analog-to-digital converter values of the entire frame (n=5 embryos, 12 sections, $^{**}P<0.01$). Very similar results were obtained when a region of interest was selected to encompass a smaller, designated portion of the brain.

Fig 7: A working model of how mutation of *dbt* results in abnormal, accordion behavior. Similar to mammalian systems, we propose that wild-type zebrafish regulate metabolism of BCAAS via the BCKD complex. Many of these metabolic or molecular steps (black arrows) might occur in organs in the gut (such as the liver and intestine) but also the CNS. Amino acids (AA), such as

glutamine, are transported across the blood-brain barrier and used to generate glutamate, GABA and other neurotransmitters (NT). These neurotransmitters are required for coordinated nervous system output to orchestrate swimming behavior. In *que* mutants, we propose that impaired BCKD function results in the accumulation of BCAA and α-keto acids. This yields reduced retention and metabolism, and reduced transport of other amino acids (white arrows) across the blood-brain barrier, yielding diminished neurotransmitter synthesis. The abnormal levels of neurotransmitters contribute to aberrant nervous system output and abnormal, accordion behavior. It is also possible that elevated concentrations of α-keto acids directly disrupt neural circuits to cause accordion behavior.

Figure 1

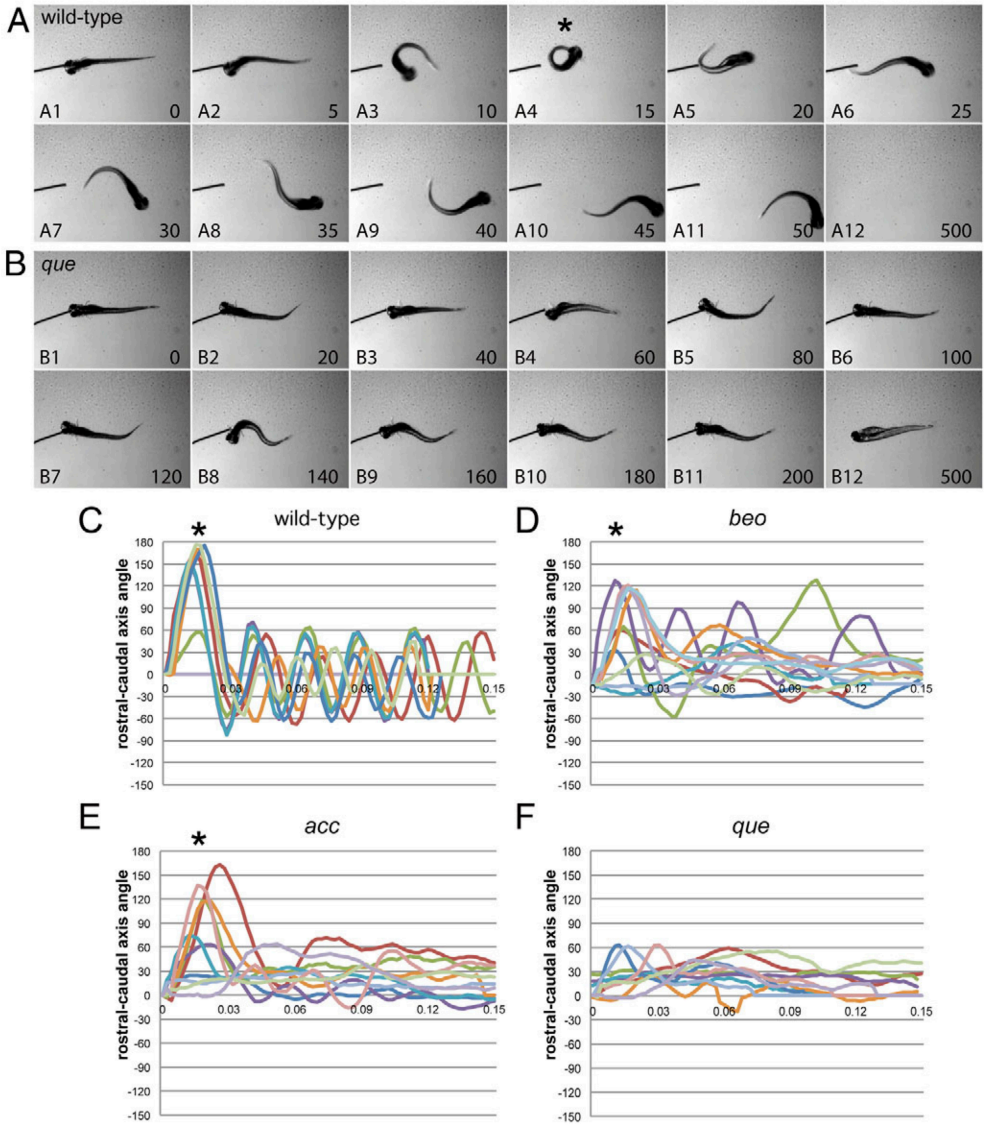
A
wild-type
A1 0
A2 5
A3 10
A4 15
A5 20
A6 25
A7 30
A8 35
A9 40
A10 45
A11 50
A12 500
B
que
B1 0
B2 20
B3 40
B4 60
B5 80
B6 100
B7 120
B8 140
B9 160
B10 180
B11 200
B12 500
C
wild-type
D
beo
E
acc
F
que
rostral-caudal axis angle
180
150
120
90
60
30
0
-30
-60
-90
-120
-150
0
0.03
0.06
0.09
0.12
0.15

Table 1

	Wild type	*que* mutants
No. of bouts	1.9±0.9	8.6±7.3*
Bout duration (msec)	329.1±60.4	285.2±148.8
No. of bursts per bout	9.5±1.9	9.7±3.6
Burst duration (msec)	13.3±2.8	12.4±1.7
Burst duty cycle (%)	30.9±11.8	39.6±6.8
Burst frequency (Hz)	31.6±4.6	37.6±9.3
Mean contralateral phase (%)	49.6±1.2	50.4±7.7
Bursting overlap (%)	6.5±6.0	19.1±11.3**

All values presented as mean ± s.d. Significant differences are indicated by *$P<0.05$ or **$P<0.01$.

Figure 2

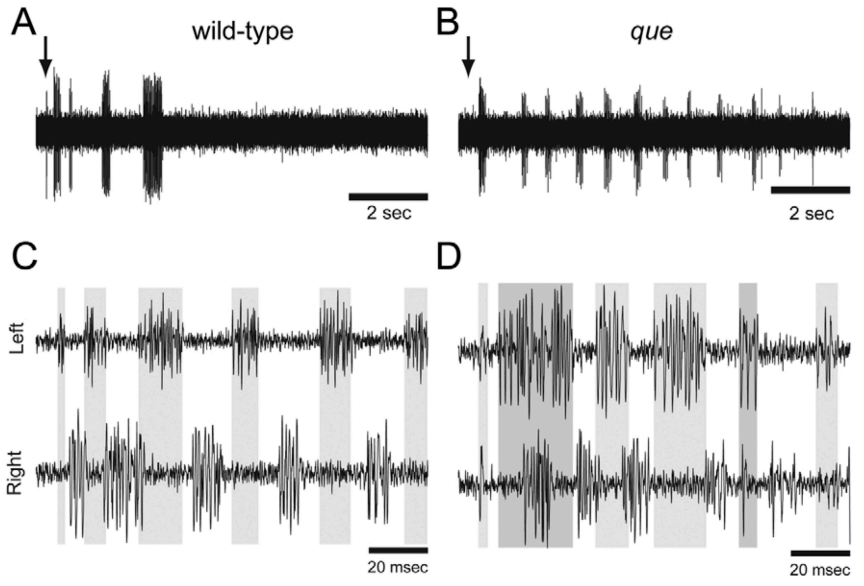

Figure 3

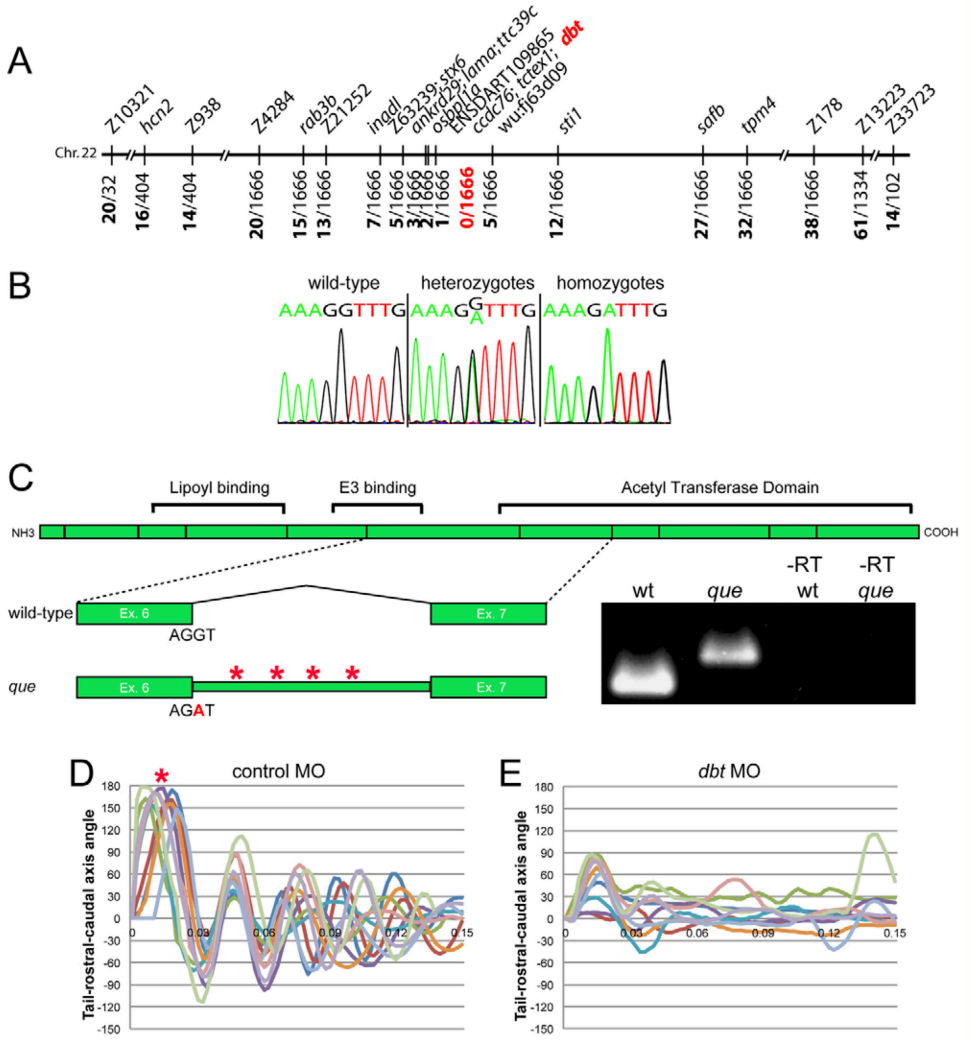
A
Z10321
hcn2
Z938
Z4284
rab3b
Z21252
ingdl
Z63239; stx6
ankrd29; lama; ttc39c
osbpl1a
ERLEC1; ART109865
ccdc76; tctex1; dbt
wu:fj63d09
sti1
safb
tpm4
Z178
Z13223
Z33723
Chr. 22
20/32
16/404
14/404
20/1666
15/1666
13/1666
7/1666
5/1666
3/1666
2/1666
1/1666
0/1666
5/1666
12/1666
27/1666
32/1666
38/1666
61/1334
14/102
B
wild-type
heterozygotes
homozygotes
AAAGGTTTG
AAAGATTTG
C
Lipoyl binding
E3 binding
Acetyl Transferase Domain
NH3
COOH
wild-type
Ex. 6
Ex. 7
AGGT
que
AGAT
wt
que
-RT wt
-RT que
D
control MO
E
dbt MO
Tail-rostral-caudal axis angle

Figure 4

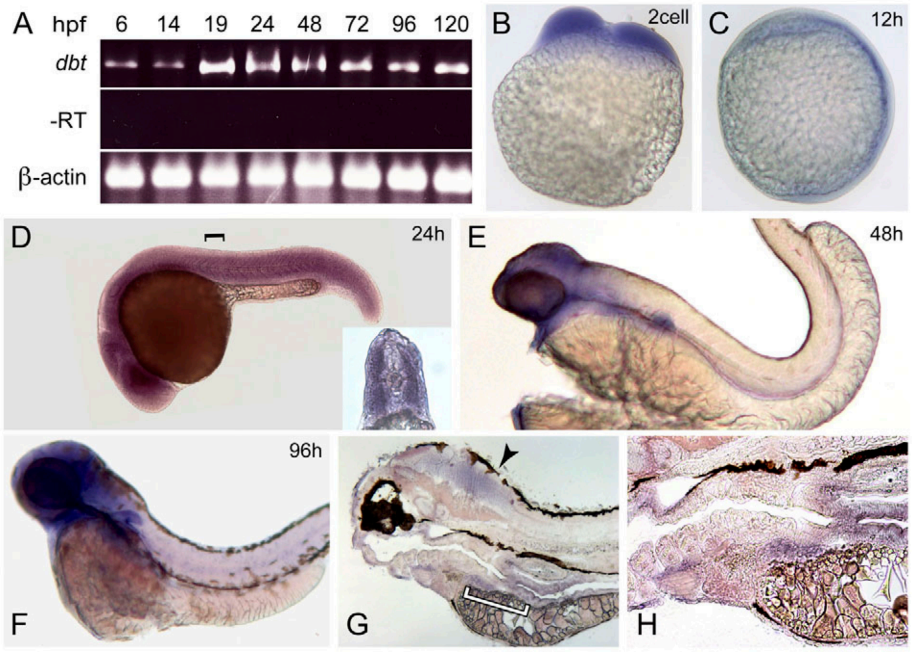
A
hpf
6
14
19
24
48
72
96
120
dbt
-RT
β-actin
B
2cell
C
12h
D
24h
E
48h
F
96h
G
H

Figure 5

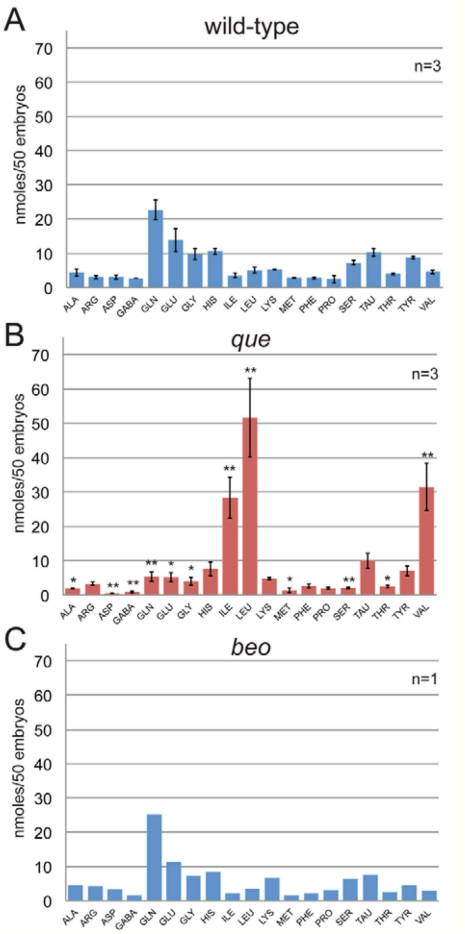
A
wild-type
n=3
nmoles/50 embryos
0
10
20
30
40
50
60
70
ALA
ARG
ASP
GABA
GLN
GLU
GLY
HIS
ILE
LEU
LYS
MET
PHE
PRO
SER
TAU
THR
TYR
VAL
B
que
n=3
nmoles/50 embryos
C
beo
n=1
nmoles/50 embryos

Figure 6

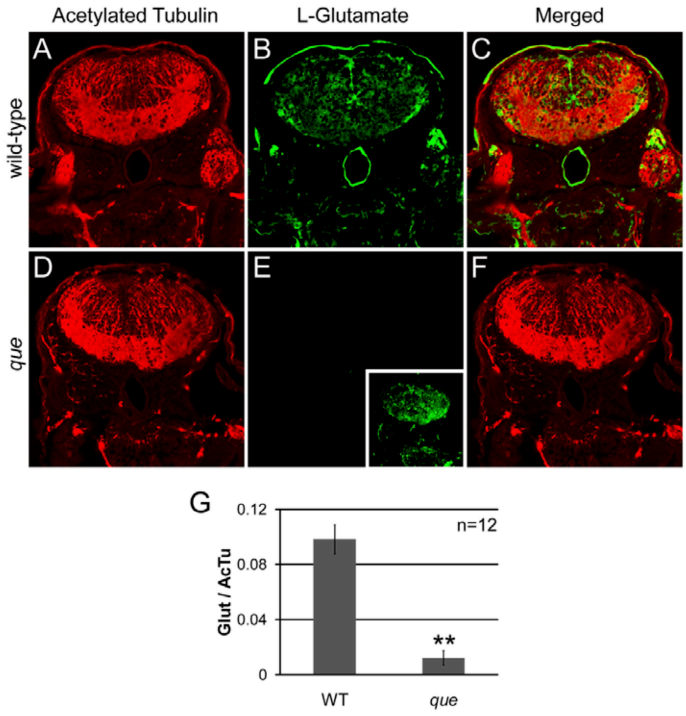
Acetylated Tubulin
L-Glutamate
Merged
A
B
C
D
E
F
wild-type
que
G
0.12
0.08
0.04
0
Glut / AcTu
n=12
**
WT
que

Figure 7

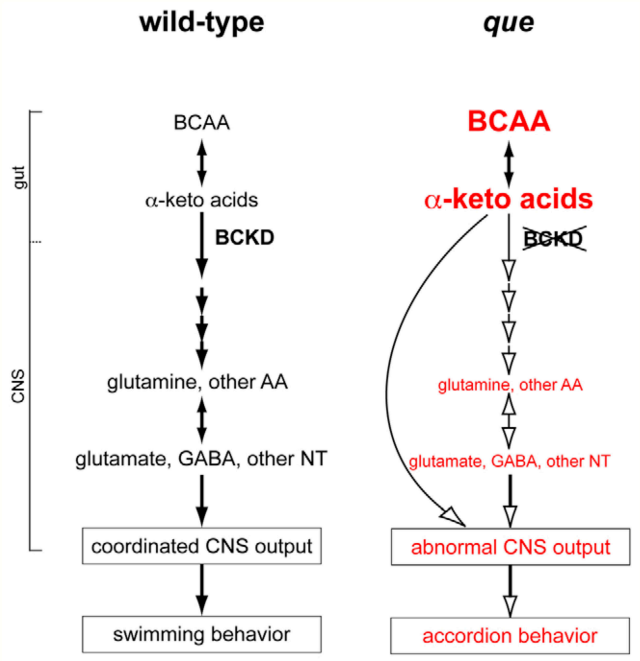
wild-type
que
gut
CNS
BCAA
α-keto acids
BCKD
glutamine, other AA
glutamate, GABA, other NT
coordinated CNS output
swimming behavior
BCAA
α-keto acids
BCKD
glutamine, other AA
glutamate, GABA, other NT
abnormal CNS output
accordion behavior

Appendix 2B: Abnormal differentiation of dopaminergic neurons in zebrafish *trpm7* mutant larvae impairs development of the motor pattern.

Summary

Transient receptor potential, melastatin-like 7 (Trpm7) is a combined ion channel and kinase implicated in the differentiation or function of many cell types. Early lethality in mice and frogs depleted of the corresponding gene impedes investigation of the functions of this protein particularly during later stages of development. By contrast, zebrafish *trpm7* mutant larvae undergo early morphogenesis normally and thus do not have this limitation. The mutant larvae are characterized by multiple defects including melanocyte cell death, transient paralysis, and an ion imbalance that leads to the development of kidney stones. Here we report a requirement for Trpm7 in differentiation or function of dopaminergic neurons in vivo. First, *trpm7* mutant larvae are hypomotile and fail to make a dopamine-dependent developmental transition in swim-bout length. Both of these deficits are partially rescued by the application of levodopa or dopamine. Second, histological analysis reveals that in *trpm7* mutants a significant fraction of dopaminergic neurons lack expression of tyrosine hydroxylase, the rate-limiting enzyme in dopamine synthesis. Third, *trpm7* mutants are unusually sensitive to the neurotoxin 1-methyl-4-phenylpyridinium, an oxidative stressor, and their motility is partially rescued by application of the

iron chelator deferoxamine, an anti-oxidant. Finally, in SH-SY5Y cells, which model aspects of human dopaminergic neurons, forced expression of a channel-dead variant of TRPM7 causes cell death. In summary, a forward genetic screen in zebrafish has revealed that both melanocytes and dopaminergic neurons depend on the ion channel Trpm7. The mechanistic underpinning of this dependence requires further investigation.

Introduction

Transient receptor potential melastatin-like 7 (TRPM7), a widely-expressed divalent-cation channel with intrinsic kinase activity, has cell-type- and context-dependent roles in cell survival and physiology. Mouse and frog embryos depleted of the *Trpm7* gene die during early morphogenesis (Jin et al., 2008; Ryazanova et al., 2010; Liu et al., 2011). Cell-lineage-specific deletion of *Trpm7* in mice indicates that Trpm7 is essential for the terminal differentiation of thymocytes and of certain neural-crest derivatives, including melanocytes and sensory neurons (Jin et al., 2008; 2012). Studies in cell lines or primary cells in vitro have suggested roles for TRPM7 in Mg^{2+} homeostasis (Nadler et al., 2001; Chubanov et al., 2004) , cell proliferation (Hanano et al., 2004), cell adhesion (Su et al., 2006), and cholinergic synaptic transmission (Krapivinsky et al., 2006). The lack of TRPM7 causes cell-death due to a disruption of magnesium homeostasis in some cell lines (Nadler et al., 2001; Kim et al., 2008). Conversely, its presence appears to sensitize at least one cell type to zinc-ion poisoning (Inoue et al., 2010), and the reduction of *TRPM7* expression in fibroblasts decreased markers of oxidative stress and increased cellular resistance to apoptotic stimuli (Chen et al., 2012b). Moreover, when extracellular levels of divalent cations drop below normal physiological levels TRPM7 permits an influx of Ca^{2+} which may contribute to excitotoxicity (Aarts et al., 2003; Wei et al., 2007; Sun et al., 2009). Supporting this model, reduction of *Trpm7* expression in the rat hippocampus

was found to lessen the amount of neuronal cell death caused by ischemia (Sun et al., 2009). In summary, studies in cell lines and limited tissue specific knock-outs in rodents indicate that the physiological role for TRPM7 is cell-type dependent.

Additional roles for Trpm7 in vertebrate development were uncovered through forward genetics in zebrafish. Independent screens for mutations that disrupt melanophore development, early motility, or adult growth each identified *trpm7* mutants (Kelsh et al., 1996; Arduini and Henion, 2004; Cornell et al., 2004; Elizondo et al., 2005; Low et al., 2011). In *trpm7* loss-of-function mutants, embryonic melanophores (the melanin-producing cells of fish) succumb to cell death (Arduini and Henion, 2004; Cornell et al., 2004), and the melanosomes (the organelles that confine melanin) are structurally abnormal (McNeill et al., 2007). Because Trpm7 is required within melanophores (Arduini and Henion, 2004; Cornell et al., 2004), the melanophore cell-death in *trpm7* mutants may result from the release of toxic intermediates of melanin synthesis into the cytoplasm (HOCHSTEIN and COHEN, 1963; Hochstein and Cohen, 2006; McNeill et al., 2007). Additionally, *trpm7* mutant larvae are unresponsive to touch for a period of about 12 h during development (Kelsh et al., 1996; Arduini and Henion, 2004; Cornell et al., 2004; Low et al., 2011). This phenotype can be alleviated by forcing the expression of *trpm7* in primary sensory neurons, implying that Trpm7 is required transiently for function or

differentiation of embryonic primary sensory neurons (Low et al., 2011). Finally, global homeostasis of divalent cations including calcium and magnesium is abnormal in *trpm7* mutant larvae leading to aberrant calcification of developing bones. This suggests a function for Trpm7 in the kidney-associated Corpuscle of Stannius where it is highly expressed (Elizondo et al., 2005; 2010). Consistent with conservation of Trpm7 function at least in some tissues, *trpm7* mutant larvae exhibit bradycardia and mice with depletion of Trpm7 in cardiac myocytes exhibit arrhythmia (Arduini and Henion, 2004; Sah et al., 2013). Analysis of zebrafish *trpm7* mutant larvae has complemented mammalian studies.

Here we report additional analyses of a zebrafish *trpm7* mutant and describe the consequences to a human dopaminergic cell-line of reducing TRPM7 activity. We identify behavioral and developmental defects in *trpm7* mutants that can be partially reversed by exogenous dopamine. Further we find abnormal gene expression, and increased sensitivity to a toxin, in dopaminergic neurons of such mutants. Dominant negative interference with TRPM7 causes death of the human dopaminergic cell line, suggesting a conserved role for TRPM7 in dopaminergic neurons. In summary, the result of a forward genetic screen in zebrafish has identified a previously unrecognized genetic requirement for Trpm7 in function and possibly survival of dopaminergic neurons.

Methods

Fish and embryo rearing. All standard animal protocols were approved by the Institutional Animal Care and Use Committee, and comply with USDA laws as well as PHS Guidelines. Zebrafish progeny and adults were reared under supervision of the University of Iowa Animal Care Unit, at 27.5 °C on a normal illumination cycle (i.e., 14 h light, 10 h dark) unless otherwise noted. Embryos were generated and handled following standard methods (Westerfield, 2007), and staged by hours post fertilization (hpf) at 28.5 °C (Kimmel et al., 1995). The highly penetrant *trpm7b508* (Elizondo et al., 2005), and *mitfaw2* (Lister et al., 1999) alleles were used for all experiments. Until the beginning of each experiment, all fish were raised in fish water (distilled water further purified by reverse osmosis and then supplemented with 0.30 g Crystal Sea® (Marinemix) (Marine Enterprises International; Baltimore, MD) per liter).

***Motility assay*.** Motility was monitored using ZebraBox and Viewpoint software (version 3,10,0,42; Viewpoint Life Sciences, Inc.; Montreal, Quebec, Canada) under infrared light. Larvae were exposed to alternating cycles of light and dark, invisible to the camera, every 30 min as described (Emran et al., 2008); each light transition took approximately 1 ms. A 96-well plates (Costar) were used for all experiments. At 4 days post fertilization (dpf), larvae were singly placed in wells with 300 µl of fish water. Larvae were placed into a 28.5 °C incubator on a normal light cycle overnight. All experiments were completed in a quiet room at 5

dpf, between 10 AM and 2 PM. Larvae were allowed to acclimate in the Zebrabox measurement apparatus for 2 h before recording began. Larval locomotion was tracked with ViewPoint software. We defined motility as tracks moving less than 10 cm/s but more than 0.1 cm/s. Location and distance traveled were recorded and binned every 5 min as presented in Fig 2.

Cultured melanocytes. The 30 hpf control embryos, defined as the wild-type and heterozygous mutant siblings of *trpm7* homozygous mutants, and *trpm7* homozygous mutant embryos (hereafter, *trpm7* mutants), identified by the strong reduction of cutaneous melanocytes, were transferred to calcium-free medium supplemented with 0.05% trypsin and 5 mM EDTA, crushed with a plastic pestle, incubated at 33 °C, and gently triturated every 10 min for 30 min. Cultures were gently spun, the supernatant discarded, and the tissue pellet resuspended in cell medium. Cells were cultured overnight at 30 °C, and electrophysiology carried out at room temperature (RT) the next morning. Cell medium, adapted from (Badakov and Jaźwińska, 2006), is DMEM (Gibco, Invitrogen, Carlsbad, CA) supplemented with 15% (v/v) fetal bovine serum (FBS; Atlanta Biologicals, Lawrenceville, GA), 100 units/ml penicillin (Gibco), 100 mg/ml streptomycin (Gibco), 1% (v/v) trout serum (Seagrow, product JJ80**,** East Coast Biologicals, North Berwick, ME), 20 ng/ml bovine insulin (Sigma, St. Louis, MO), 50 ng/ml basic fibroblast growth factor (Sigma), 62.5 µg/ml ampicillin, 25 ng/ml epidermal growth factor (Sigma), 1% embryo extract. 100% embryo extract

consists of 200 embryos at 3 dpf rinsed in 0.5% bleach for 2 min then rinsed in calcium-free Ringer's solution (defined in (Westerfield, 2007)) for 2 min; the embryos were homogenized without liquid and suspended in 1 ml of cell medium without fetal bovine serum (FBS).

Cell culture and adenoviruses. The 293-TRPM7 cell line was employed to express hemagglutinin (HA)-tagged murine TRPM7 and has been previously described (Su et al., 2006). 293-TRPM7 cells were cultured in Dulbecco's Modified Eagle Medium (D-MEM) with 10% FBS. The overexpression of HA-tagged TRPM7 in 293-TRPM7 cells was induced by the addition of tetracycline (1 μg/ml) to the growth medium for 24 h. To assess the dominant-negative potential of the TRPM7-E1047K pore mutant (TRPM7-DN), 293-TRPM7 cells were treated with tetracycline and transiently transfected with pcDNA5/FRT/TO-HA-TRPM7-E1047K, which has been previously described (Li et al., 2007a). SH-SY5Y cells were maintained in D-MEM/F-12 with 10% FBS and 5% horse serum, and were differentiated in complete medium with 10 μM retinoic acid (RA), as previously described with the following modifications (Cheung et al., 2009). SH-SY5Y cells were placed in differentiation medium for 3 days prior to viral transduction. After the recombinant adenoviruses were applied at a multiplicity of infection (M.O.I.) of 30, cells were cultured in differentiation medium for another 3 days unless otherwise specified. Cell viability was quantified by manual cell counting and trypan blue exclusion. The recombinant adenoviruses expressing LacZ and GFP have been previously described (Su et al., 2011). The

recombinant adenovirus expressing TRPM7-DN was engineered as follows. First, the AfeI/BglII fragment from pcDNA5/FRT/TO-HA-TRPM7-E1047K was exchanged with the AfeI/BglII fragment from pENTR/D-TOPO-SR-TRPM7 to create pENTR/D-TOPO-SR-TRPM7-E1047K. The SR-TRPM7-E1047K cassette was then transferred to the destination vector pAd/CMV/V5-DEST (Invitrogen) by recombination using the Gateway® system (Invitrogen) following the manufacturer's instructions. The recombinant adenoviruses expressing SR-TRPM7-DN was then made using pAd/CMV/V5-SR-TRPM7-E1047K and the ViraPower Adenoviral Expression System (Invitrogen) following the manufacturer's instructions. The TRPM7-DN recombinant adenovirus was amplified and concentrated from two 150 mm plates of HEK-293 A cells (Invitrogen) using the Adenopack 100 kit (Sartorius Stedim Biotech) following manufacturer's instructions.

Drug treatments. All drugs were purchased from Sigma-Aldrich (St. Louis, MO). Levodopa (L-dopa; 20 mM) was applied with ascorbic acid (100 μM) to delay oxidation of the former; ascorbic acid alone was applied in control experiments. L-dopa was applied in the morning at 5 dpf, and larvae were allowed to incubate for one hour before behavior recordings began. Dopamine (DA; 20 μM) was applied to both behavioral (free-swimming) and fictive preparations and had locomotor effects within 5 to 20 min, similar to the time course reported in previous studies (Thirumalai and Cline, 2008; Souza et al., 2011; Lambert et al., 2012). The effect of DA on episode duration was quantified

during 20–30 min into the drug application. MPP^+ was applied at 500 µM. It was dissolved immediately prior to application at 50 hpf, and refreshed daily. Larvae were fixed for immunohistochemistry at 5 dpf. All drugs were diluted in fish water except in the case of peripheral nerve recordings (see below), in which drugs were diluted in extracellular recording solution.

Whole-cell voltage clamp recordings. The cells were kept under continuous perfusion of standard extracellular solution containing (in mM): 135 Na-methanesulfonate (Na-$MeSO_3$), 5 CsCl, 1 $CaCl_2$ and 10 HEPES, pH 7.4 (adjusted with NaOH). A volume of 1 µM tetrodotoxin (TTX) was added to the extracellular buffer, in order to block voltage-gated Na^+ channel currents. Patch pipettes were pulled from borosilicate glass tubes (TW150F-4, World Precision Instruments, Sarasota, FL) and heat-polished at the tip to give a resistance of 3–5 mΩ when filled with the pipette solution containing (in mM): 120 Cs-$MeSO_3$, 5 CsCl, 2 $CaCl_2$, 10 EGTA and 10 HEPES, pH 7.2 (adjusted with CsOH). The free Ca^{2+} concentration in the pipette solution was calculated as 60 nM (MaxChelator, Stanford). All currents were recorded at room temperature using an Axopatch 200B patch-clamp amplifier (Molecular Devices, Sunnyvale, CA), low-pass filtered at 5 kHz and sampled at 10 kHz. All current acquisitions were made with the pClamp10 software (Molecular Devices, Sunnyvale, CA) and analyzed with Origin 7 software (OriginLab Corporation, Northampton, MA). The holding potential was −70 mV and the currents were recorded by applying a voltage-ramp from −120 mV to +100 mV for 500 ms. To determine the Trpm7 current

component, recordings were performed from cells superfused with extracellular solution containing 10 mM NH_4Cl or 10 mM $MgCl_2$ for 2 min after the first set of recordings under standard extracellular conditions.

Whole-cell voltage clamp recordings of TRPM7 currents in 293-TRPM7 cells were elicited by voltage stimuli lasting 250 ms delivered every second using voltage ramps from −120 mV to +100 mV. Data were digitized at 2 kHz and digitally filtered at 1 kHz. The internal pipette solution for macroscopic current recordings contained (in mM) 145 Cs-methanesulfonate, 8 NaCl, 10 EGTA, and 10 4-(2-hydroxyethyl)-1-piperzineethanesulfonic acid (HEPES), pH adjusted to 7.2 with CsOH. The extracellular solution for whole-cell recordings contained (in mM) 140 NaCl, 5 KCl, 2 $CaCl_2$, 20 HEPES, and 10 glucose, pH adjusted to 7.4 with NaOH.

Peripheral nerve recordings. Fictive swimming was assessed via peripheral nerve recordings in vivo as described previously (Masino and Fetcho, 2005). Briefly, control and *trpm7* mutants were anesthetized with 0.02% Tricaine-S (Western Chemical) in extracellular recording solution (Lambert et al., 2012) and paralyzed with 0.1% (w/v) α-Bungarotoxin (Sigma). Larvae were pinned in a lateral position to a Sylgard-lined petri dish and the skin was removed. Subsequently, larvae were transferred to the stage of an Olympus BX51 WI microscope and extracellular recording solution was superfused continuously at 1 ml/min at room temperature. Extracellular suction electrode recording

techniques (Masino and Fetcho, 2005) were used to monitor the activity of peripheral nerves during fictive behavior; the tip of the extracellular suction electrode (6–15 μm tip diameter) was positioned near the dorsoventral midline of an intermyotomal cleft where the skin had been removed. Spontaneous activity was acquired for a minimum of 30 min for each preparation and, for experiments in which DA was applied, samples were subsequently perfused with 20 μM DA in extracellular recording solution. All recordings were between body segments 10 and 20. A MultiClamp 700B (Molecular Devices, Sunnyvale, CA) amplifier was used to monitor extracellular voltage in current-clamp mode at a gain of 2,000 (***Rf***=50 MΩ), with the low- and high-frequency cut-off at 300 and 1000 Hz, respectively. Recordings were sampled at 10 kHz, digitized using a digitizing board (DigiData series 1440A, Molecular Devices, Sunnyvale, CA) and acquired using pClamp 10 software. Analysis of peripheral nerve activity was performed as described previously (Lambert et al., 2012; Wiggin et al., 2012), using custom scripts written in MATLAB (Mathworks, Natick MA). Briefly, the occurrence times of rhythmic fictive locomotor bursts were determined from a rectified and smoothed version of the voltage recording. These bursts were then grouped into episodes and used to determine the episode durations for each voltage trace. Values for fictive episode durations are expressed as mean±SEM (standard error of the mean).

Electroretinogram recordings. Electroretinograms (ERGs) were recorded as described previously (Lewis et al., 2011). Briefly, 6 dpf larvae were anesthetized

in 0.02% Tricaine-S, and eyes were removed using a fine tungsten wire loop. Excised eyes were then placed in an oxygenated Ringer's solution (in mM; 130 NaCl, 2.5 KCl, 20 $NaHCO_3$, 0.7 $CaCl_2$, 1.0 $MgCl_2$, and 20 glucose), and a glass electrode was positioned directly onto the cornea. After 3 min of dark adaptation, eyes were exposed to white light flashes in the presence or absence of background light, and their electrical responses were recorded. Data were acquired and processed as described previously (Van Epps et al., 2001). Peak values are listed as the mean±SD (standard deviation) from at least three animals.

Free-swimming assay. Video acquisition and analysis were performed as described previously (Lambert et al., 2012). Briefly, a group of 10 larvae in embryo medium or embryo medium containing 20 μM DA was placed in a 50 mm watch glass (Fisher Scientific) atop a transmitted light stage (Schott TLS and MC-1500 LED Controller). The larvae were allowed to acclimate to the recording arena for 5 min prior to the start of video recording. Subsequently, spontaneous free-swimming was recorded for 10 min at 60 frames per second, using a digital CMOS camera (Point Grey, Firefly M) with an attached 50 mm macro lens (Sigma Corporation, Ronkonkoma, NY). Videos were acquired with Fview (open-source software; (Straw et al., 2011)), in uncompressed Fly Movie Format (FMF). The FMF files generated by Fview were imported into the California Institute of Technology Fly Tracker (Ctrax) (open-source software; (Branson et al., 2009)) to obtain independent trajectories of each target within the arena. We subsequently

used the open-source Fix Errors MATLAB Toolbox, provided by the creators of Ctrax (Branson et al., 2009)), to identify and fix tracking errors (such as swapping of target identities). The total number of errors per 10-min video was 4.49±0.55 (***n***=23 videos) and all errors were corrected via the FEMT. Subsequently, scripts from the open-source Behavioral Microarray MATLAB Toolbox, provided by the creators of Ctrax (Branson et al., 2009), were implemented to compute descriptive statistics of a suite of behavioral parameters for each of the individual targets from the fixed Ctrax trajectories. The target speed function, velmag, was extracted for each target and custom scripts were written to define and detect swimming episodes using the same criteria as employed previously (Lambert et al., 2012), namely: signal threshold of 1.5 mm/s, minimum episode duration of 66.6 ms (4 frames), minimum average swimming speed of 3 mm/s, and concatenation of signals within a 300 ms (18 frame) inter-signal interval. Identical filters were applied for all videos across all ages and experimental groups. Once all swimming episodes were identified, we quantified the total distance traveled per individual in centimeters (sum of instantaneous speeds during swimming episodes divided by the frame rate) and mean swimming episode duration per individual in milliseconds (mean duration from the onset to the offset of each individual episode) over the 10-min recording period. Sample sizes were ultimately smaller for quantifying episode duration compared with total distance traveled because episode duration could not be obtained from animals that did not move during the recording session.

Histology. Larvae were fixed in 4% paraformaldehyde overnight at 4 °C. Whole-mount larvae were washed out of fixative with double-distilled water (ddH_2O), permeabilized by either 5 h incubation at room temperature in ddH_2O or 30 min treatment with 40 mg/ml ProtK, blocked in PBDT (Phosphate buffered solution, 2.5% Goat serum, 1% bovine serum albumin, 1% DMSO, 0.5% Tritonx-100) for 1 h, and incubated in primary antibody [mouse anti-tyrosine hydroxylase (1:500, Sigma-Aldrich) or rabbit anti-5HT] diluted in PBDT overnight at 4 °C. In experiments where we used the peroxidase anti-peroxidase system (Jackson Immunoresearch Laboratories, West Grove, PA), we subsequently incubated embryos in 2° goat anti-mouse antibodies and 3° mPAP antibody. Samples were incubated in 1% hydrogen peroxide for 30 min in between application of the 2° and 3° antibodies, and then developed using 3-3′-diaminobenzidene (DAB, Sigma Aldrich). Whole-mount larvae were alternatively prepared using Alexa 488 conjugated secondary antibodies and optically sectioned using a Zeiss 700 confocal microscope and ZEN 2010 software (Carl Zeiss Inc., Germany). Optical sections were compressed into single images by projecting the maximum intensity signal of each pixel of each section using ImageJ (National Institutes of Health) for approximately 500×500×150 µm (width x height×depth) at a resolution of 1.087 pixels per µm. In situ hybridization for *th2*and *dat* were carried out as described (Sallinen et al., 2010).

Reverse transcriptase-polymerase chain reaction (RT-PCR). Whole-animal mRNA was isolated at 5 dpf using Trizol (Invitrogen), from which cDNA was synthesized using oligo-dT(16) primers and the cDNA SuperScript cDNA synthesis kit (Qiagen). MMLV enzyme (Promega) was used for the reverse transcriptase reaction. Quantities of mRNA were calculated relative to levels of *beta-actin*. Primers for *beta-actin* forward 5′-gagatgatgcccctcgtg-3′ reverse 5′-gctcaatggggtatttgagg-3′; *th1* primers forward 5′-catatgtgacccgcatcaag-3′ reverse 5′-caacacattcagggcatctg-3′; *th2* primers forward 5′-agcttcgtgtttgaggagga-3′ reverse 5′-ctctttctgctcgctcgact-3′;*dat* primers forward 5′-agacatctgggaaggtggtg-3′ reverse 5′-tgtagctggagaaggcgatt-3′; *bdnf* primers forward 5′-tggcggcatccaggtagt-3′ reverse 5′-tcgaaggacgttgacctgtatg-3′.

Statistics. Levene's test for equality of variances was used to test assumptions about error variances for Student's ***t***-test. For experiments that involved comparisons of two means, one-tailed Student's *t*-tests were performed when error variances were equal. Significance was determined at the $p<0.05$ level. A Welch *t*-test was used instead when error variances were unequal. Multiple comparisons of means were made using two-way analysis of variance and Bonferroni post-hoc tests. SPSS Statistics (IBM version 19 was used for all above tests. A χ^2 test was conducted assuming Mendelian ratios of inheritance and 3 degrees of freedom, using Microsoft Excel.

Calcification assays. Kidney stones were visualized as previously described (Elizondo et al., 2005). Briefly, live larvae were submerged in 0.004% alizarin red in Ringer's solution overnight. They were washed 2× in Ringer's solution before visualizing live under Texas Red filter.

Results

Sequence analysis of *trpm7* cDNA generated from *trpm7b508* mutants indicated that the encoded TRPM7 protein is truncated in the cytoplasmic carboxy terminus upstream of the kinase domain; however it did not clarify whether this variant retains channel function (Elizondo et al., 2005)**.** Application of a voltage ramp to melanocytes isolated from wild-type embryos at 48 h post fertilization (hpf) produced currents characteristic of those mediated by TRPM7 (Fig 1A). Subjecting rare surviving melanocytes isolated from 48 hpf *trpm7* mutants to the same procedure revealed that these produce virtually no such current (Fig 1B). These findings suggest that, in vivo, *trpm7b508* encodes a Trpm7 protein that either lacks channel function or fails to reach the plasma membrane. They are consistent with conclusions derived from forced expression of *trpm7b508* in Xenopus oocytes (Low et al., 2011).

Because an allele of *TRPM7* was reported to be associated with a parkinsonian condition (Hermosura et al., 2005), we observed motility in zebrafish *trpm7* mutant larvae at 5 days post fertilization (dpf). We monitored motility in larvae in alternating 30-min periods of light and dark because the light-to-dark transition strongly stimulates swimming (Burgess and Granato, 2007b; Emran et al., 2008). In dark periods and in light periods, *trpm7* homozygous mutants traveled a shorter distance than their siblings (wild-types and

heterozygous mutants; hereafter, control larvae) (Fig 2, statistical analysis in the figure legend). In both mutants and control larvae, motility was lower in light periods than in dark periods; in light periods mutants were virtually still. To test whether a deficit in dopaminergic signaling causes hypomotility in *trpm7* mutants, we treated *trpm7* mutants and control larvae with levodopa (L-dopa), a precursor of dopamine (DA), and assayed their motility. In dark periods, L-dopa-treated mutants moved significantly more than vehicle-treated mutants, while L-dopa treatment did not affect the motility of control larvae (Fig 2). The effectiveness of the light-to-dark stimulus depends on intact visual processing and on non-visual light sensors (Emran et al., 2008; Fernandes et al., 2012). To test whether vision is grossly affected in *trpm7* mutants we subjected larvae to micro-electroretinography. We found that beta waves were indistinguishable between mutants and control larvae (Fig S1). We conclude that hypomotility of the mutants is unlikely to be caused by abnormal vision or other gross defects. The simplest explanation of these observations is that hypomotility in *trpm7* larvae is at least partly the result of sub-threshold dopaminergic signaling in the central nervous system.

To test the possibility that dopaminergic signaling is lower than normal in *trpm7* mutants, we examined a developmental milestone in zebrafish that depends on intact dopaminergic signaling. Between 3 and 4 dpf, wild-type zebrafish larvae undergo a developmental switch in their locomotor pattern,

transitioning from long to short swimming episodes (Buss and Drapeau, 2001; Lambert et al., 2012). The latter pattern persists into adulthood (Fuiman and Webb, 1988; Muller et al., 2000). This developmental switch is mediated by central dopaminergic signaling, which originates in the caudal diencephalon and acts in the spinal cord via the diencephalospinal tract (Lambert et al., 2012). Using videography, we measured swimming speed and episode duration before (3 dpf) (Fig S2) and after (5–6 dpf) (Fig 3A, top) the developmental switch. In addition to these behavioral parameters, we measured the duration of fictive swimming episodes by carrying out extracellular recording of peripheral nerve activity (Fig 3A, bottom). At 3 dpf, there was no difference in episode duration between *trpm7* controls and mutants, regardless of whether examined in the behavioral or fictive swimming preparations (Fig S2). However, at 5–6 dpf, the durations of behavioral and fictive episodes in *trpm7* mutants were significantly longer than those of controls (Fig 3A and B), indicating that the mutants did not properly execute the stereotypic switch from long to short episodes. By contrast, in 5–6 dpf *trpm7* mutants treated with 20 μM exogenous DA, the episode duration during both the behavioral and fictive assays was significantly shorter than in untreated *trpm7* mutants, but not different from that in controls (Fig 3A and B). Because the long-episode behavioral phenotype of *trpm7* mutants is recapitulated in the fictive swimming preparation, and because the exogenous application of DA is sufficient to rescue the developmentally appropriate locomotor pattern, we conclude that this phenotype is not caused by a deficit in

muscle or body morphology but rather by to a lack of central dopaminergic signaling (Lambert et al., 2012).

We next used histology to determine if dopaminergic neurons and other neuronal sub-types are present in*trpm7* mutants. Tyrosine hydroxylase is the rate-limiting enzyme in dopamine synthesis. There are two orthologs of *tyrosine hydroxylase* in zebrafish, Th1 and Th2 (Holzschuh et al., 2001; Chen et al., 2009; Filippi et al., 2010; Yamamoto et al., 2010). There is recent evidence that Th2 contributes to serotonin synthesis in larvae (Ren et al., 2013), although in some cells Th2 is detected together with DA in the absence of Th1, implying it contributes to dopamine synthesis (Yamamoto et al., 2011). Clusters of anti-Th1 immunoreactive (IR) cells (Th1 IR cells, hereafter) are present in several discrete clusters within the brains of 5-dpf zebrafish larvae (Fig 4M; the labeling scheme used here (Sallinen et al., 2009) is compared to an alternative scheme (Rink and Wullimann, 2002) in Table S1). The number of Th1 IR cells in all of these clusters appeared grossly reduced in mutants in comparison to controls. To quantify this effect, we focused on a cluster in the pretectum (group 7), which is well-separated from the other clusters, and on a cluster in the periventricular hypothalamus (group 13), because neurons here exhibit a high level of immunoreactivity and are less densely packed than elsewhere. We found that the number of Th1 IR cells in both clusters trended lower in *trpm7* mutants than in control larvae; this difference reached significance in the pretectum (Fig 4A, B).

The number of cells expressing *th2*, which are found only in a preoptic cluster (group 3b), a diencephalic cluster (group 8b), and a posterior paraventricular organ cluster (group 10b), was also clearly reduced in *trpm7* mutants compared to controls (Fig 4K and L). The reduction in the number of *th1*- and *th2*-expressing cells was mirrored by a reduction of the total amount of *th1* and *th2*mRNA in mutants with respect to siblings, as monitored by qRT-PCR (Fig 5H). In contrast to expression of*th* paralogs, expression of *dopamine transporter* (*dat*), a second marker of dopaminergic neurons, appeared grossly equivalent in *trpm7* mutants and controls (Fig 5E and F). Confirming this impression, we found the number of cells expressing GFP in the *Tg*(*dat*:*gfp*) transgenic line (Xi et al., 2011) was not significantly different in *trpm7* mutants relative to control larvae (Fig 5C and D). The number of sensory neurons in the dorsal root ganglia and the number of serotoninergic neurons in the pretectum, recognized by anti-Hu and anti-5-hydroxytryptophan (5HT) immunoreactivity, respectively, were equivalent in mutants and controls (Fig 5G and legend to Fig 5). We also found no difference between message levels of *brain derived neurotrophic factor* (*bdnf*), a gene expressed in many regions of the brain (Fig 5H). These findings indicate that, in contrast to embryonic melanophores, which undergo cell death, dopaminergic neurons and other categories of neurons examined are present in normal numbers in *trpm7* mutants. However, abnormally low expression of *th* paralogs in such mutants indicates faulty differentiation or

physiology of dopaminergic neurons and possibly a subset of serotoninergic neurons (i.e., those expressing Th2).

Embryonic melanophores in *trpm7* mutants are poisoned by the oxidative intermediates of melanin synthesis (McNeill et al., 2007), and such intermediates are related to dopamine; therefore we reasoned that dopaminergic neurons in *trpm7* mutants may similarly experience elevated levels of oxidative stress. In this case they may be hypersensitive to oxidative stressors. The neurotoxin 1-methyl-4-phenylpyridinium ion (MPP^+) is transported by the dopamine transporter into neurons, where it interferes with complex I of the mitochondrial electron transport chain, depleting the cell of ATP and elevating levels of reactive oxygen species (ROS) (reviewed in (Segura Aguilar and Kostrzewa, 2004). We examined Th1 IR neurons in control and *trpm7* mutant larvae treated chronically with MPP^+. In control larvae, this treatment caused a 15% reduction (relative to untreated larvae) in the number of Th1 IR cells in the pretectal area, whereas in *trpm7* mutants it caused a 50% reduction (relative to untreated *trpm7* mutants) (Fig 4A–D, I). The increased sensitivity of *trpm7* mutants to the effects of MPP^+ was also apparent in the hypothalamus (Fig 4E–H, J). In principle, abnormally high levels of *dat* expression might explain the elevated sensitivity to MPP^+, but we found that the *dat* levels in mutants and siblings are comparable (as measured by qRT-PCR,Fig 5H). Instead, the increased sensitivity

of *trpm7* mutants versus control larvae to MPP^+ implies that the absence of Trpm7 elevates oxidative stress in DA neurons.

We next asked whether treatments that protect DA neurons from MPP^+ similarly protect them from the absence of Trpm7. Deferoxamine (DFO) chelates iron and thereby inhibits the iron-catalyzed conversion of hydrogen peroxide to the more highly reactive hydroxyl ion (Menasche et al., 1987). DFO protects against degeneration of dopaminergic neurons induced by 6-hydroxydopamine (6-OHDA) or MPTP (the MPP^+precursor) in animal models (Ben-Shachar et al., 1992; Lan and Jiang, 1997). We treated *trpm7*mutants and controls chronically with DFO and measured their motility. Mutants treated with DFO moved significantly more than untreated mutants (Fig 6), whereas control siblings were not affected by DFO treatment. DFO treatment did not have a detectable effect on the number of Th1 IR cells or on the quality of melanocytes in *trpm7* mutants (data not shown). Of note, treatment of *trpm7* mutant larvae with DFO, similar to their treatment with L-dopa, increased motility after the dark-to-light transition, but not after the light-to-dark transition. This suggests that DFO treatment partially rescues the function of dopaminergic neurons in *trpm7* mutants, and therefore that the defect in such neurons caused by the absence of Trpm7 is similar to that induced by 6-OHDA or MPTP treatment.

Because parkinsonian features can result from the calcification of basal ganglia (Koller et al., 1979), we considered the possibility that the effects of Trpm7 on dopaminergic neurons may be indirect. As previously reported (Elizondo et al., 2010), *trpm7* mutant embryos had significantly more kidney stones than controls. However we did not detect calcification in the brains of either genotype. We also found no correlation between average distance moved in the light-dark analysis and the presence of kidney stones (Pearson correlation coefficient of 0.015, n=43, two-tailed p=0.51). These findings support the possibility that Trpm7 is required within dopaminergic neurons in zebrafish larvae, although this remains to be tested experimentally.

Because of distinct phenotypes in zebrafish and mouse *Trpm7* loss-of-function mutants, it is unknown whether there is requirement for TRPM7 within mammalian dopaminergic neurons. SH-SY5Y is a dopaminergic, neuroblastoma-derived cell line that can be induced to differentiate in vitro (Encinas et al., 2000). We infected SH-SY5Y cells with adenovirus encoding the TRPM7-E1047K channel-pore mutant form of TRPM7 (TRPM7-DN), or with a control adenovirus expressing LacZ. Electrophysiological recordings in HEK-293 cells confirmed our expectation that TRPM7- E1047K acts in dominant-negative fashion, suppressing wild-type TRPM7 currents (Fig 7A and B). In comparison to non-transduced and LacZ-expressing SH-SY5Y cells, TRPM7-DN-expressing counterparts underwent cell death at an elevated rate, whether or not they were

induced to differentiate (Fig 7C and D). Treatment with DFO did not alleviate the toxicity of TRPM7-DN (Fig S3). These findings suggest that survival of a human dopaminergic cell-line requires TRPM7 in a cell-autonomous fashion.

Discussion

The zebrafish *trpm7* mutant provides an unusual opportunity to explore the roles for Trpm7 in cell differentiation and physiology at stages of development later than gastrulation, the stage when mice and frogs depleted of Trpm7 die. Here we have presented several pieces of evidence that in zebrafish *trpm7*loss-of-function mutants there is defective function of dopaminergic neurons leading to behavioral phenotypes. First, motility in *trpm7* mutant larvae in the dark can be elevated by a concentration of L-dopa that has no effect on sibling larvae. Tonic application of L-dopa probably poorly mimics endogenous dopamine (DA) signaling and may have indirect compensatory effects on Trpm7-dependent neuronal populations controlling motility. Nonetheless, these findings suggest that within *trpm7* mutants there is a defect in the production or release of DA while other elements of DA signaling relevant to motility remain intact. Second, the observation that *trpm7* mutants do not undergo the stereotypic, DA-dependent developmental switch from long to short swimming episodes but will do so if provided with exogenous DA also suggests there lower-than-normal levels of dopaminergic signaling in *trpm7* mutants. It also implies that the signaling mechanisms and neural circuits that result in DA-mediated shortening of swimming episodes, which were previously shown to be separable from those that set motility levels (Lambert et al., 2012), function properly. Third, the numbers of expressing *th1*-expressing and *th2*-expressing neurons are modestly

but significantly reduced in *trpm7* mutant larvae in comparison to sibling larvae. A concomitant reduction in DA production in the brain may account for motility defects in mutants. We conducted an HPLC analysis of biogenic amines in whole embryo lysates but, because of confounding effects of melanocytes, it was not sensitive enough to detect changes in levels of biogenic amines of the magnitude as changes in *th*expression (data not shown). A similar analysis of isolated brains may suffice to do so. Alternatively, the cause of lower-than-normal dopaminergic signaling in Trpm7 mutants may be other than reduced DA production; for instance there may be a defect in evacuation of DA from synaptic vesicles, as has been proposed in cholinergic vesicles (Krapivinsky et al., 2006; Brauchi et al., 2008). Because motility of*trpm7* mutants after a dark-to-light transition is not measurably restored by L-dopa treatment, there may be separate contributions of Trpm7 to motility other than its role in development or function of DA neurons. There is a recent report that Th2 has tryptophan hydroxylase activity (Ren et al., 2013). While the number of neurons that are immunoreactive for 5HT appears to be normal in Trpm7 mutant larvae, we cannot rule out a role for Trpm7 in function of serotonergic neurons. In summary, the physiological role of Trpm7 in motility of 5 dpf zebrafish larvae in dark periods is largely explained by a direct or indirect requirement for Trpm7 in dopaminergic neurons, while its role in motility in the light phase remains unexplained.

The mechanistic underpinnings of the defect in the DA neurons in *trpm7* mutants remain unclear. However, two observations suggest that in DA neurons, as in melanocytes but in contrast to in other cell types (Chen et al., 2012b), loss of Trpm7 elevates oxidative stress. First, *trpm7* mutants are unusually sensitive to treatment with MPP^+, a toxin that raises levels of reactive oxygen species and that prevents the differentiation of, and may kill, dopaminergic neurons in zebrafish (Burns et al., 1983; Sallinen et al., 2010). Second, mutants treated with DFO, an iron chelator and anti-oxidant that halts the Fenton reaction, were more motile than untreated animals. How might the loss of Trpm7 lead to increased oxidative stress in dopaminergic neurons in vivo? The primary defect may be a disruption of cellular magnesium homeostasis, as organismal magnesium levels are abnormal in zebrafish *trpm7* mutants (Elizondo et al., 2010), and there is some evidence connecting abnormal cellular magnesium homeostasis and risk for Parkinson's disease (see references in (Kolisek et al., 2013)). In zebrafish *trpm7*mutants, melanocytes have abnormally shaped melanosomes and undergo cell death that is rescued by inhibition of tyrosinase (McNeill et al., 2007). Perhaps in the absence of Trpm7 the integrity of dopaminergic vesicles is also compromised, and the toxic molecule dopamine is released into the cytoplasm. How Trpm7 affects the integrity of these vesicles is unknown, but it is noteworthy that calcium channel blockers can cause a loss of the ATP-dependent proton gradient in catecholaminergic vesicles, reduce DA content, and can promote cell death among dopaminergic neurons (Terland and Flatmark,

1999). In summary, a plausible model that warrants further testing is that in the absence of Trpm7, defective cation homeostasis leads to elevated oxidative stress which disrupts function, differentiation, and survival of dopaminergic neurons.

While there is no clear link between TRPM7 and any human disorder, the mechanisms by which DA neurons are compromised in the zebrafish *trpm7* mutants may be relevant to clinical conditions. Amyotrophic lateral sclerosis/parkinsonian dementia complex (ALS/PDC) is a disease to which epidemiologists have long ascribed an environmental cause (Banack and Cox, 2003). A variant of TRPM7 with increased sensitivity to inhibition by magnesium was found to be over-represented in families with ALS/PDC in Guam (Hermosura et al., 2005) but not in the Kii peninsula of Japan (Hara et al., 2010). Evidence of a role for this ion channel in function and maintenance of dopaminergic neurons presented here supports further investigation into the possibility that mutations in *TRPM7* predispose individuals to ALS/PDC. Indeed, zebrafish *trpm7* mutants may serve as a model for the gene-environment interaction underlying ALS/PDC. Also, there is an association between risks for Parkinson's disease and metastatic melanoma (Pan et al., 2011; Su et al., 2011). This association has been proposed to result from failure of a mechanism used to contain quinone-related toxins in both dopaminergic neurons and melanocytes (Herrero Hernández, 2009); TRPM7 may contribute to such a mechanism. Finally, stem

cell-based therapies have the potential to restore the damage caused by neurodegenerative diseases. Such therapies require a clear understanding of the mechanisms that govern the differentiation and survival of dopaminergic neurons, including the role of TRPM7 in these processes (Hegarty et al., 2013).

Figure Legends

Fig 1. The TRPM7-like current is dramatically reduced in *trpm7b508* mutants. Representative whole-cell current recordings of melanophores isolated at 32 hpf, in (A) control or (B) *trpm7* mutant embryos, in response to voltage ramps from −100 mV to +100 mV for 500 ms. (A) Control melanocytes exhibited outwardly rectifying currents that are potentiated by the extracellular application of 10 mM NH_4Cl, and inhibited by the application of 10 mM $MgCl_2$, properties that are characteristic of TRPM7-mediated currents. (B) The mutant melanophores did not exhibit any TRPM7-like outwardly rectifying currents. The slight outward rectification of currents in mutant melanophores indicates that the cells were alive. Control, *n*=7 cells; mutant, *n*=3 cells.

Fig 2. The hypomotility of *trpm7* mutants is levodopa responsive. Bar chart showing results of automated analysis of motility was carried out during daytime, over one cycle of 30 min exposure to light (white horizontal bar) followed by 30 min of darkness (black horizontal bar). Vertical bars indicate average distance moved during 5 min intervals. The average movement of mutants over the hour was significantly lower than that of controls (Welch *t*-test, $p<0.001$). For each experiment, half of a single clutch of larvae from*trpm7* heterozygous adults was treated with 30 μM L-dopa for 3 h before recording. The motility of *trpm7* mutants was significantly increased by L-dopa treatment during the first 10 min after the

light-to-dark shift (Student's *t*-test, p=0.004 and Welch *t*-test,p=0.017 for the first and second 5 min intervals after the light-to-dark transition, respectively). By contrast, control larvae were unaffected by L-dopa (Student's *t*-test, p=0.097 and p=0.070 for the first and second 5 min intervals after the light-to-dark transition, respectively). Each group tested consisted of 22–24 animals. Error bars represent SEM in one single hr. Asterisks, values significantly different.

Fig 3. Dopamine rescues behavioral and fictive locomotor patterns of the *trpm7* mutant. (A) (Top row) Representative recordings of speed and (bottom row) extracellular peripheral nerve recordings in fictive swimming preparations for discrete swimming episodes of 5–6 dpf control siblings (left), *trpm7* mutants (middle), and *trpm7* mutants+DA (20 μM; right). Grey bars below x-axes of speed plots represent episode durations whose beginnings and ends are defined by the filter settings. (B) Summary plot of the mean durations of behavioral and fictive swimming episodes for each group. Asterisks indicate significant difference; $^{***}p$<0.001. Numbers at the base of bars in graph denote number of larvae observed for each experimental group. Error bars represent SEM.

Fig 4. *trpm7* mutants are sensitized to MPP^+. (A–H) Dorsal views of 5-dpf larvae of the indicated genotype, treated with 500 μm MPP^+ or vehicle control as indicated. Individual panels show distinct groups of Th1 IR cells in the following

brain regions: (A–D) pretectal diencephalon (group 7); (E–H) periventricular hypothalamus (group 13); and I and J) bar chart showing average numbers of Th1 IR-positive cells in each group (*n*=11 animals scored). In the untreated samples, the number of Th1 IR cells was significantly lower in mutants than controls in group 7 (control avg. +/- SEM: 44 +/- 2, mutant: 36 +/- 2; Two way ANOVA with Bonferroni post-hoc test,*p*<0.001).. In group 13, (control: 56 +/- 1, mutant: 51 +/- 2) there was not a significant difference in the number of Th1 IR cells between untreated controls and untreated mutants. In both groups, MPP^+ treatment effected a larger reduction in the number of Th1 IR cells in mutants than in controls (group 7, control+MPP^+: 39 +/- 2, mutant+MPP^+: 17 +/- 2; group 13, control+MPP^+: 53 +/- 2, mutant+MPP^+: 37 +/- 3). In group 7 the effect of MPP^+ in mutants was almost three times larger than in controls, and in group 13 it was over four times larger; in both groups, mutants were significantly more sensitive to MPP+ treatment than controls (*p*<0.001). (K and L) Dorsal views of dissected brains from (K) control or (L) *trpm7* mutant larvae, processed to reveal *th2* mRNA. The pre-optic area (group 3b) is outlined in white. (*th2*-positive cells: control: 14 +/- 1, *n*=9; mutant: 7 +/- 5, *n*=12; *p*<0.001). Scale bar in A=50 μm, applies to A-H. Scale bar in K, =100 μm, applies to K,L. (M) Schematic illustrating the numbering scheme of Th1 and *th2* positive (outlined in black) neuron clusters where darkness indicates more ventral groups (1 olfactory bulb; 2 subpallium; 3–4 preoptic area; 5,6,11 diencephalon; 7 pretectum; 8 anterior paraventricular organ; 9 interior paraventricular organ; 10 posterior

paraventricular organ; 12 posterior tuberal nucleus; 13 hypothalamus; 14 locus coeruleus; 15-16 medulla oblongata; 17 area postrema; see Table S1 for additional details) (modified from (Sallinen et al., 2009)).

Fig 5. Numbers of serotonergic neurons and neurons expressing *dat* are normal in *trpm7* mutants. (A,B; A′,B′) Dorsal views of the (A and B) pre-tectum (Th1 group 7) and (A′ and B′) hypothalamus (Th1 group 13) in 5 dpf control and *trpm7* mutant larvae, as indicated, processed to reveal anti-5HT (red) and anti-Th1 (green) immunoreactivity (IR). Th1 IR cells were reduced in mutants (quantified inFig 4), 5HT IR cells were normal in number (below). Scale bar in *A*=30 μm and applies to A–D; scale bar in *A′*=50 μm and applies to A′–B′ and E, F. (C and D) Dorsal views of 5 dpf *Tg*(*dat*:*gfp*) larvae focused on the pretectum (group 7). GFP-expressing neurons were equally abundant in *trpm7* mutants and controls (control: 65 +/- 7; mutant: 60 +/- 10). (E and F) Ventral view of hypothalamus (group 13) in embryos of the indicated genotype processed to reveal *dat* expression by in situ hybridization. (G) Bar chart indicating numbers of 5HT IR and GFP-expressing neurons within the pretectum (group 7) of *trpm7* mutants (or *trpm7* mutant; *Tg*(*dat*:*gfp*) transgenic) and controls. Number of neurons was not significantly different between the genotypes. (Anti-Hu IR-positive cells in DRG caudal to hindyolk at 5 dpf, control: 32± 0, mutant: 31±1). **(**H) qRT-PCR analysis of mRNA levels of *th1*, *th2*, *dat*, and *bdnf*. Asterisks indicate significant difference; $^{*}p<0.001$. Error bars represent

SEM. (For interpretation of the references to color in this figure legend, the reader is referred to the web version of this article.)

Fig 6. DFO partially rescues hypomotility of *trpm7* mutants. DFO treatment increased spontaneous motility of 5-dpf, *trpm7b508* mutant larvae. Automated analysis of motility was carried out as in Fig 2. For each experiment, half of a single clutch of larvae from *trpm7* heterozygous adults was treated with 50 μM DFO from 2–5 dpf. Motility of control larvae was unaffected by DFO treatment (Student's *t*-test, $p>0.4$). Motility of the *trpm7* mutant was significantly increased by treatment with DFO in darkness (Student's *t*-test, $p<0.05$). Each group tested consisted of 23–24 animals. Error bars represent SEM. Asterisks, significantly different values.

Fig 7. Expression of TRPM7 dominant-negative (TRPM7-DN) suppresses differentiation by causing cell death. (A) Representative traces show the current-voltage relationship in HEK-293 cells with expression of wild-type TRPM7 alone or with coexpression of wild-type TRPM7 and the TRPM7-E1047K pore mutant (TRPM7-DN). (B) Co-expression of TRPM7-DN with wild-type TRPM7 in HEK-293 cells suppressed TRPM7 current densities at −120 mV and +100 mV. (C) Representative phase-contrast images of SH-SY5Y cells treated with retinoic acid (RA), at 4 and 6 days after plating. Shown are non-transduced (NT) cells, cells transduced with LacZ for 2 and 4 days, and cells transduced with TRPM7-

DN for 2 and 4 days. Scale bar=200 μm. (D) Cell viability of non-transduced (NT), LacZ expressing, and TRPM7-DN expressing SH-SY5Y cells treated with RA 6 days after plating and 3 days post-transduction. Viability of TRPM7-DN transduced and NT cells was significantly different (Student's *t*-test, p=0.006). Viability was expressed as percent of non-transduced (% NT) cells.

Figure 1

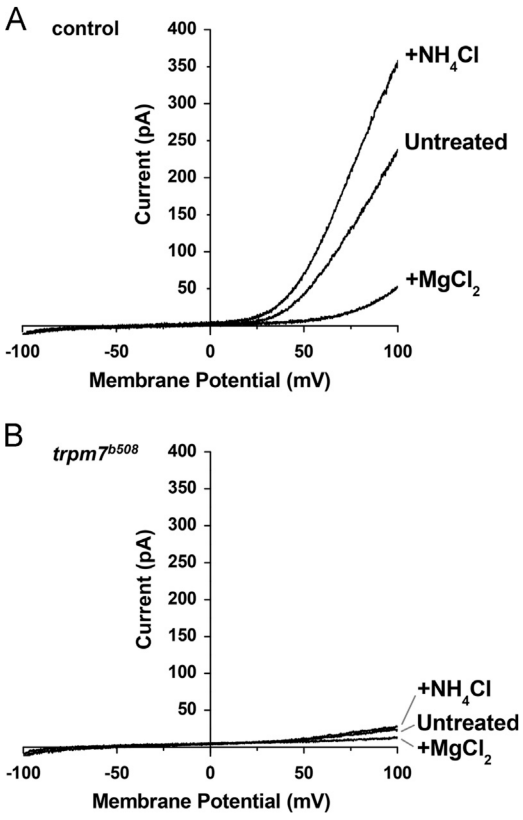
A
control
+NH4Cl
Untreated
+MgCl2
Current (pA)
400
350
300
250
200
150
100
50
-100
-50
0
50
100
Membrane Potential (mV)
B
trpm7b508
+NH4Cl
Untreated
+MgCl2
Current (pA)
Membrane Potential (mV)

Figure 2

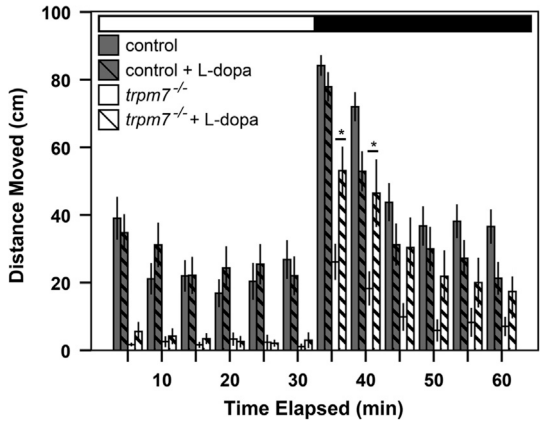
control
control + L-dopa
trpm7 -/-
trpm7 -/- + L-dopa
Distance Moved (cm)
Time Elapsed (min)
0
20
40
60
80
100
10
20
30
40
50
60
*
*

Figure 3

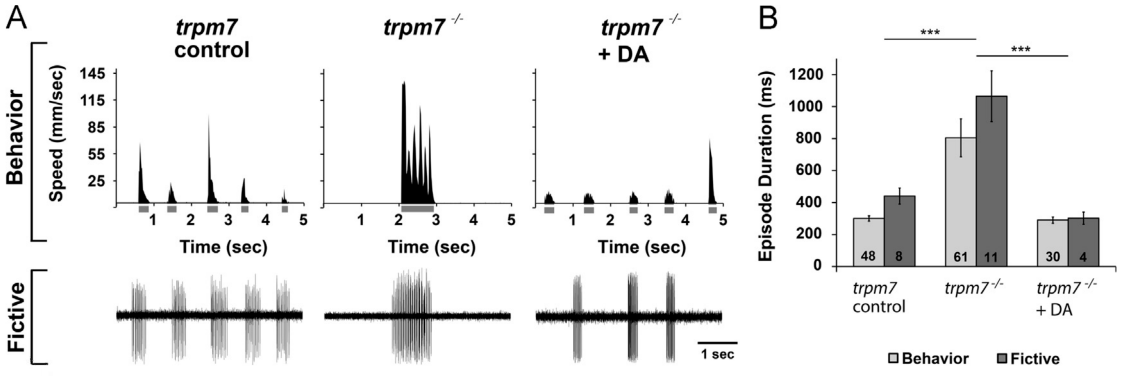
A
trpm7
control
trpm7 -/-
trpm7 -/-
+ DA
Behavior
Speed (mm/sec)
145
115
85
55
25
1 2 3 4 5
Time (sec)
Fictive
1 sec
B
***
***
Episode Duration (ms)
1200
1000
800
600
400
200
0
48 8
61 11
30 4
trpm7
control
trpm7 -/-
trpm7 -/-
+ DA
Behavior
Fictive

Figure 4

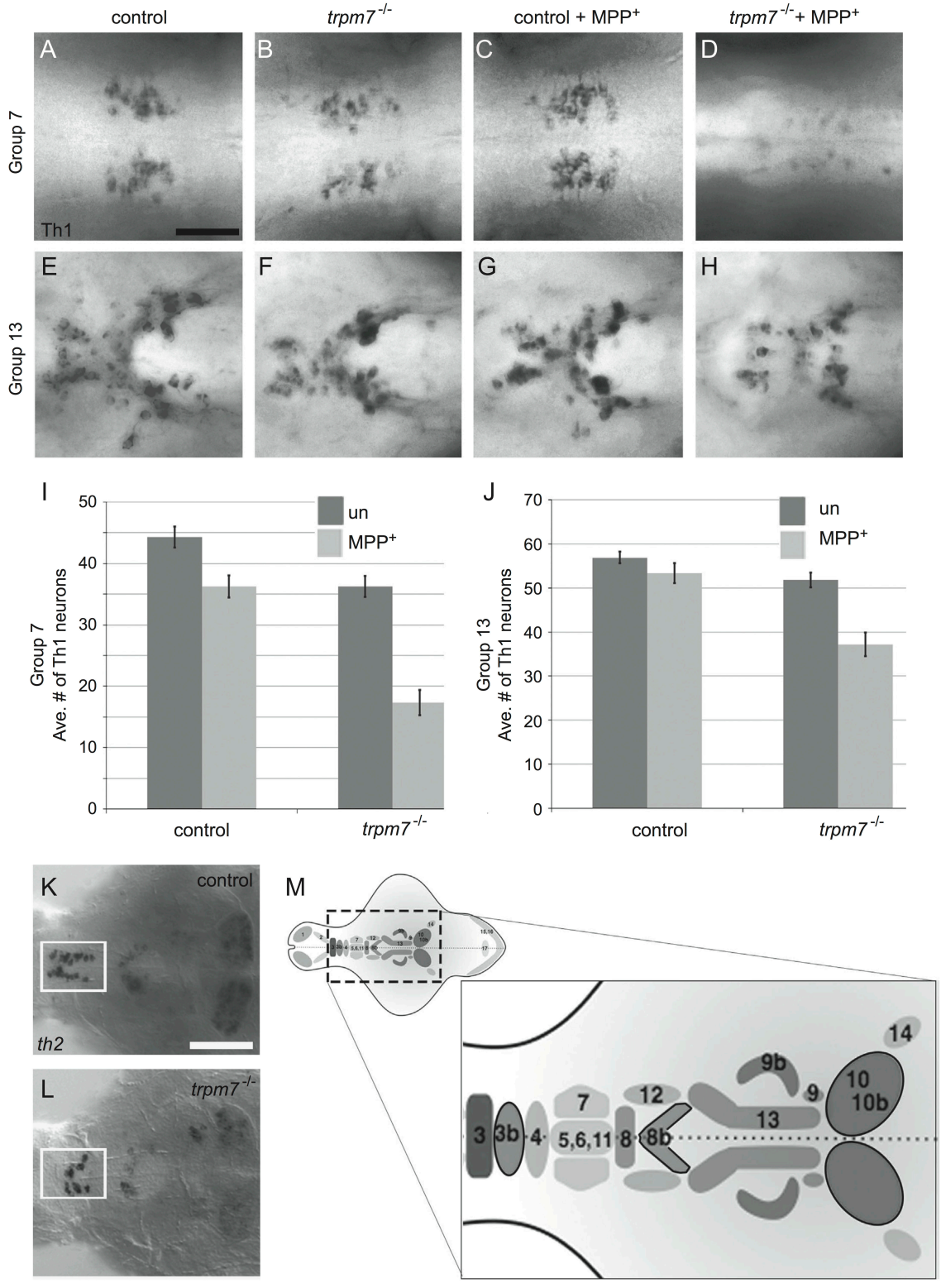
control
trpm7 -/-
control + MPP+
trpm7 -/- + MPP+
A
B
C
D
Group 7
Th1
E
F
G
H
Group 13
I
Group 7
Ave. # of Th1 neurons
un
MPP+
control
trpm7 -/-
J
Group 13
Ave. # of Th1 neurons
un
MPP+
control
trpm7 -/-
K
control
th2
L
trpm7 -/-
M
14
9b
9
10
10b
12
7
13
3
3b
4
5,6,11
8
8b

Figure 5

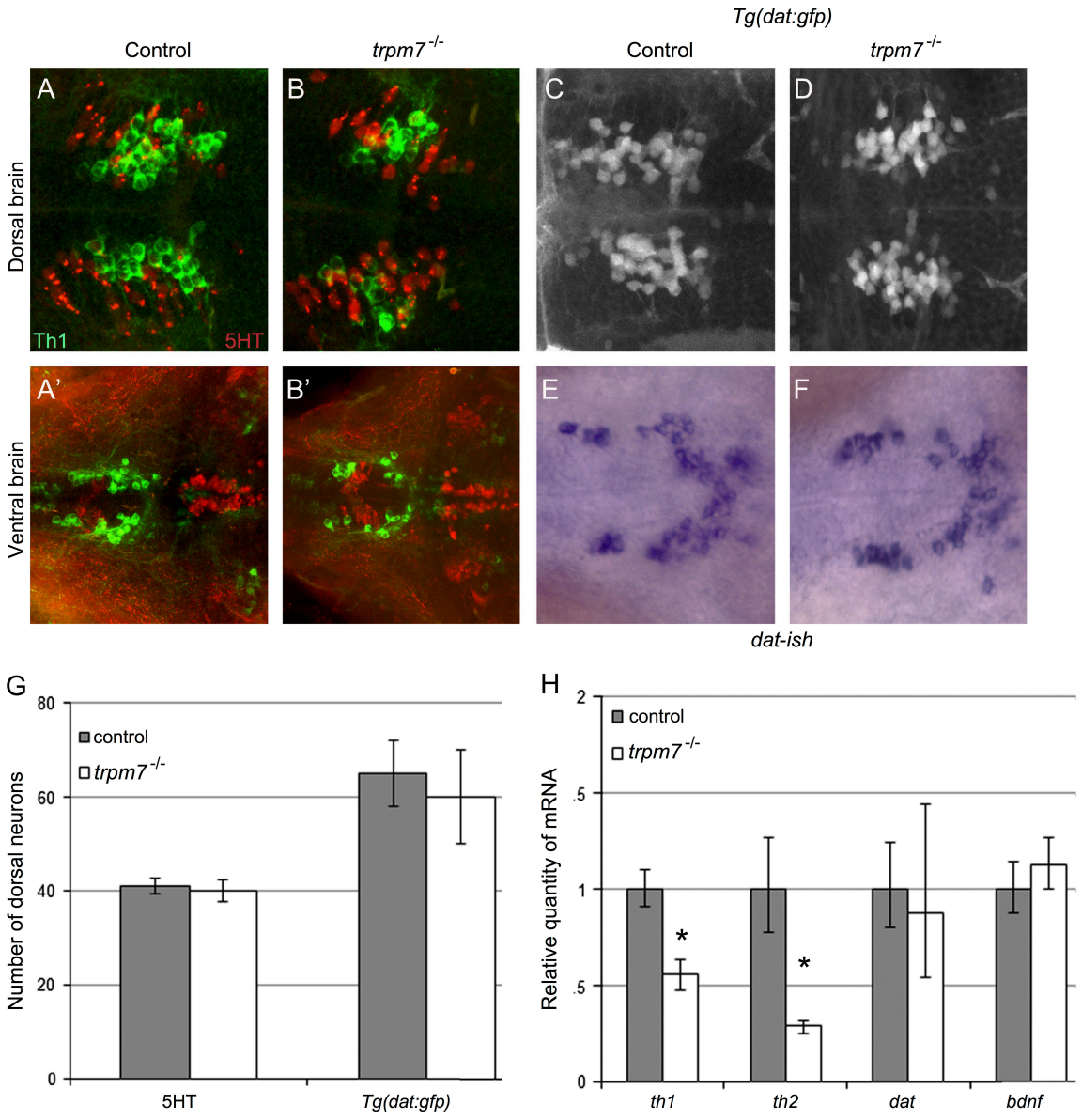
Tg(dat:gfp)
Control
trpm7 -/-
Control
trpm7 -/-
Dorsal brain
A
B
C
D
Th1
5HT
Ventral brain
A'
B'
E
F
dat-ish
G
Number of dorsal neurons
80
60
40
20
0
control
trpm7 -/-
5HT
Tg(dat:gfp)
H
Relative quantity of mRNA
2
1.5
1
.5
0
control
trpm7 -/-
*
*
th1
th2
dat
bdnf

Figure 6

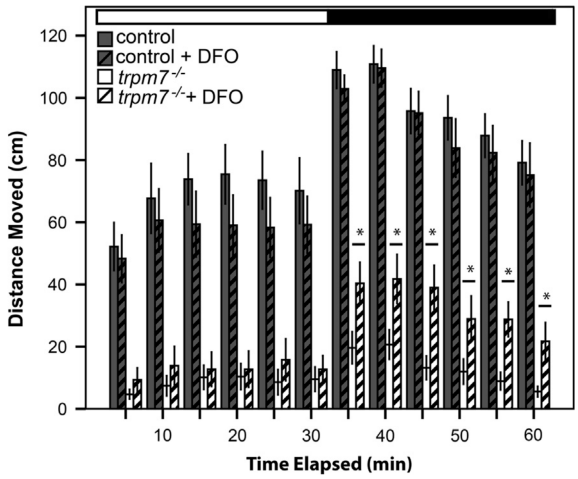
control
control + DFO
trpm7-/-
trpm7-/-+ DFO
Distance Moved (cm)
0
20
40
60
80
100
120
10
20
30
40
50
60
Time Elapsed (min)
*

Figure 7

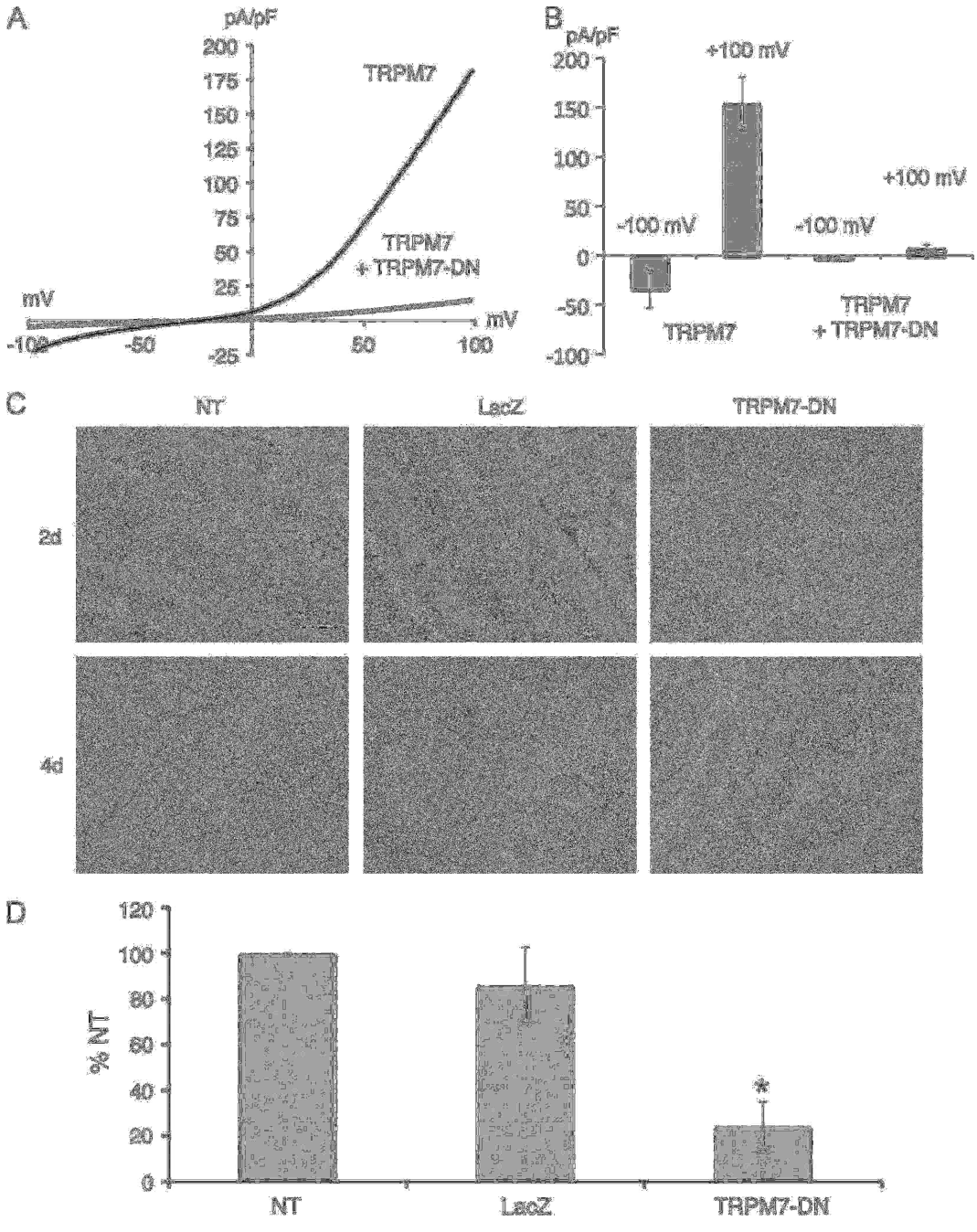
A
pA/pF
200
175
150
125
100
75
50
25
TRPM7
TRPM7
+ TRPM7-DN
mV
-100
-50
-25
50
100
mV
B
pA/pF
200
150
100
50
0
-50
-100
+100 mV
-100 mV
-100 mV
+100 mV
TRPM7
TRPM7
+ TRPM7-DN
C
NT
LacZ
TRPM7-DN
2d
4d
D
% NT
120
100
80
60
40
20
0
*
NT
LacZ
TRPM7-DN

Appendix 2C: Amelioration of vestibular and auditory deficits in Myo7a mutants via high-throughput genomic and pharmacological interventions.

I am sharing my novel methodologies and expertise for videography in zebrafish in a joint zebrafish collaboration with the Schimmenti lab (University of Minnesota- Twin Cities) and the Ekker lab (Mayo Clinic). The goal of the study is to explore pharmacological and genomic therapies in a zebrafish model of hearing loss, called the mariner mutant (Ernest, 2000). This mutant exhibits a phenotype very distinguishable from a wild-type fish. The mariner mutants are deaf and demonstrate abnormal circular swimming. The current study (Appendix 2c) is performing a calcium-driven drug screen and TALEN knockdown screen (Bedell et al., 2012) for potential pharmacological and genomic interventions that ameliorate the observed hearing deficiency and abnormal swimming during development of the mariner mutants. The intentional hypothesis is to modulate the function of the mechanotransducer (MET) channel in order to compensate for the loss of tension on the tip link typically generated by tethering of the tip link to Myosin 7a (Myo7a), a motor protein specific to hair cells of the inner ear. The drugs and genome-editing will be chosen based on their putative ability to modulate the MET channel as well as those that target the voltage-gated calcium channel at the lower periphery of the cell. The efficacy of each drug will be evaluated through a series of behavioral, imaging, and hearing assays. The behavioral assays will employ my adaptation of high-throughput behavioral

analyses (Branson et al., 2009) in zebrafish (Lambert et al., 2012), with additional novel kinematic assessments that I have developed but have yet to be published. My preliminary data reveal that the circular swimming of *myo7a* mutants occurs exclusively during sensory-induced startle responses, either from fish-to-fish contact (Fig 1) or explicit mechanosensory stimulation via touching larvae with a fine probe (Fig 2). Finally, this study has translational potential, because any auspicious candidates from this chemical screen would be potential lead compounds for downstream clinical applications for the prevention of genetic-based newborn hearing loss.

Figure 1

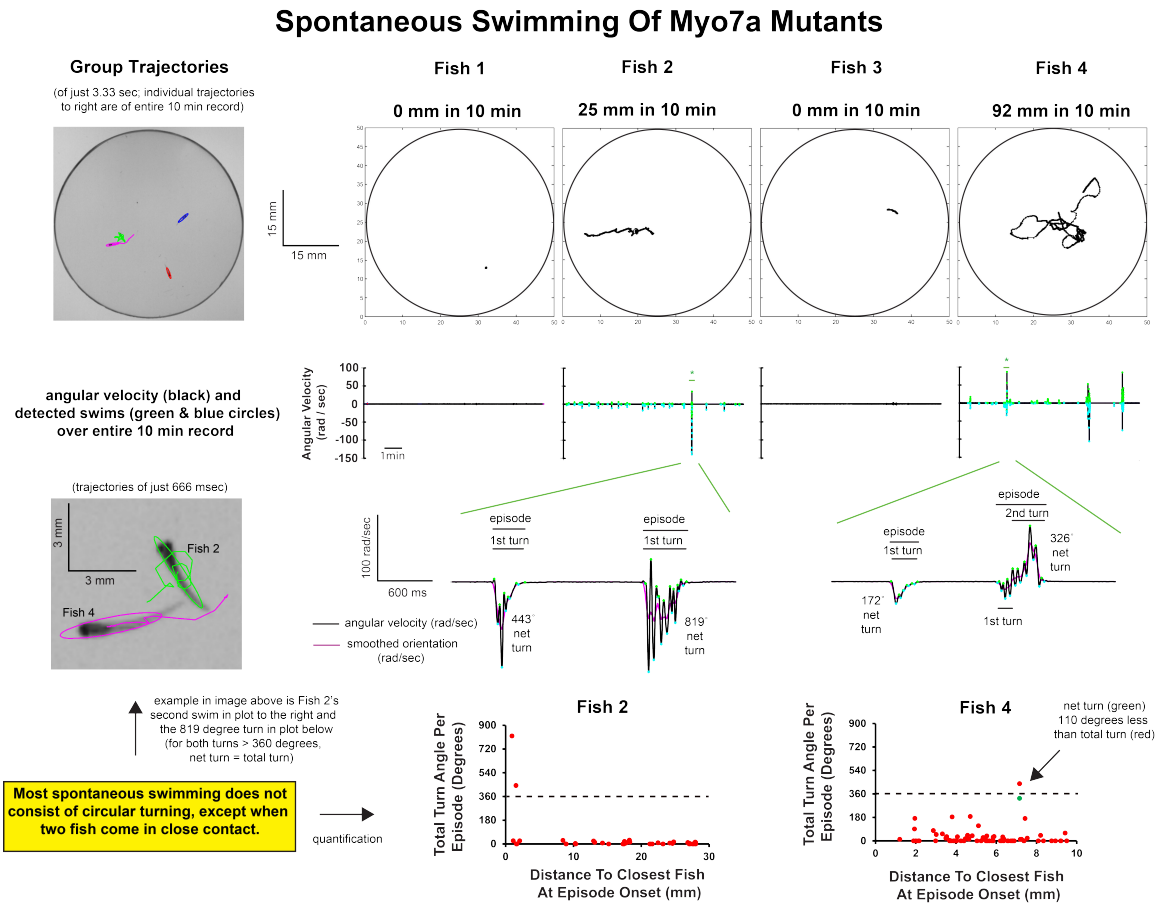
Spontaneous Swimming Of Myo7a Mutants
Group Trajectories
(of just 3.33 sec; individual trajectories to right are of entire 10 min record)
Fish 1
Fish 2
Fish 3
Fish 4
0 mm in 10 min
25 mm in 10 min
0 mm in 10 min
92 mm in 10 min
15 mm
15 mm
angular velocity (black) and detected swims (green & blue circles) over entire 10 min record
Angular Velocity (rad / sec)
1min
(trajectories of just 666 msec)
3 mm
3 mm
Fish 2
Fish 4
100 rad/sec
600 ms
episode
1st turn
443° net turn
819° net turn
172° net turn
326° net turn
2nd turn
1st turn
angular velocity (rad/sec)
smoothed orientation (rad/sec)
example in image above is Fish 2's second swim in plot to the right and the 819 degree turn in plot below (for both turns > 360 degrees, net turn = total turn)
Most spontaneous swimming does not consist of circular turning, except when two fish come in close contact.
quantification
Fish 2
Fish 4
net turn (green) 110 degrees less than total turn (red)
Total Turn Angle Per Episode (Degrees)
Distance To Closest Fish At Episode Onset (mm)

Figure 2

Escape Response To Mechanical Stimualtion (Probe To Head)

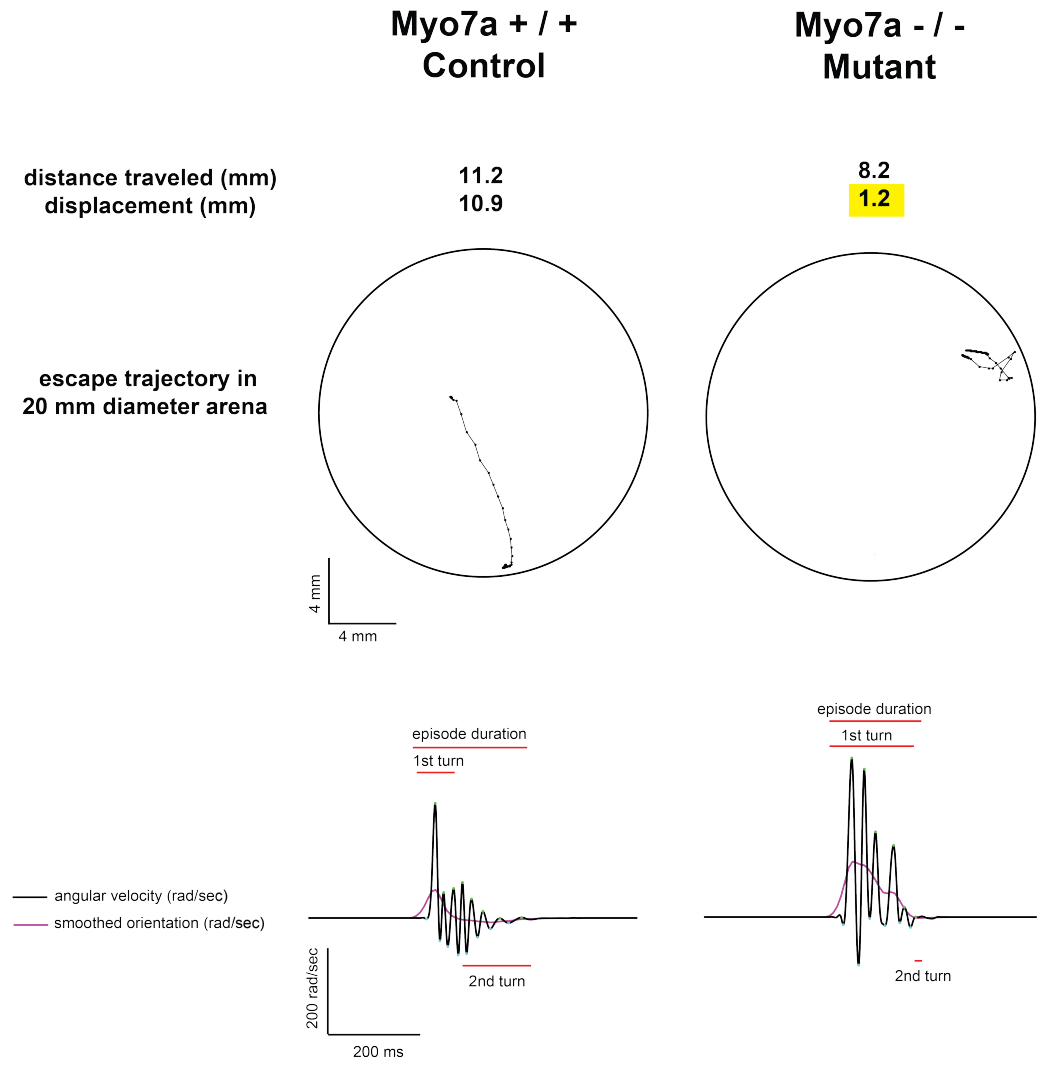

episode duration (ms)	250	200
mean speed (mm/sec)	45	41
peak speed(mm/sec)	138	138
first turn duration (ms)	83	183
first turn angle (degrees)	158	711
total turn angle (degrees)	214	714
net turn angle (degrees)	102	708

Appendix 2D: High-throughput genomic and pharmacological targeting of bioaminergic targets for regeneraton in the planarian Dugesia japonica.

I have also employed my adaptation of high-throughput videography for a collaboration with the Marchant lab (University of Minnesota- Twin Cities). This project is investigating the effects of bioaminergic ligands on the locomotion of planarians. These are aquatic, free-living flatworms that are a classic model for developmental biologists to study the process of regeneration. Worms maintain an adult population of multipotent stem cells that allows regeneration of missing body parts with correct size and polarity. The Marchant group is interested in studying the effects of genetic (by RNAi) and pharmacological inhibition of gene products involved in regeneration, and assessment of locomotor phenotypes provides a good way for screening the efficacy of these interventions as planarian polarity genes are expressed in muscle. My preliminary data provide proof of principle that multiple flatworms can be individually tracked in a group setting and analyzed for multiple locomotor parameters with high fidelity (Fig 1).

Figure 1

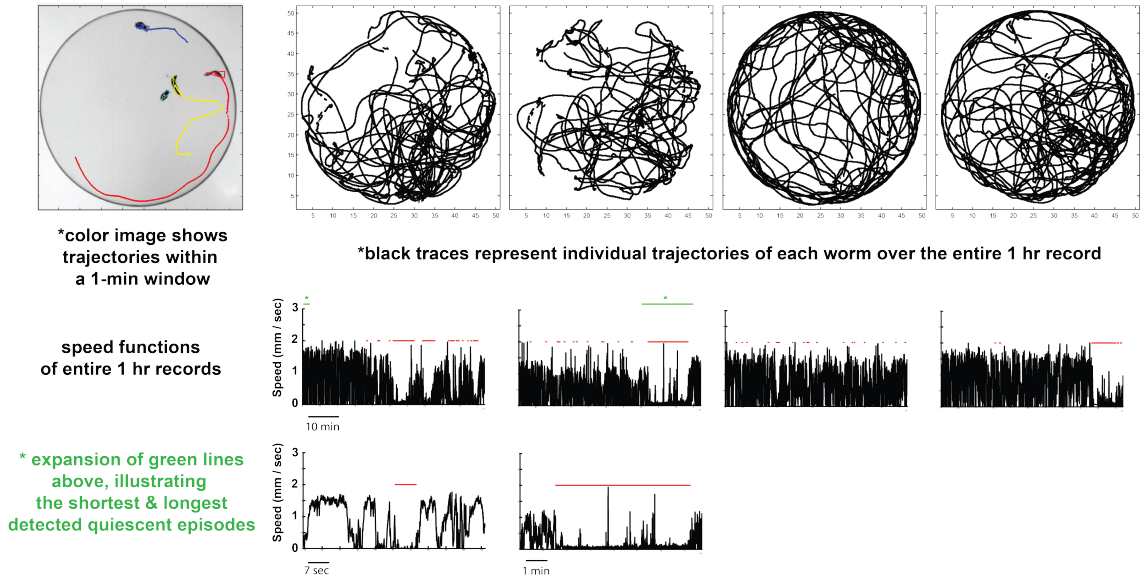

	Worm 1	Worm 2	Worm 3	Worm 4
# quiescent episodes	13	11	16	5
mean quiescent duration (sec)	73	87	14	106
min quiescent duration (sec)	8	9	7	9
max quiescent duration (sec)	399	760	59	460
mean interquiescent duration (sec)	180	186	187	376